Strut-and-Tie Design and Evaluation of Reinforced Concrete Bridge Bent Caps

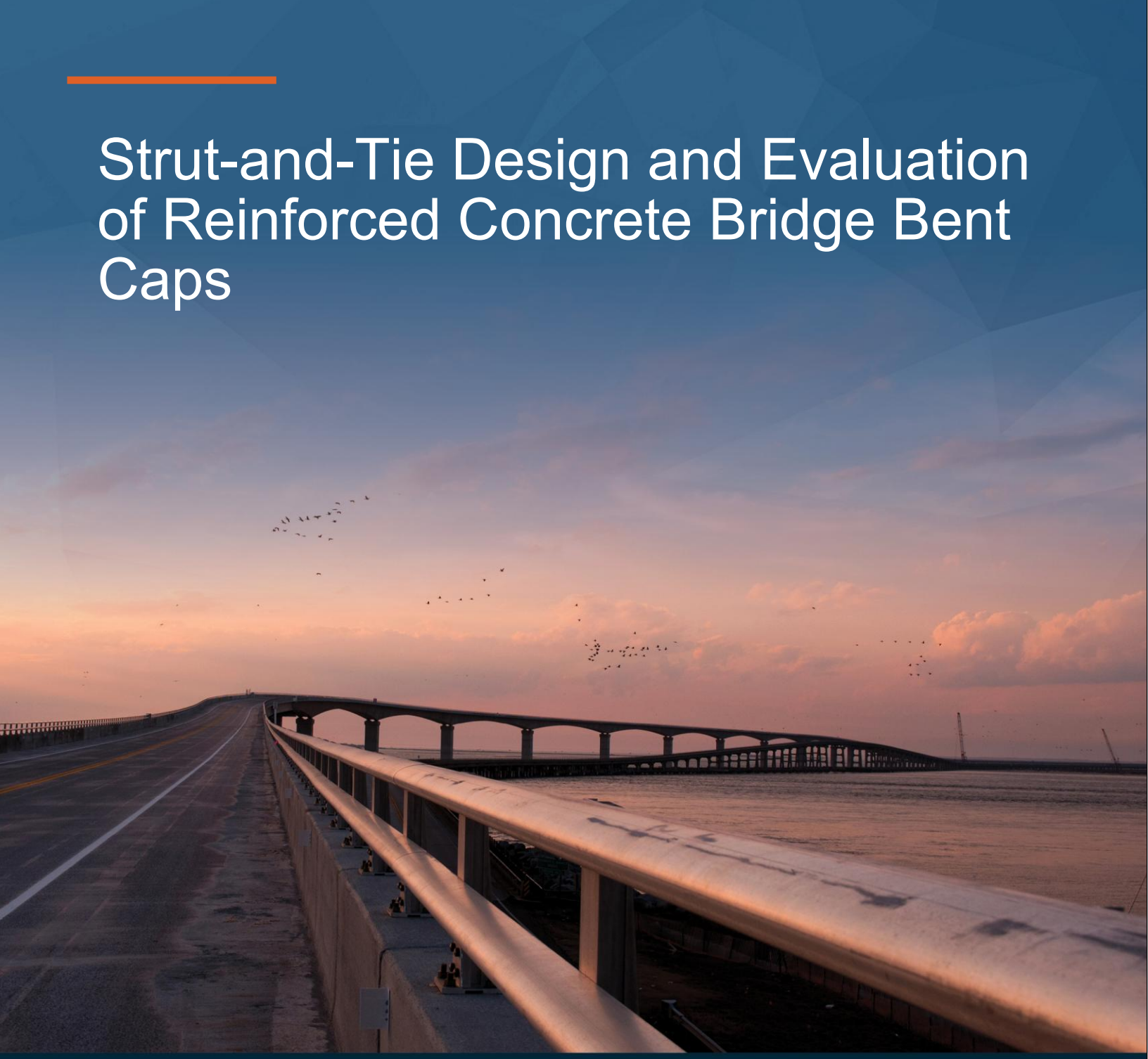

NCDOT Project 2022-09
FHWA/NC/2022-09
August 2025

Vishnu Punithavel
Luis Medina Martinez
Giorgio T. Proestos, Ph.D.
Department of Civil, Construction, and Environmental Engineering
North Carolina State University

RESEARCH & DEVELOPMENT

Technical Report Documentation Page

1. Report No. FHWA/NC/2022-09	2. Government Accession No.	3. Recipient's Catalog No.
4. Title and Subtitle Strut-and-Tie Design and Evaluation of Reinforced Concrete Bridge Bent Caps		5. Report Date August 21, 2025
		6. Performing Organization Code
7. Author(s) Vishnu Punithavel Luis Medina Martinez Giorgio T. Proestos, Ph.D., https://orcid.org/0000-0003-4172-442X		8. Performing Organization Report No.
9. Performing Organization Name and Address Department of Civil, Construction, and Environmental Engineering College of Engineering North Carolina State University 3250 Fitts-Woolard Hall 915 Partners Way Raleigh, NC 27606		10. Work Unit No. (TRAIS)
		11. Contract or Grant No.
12. Sponsoring Agency Name and Address Research and Development Unit 1549 Mail Service Center Raleigh, North Carolina 276699-1549		13. Type of Report and Period Covered Final Report Aug 2021 – May 2025
		14. Sponsoring Agency Code RP2022-09
Supplementary Notes:		

16. Abstract

This report investigates the application of the Strut-and-Tie Method (STM) for the design and evaluation of reinforced concrete bridge bent caps in North Carolina. The study addresses practical challenges in implementing STM, seeks to improve design and assessment consistency, and examines structural performance under both ultimate and service load conditions. A literature review was conducted to establish the foundation for STM design. Multiple bent cap typologies common in North Carolina were identified, and templates were developed to guide engineers through STM design in alignment with AASHTO LRFD provisions. An experimental program involving six large-scale deep beam specimens was undertaken to validate the STM templates and assess the influence of different reinforcement levels and geometries. Specimens were constructed with transverse and horizontal reinforcement ratios of 0%, 0.13%, and 0.30%. Results demonstrated that transverse reinforcement significantly improves shear capacity and serviceability. Members with 0.13% reinforcement achieved higher shear capacities than unreinforced specimens, while those with 0.30% reinforcement offered improved crack control with only modest strength gains. Reinforcement also influenced crack width distribution, with higher ratios resulting in smaller crack widths and more crack control. Geometric parameters, particularly shear span-to-depth ratio, affected crack behavior, with shorter spans exhibiting smaller crack widths. Based on these findings, a minimum distributed reinforcement ratio of 0.13% to 0.30% is recommended to ensure adequate service-level performance. The results also support the use of full nodal efficiency factors in evaluating existing members with distributed reinforcement that may be less than the minimum. This work provides a description for integrating STM into the NCDOT's design workflow and offers guidance for both new and existing bent cap evaluation.

17. Key Words Concrete, Bridge Design, Bents, Strut and Tie Method, Experiments, Testing, Cracking	18. Distribution Statement		
19. Security Classif. (of this report) Unclassified	20. Security Classif. (of this page) Unclassified	21. No. of Pages 133	22. Price

Form DOT F 1700.7 (8-72) **Reproduction of completed page authorized**

DISCLAIMER

The contents of this report reflect the views of the author(s) and not necessarily the views of the University. The author(s) are responsible for the facts and the accuracy of the data presented herein. The contents do not necessarily reflect the official views or policies of either the North Carolina Department of Transportation or the Federal Highway Administration at the time of publication. This report does not constitute a standard, specification, or regulation.

Acknowledgements

The authors would like to thank the North Carolina Department of Transportation for their support of this research. Their continued support of studies on the design and evaluation of bridge infrastructure is greatly appreciated. The authors also wish to thank the steering committee and research manager for their collaboration and contributions throughout the project. Their input has significantly improved the research. Some of the reinforcing bars used in the construction of the test specimens were generously donated by Headed Reinforcement Corporation. Finally, the authors would like to thank the Constructed Facilities Laboratory and its staff for their continued assistance in constructing and testing the experiments in this research.

Executive Summary

This report presents an investigation into the application of the Strut-and-Tie Method (STM) for the design and evaluation of reinforced concrete bridge bent caps in North Carolina. The study aims to address practical challenges associated with STM, enhance design and assessment consistency, and examine the performance of bent caps under both ultimate and service load conditions. The report includes a literature review on the use of STM for bridge structures, identifies bent cap typologies that are classified as deep beams and are well-suited for STM design and evaluation, develops a series of templates to support the design and evaluation process, summarizes an experimental program involving six large-scale deep beam specimens representative of North Carolina bent caps, and provides recommendations for the application of STM in bridge design and evaluation practice.

Reinforced concrete bridge bent caps are structural elements that transfer loads from the superstructure to the substructure. Due to their short shear-span-to-depth ratios, most bent caps in North Carolina behave as deep beams. Traditional sectional design methods often result in conservative estimates of strength for deep beams. The AASHTO LRFD Bridge Design Specifications STM approach provides a more accurate representation of internal force flow and allows for more efficient designs.

This study was undertaken with four primary goals:

1. Review and summarize relevant literature and guidance for application of the STM to bridge bent caps.
2. Develop STM templates for common bent cap typologies used in North Carolina.
3. Experimentally evaluate the behavior of bent caps under different reinforcement and geometric conditions.
4. Provide practical recommendations for the use of STM within NCDOT's design and evaluation framework.

Twelve common bent cap typologies were identified from NCDOT bridge projects and used to develop Excel-based STM templates. These templates guide engineers through the design process by defining geometry, inputting material properties, loads, performing force equilibrium calculations, checking nodal strength, and calculating required reinforcement. The templates align with AASHTO LRFD STM and can be integrated with current NCDOT tools such as RC-Pier and LEAP Bridge Concrete.

In the design of bent caps using AASHTO LRFD based STM, the 0.30% minimum required reinforcement in both orthogonal directions allows the use of the larger nodal efficiency factors specified in AASHTO LRFD Table 5.8.2.5.3a-1. Most studies indicate this will give conservative designs under ultimate limit state conditions. This relatively large quantity of reinforcement will assist in crack control under service conditions. In members that are not heavily loaded in shear, the designer can reduce this quantity of distributed reinforcement and use the lower nodal efficiency factor (a value of 0.45) as described in the AASHTO LRFD STM provisions. While there is substantial research on the application of the STM under ultimate conditions, there is little research exploring the influence of different reinforcement ratios, and other member properties, on performance under service conditions.

An experimental program was conducted to verify and validate the STM templates and to investigate how different transverse and horizontal reinforcement ratios influence the structural performance of bent caps

under both service and ultimate load conditions. Six large-scale specimens, representative of North Carolina bridge bent caps, were tested with transverse and horizontal reinforcement ratios of 0%, 0.13%, and 0.30%. These values were chosen to examine the behavior of members without distributed reinforcement, members with moderate quantities of distributed reinforcement, and members meeting the AASHTO minimum reinforcement for full nodal efficiency when using the STM. Instrumentation included full field-of-view digital image correlation (DIC), strain gauges, and displacement transducers, which provided detailed insights into displacement fields, strain fields and cracks throughout loading.

The results demonstrated that the inclusion of transverse reinforcement significantly improves shear capacity compared to members without transverse and horizontal distributed reinforcement. Beams with 0.13% reinforcement showed higher shear capacities over those without any reinforcement, and those with 0.30% reinforcement exhibited similar capacities to specimens reinforced with 0.13% reinforcement. While the increase in ultimate strength, if any, between 0.13% and 0.30% reinforcement was relatively small, the member strengths were higher than those predicted by the STM.

In addition to strength, transverse and horizontal reinforcement had a significant effect on crack control at service loads. Members without distributed reinforcement developed wider, localized shear cracks. In contrast, members with 0.13% reinforcement showed smaller, more distributed cracking, and those with 0.30% reinforcement exhibited the most crack control. Increasing the reinforcement ratio reduced crack widths and improved the overall serviceability of the beams.

The Manual for Bridge Element Inspection for reinforced concrete bent caps suggests crack widths as large as 0.0625 in. to 0.125 in. (1.6 mm to 3.2 mm) corresponds to "narrow to moderate" crack widths, resulting in a Condition State less than 3. Shear cracks in disturbed regions can become concerning at lower values. Additionally, other guidance documents suggest that crack widths near service loads should be limited to approximately 0.016 in. (0.40 mm). Based on the results of this study, a minimum quantity of distributed reinforcement in both orthogonal directions of approximately 0.13% to 0.30% is recommended to achieve this level of crack control performance.

The tests also showed that geometric factors, such as the shear span-to-depth ratio, influence crack widths. Beams with shorter shear spans generally exhibited smaller crack widths for the same reinforcement levels, confirming that member specific geometry, such as shear span-to-depth ratio, influences crack widths at service and ultimate loads.

Overall, the experimental results confirm that using a minimum of 0.13% transverse and horizonal reinforcement significantly enhances shear performance and crack control in deep beams. Increasing to 0.30% distributed reinforcement provides additional benefit, particularly in terms of serviceability, and is recommended where crack control is of particular importance. It should be noted that as the shear span-to-depth ratio, quantity of flexural reinforcement, concrete strength, concrete clear cover, reinforcement bar sizes and other member specific factors change, the minimum amount of distributed reinforcement to achieve the desired performance at service loads may also be affected.

In evaluating existing members that may contain less than 0.30% distributed reinforcement, but more than zero distributed reinforcement, the results of this study indicate that it may be appropriate to use the nodal factors in AASHTO LRFD Table 5.8.2.5.3a-1, rather than using a value of 0.45. This could be considered in evaluating existing bent caps or bent caps that, for example, may have been designed using sectional methods and contain lower quantities of transverse reinforcement (approximately 0.13%).

Table of Contents

List of Figures

List of Tables

Limitations and Public Notice

This report was written for the North Carolina Department of Transportation for its use. The assumptions, drawings, calculations, and recommendations included in this report are applicable to the specific structures and conditions described in the report and may not be applicable or appropriate in other applications. It is expected that the North Carolina Department of Transportation will use engineering judgment to apply the contents of this report in its works.

The public should be put on notice that the contents of this report is not a certified document and shall not to be used for construction. For the purposes of the public, this report is: “Preliminary - Do not use for construction”.

Glossary

A_c: Cross-sectional area of strut

A_{cn}: Effective cross-sectional area of the node face as specified in AASHTO LFRD.

A_{cs}: Effective cross-sectional area

A_{sb}: Area of bottom reinforcement

A_{st}: Area of steel

A_v: Area of transverse reinforcement

A_h: Total area of horizontal crack control reinforcement within spacing S_h

D: Length between forces from columns in design templates

F_u: Factored load

F_y: Yield strength

$L_{\#}$: Length of section in design templates

$P_{\#}$: Point loads

$R_{\#}$: Reaction force

S_h: Spacing of horizontal crack control reinforcement

S_v: Spacing of vertical crack control reinforcement

β_c: Strut/node confinement modification factor

k_s: Conversion factor for the efficiency of the face of a node abutting a strut

l_b: Length of bearing

m: Confinement modification factor

v: Concrete efficiency factor

ϕ: Resistance factor

h_a: Height of the back face of the node

ϕ_c: Resistance factor for concrete

ρ_h: Horizontal reinforcement ratio

ρ_v: Transverse reinforcement ratio

β_s: Strut coefficient

b_w: web width

b_v: web width

d: Effective depth

d_{ba}: Diameter of bottom longitudinal bar

d_{ta}: Diameter of top longitudinal bar

d_v: Diameter of transverse reinforcement

ϵ: Strain

ϵ_u: Strain at ultimate strength

ϵ_y: Yield strain

ϵ_{sh}: Strain hardening strain

f'_c: Concrete cylinder compressive strength

f_s: Allowable stress in steel under service load

f_u: Ultimate strength

f_y: Yield strength

f_{ce}: Strength of concrete strut

f_{cu}: Limiting compressive stress

f_{yl}: Longitudinal reinforcement bars yield strength

f_{yv}: Vertical reinforcement bars yield strength

h: Height of beam

h_{STM}: Height of STM model

1 INTRODUCTION

Bridges are integral to the highway network as they provide a mechanism to support roadways and rail systems. There are more than 617,000 bridges across the United States, and between $14.4 and $22.7 billion are spent annually on rehabilitating the bridges (ASCE's Report Card for America's Infrastructure 2025).

Bridges are composed of various structural components. Among these, bent caps transmit loads from the superstructure to the substructure. The superstructure generally consists of decks and girders. Load is transferred to the substructure through the bent caps to the columns or piers, and then to the pile caps or spread footings. The bent caps are typically constructed from reinforced concrete and often support the superstructure through bearings on top of the bent caps. The loads applied to the bent caps from the supported girders can be idealized as point loads. Bent caps are typically supported by closely spaced columns, leading to small shear span to depth ratios (a/d) ratios (less than 2.5). As a result, most bent caps are classified as deep beams (disturbed regions) rather than slender beams (beam regions). Figure 1-1 shows a typical four-column bent cap, where the shear span-to-depth (a/d) ratio is approximately 0.85. This ratio varies slightly from span to span but all the shear spans in this bent cap would be classified as a deep beam or disturbed region.

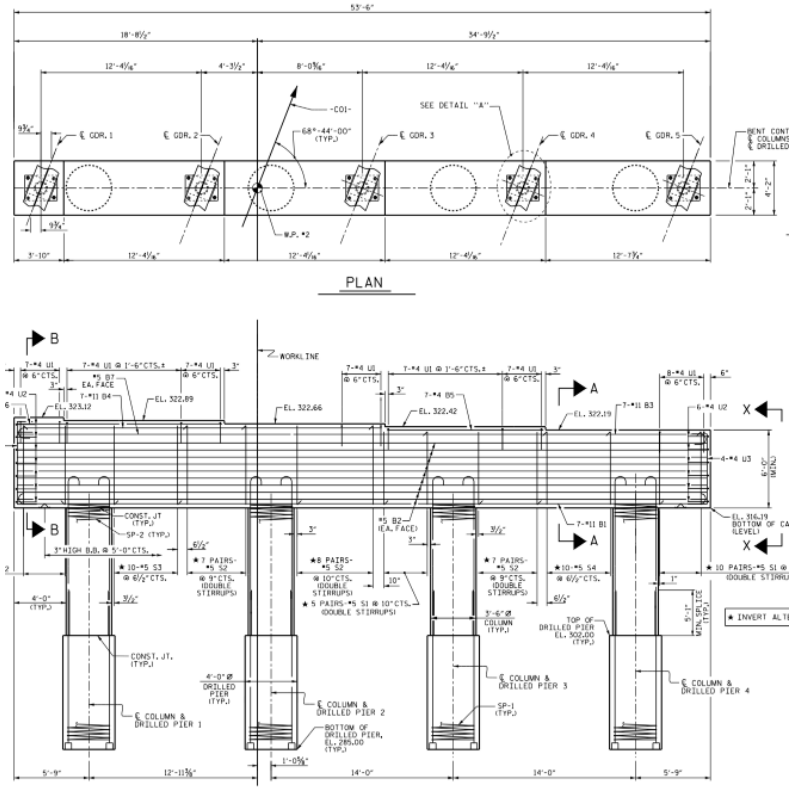

Figure 1-1: A typical four-column bent cap located in Wake County.

Reinforced concrete deep beams are defined by their small shear-span-to-depth ratios (a/d ratios). The response of deep beams is governed by strut action rather than beam action. This strut action is characterized

by direct compression that connects the loading and supporting elements. In these scenarios, plane sections do not remain plane and the strain distribution through the depth of the member is non-linear. The shear strength of deep beams where the shear span to depth ratio is less than about 2 or 2.5, is often much higher than what would be predicted by sectional methods. Since reinforced concrete bridge bent caps are often in this category of deep beams, if these members are designed using traditional sectional analysis methods, it can result in the structure being overly conservative in shear. This can result in congested transverse reinforcement arrangements. The AASHTO LRFD Bridge Design Specifications 9th Edition (AASHTO LRFD) allows the use of strut-and-tie procedures for the design of these members (AASHTO 2020). The application of strut-and-tie procedures can result in more efficient structural designs that also better represent the load-carrying mechanisms of the members.

The Strut-and-Tie Method (STM) is a powerful tool used in the design and assessment of reinforced concrete disturbed regions, such as bridge bent caps. It is used to model the internal flow of forces and determine if the structure is capable of transmitting these loads through compression struts and tension ties. *Figure 1-2* depicts a strut-and-tie model developed for a deep beam carrying a point load.

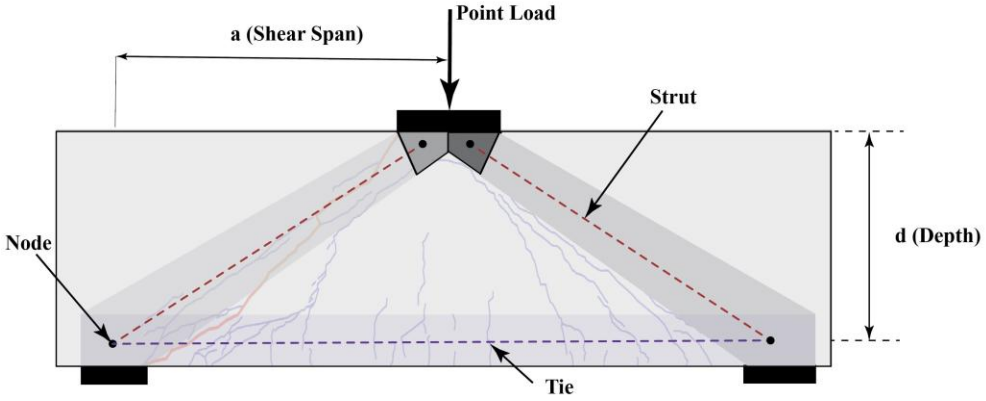

Figure 1-2: Strut-and-tie model developed for a deep beam.

The application of STM in practice can present several challenges. Developing strut-and-tie models and determining the geometry of struts and ties, particularly in complex scenarios, can be difficult. Additionally, different engineers may arrive at different plausible models thereby raising the question of which model is most appropriate. Multiple different models can present challenges in checking the calculations and of other engineers. Another challenge in the STM is the consideration of multiple load combinations. This includes different combinations of live and dead loading (among other load combinations) that can arise from different load conditions. This poses a challenge when using the STM, because different strut-and-tie models may need to be developed for each loading scenario. Envelopes of load, generally, cannot be used with the STM since individual loading scenarios that satisfy equilibrium need to be considered independently. Additionally, each load combination may affect the strut-and-tie geometry differently, requiring a unique strut-and-tie model for each combination. Another challenge in using strut-and-tie models is the consistency of assumptions regarding load path from supported and supporting elements. For example, if in the structural analyses, it is assumed that the columns or piers supporting bent caps transmit moment, this must be consistently applied in strut-and-tie models being developed. Another common consideration needed is how to address the use of STM in scenarios with indeterminate bent caps supported

by more than two supports. Thus, when using the strut-and-tie model, it can be important to consider the moment transmitted at the bent cap and column interface, as this moment affects the distribution of forces and the layout of the strut-and-tie model. Not addressing this moment transfer can lead to inconsistent load path assumptions for the design of the piers and columns and the bent caps. Another practical challenge that can arise relates to minimum reinforcement requirements. The AASHTO LRFD Bridge Design Specifications requires a minimum reinforcement ratio (0.30%) for the use of certain strut-and-tie model assumptions. In some scenarios this quantity may be higher than lightly transverse reinforced members designed with sectional design procedures. Additionally, the STM is a tool for the design and assessment of members in ultimate load conditions. The STM does not provide insight on the performance of structures under serviceability conditions.

This research and report address some of these challenges in applying the STM for reinforced concrete bridge bent caps in North Carolina. First this report provides a literature review focused on the use of STM models for bridge bent cap components. The literature review is also used to support typical assumptions made in developing strut-and-tie models.

Second, as previously introduced the STM provides significant flexibility in being able to design and evaluate complex structures under any loading condition, near supports or complex disturbed regions. While this flexibility and generality is powerful, it poses the challenge that it can make designs difficult to check or can give different models that provide different levels of conservatism. To address this challenge, this research and report shows the development of spreadsheet-based templates that can be used for common bent cap typologies identified in North Carolina. These templates help users select a suitable strut and tie model from a set of available options based on the structure's geometry and loading conditions. Once an appropriate typology is selected, a corresponding set of struts, ties, and nodes is defined to represent the internal flow of forces. Key parameters such as structural dimensions, material strengths, support and bearing dimensions, and applied loads are then input into the template. Using the method of joints, the internal forces within each member are determined based on static equilibrium. Once the model is analyzed, the suitability of the selected strut-and-tie model is verified through nodal checks as described in the AASHTO LRFD Bridge Design Specifications provisions. The required longitudinal and transverse reinforcement is then determined based on the selected model, the forces in the ties and reinforcement bar size selected. The development and application of these templates are based on a series of assumptions that provide more consistency in how the design or evaluation of a particular bent cap is conducted. It also provides the conceptual basis upon which other templates and models can be developed. Section 3 of this report discusses the process used to developed the strut-and-tie templates introduced.

As previously noted, the STM was developed and is typically applied to addresses designs under ultimate conditions for flexure and shear. Strut-and-tie models are limited in their ability to predict structural performance under service loads. While STM ensures the safety of a structure under ultimate conditions, it does not address serviceability issues, such as crack widths, that can affect a member's long-term durability and aesthetic appearance. Therefore, as a part of this study, the minimum reinforcement quantities are investigated through an experimental program, in part to address serviceability considerations. The investigation also provides a basis to examine the performance of members that may contain less than the minimum reinforcement. Section 4 provides a detailed discussion of the experimental program developed to investigate the behavior of representative beams under serviceability and ultimate loading conditions. The study examines the effects of different reinforcement ratios and shear span-to-depth ratios, to

investigate their influence on cracking, deflections, and overall structural performance throughout loading. Six large-scale experiments, representative of North Carolina bridge bent cap conditions were conducted. The shear span-to-depth (a/d) ratios were selected to reflect the those commonly found in bent caps used by the North Carolina Department of Transportation (NCDOT). The specimens were constructed with varying transverse reinforcement ratios: 0%, 0.13%, and 0.30%. These values were chosen to represent three scenarios, the unreinforced condition (used as a baseline and lower bound), a transverse reinforcement ratio that is associated with lightly reinforced members identified as a value that is used by the NCDOT in existing bent caps, and the AASHTO-recommended minimum reinforcement limit required to use strut-and-tie efficiency factors without reduction. The specimens were instrumented with a three-dimensional Digital Image Correlation (DIC) equipment used to measure the full displacement field of the specimens throughout loading. This was also supplemented with data collected from an OptoTrack system that uses infrared light emitting diodes (LEDs) to monitor the three-dimensional displacement field at discrete locations. Conventional strain gauges and displacement transducers were also used to measure the response of the specimens. These results were used to evaluate the performance of the members throughout loading at service and ultimate conditions.

1.1 Layout of the Report

Section 1 introduces the Strut-and-Tie Method (STM) and its application for the design and evaluation of reinforced concrete bent caps. It outlines the fundamental principles of STM, its advantages over traditional design methods, and the challenges associated with its implementation. For brevity, a comprehensive literature review as it relates to the design of bridge bent caps that includes an in-depth discussion on the STM, including theoretical background, additional design considerations, and existing research, is provided in Appendix A.

Section 2 presents the approach by which the STM is applied to bridge bent caps in North Carolina consistent with the AASHTO LRFD Bridge Design Specifications provisions. It outlines the steps involved in developing and applying the proposed STM templates, including fundamental assumptions, nodal checks, design of tie reinforcement and other relevant simplifications.

Section 3 discusses the development of the templates which use the STM for the design or evaluation of reinforced concrete bent caps. The section also discusses how these templates fit into the existing NCDOT design process and workflow. Additionally, this section discusses how the templates align with AASHTO LRFD design provisions and provides a description of various assumptions used in the proposed methods. A detailed example of a two-column bent cap is provided to illustrate the step-by-step application of the templates for design. A comprehensive summary of the templates is also provided in this section.

Section 4 discusses the results and observations from the experimental program. The section outlines the variables of the experimental series and describes their significance in the context of this study on the design of bent caps using the STM. For brevity, the most important results and observations are discussed in this section with additional information provided in Appendix E and Appendix F. Appendix E provides additional information on the experiment setup and specimens. Appendix F provides a detailed summary of photos of the experiments, crack width diagrams, and crack patterns observed.

Section 5 summarizes the recommendations and conclusions of the study based on the development of the typologies, the experiments and modeling conducted. The section discusses assumptions made in the development of the strut-and-tie models, a summary of conclusions from the experimental series, recommendations on the quantity of minimum reinforcement and a discussion of how the STM fits within the NCDOT processes and workflow. The section provides a discussion of results in the context of service and ultimate conditions.

Appendix A presents a detailed literature review related to the strut-and-tie design and evaluation of bridge bent caps, including a discussion of the STM using various design codes and methods, summaries of related experimental programs, and a discussion of assumptions or approaches adopted by other Departments of Transportations or found in guidance documents.

Appendix B provides a detailed example for a two-column bent cap, including sample calculations for various loading scenarios, a summary of nodal checks and the tie reinforcement design.

Appendix C presents sample designs obtained from sample templates and compares the designs with analyses of nonlinear finite element models.

Appendix D provides additional details on how the strut-and-tie design and evaluation process can be used in conjunction with RC-Pier and LEAP Bridge Concrete.

Appendix E provides additional details of the experimental program, including the experimental setup, instrumentation arrangement, material properties, and additional details of the specimens.

Appendix F provides additional data obtained from the experimental series. The appendix summarizes measurements from strain gauges and summarizes photographs and crack patterns observed at the peak load.

Appendix G summarizes a list of related references reviewed and determined to be relevant to this study but not directly referenced elsewhere.

2 AASHTO BASED STRUT-AND-TIE DESIGN PROCESS

In this chapter, the Strut-and-Tie Method (STM) based on AASHTO LRFD Bridge Design Specifications 9th Edition are discussed in the context of bridge bent caps in North Carolina. The STM process begins by identifying nodes, which are the connection points where struts (compression elements) and ties (tension elements) meet. Next, a truss model is developed to represent the internal force flow within the structure. The forces in struts and ties are then determined from equilibrium. From the forces in the struts and ties, the stresses in the nodes are checked and the quantity of reinforcement in the ties can be determined. This section provides an overview of this process and the assumptions in the development of strut-and-tie models for bridge bent caps.

2.1 Overall Assumptions for The Design of Bent Caps Using AASHTO LRFD Based STM

Step 1: Initial Load Analysis and Calculating Reactions

As the first step, the factored loads for a particular load case and load arrangement are applied to the bent cap at the bearing locations as point loads (see example in Figure 2-1). The designer should consider how the flow of forces are assumed to pass through the bent cap into the supporting members. That is, if a linear structural analysis has been conducted for the bent cap and includes moment transfer to piers or columns, this should be considered in the strut-and-model and analysis. The applied loads and reactions from the linear structural analysis of the bent cap beam model will be used as inputs to the strut-and-tie model. For structures that are statically determinate a linear model for the bent cap would be trivial, but in many cases the bent cap has multiple column or pier reactions and is statically indeterminate. Therefore, in these cases a linear model of the bent cap can be used to determine the reactions from the applied loads for a particular load case. It should be noted that in general when using strut-and-tie methods for statically indeterminate structures, any reasonable distribution of the reactions can be used, a linear analysis is not required. However, since for this study, the discussion is on bent caps, consistency should be maintained with the design of the superstructure and supporting elements, thus the reactions as determined from a linear elastic beam analysis of the bent cap is recommended.

One advantage of strut-and-tie methods are that they are compatible with any reasonable assumed load path, if equilibrium is satisfied. That is, if a designer has decided on how the applied loads on the bearings will flow through the bent cap, the strut-and-tie model can be arranged to accommodate this.

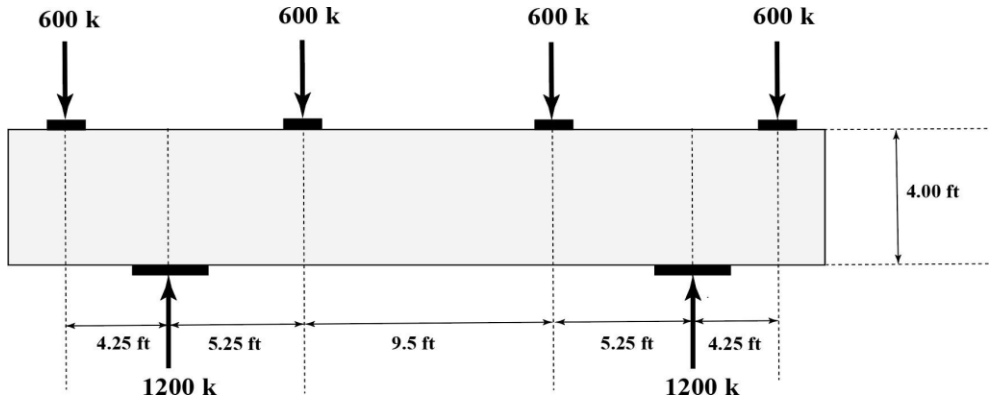

Figure 2-1: Example loads applied as point loads on a bent cap.

Figure 2-2 shows how the strut-and-tie models developed can be arranged to accommodate moment transfer into the columns or piers. The moment and axial load that is determined from a structural analysis will be converted to two-point loads separated by a distance. If there is no moment transmitted into the supporting elements each of the two vertical reactions will be equal. The two-point loads will be separated by a characteristic distance approximating the flexural lever arm in the supporting member.

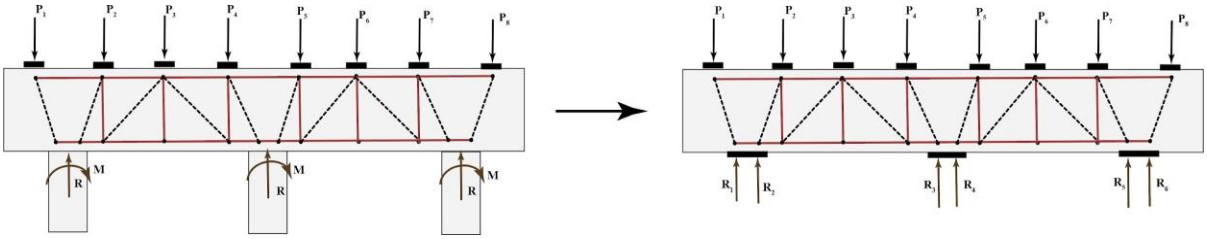

Figure 2-2: Moments idealized as two-point loads separated by a distance within the column.

It is important to note that the location and geometry of these applied forces must align with the resultant force acting on the bearing plate. Since the support reactions are prorated based on tributary areas and the effective bearing length (l_b) may vary across different supports, the point of action of each force should be centered over its assigned portion of the plate. The engineer must ensure that the assumed strut-and-tie geometry correctly reflects these centroids of bearing to maintain force equilibrium and compatibility. Therefore, the input geometry should be carefully checked and adjusted so that the resultant force direction and location are consistent with the distribution of loads on the support plates.

Step 2: Developing an Appropriate Strut-and-Tie Model

The first step in developing the strut-and-tie model for a particular bent cap beam involves positioning the top and bottom chords at the appropriate locations. The diagonal compressive elements (struts) and vertical tension elements (ties) are added based on the assumed internal load path. In North Carolina, bent caps often have more than two columns and may contain overhangs which means that in many cases there can be both positive and negative moments along the bent cap and over the columns. Therefore, almost all the bent caps have both top and bottom longitudinal reinforcement. Even in scenarios where there are only two

supporting elements, the overhangs often create negative moments, and thus, the bent cap would require top reinforcement. The centroids of the compression and tension chords should coincide to avoid the need to build complex strut-and-tie models that redirect the chord forces. When a chord is under compression on both sides of a node, such as in the region between two compression-dominated members, the location of the chord centroid is governed by the geometry of the node (back face of the node). In this case, the compressed concrete or member profile around the node determines the effective centroid. On the other hand, when the chord is under tension on both sides of the node, such as in a continuous beam passing over a column, the centroid of the chord coincides with the centroid of the flexural tension reinforcement, which carries the tensile force through the node. Ensuring that these centroids align in both tension and compression helps maintain consistent force paths and avoid the need to develop more complex strut-and-tie models to move the centroid of the chord forces up or down in the section (see Figure 2-3).

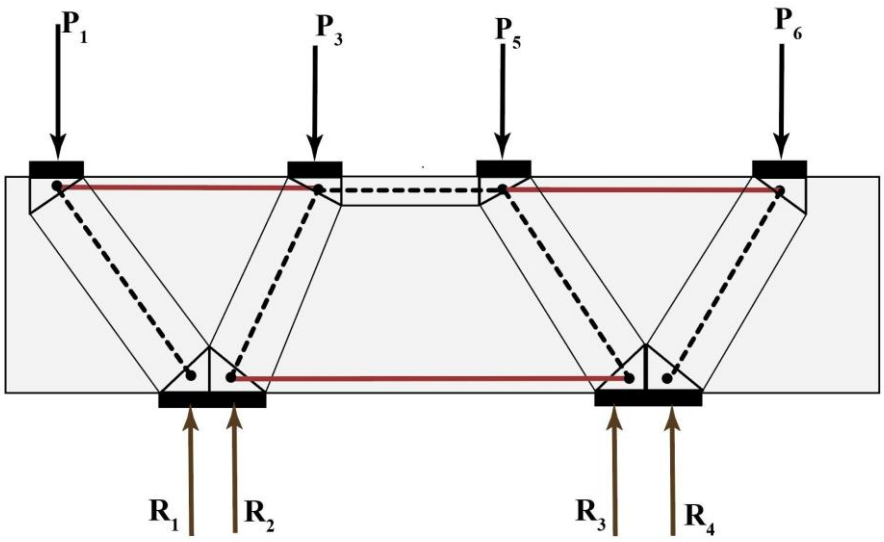

Figure 2-3: An illustration showing the ties and the centroids of the chords coincide.

In scenarios where the top or bottom chords switch from tension to compression, it is convenient to model the chord as straight so that additional, local modifications, to the strut-and-tie model are not needed to deviate the compression strut from the location of the tension tie. Thus, for simplicity it is suggested that the location of the top and bottom chords be selected and remain constant over the length of the member. This may mean accommodating the location of the compression strut or tension tie in the model so that they coincide. See Figure 2-3.

Figure 2-4 presents a schematic cross-section used to define the input parameters for the strut-and-tie model as required in the AASHTO LRFD Bridge Design Specifications. This figure illustrates the key geometric dimensions involved in modeling the internal flow of forces through concrete elements. These geometric inputs are derived based on the physical layout of the structure, such as the position and width of load bearings and supports.

The dimension h_{STM} represents the total height of the STM region. The dimension h_a refers to the height of the node under bearing or support area. The horizontal distance l_b denotes the length which refers to the

tributary length of the applied load that contributes to a specific node**.** The applied load is often spread over a wider area (such as a bearing pad or load plate), and each node in the STM only receives the portion of that load which lies within its zone of influence.

These values determine the location and angle (θ_s) of the strut, which affects how efficiently compressive forces are transferred through the concrete. From trigonometric relationships, the dimensions of the nodes are calculated as shown in Figure 2-4. These are used in conducting nodal capacity checks.

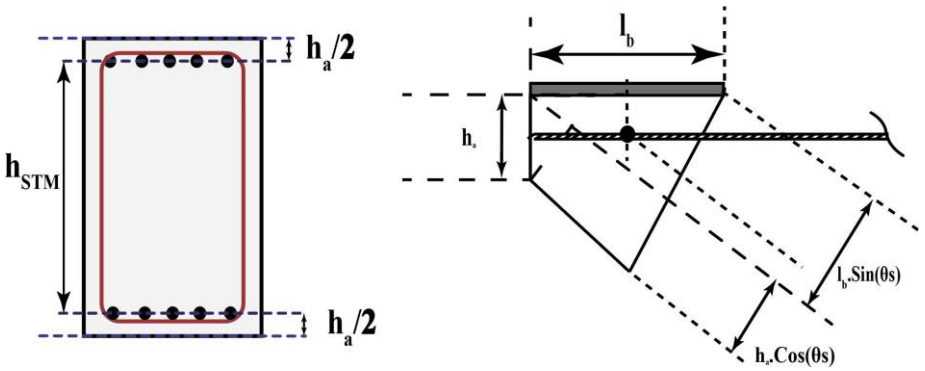

Figure 2-4: Portion of the strut-and-tie model and the depth of the centroid of a generic node.

In strut-and-tie modeling when multiple compressive struts converge at a single face of a node, such as at a bearing or support region (see Figure 2-5), it becomes necessary to determine the resultant compression force and its direction. This is particularly important in regions where more than two struts merge, as the concrete must be able to sustain the combined effect of these forces.

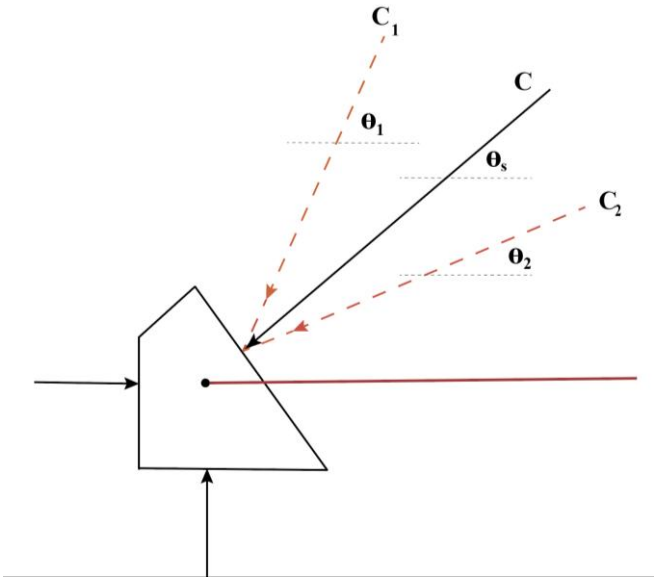

Figure 2-5: Resultant compression force (C) formed by two struts (C_1 and C_2) acting at angles θ_1 and θ_2. The direction θ_s is based on vector summation.

Figure 2-5 illustrates the procedure used to calculate the resultant compression force (C) and its angle (θ_s) when two compressive forces (C_1 and C_2) act at angles θ_1 and θ_2, respectively, relative to the horizontal. Each individual compression force is first resolved into its horizontal and vertical components using basic trigonometric relationships. The total horizontal and vertical components of the resultant force C are found by summing the corresponding components of C_1 and C_2. The magnitude of the resultant compression force is then calculated and the angle of the resultant force, denoted θ_s, is determined.

This method aligns with the approach described in the AASHTO LRFD Bridge Design Specifications Commentary, where a general situation involving non-symmetric struts is simplified by resolving forces into resultants on each side of the node, see C5.8.2.2-4 (AASHTO 2020). There, the load is statically divided and attributed to the center of tributary areas for each CCC node, illustrating how resultant forces help in simplifying complex nodes.

2.2 Topology of Struts and Ties

As discussed earlier, in the strut-and-tie method, the concrete carries compression (struts), and the reinforcement carries tension (ties). Figure 2-6 illustrates a typical strut-and-tie model where transverse reinforcement is in tension and diagonal struts are in compression. The figure also illustrates the "panel" (a term commonly used to describe each part of the truss model separated by vertical ties). The typology, shown in Figure 2-6(a) has three panels in the shear span, whereas Figure 2-6(b) has only one panel to carry the shear on the left of the applied load. Generally, when the number of panels increases, the compression force on the diagonal struts will reduce. However, the requirement for transverse reinforcement will increase. As shown in Figure 2-6(a), in order to carry a shear force of 57.1 kips with 3 panels, the struts have to carry a load of 80.8 kips, and transverse reinforcement has to carry 57.1 kips, whereas the same shear force is carried with just one panel where the strut carries 180.7 kips, and zero force in the vertical member, see Figure 2-6(b). Unnecessarily increasing the number of panels will result in inefficient strut-and-tie models (congested transverse reinforcement) and a model that does not agree with the flow of internal forces. Additionally, AASHTO LRFD limits the angle between any strut and tie entering the same node to be no less than 25 degrees and therefore also puts an effective limit on the number of panels within a geometry (AASHTO LRFD 5.8.2.2.).

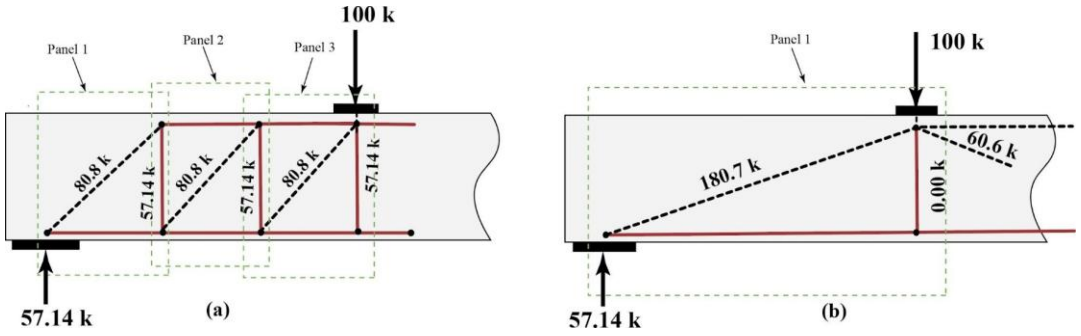

Figure 2-6: Comparison of internal strut-and-tie forces when the number of panels is increased.

2.3 Equivalent Size of Bearings

Torsion can be considerable if the superstructure spans (girders) from both sides of the bent cap are unequal or in certain loading scenarios. In these cases, a strut-and-tie model of a tributary portion of the width of the bent cap can be conducted in proportion to the corresponding bearing.

When torsion is not significant, the two bearings can be idealized as one single bearing of square shape. Figure 2-7 shows the conversion of two skewed bearings into one idealized square-shaped bearing. Figure 2-8 shows an example of the idealization of two bearings into a square-shaped bearing.

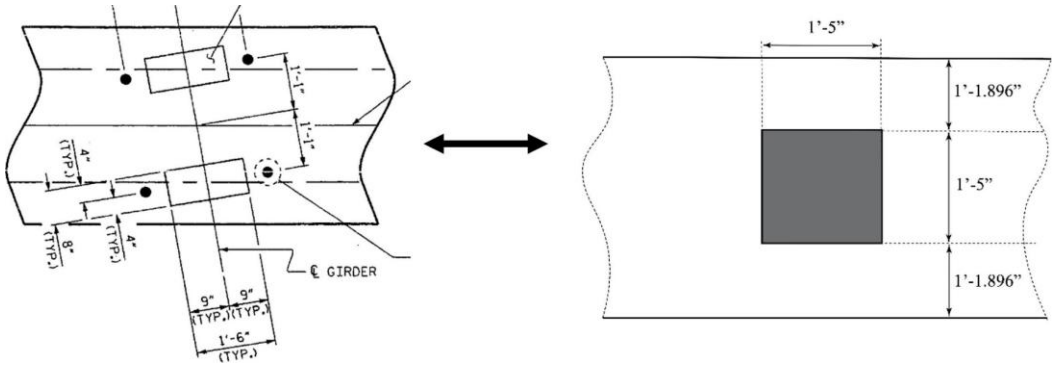

Figure 2-7: Bearings (skewed) converted to the equivalent square area (Ref: Project No. B-4499, Davidson County, Sheet No. S-5).

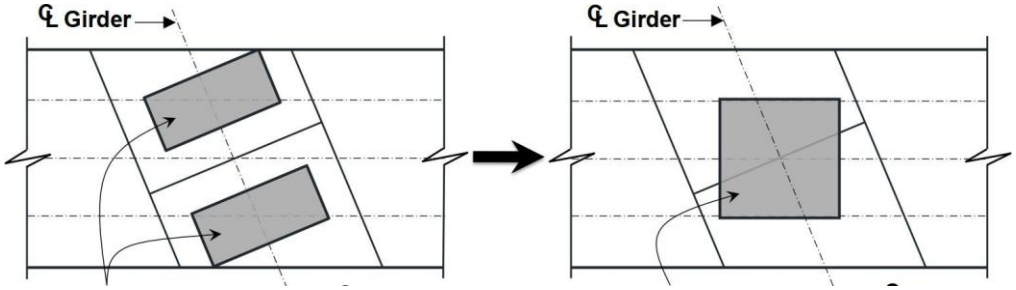

Figure 2-8: Two Bearing areas combined as a single idealized square load (Technical report FHWA/TX-12/5-5253-01-1).

2.4 Load Combinations

A load combination occurs when multiple types of loads act simultaneously on a structure. A given bent cap may be subject to numerous load combinations, and the total number of combinations to be considered is often quite large. However, not all combinations are critical for design. As discussed in Section 2.5, vehicular live loads typically introduce some of the most significant and distinct load cases. Table 3.4.1.1 of the AASHTO LRFD 9th Edition summarizes the common critical load combinations used in bridge

design. While multiple strength limit states are examined in design, the strut-and-tie method provides a method for evaluation of the bent cap ability to resist ultimate loads. The Strength I load combination is the primary load combination for evaluating the resistance of structural members under full live load conditions without wind effects. A load factor of 1.75 is applied to the live load for this load combination. It should also be noted that strut-and-tie methods require the evaluation to occur on a set of loads and reactions that are in equilibrium. Envelope values cannot be used in strut-and-tie models. When using strut-and-tie methods, each load condition should be checked and the maximum reinforcement required in any load combination should be provided.

2.5 Load Cases

One of the objectives of this research study is to develop strut-and-tie models for typical typologies of bent caps. The layout of the strut-and-tie models depends on the loading arrangements. Therefore, as a part of developing the strut-and-tie templates and typologies, vehicular pattern loading was considered in order to prepare reasonable templates and typologies. As a representative case study, a two-column bent cap supporting four traffic lanes is discussed below. This bent cap, shown in Figure 2-7 is based on a bent cap from the Davidson County - Project No. B-4499, Sheet No. S-22 structure. It was chosen due to the unique challenges it presents in typology classification, particularly its geometric asymmetry and overhangs. Following initial analyses, nine load cases were identified as possibly critical for this simplified example, they are illustrated in Figure 2-9. In general design situations software will be employed to determine the loading combinations on the structure. For example, at present, the NCDOT uses the LEAP Bridge Concrete software to consider different load cases and provides the loads which are then applied on the bent caps using the RC-Pier software.

It is important to note that in general, when using strut-and-tie templates described in this research report and study, the loads for each load case can be obtained from LEAP Bridge Concrete Reactions can then be determined using RC-Pier software or another method to carry out an elastic analysis of the bent cap beam for the specific load case. These reactions, along with the loads from LEAD Bridge software, are input into the strut-and-tie model. The reactions must be calculated separately for each load case to ensure that equilibrium is satisfied for each case. As previously described, envelope values should not be used. Appendix D describes how the STM templates can be integrated into existing bridge substructure workflows, using tools such as RC-Pier and LEAP Bridge Concrete. This approach leverages widely used tools like RC-Pier and LEAP Bridge Concrete to transition from traditional sectional design methods to STM-based templates that utilize factored loads as direct inputs.

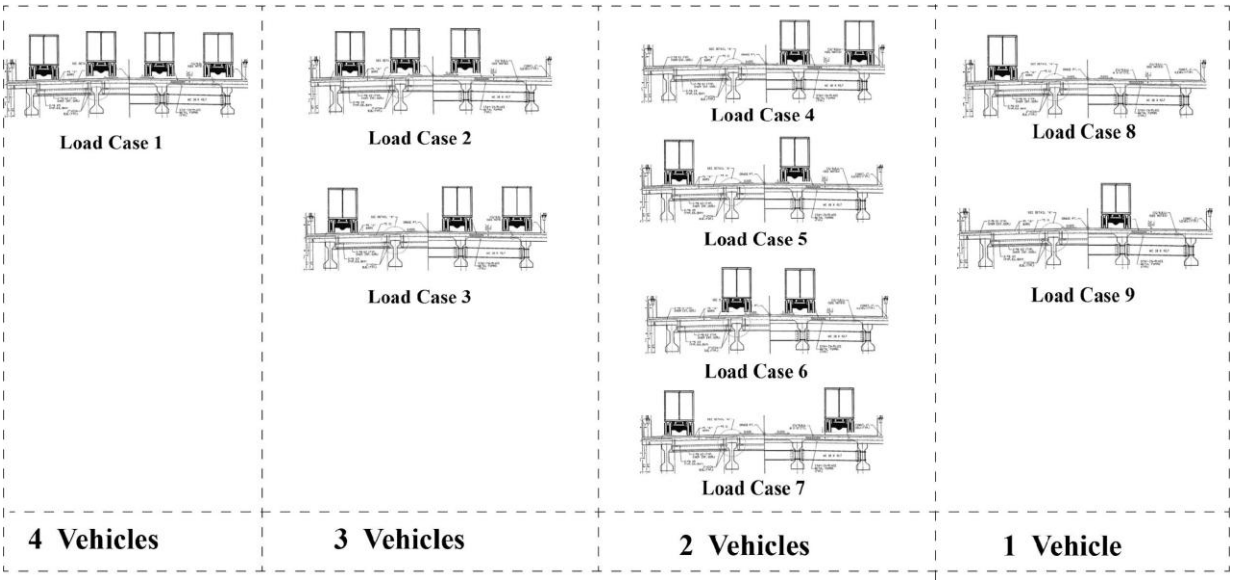

Figure 2-9: Critical load cases, considering pattern loading for two column bent cap.

2.6 Calculating Nodal Strength

Nodes are points where at least three forces intersect in a strut-and-tie model. Equilibrium must be enforced at the nodes. Nodes can be divided into 4 main categories: CCC, CCT, CTT and TTT, where C stands for compression, and T stands for tension. In the analysis of forces in the strut-and-tie model, the nodes are assumed to be pinned joints. Each node has geometry of intersecting struts and/or ties. For nodal faces in compression, if the factored force applied at any face of the node is greater than the strength at the face of the node, that implies that the strut-and-tie model cannot carry the loads. A different model needs to be attempted, the size of the loading or supporting elements needs to be modified, the member geometry needs to be revised, or the material properties need to be revised. The process of checking nodal capacity is explained in Section 3.2.7. The limiting compressive stresses (f_{cu}) at the face of the node are defined in AASHTO LRFD (AASHTO 2020), as shown in Figure (2-1) below.

$$f = m \cdot v \cdot f'_c \qquad (2\text{-}1)$$

Where:

f_{cu}= limiting compressive stress.

m = confinement modification factor.

f'_c = compressive strength used in the design.

Step 1: Calculating Confinement Modification Factor

The confinement modification factor is used to account for the vertical stress distribution, where the bearings or supports are smaller than that of the structural members. The increased strength can be assumed for all the faces of the node. When there are drops (i.e., changing of the width along the load path) in the bent caps, see Figure 2-10(a), the load distribution should be calculated as shown in Figure 2-10(b) and Figure 2-10(c).

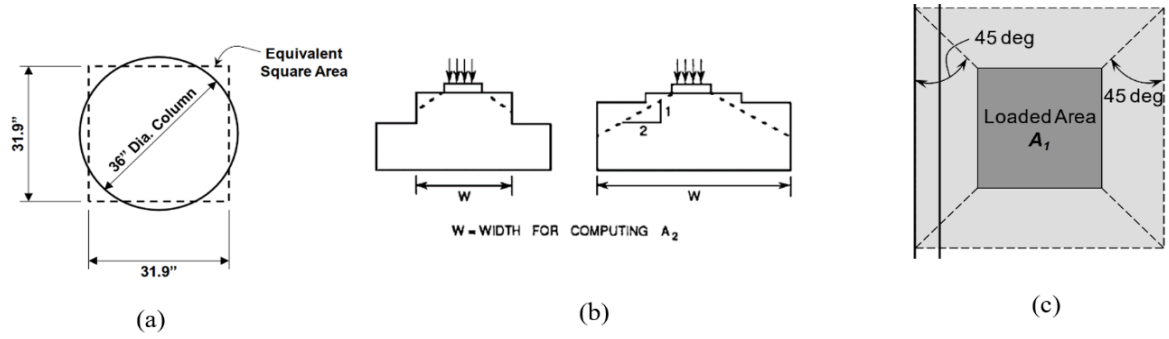

Figure 2-10: a: Equivalent square area of circular Column. b: Load distribution in stepped supports and c: Load distribution from the plan (AASHTO Fig.5.6.5.2).

Step 2: Calculating Concrete Efficiency Factor (ν)

In strut-and-tie modelling, the efficiency factor is used to take into account the lower strength of struts relative to the uniaxial strength of the concrete. When concrete compressive fields co-exist with perpendicular strain fields, the maximum compressive stress that can be achieved is lower than the uniaxial concrete strength. This is called compression softening (Vecchio and Collins, 1986). While some codes explicitly calculate this effect based on the tensile strain in the ties, in AASHTO LRFD constant limits are used based on the node type. The concrete efficiency factor (5.8.2.5.3a AASHTO) depends on the type of node and the face of the node under consideration. Figure 2-11 summarizes the concrete efficiency factor and how it varies on each face. The images are extracted from AASHTO Table 5.8.2.5.3b and Figure C5.8.2.5.3a-1.

As outlined in Article 5.8.2.6 (AASHTO LRFD), these efficiency factors are applicable only if crack control reinforcement is provided. AASHTO LRFD Article 5.8.2.6, indicates crack control reinforcement should be provided in an orthogonal grid. The minimum spacing of the reinforcement should be a minimum of (d/4 or 12 in.). The quantity of vertical and horizontal crack control reinforcement should be at least 0.30% as shown in Equation (2-2). When these minimum limits are not provided AASHTO LRFD suggests that an efficiency factor of 0.45 be used.

$$\frac{A_v}{b_w.s_v} \geq 0.003 \; and \; \frac{A_h}{b_w.s_h} \geq 0.003 \qquad (2\text{-}2)$$

Where:

A_v = Total area of vertical crack control reinforcement within spacing s_v (in^2).

b_w= Width of member's web (in).

s_v, s_h = Spacing of vertical and horizontal crack control reinforcement, respectively (in).

A_h = Total area of horizontal crack control reinforcement within spacing s_h (in^2).

	Node Type		
Face	**CCC**	**CCT**	**CTT**
Bearing Face	0.85	0.70	$0.85-\frac{f'_c}{20\ \text{ksi}}$ $0.45 \le v \le 0.65$
Back Face			
Strut-to-Node Interface	$0.85-\frac{f'_c}{20\ \text{ksi}}$ $0.45 \le v \le 0.65$	$0.85-\frac{f'_c}{20\ \text{ksi}}$ $0.45 \le v \le 0.65$	

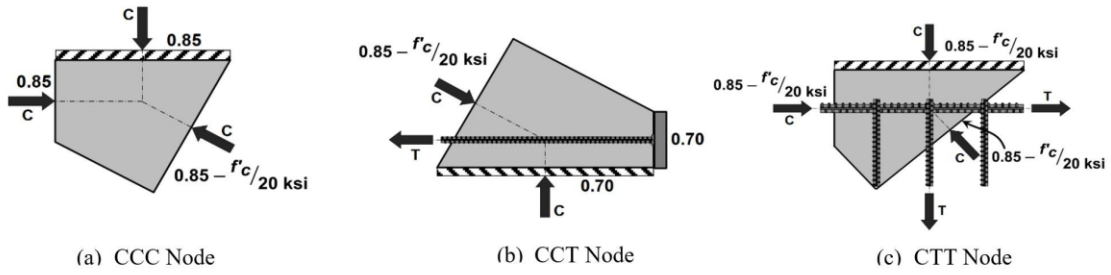

(a) CCC Node (b) CCT Node (c) CTT Node

Figure 2-11: Summary of efficiency factors in AASHTO LRFD (AASHTO,2020).

2.7 Proportioning of Ties

The proportioning of ties is addressed in Clause 5.8.2.4 of the AASHTO LRFD Bridge Design Specifications, 9th Edition. The nominal resistance of tie is taken as given in equation (*2-3*) and the factored resistance is given in equation *(2-4)*.

$$P_n = f_y . A_{st} + A_{ps.}[f_{pe} + f_y] \qquad (2\text{-}3)$$

$$P_r = \emptyset\ P_n \qquad (2\text{-}4)$$

Where:

f_y = Yield strength of non prestressed longitudinal reinforcement (ksi).

A_{st} = Total area of non-prestressed longitudinal reinforcement (in^2)

A_{ps} = Area of prestressing steel (in^2).

f_{pe} = Effective stress in prestressing steel (ksi).

ϕ = Reduction Factor

The required amount of steel reinforcement to resist the factored load is given by the Equation (2-5) below:

$$A_{st} = \frac{F_u}{\emptyset \times f_y} \qquad (2\text{-}5)$$

Where:

A_{st} = Required amount of steel (in^2)

F_u = Factored Load (ksi)

F_y = Yield Strength (ksi)

ϕ = Reduction Factor

It should be noted that AASHTO LRFD provisions apply only to components with reinforcement having a yield strength of less than 75.0 ksi and normal-weight concrete with a compressive strength below 15.0 ksi. These limits should be considered when determining the efficiency factor and inputting material strength values in design templates.

3 DEVELOPMENT OF STRUT-AND-TIE TEMPLATES FOR BRIDGE BENT CAPS IN NORTH CAROLINA

This section summarizes the development of strut-and-tie design and evaluation templates for bridge bent caps in North Carolina.

In collaboration with NCDOT personnel, typical bent cap typologies were identified. For these typical typologies identified, templates were developed to be able to carry out the design or evaluation of the bent caps using the methods consistent with the AASHTO LRFD described in the previous section.

For this study and research report, bent caps are divided into multiple typologies based on the number of columns or supporting elements. Based on drawings provided by the NCDOT (including project No. B-4499-Davidson County, project No. B-2506-Anson County, Project No. I-5700-Wake County, Project No. B-5406-Forsyth County, Project No. U-2810B-Cumberland County), the shear span to depth ratio of the bent cap shear spans are found to vary between 0.75-1.97. This indicates that the members can be considered deep beams in most cases identified. The bent caps identified in the state of North Carolina are typically rectangular in shape.

This section presents the design of a two-column bent cap to familiarize the readers with the implementation of the strut-and-tie modeling procedure and to demonstrate the information and data workflow needed for strut-and-tie design or evaluation. Columns with more than two columns are encountered routinely and the general guidance provided here can also be extended to the other scenarios. Additional templates with multiple columns or supporting elements are also shown. This section provides a complete example of a two-column bent cap considering several possible load cases and step-by-step calculations for nodal geometries. Additional and related information can also be found in Appendix B and Appendix C.

3.1 Introduction to the STM Templates

Figure 3-1 illustrates a typical strut-and-tie model where dashed lines represent compression struts and solid lines represent tension ties. When the overall geometry of a particular strut-and-tie model, loading conditions and support conditions are similar, a template can be developed to model the structure. That is, when bent cap geometries and loading arrangements are sufficiently similar, a single model template can be developed.

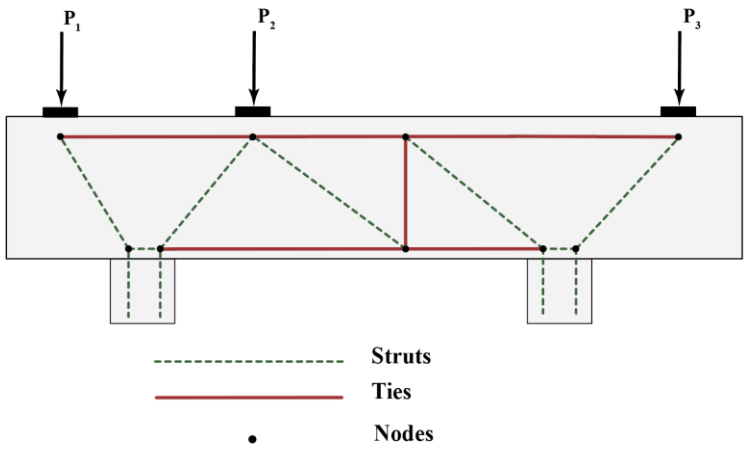

Figure 3-1: Strut-and-tie model of a beam.

The templates developed for this study are developed in Excel spreadsheets. However, it is expected that it will be more appropriate for simple computer programs to be developed through the internal NCDOT implementation process for use in their calculations. To use the templates, the first step involves selecting the appropriate strut-and-tie typology from a set based on specific loading and supporting conditions. Namely, the number of applied loads to the bent cap and the number of supporting elements. Key parameters, including structural dimensions, material strengths, support dimensions, bearing dimensions, and magnitude of the factored loads, are then input into the template. The method of joints is used to solve the forces in the selected typology. For indeterminate structures, the known reactions from elastic analyses are used to solve the system of equations and are the assumed distribution of the loads for the strut-and-tie model. Once the forces in the struts and ties are determined, the ability for the structure to transmit the applied loads is assessed by conducting nodal checks for each node in accordance with the AASHTO LRFD provisions. Finally, the reinforcement required for the tension ties is proportioned. The templates then determine the required longitudinal and transverse reinforcement.

Through collaborations with the NCDOT personnel, 12 bent cap typologies were identified as common in North Carolina and appropriate for the development of templates. Table 3-1 summarizes the templates developed as a part of this study. Figure 3-8, Figure 3-9 and Figure 3-10 illustrate representative examples of the nomenclature used to categorize various loading and support configurations: namely, “10 Loads Symmetric”, “10 Loads Asymmetric 1”, and “10 Loads Asymmetric 2”, respectively.

The designation “10 Loads Symmetric” refers to a structural configuration comprising three columns, ten vertically applied loads, and a strut arrangement that is symmetric with respect to the midspan of the beam. In contrast, “10 Loads Asymmetric 1” and “10 Loads Asymmetric 2” represent configurations that also contain ten loads and three columns, but feature strut layouts that are asymmetric. These asymmetric strut-and-tie models are needed in scenarios when the loading is not symmetric. It is important to note that the asymmetric strut-and-tie models can be reflected or mirrored about the beam’s centerline to represent load asymmetries occurring from the opposite side. This allows the same model to be used for different asymmetric loading conditions without creating entirely new configurations.

The naming convention is designed to convey information regarding the number of applied loads, the presence or absence of symmetry in the structural layout, and the number of columns or supporting elements used.

All of the typologies summarized in Table 3-1 are illustrated in Figure 3-2 through Figure 3-13. These figures provide a visual reference for the various structural templates considered in this study, allowing for identification and comparison based on the established naming scheme.

It should be noted that in some cases models with additional panels between bearing or supports may be desired. In these cases, additional templates can be developed or templates with an artificially higher number of bearings or supports can be used with the bearing or support load set to zero. This will effectively provide a model with additional panels between the actual bearings, if such a model is needed. Alternatively additional models can be developed and deployed using the same principles, as needed. Some zero force elements are included for numerical stability.

Table 3-1: Summary of templates developed as a part of this study.

Template #	Number of Columns or Supporting Elements	Template Name and Description
1	2	4 Loads Symmetric/Asymmetric
2	2	5 Loads Symmetric
3	2	5 Loads Asymmetric 2
4	3	4 Loads Symmetric/Asymmetric
5	3	6 Loads Asymmetric 1
6	3	6 Loads Asymmetric 2
7	3	10 Loads Symmetric
8	3	10 Loads Asymmetric 1
9	3	10 Loads Asymmetric 2
10	4	5 Loads Symmetric/Asymmetric
11	4	8 Loads Asymmetric 1
12	4	8 Loads Asymmetric 2

The design flowchart presented in Figure 3-14 outlines the step-by-step procedure that could be used for incorporating the strut-and-tie templates into the bent cap design process currently used by the North Carolina Department of Transportation (NCDOT). This flowchart illustrates how the template-based methodology generally fits within the broader design workflow. It also should be noted that the templates can be used to evaluate existing designs conducted by others or in evaluating the safety of existing structures. Appendix D contains more information on the STM in the context of NCDOT workflows.

The process shown in Figure 3-14 begins with the calculation of factored loads, typically performed using RC-Pier software, followed by the determination of preliminary bent cap dimensions. Then, an appropriate template is selected from a predefined set of configurations based on the number of supports, the nature of the applied loads, and the strut-and-tie arrangement. The loads, geometric conditions, material properties, including the concrete compressive strength and the yield stress of reinforcing steel, and other details are input into the appropriate template.

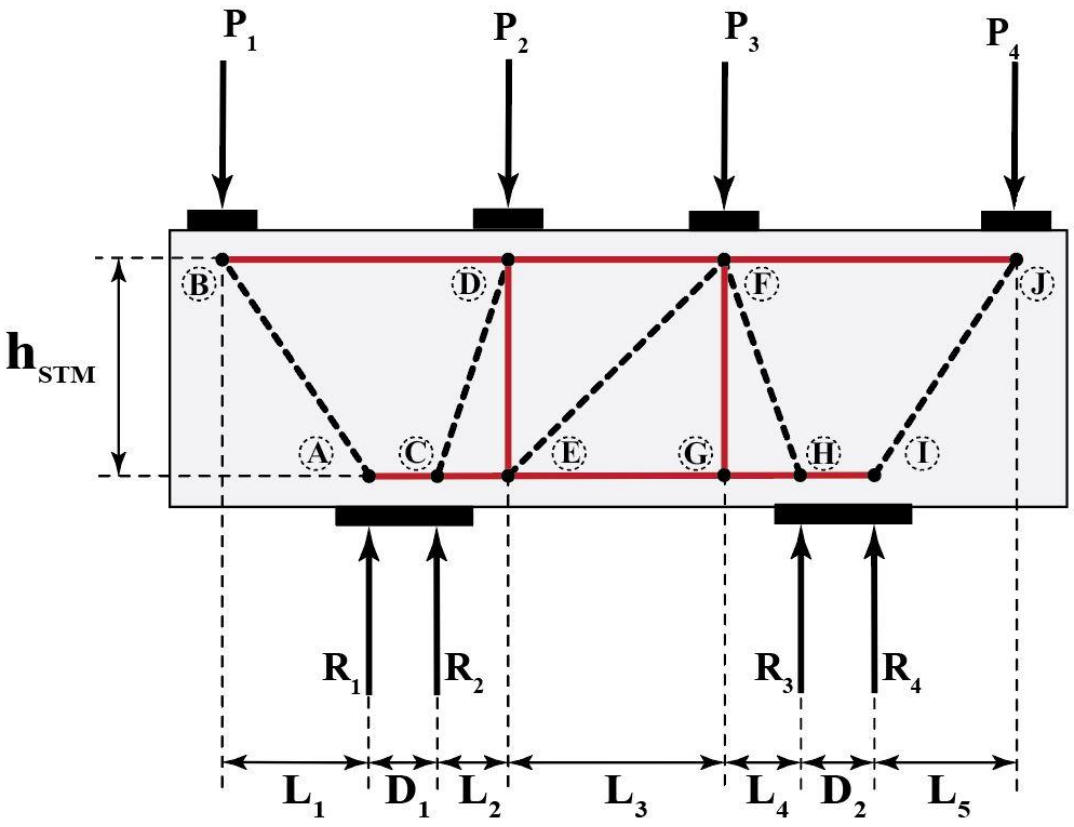

Figure 3-2: Two column bent cap - 4 loads asymmetric.

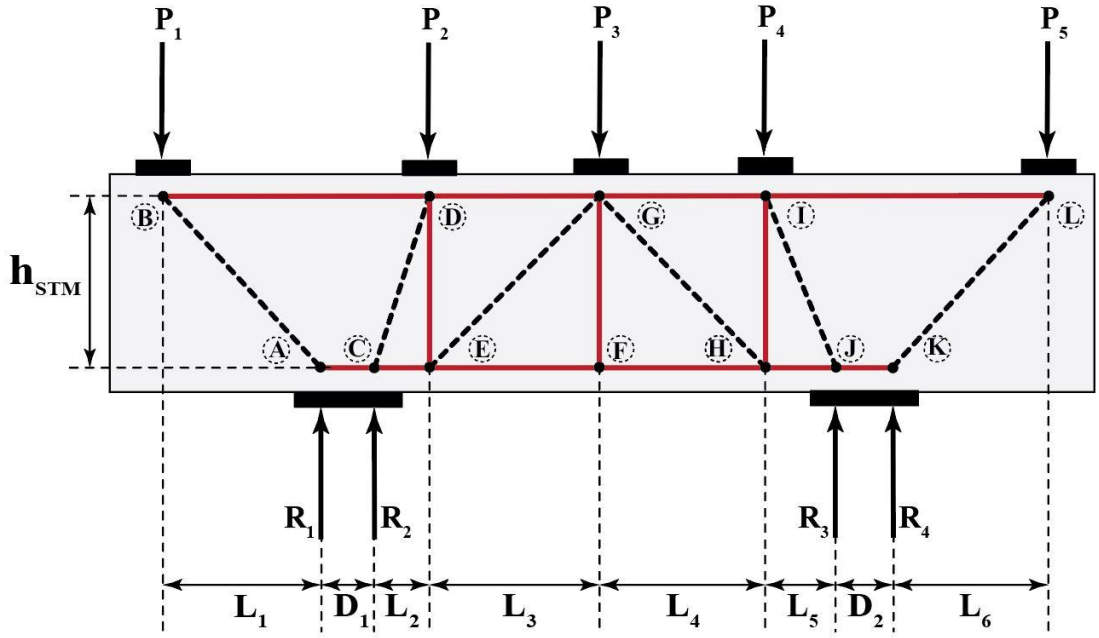

Figure 3-3: Two column bent cap - 5 loads symmetric.

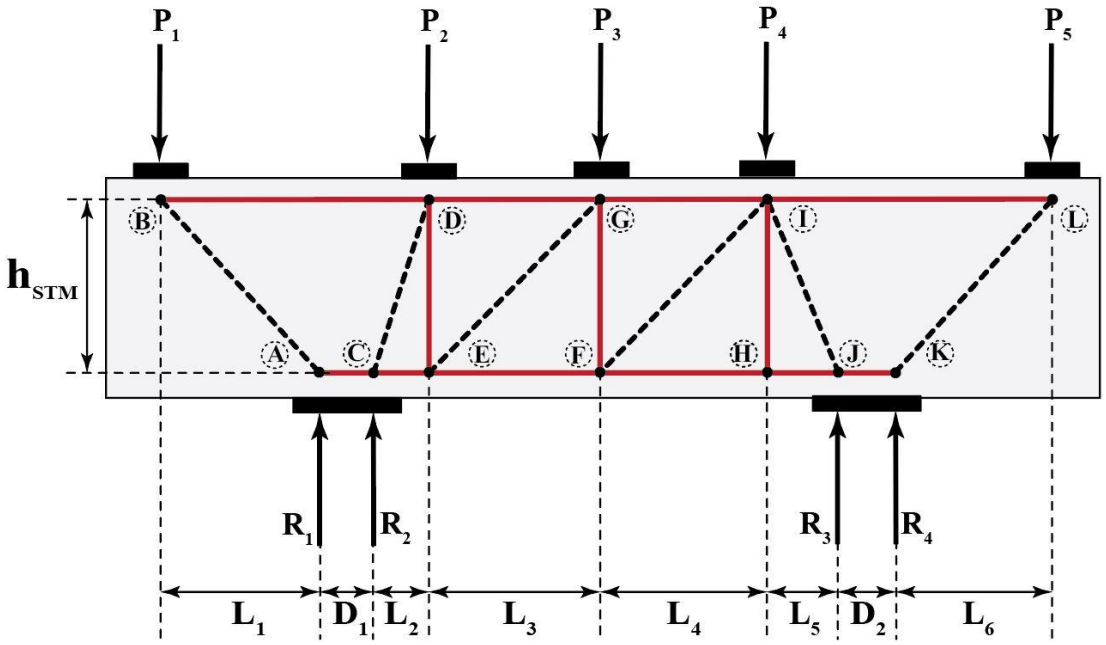

Figure 3-4: Two column bent cap - 5 loads asymmetric 2.

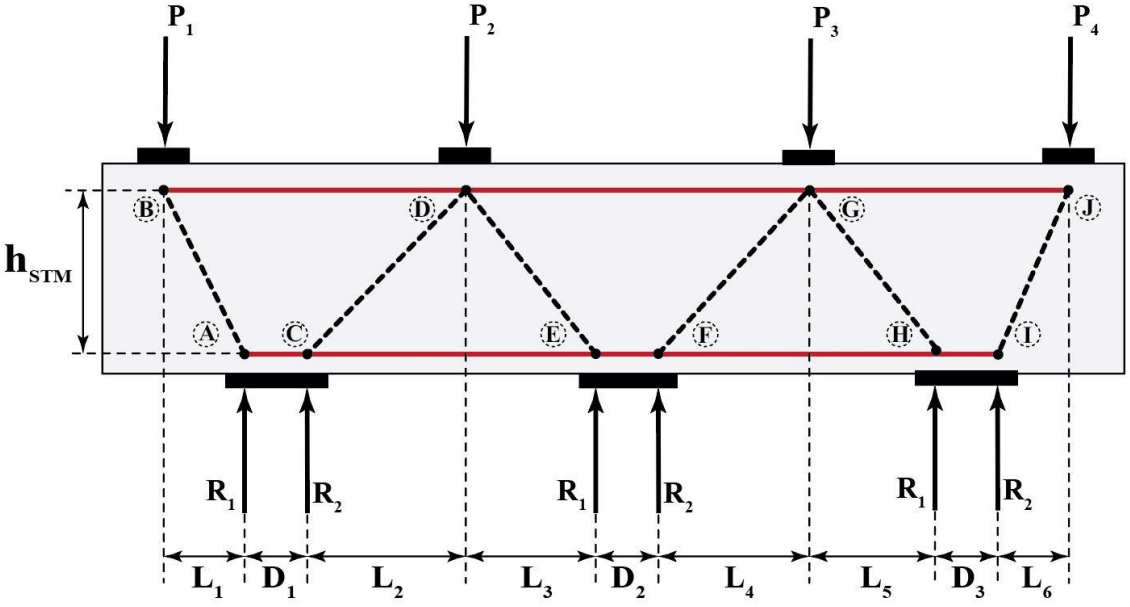

Figure 3-5: Three column bent cap - 4 loads symmetric/asymmetric.

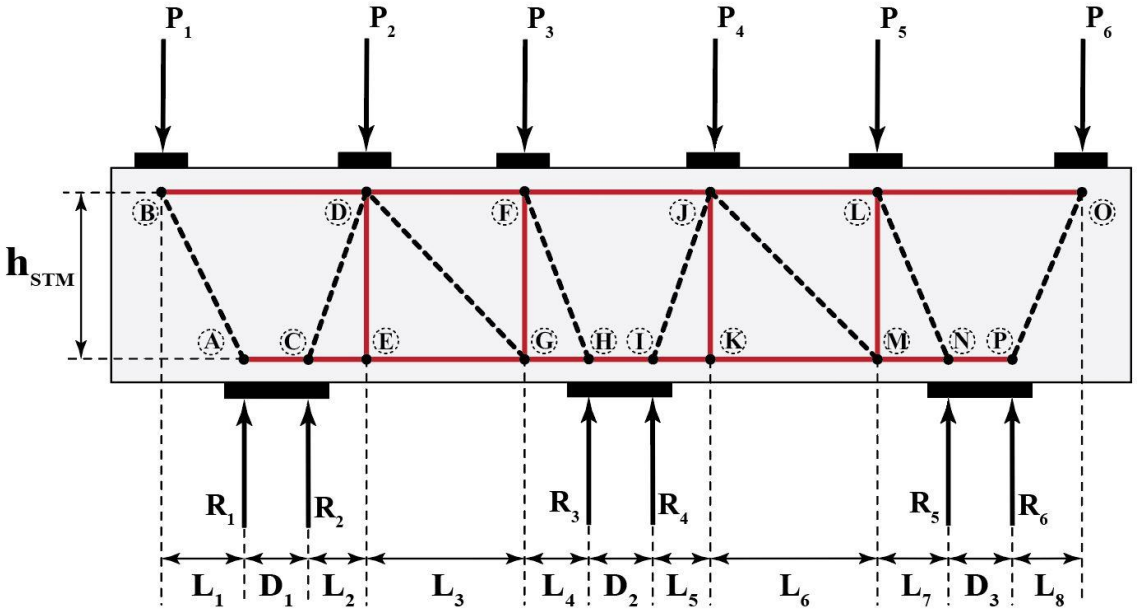

Figure 3-6: Three column bent cap - 6 loads asymmetric 1.

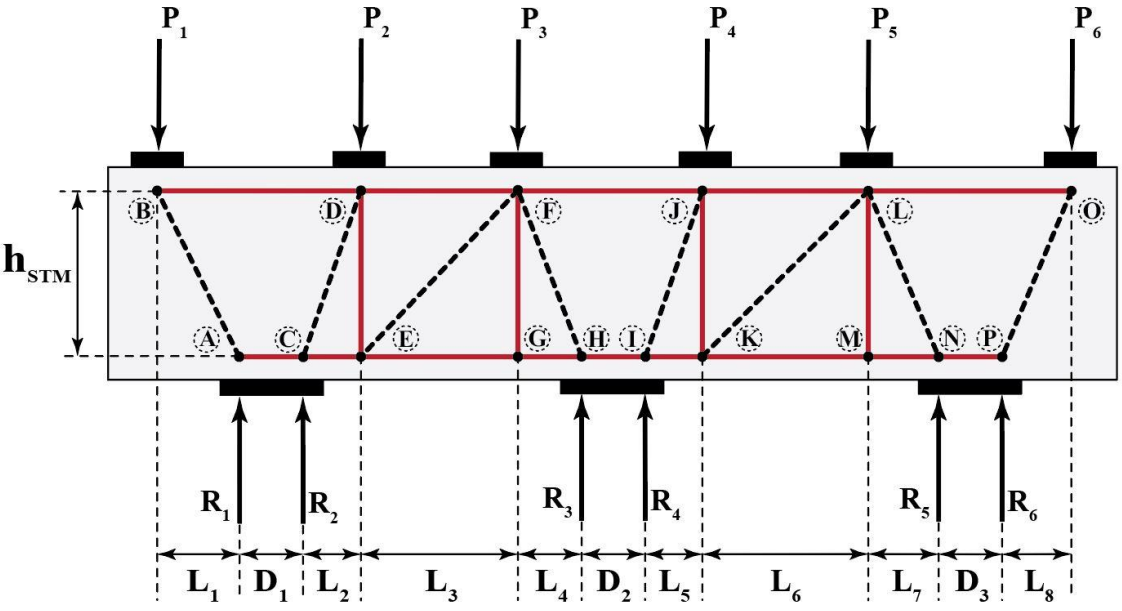

Figure 3-7: Three column bent cap - 6 loads asymmetric 2.

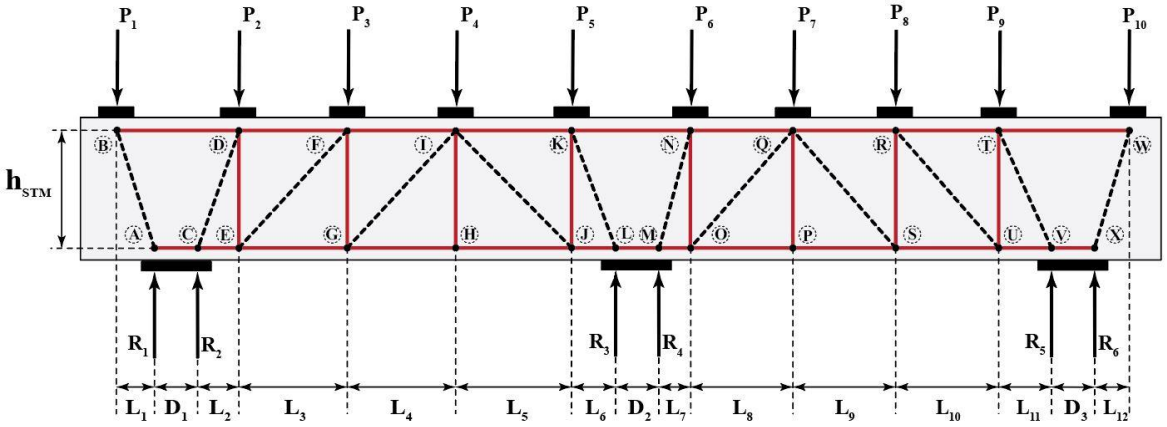

Figure 3-8: Three column bent cap - 10 loads symmetric.

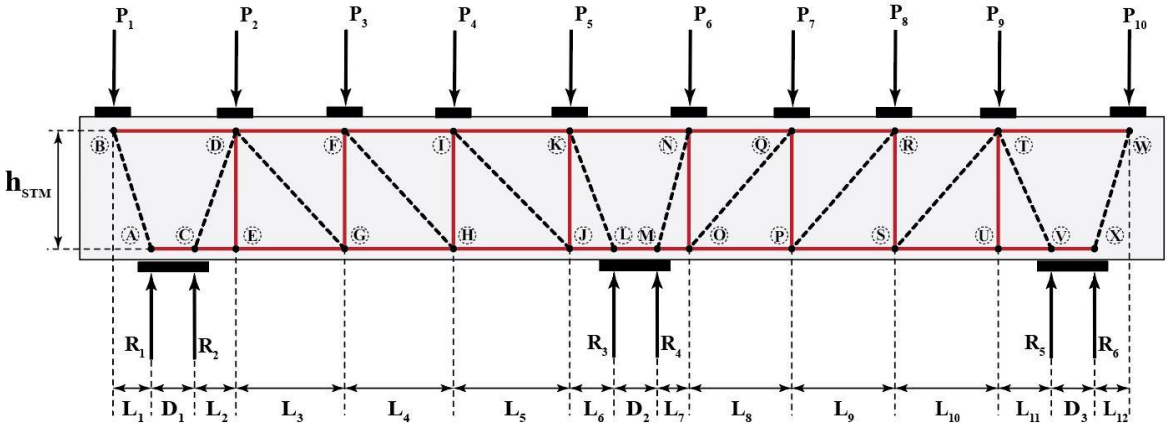

Figure 3-9: Three column bent cap - 10 loads asymmetric 1.

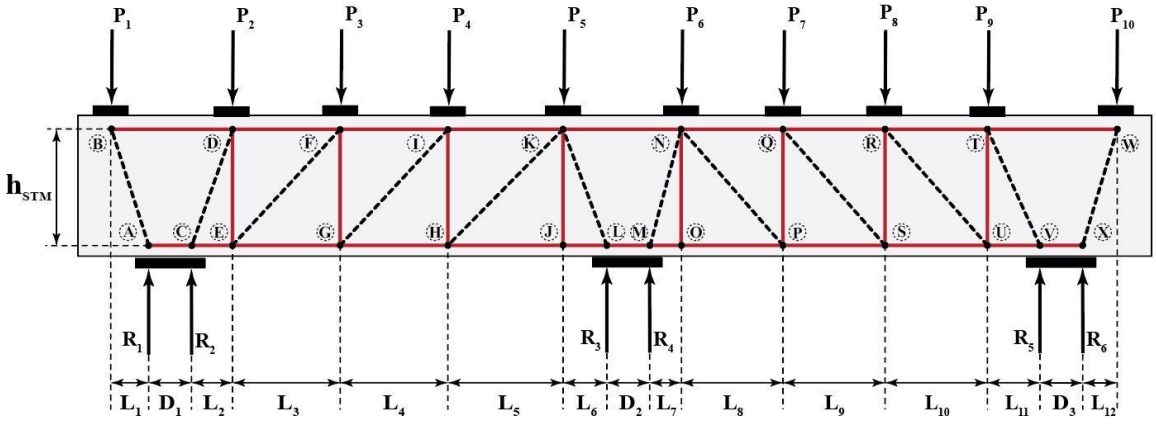

Figure 3-10: Three column bent cap - 10 loads asymmetric 2.

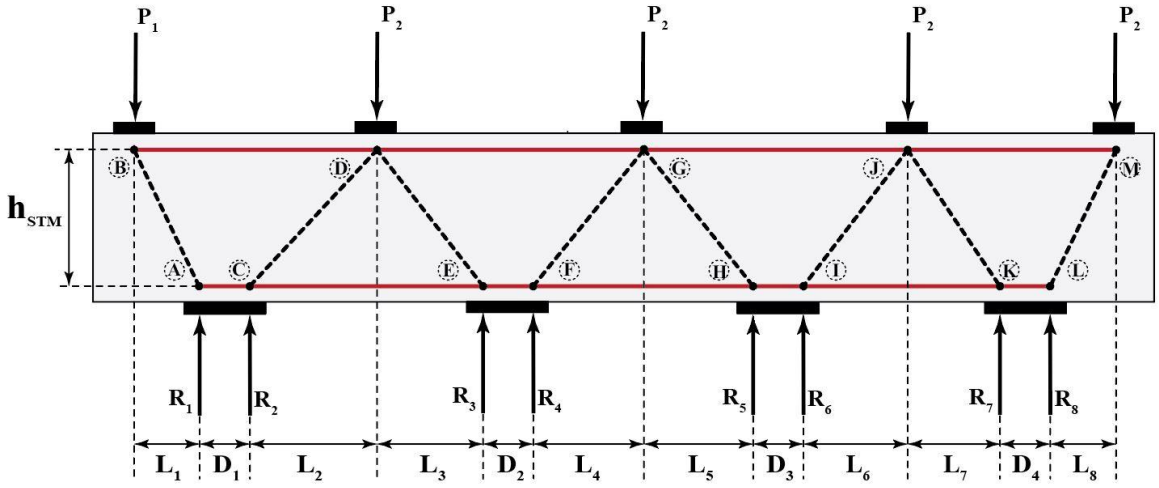

Figure 3-11: Four column bent cap - 5 loads symmetric/asymmetric.

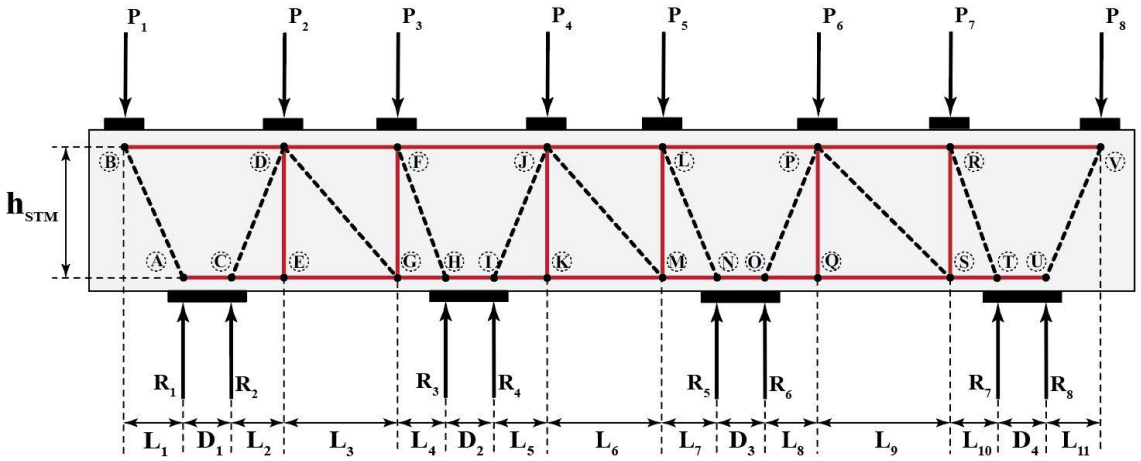

Figure 3-12: Four column bent cap - 8 loads asymmetric 1.

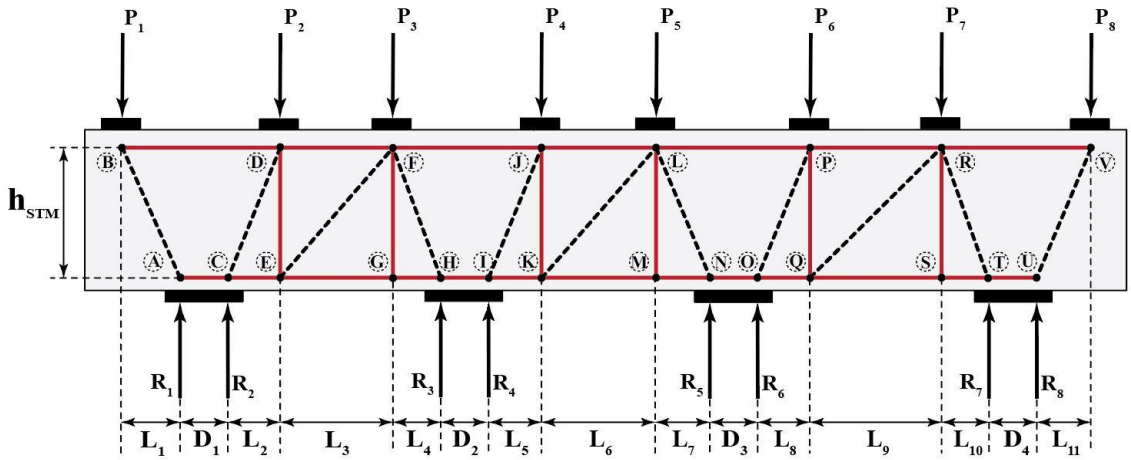

Figure 3-13: Four column bent cap - 8 loads asymmetric 2.

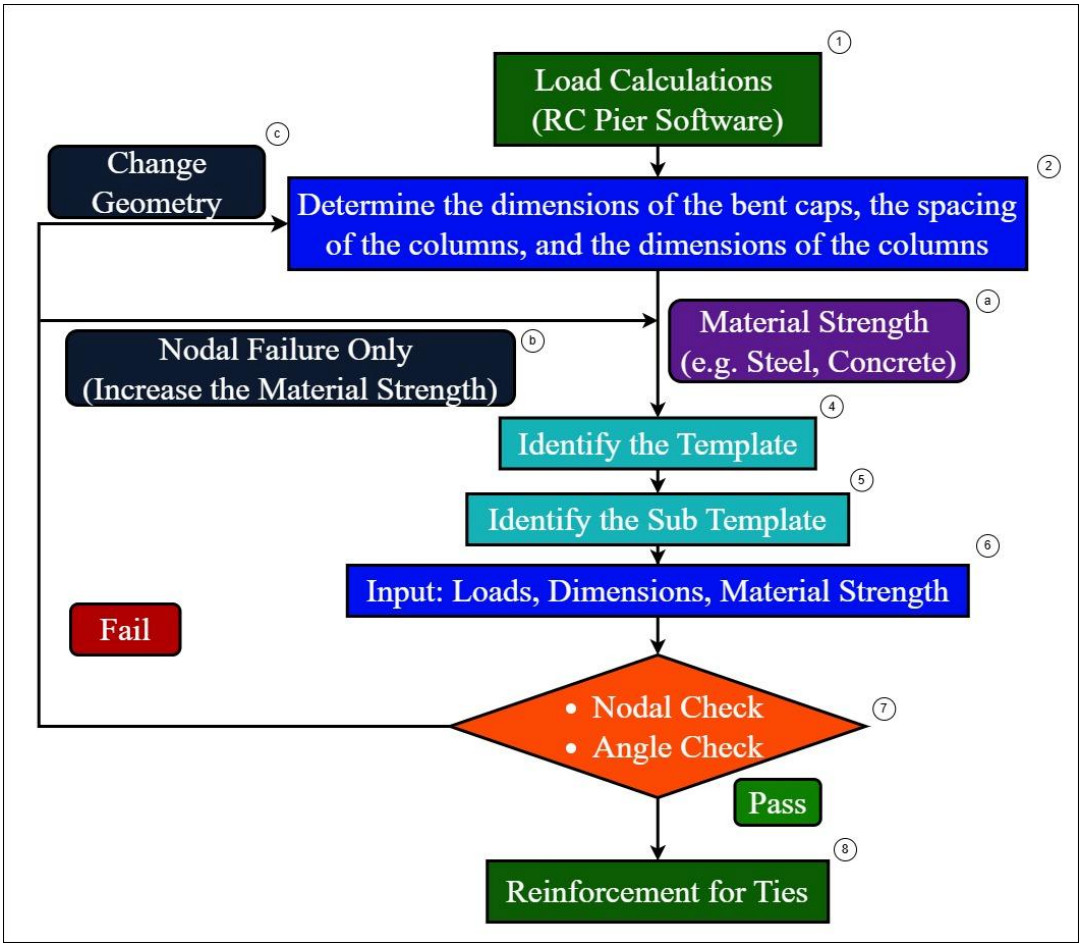

Figure 3-14: Information and design workflow for use with strut-and-tie templates.

Once the information in the specific template is populated, the template uses the provided information to conduct an analysis of the truss forces, checks on the nodal strengths and provides the quantity of tie reinforcement needed. These checks are consistent with the AASHTO LRFD specifications for strut-and-tie procedures. These include nodal strength checks to confirm that all strut-and-node regions possess adequate capacity, as well as angle checks to verify that the orientation of compression struts satisfies the minimum geometric requirements indicated in AASHTO LRFD. Based on the input information provided the quantity of reinforcement is proportioned.

The flowchart shown in Figure 3-14 also provides guidance on how to proceed in cases where a particular check is not satisfied, such as revising the geometry, altering the reinforcement layout, or selecting a different template. Overall, the flowchart serves as both a procedural guide and a decision-making framework that supports iterative refinement in scenarios that are initially not satisfactory.

It also should be noted that other templates can be developed based on the templates already provided. That is, the fundamental application of the STM will remain the same and only the solving of the strut-and-tie model truss will change. Therefore, as the implementation of these methods occurs, it is expected that other typologies can be extrapolated from the set of 12 introduced as a part of this study. It is also expected that the 12 templates presented in his study represent a large range of different geometric scenarios that can

arise in general and thus provide a wide breadth of examples that can be used as a starting point for other designs. It should also be noted that in some cases loads of zero can be applied to accommodate similar loading arrangements and therefore use the templates provided for similar but not identical scenarios.

Section 3.2 provides a detailed example of the template development for a two-column bent cap. This example is representative of the development of the templates in this study.

3.2 Example Template Development for A Two-Column Bent Cap

The strut-and-tie design process is demonstrated for a two-column skew bent cap which was identified in Project No. B-4499 in Davidson County (see Figure 3-15). The shear span to depth ratio of the bent cap is 1.97. The bent cap configuration can be idealized as 4-point loads (from 4 pairs of girders being supported) with two supports (columns). The following subsections describe the assumptions and steps used in the development of the associated template, it should be noted that to use the template directly is more straightforward than its development. The assumed loads for this example are simplified from what would otherwise come from a complete structural analysis of the super and substructure and is described in Section 3.2.3. The proportioning of tie reinforcement and nodal strength checks are discussed. Section 3.3 then provides a summary of using the templates once developed with example values.

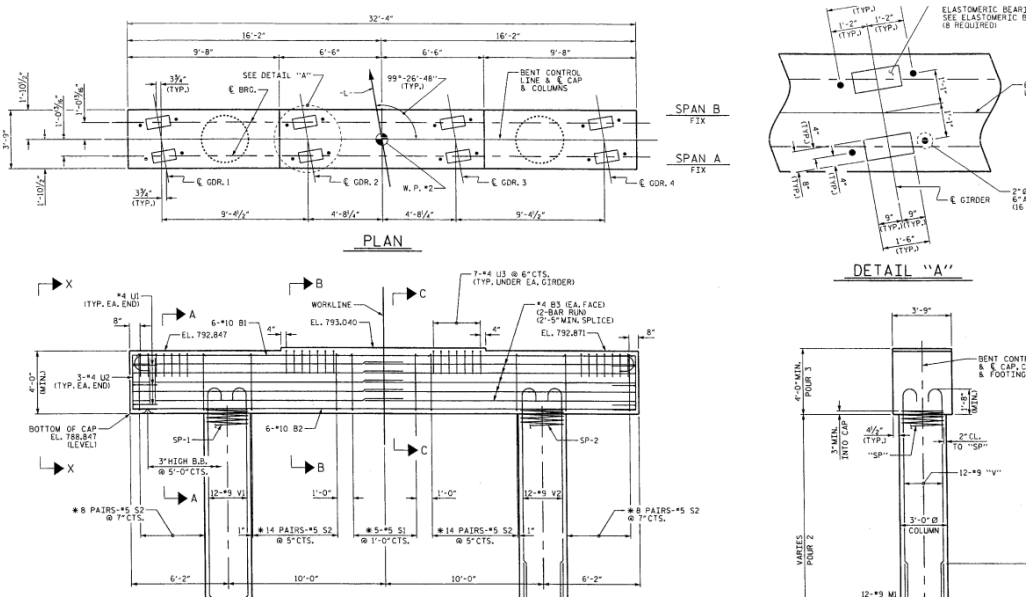

Figure 3-15: Plan and elevation of two-column skew bent cap and section (Ref: Project No. B-4499, Davidson County, Sheet No. S-22).

3.2.1 Equivalent Length of Bearings

When bearings or supporting elements are not rectangular in shape, an equivalent rectangular area should be used. For example, since the columns are often circular in shape, the circular shape should be converted

into an equivalent rectangular shape in order to simplify the calculations. This approach is adapted from the methodology presented in the Strut-and-Tie Model Design Examples for Bridge Structures (Frosch et al., 2012). Figure 3-16 shows how a circular cross-section is converted into an equivalent square shape. This is conducted on an equivalent area basis. For example, if the diameter of the column considered is 3 ft (36 in), the equivalent dimension of the square is 31.9 in.

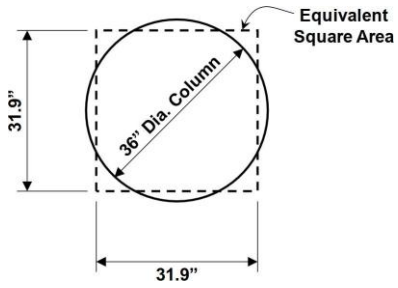

Figure 3-16: Equivalent square cross section for columns.

3.2.2 Strut-And-Tie Model Typology Selection

Two-column bent caps can have a higher number possible strut-and-tie model configurations compared to other members because the geometry allows for different arrangements of struts-and-ties to fit in the shear span space. Additionally, different load combinations can significantly change the typology of the strut-and-tie model. This is not always the case and in scenarios where there are many supported girders and supports, the number of possible typologies may actually decrease since there is less space and freedom to change the typology layout. The two-bent-column typology considered is shown in

Figure 3-17. The tie EJ is a zero-force member under the applied loading, as determined by the equilibrium of the strut-and-tie model. However, in practice, reinforcement is typically provided along this tie due to symmetry considerations and to satisfy the minimum transverse reinforcement requirements specified by design codes.

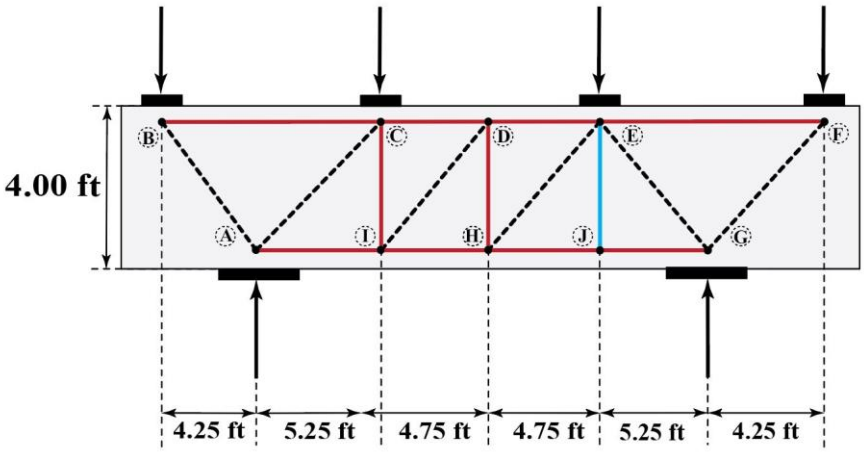

Figure 3-17: The typology considered for Two-Column Skew Bent Cap and Section (Ref: Project No. B-4499, Davidson County, Sheet No. S-22).

3.2.3 Load Cases Considered for The Typology Selected

The strut-and-tie design process is demonstrated for a two-column skew bent cap from Project No. B-4499 in Davidson County. For demonstration purposes, a dead load of 200 kips and live loads totaling 400 kips were assumed. Based on these loads, nine load cases were generated as discussed in section 2.5. The load cases were analyzed following the methodology outlined in Section 3.2.4 and the analysis results are summarized in section 3.2.5. The Figure 3-18 illustrates the pattern loading of the live loads considered.

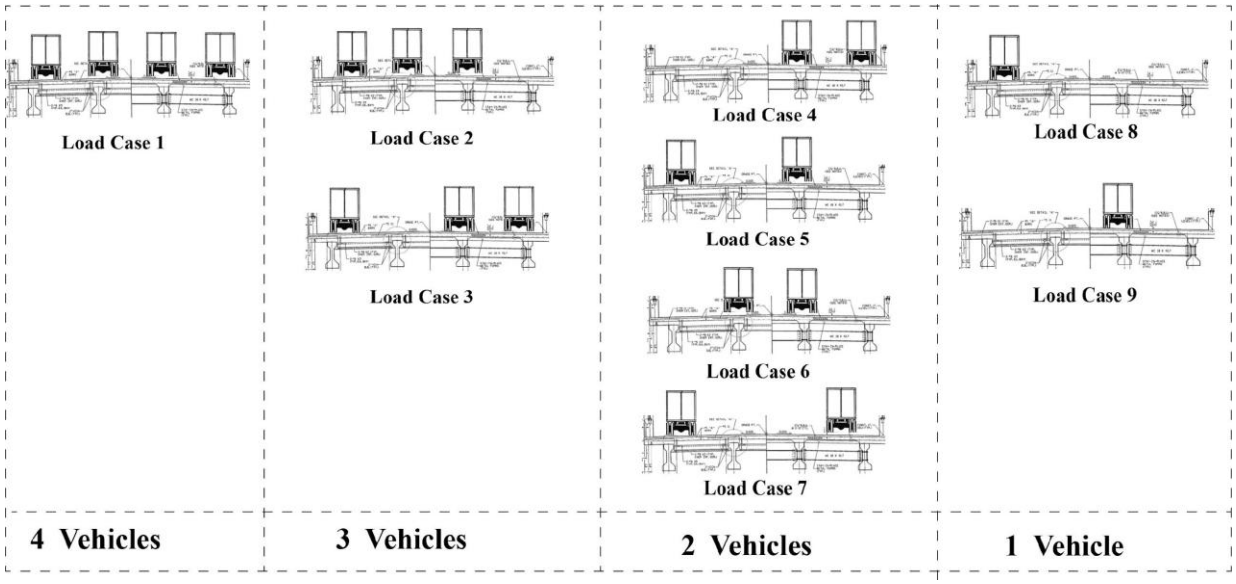

Figure 3-18: Critical load cases, considering pattern loading for two column bent cap.

3.2.4 Matrix-Based Solution of the Strut-and-Tie Model

To solve the truss that makes up the strut-and-tie model generated by the template a matrix-based approach is adopted using the method of joints. Each node has two degrees of freedom, one in the horizontal direction and one in the vertical direction. This results in a global equilibrium matrix of size 2n×2n, where n is the total number of nodes. The system is often statically indeterminate. To address this, the template prompts the user to provide appropriate reaction forces to make the system determinate. These reactions can be obtained from a beam (stick) model or from any other elastic analysis of the bent cap under the specific load case being considered. Once the system is determinate, the internal forces in the struts and ties are calculated by solving the global system of equations. Individual load cases need to be provided that each satisfy equilibrium, rather than envelope values.

A typical approach to solve indeterminate trusses, is using stiffness method, however this requires assumptions regarding the structural stiffness of compression and tension members. It has been shown that using the stiffness method to solve for indeterminate strut-and-tie truss models is not generally appropriate. This study does not recommend that approach.

Theoretically, for indeterminate structures designed with strut-and-tie, since a lower bound approach is assumed, any load distribution that satisfies equilibrium can be used. Since the NCDOT uses a linear elastic software to determine the distribution of loads in the bent caps and supporting elements, this is the load distribution assumed for the templates discussed and is the procedure recommended as a part of this study. That is, for determinate and indeterminate structures, the distribution of forces determined from elastic analysis should be used, including moments in the supporting element. Since the assumed load path often includes the moments transferred to columns, they should be included in the strut-and-tie model to ensure consistent load path assumptions. These moments from the linear analysis are also used.

It should be noted that a significant part of the template development is in developing and checking the equations to solve for the internal forces in the truss elements. As the NCDOT develops its own templates and procedures, this could be accomplished with typical structural engineering software or a computer program. It should be emphasized that the solution should not rely on the stiffness of the truss elements and the use of the reactions from the elastic analysis should be used to effectively make the internal truss statically determinate. If this procedure is conducted in this manner the development of strut-and-tie models becomes a rapid exercise, after which the nodal checks and proportioning of tie reinforcement would be conducted as outlined for all other nodes in the existing templates and specified in AASHTO LRFD.

3.2.5 Summary of Forces for the 9 Load Cases Considered for Example

As discussed in Section 3.2 a two-column bent cap with four lanes (Ref: Project No. B-4499, Davidson County, Sheet No. S-22) was considered for the case study. After initial analysis, 9 load cases were considered of importance for this analysis and example. The strut-and-tie model was analyzed for all nine cases and summarized below in Figure 3-19.

	Element Forces	Load Case_1	Load Case_2	Load Case_3	Load Case_4	Load Case_5	Load Case_6	Load Case_7	Load Case_8	Load Case_9	Dead Load Only	Tension	Compression
	A_B	-786	-867	-854	-577	-856	-588	-848	-852	-580	-553	Compression Only	-867
	B_C	507	626	606	415	611	430	600	605	419	382	626	Tension Only
	C_D	-173	-211	-2.36	-130	-34.0	-343	54	16	-166	-115	54	-343
	D_E	-173	-258	-70.6	-144	-144	-343	54	-31	-229	-115	54	-343
	E_F	507	427	606	621	425	430	600	410	426	381	621	Tension Only
	F_G	-786	-585	-853	-864	-584	-588	-848	-575	-585	-552	Compression Only	-882
	G_H	174	305	138	160	254	343	-53	78	292	116	343	-53
	H_I	174	258	70	145	145	343	-53	31.2	229	116	343	-53
	A_I	174	212	236	130	340	343	343	343	343	116	343	-343
	A_C	-907	-1050	-756	-682	-804	-980	-674	-731	-736	-627	Compression Only	-1050
	C_I	0	34	50	12	80	0	0	34	46	0	80	Tension Only
	D_I	0	-58	-84	-19.5	-135	0	0	-58	-77.6	0	Compression Only	-135
	D_H	0	42	50	12	80	0	0	34	46	0	80	Tension Only
	E_H	0	-58	-84	-19.5	-135	0	0	-58	-77.6	0	Compression Only	-135
	E_G	-907	-925	-926	-978	-854	-979	-674	-610	-907	-627	Compression Only	-979

	Tension Only
	Compression Only
	Tension and Compression

Figure 3-19: Summary of element forces for all 9 load cases.

3.2.6 Proportioning of Longitudinal Ties

While it is possible to adjust the longitudinal reinforcement based on the changes in forces along each tension tie, it is also possible to simply maintain a consistent reinforcement area throughout the length of the member. Figure 3-20 illustrates the design tension forces acting on both the top and bottom chords, as well as the transverse tie forces. As previously discussed, it is assumed that the centroid of the compression chord coincides with the centroid of the tension ties for the top and bottom chords in scenarios over supports where the chord force changes from tension to compression. This simplifying assumption ensures complex redirection of the compression struts and ties is not needed. More complex models could be developed if needed by the designer. It also should be noted that one approach to increasing the strength of the model limited by nodal strength, particularly when one or more faces are insufficient to withstand the compression forces, is to increase the depth of the reinforcement centroid. By doing so, the depth of the nodes is increased, thereby improving their capacity to carry the compression forces.

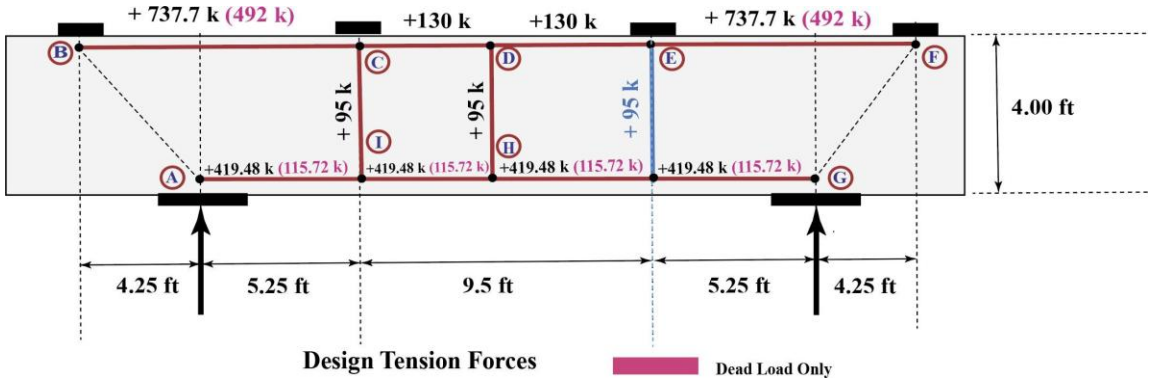

Figure 3-20: Design tension forces.

The transverse reinforcement ties represent the centroid of the reinforcement within the panel under consideration. The total reinforcement area provided is then distributed throughout the panel, ensuring the appropriate amount of reinforcement and spacing while adhering to the minimum reinforcement requirements. See AASHTO LRFD (AASHTO 2020).

The nominal resistance of tie is discussed in clause 5.8.24 AASHTO LFRD (9th edition) as shown in Equation (*3-1*).

$$P_n = f_y \cdot A_{st} + A_{ps}[f_{pe} + f_y] \tag{3-1}$$

The required amount of steel reinforcement to resist the factored load is given by the Equation (*3-2*) below:

$$A_{st} = \frac{F_u}{\emptyset \cdot f_y} \tag{3-2}$$

Where:

A_{st} = Required amount of steel (in^2)

F_u = Factored Load (ksi)

F_y = Yield Strength (ksi)

ϕ = Reduction Factor

Figure 3-21 provides a summary of the quantity of reinforcement provided in the example being considered. These minimum quantities of reinforcement to resist the applied loads, for the given strut-and-tie model should then be appropriately provided, placed and detailed.

Element Forces	Tension(kips)	ϕfy	Reinforcement Required (in^2)	Dead Load Only (kips)	Dead Load only and f_s = 22 ksi
A_B	Compression Only	54	0.00	Compression	0.00
B_C	626.0	54	11.59	382.0	19.29
C_D	54.0	54	1.00	Compression	0.00
D_E	54.0	54	1.00	Compression	0.00
E_F	621.0	54	11.50	381.0	19.24
F_G	Compression Only	54	0.00	Compression	0.00
G_H	343	54	6.35	116.0	5.86
H_I	343	54	6.35	116.0	5.86
A_I	343	54	6.35	116.0	5.86
A_C	Compression Only	54	0.00	Compression	0.00
C_I	80.00	54	1.48	0.00	0.00
D_I	Compression Only	54	0.00	Compression	0.00
D_H	80.00	54	1.48	Compression	0.00
E_H	Compression Only	54	0.00	Compression	0.00
E_G	Compression Only	54	0.00	Compression	0.00

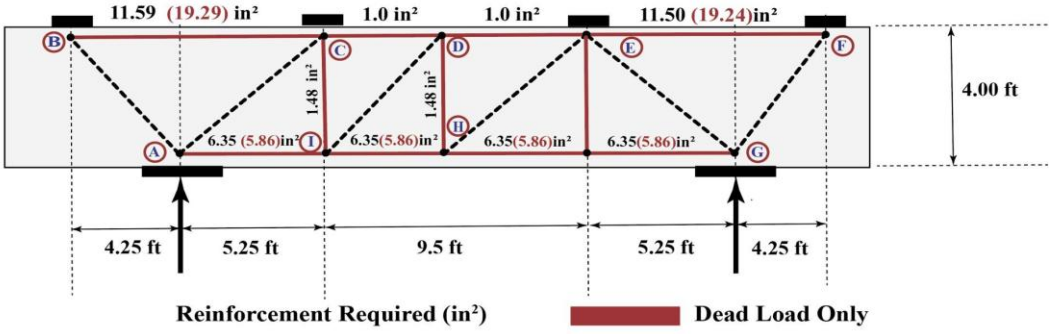

Figure 3-21: Summary of reinforcement provided.

3.2.7 Calculation of Nodal Strengths

As shown in Equation (*2-1*) in Section 2.6, the nodal strength is a product of the confinement modification factor, concrete efficiency factor, and concrete strength. The confinement modification and concrete efficiency factors were discussed in Section 2.5. For this example, the concrete strength is taken as 3.0 ksi. Nodal geometries in the strut-and-tie model are governed by the requirements outlined in Clause 5.8.2.2 of

the AASHTO LRFD Bridge Design Specifications (9th Edition). This section provides guidance on the classification of nodes based on the types of forces acting on them (CCC, CCT, and CTT) and specifies the minimum nodal dimensions and stress limits to ensure adequate anchorage and load transfer within the strut-and-tie model. The summary of nodal geometries is illustrated in Figure 3-22 below.

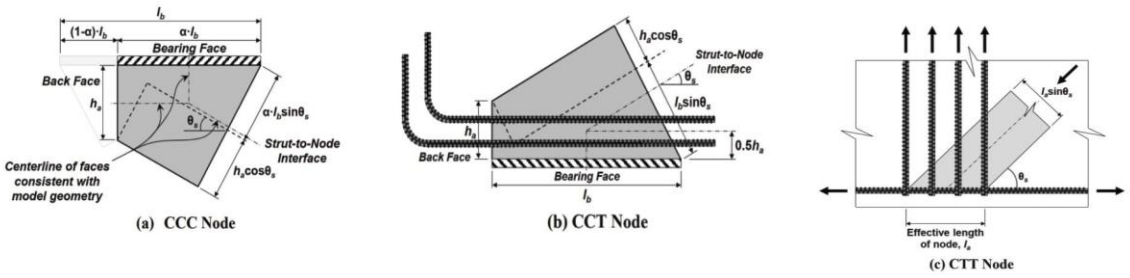

Figure 3-22: Nodal geometry (AASHTO 2020).

The nodal strength of each face of node A is calculated as shown in Figure 3-23 below.

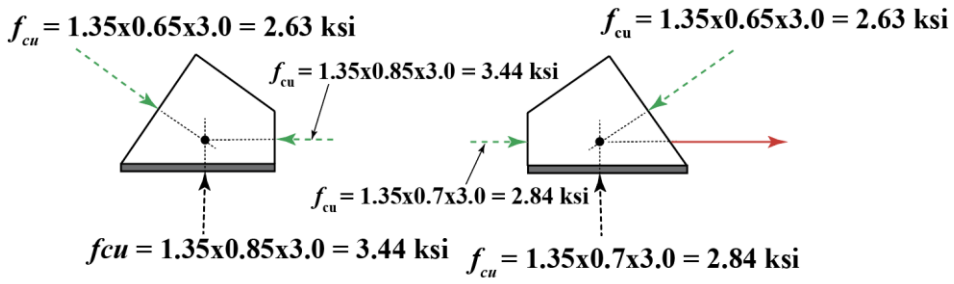

Figure 3-23: Summary of strength of each face of node A.

Similarly, the efficiency factors and nodal strength of other nodes are summarized in Appendix B. Nodal strength checks must be completed for all the nodes and load cases (see Appendix B). The strength of a face of the node is given by Equation (3-3). Some nodes can be eliminated considering symmetry or very low forces or stresses. Appendix B summarizes the nodal geometry of each node. Forces on each face of the node (for all 9 load cases) are also summarized in Appendix B.

$$P_n = f_{cu} \cdot A_{cn} \tag{3-3}$$

The factored resistance (P_r) can be calculated is given by Equation (3-4).

$$P_r = \phi \cdot P_n \tag{3-4}$$

Where ϕ = Resistance factor for compression in strut-and-tie models specified in AASHTO LFRD code (AASHTO 2020) Article 5.5.4.2 and has a value of 0.7.

The amount of applied force compared to the available capacity is expressed in percentage terms as a utilization factor. The calculations of nodal strengths and utilization factors for this example are provided in Appendix B.

3.3 Procedure for Using the STM Templates

In this section, the use of templates is illustrated through an example of a three-column bent cap (Ref: Project No. B-2506, Anson County, Sheet No. S-17). For demonstration purposes, an incorrect template was intentionally selected to highlight how specific features and behaviors of the template are presented.

After selecting a template, all the information to complete the analysis are input into the template. The following subsections provide the instructions and an example of how to use the template based on the example below in Figure 3-24.

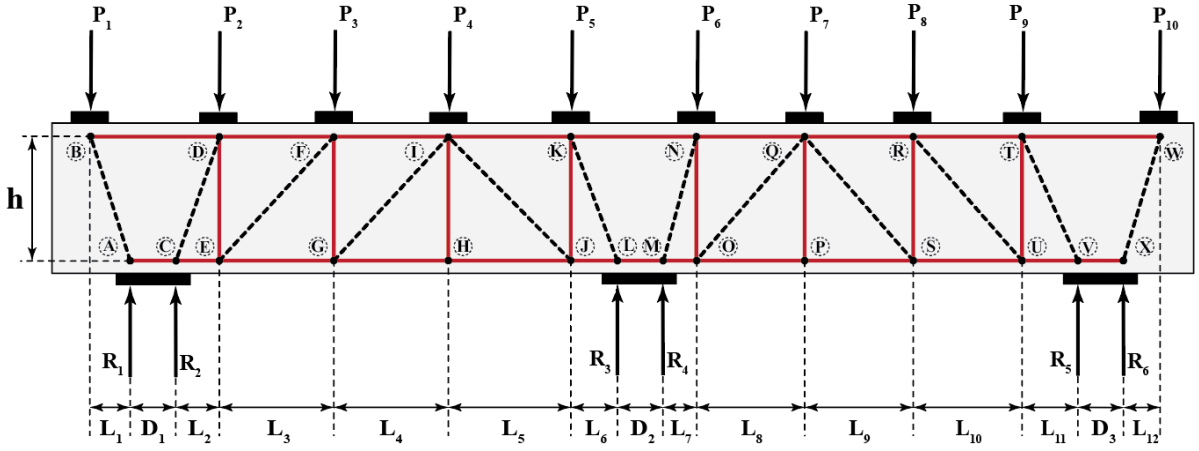

Figure 3-24: Template example - Three column bent cap 10 loads symmetric.

3.3.1 Step 1: Material Properties

Input all of the material properties such as the concrete strength f'_c (ksi), longitudinal reinforcement bars yield strength f_{yl} (ksi), the vertical reinforcement bars yield strength f_y (ksi), and the density of concrete (pcf) in the *Material Parameters* section shown in Figure 3-25.

Material Parameters			
Concrete Stength f'_c	3	ksi	
Design Strength f_{yl}	54	ksi	
Design Strength f_{yv}	54	ksi	
Density of Concrete	150	pcf	
Yield Strength f_{yl}	60	ksi	
Yield Strength f_{yv}	60	ksi	

Figure 3-25: Template material properties input table.

3.3.2 Step 2: Geometric Parameters

The length of each division in feet and inches as shown in Figure 3-26 are then input into the template. Each section is labeled from L_1, L_2, ..., L_{n-1}, L_n as shown in Figure 3-24. The user should also input D_1, D_2,….D_{n-1}, D_n which is the distance between the two reaction forces within one column. This distance represents the flexural lever arm in the supporting element and input at the judgement of the engineer. A simplifying approximation such as, 7/8d or similar elastic or cracked elastic assumption for the flexural lever arm can be used. The column is divided in half and each reaction force is applied at the center of each half of the supporting element.

Divisions	ft	in	in
L_1	3	0	36
L_2	3	0	36
L_3	3	0	36
L_4	3	0	36
L_5	3	0	36
L_6	3	0	36
L_7	3	0	36
L_8	3	0	36
L_9	3	0	36
L_{10}	3	0	36
L_{11}	3	0	36
L_{12}	3	0	36
D_1	0.25	0	3
D_2	0.25	0	3
D_3	0.25	0	3

Figure 3-26: Geometric template inputs for horizontal distances.

3.3.3 Step 3: Cross-Sectional Dimensions

Figure 3-27 shows the template variables and input information related to the cross-sectional geometry of the member, such as the cover, height of the beam (h), height of the back face of the node (h_a), effective depth (d), height of the strut-and-tie model (h_{STM}), width of the bent cap, and the width and length of the load and support bearings.

Cross Sectional Dimensions				
	ft	in	in	
Cover	0	2	2	
Height of Beam (h)	4	0	48	
d	3	8.74	44.74	
Height of Truss (h_{STM})	4	0	48	
Width of the Bentcap	4	6	54	
Width of the Loading Bearing	3	4	40	
Length of the Loading Bearing (l_b)	3	4	40	
Width of the Support Bearing	3	7	43	
Length of the Support Bearing (l_b)	3	7	43	

Figure 3-27: Template cross-sectional dimensions.

*Note: h_a may be different for top and bottom nodes. The h_a values should be changed accordingly in the nodal checks see Figure 3-33.

3.3.4 Step 4: Reinforcement Details

The reinforcement details entered in the table shown in Figure 3-28 are intended solely for cross-checking and comparative purposes. These inputs do not influence the structural analysis or the final output of the template. The template will calculate the total reinforcement area for each category and determine the required reinforcement for ties. Final decisions regarding the reinforcement arrangement are at the discretion of the engineer and may vary depending on design preferences and project requirements.

Reinforcement Details			
	Bar #	in	Number
Diameter of Bottom Lontigudinal bar (d_{ba})	10	1.27	6
Diameter of Top Longitudinal bar (d_{ta})	10	1.27	6
Diameter of Transverse Reinforcement (d_v)	4	0.50	2
		in^2	
Total Area of Bottom Reinforcement (A_{sb})		7.60	
Total Area of Top Reinforcement (A_{st})		7.60	
Total Area of Transverse Reinforcement/Per link (A_v) (in^2)		0.4	

Figure 3-28: Template reinforcement detail input.

3.3.5 Step 5: Loads

The factored loads (*P*) for a particular loading case. By inputting the load and a subset of the reactions, the truss is effectively made determinate. Although, in some cases, a reaction may be assumed or imposed by the engineer, in most cases the reactions can be calculated using an elastic analysis of the bent cap. Figure 3-29 shows example load values and an input for the variable R_4, a known reaction.

Loads			
	Load	kips	
	P_1	-200	
	P_2	-200	
	P_3	-600	
	P_4	-200	
	P_5	-200	
	P_6	-200	
	P_7	-200	
	P_8	-200	
	P_9	-200	
	P_{10}	-200	
	R_4	400.00	

Figure 3-29: Template load table input.

3.3.6 Step 6: Analysis Output

Once the forces, material properties and geometry have been input, the template will calculate the force (kips) in each member of the truss and the other reaction forces as shown in Figure 3-30. If a tie member is in tension, the required reinforcement in in^2 will be calculated. If a diagonal strut is in tension, this is not permitted and the template will highlight the member(s), to identify the problematic scenario. An example is shown in Figure 3-31.

Analysis Output			
No	Element Forces	Element Forces (Kips)	Rinforcement Required(in^2)
1	A_B	-125	Compression
2	B_D	75	1.25
3	A_C	-75	Compression
4	C_D	-720.8	Compression
5	R1	100	1.67
6	R2	576.7	9.61
7	C_E	357.5	5.96
8	D_E	0	0.00
9	D_F	-340	Compression
10	D_G	-29.2	Compression
11	E_G	357.5	5.958333333
12	F_G	23.3	0.388333333

Figure 3-30: Analysis output – no strut conflicts (tension vs compression).

Analysis Output			
No	**Element Forces**	**Element Forces (Kips)**	**Rinforcement Required(in^2)**
1	**A_B**	-250	Compression
2	**B_D**	150	2.5
3	**A_C**	-150	Compression
4	**C_D**	-583.3	Compression
5	**R1**	200	3.33
6	**R2**	466.7	7.78
7	**C_E**	200	3.33
8	**D_E**	0	0.00
9	**D_F**	-400	Compression
10	**D_G**	333.3	5.555
11	**E_G**	200	3.333333333
12	**F_G**	-266.7	Compression

Figure 3-31: Analysis output – (example indication that a strut is in tension or tie in compression).

3.3.7 Step 7: Nodal Limits

Each node requires the following information to conduct the strength checks outlined in AASHTO LRFD: the type of node (CCC, CCT, or CTT), the forces on the node, the height of the back face of the node (h_a), and the width and length (l_b) of the bearing at that node.

In the templates as a part of this study, nodal dimensions are calculated in accordance with the requirements of the AASHTO LRFD Bridge Design Specifications 9th Edition. AASHTO provides limits on the maximum compressive stress that can be applied on nodal faces, expressed as a fraction of the concrete compressive strength (f'_c) to ensure these limits are not exceeded, the required bearing area is determined by dividing the resultant compressive force by the corresponding stress. For nodes containing ties, the height of the back face of the node (h_a) is typically dimensioned as twice the distance from the reinforcement to the exterior face of the concrete member (Figure 3-32). In scenarios where compression struts define the value h_a, such as shown in Figure 3-32 estimates of the value for h_a, can be determined from the flexural compression zone size. Additionally, as previously discussed so that the compression and tension chords align, in scenarios where the chord changes from tension to compression, the location of the flexural tension reinforcement can be used so as not to complicate the geometry of the strut-and-tie model where the member chords switch from tension to compression.

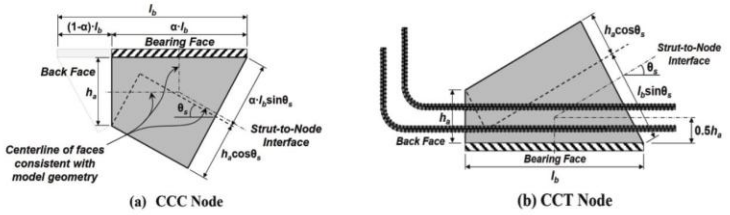

Figure 3-32: Nodal geometry (AASHTO 2020).

Please note that the back face height of the top and bottom nodes may differ and could vary between nodes, the user should ensure the correct dimension is entered for each node. If a node does not exceed the nodal limits, the word "*Ok*" will appear in green on the large upper-right square, as shown in Figure 3-33. If the node exceeds the nodal limits, the words "Nodal Failure" will appear in red, as shown in Figure 3-34, and the failure face's cell will also be highlighted in red. Multiple faces can fail simultaneously.

Node	**A**	**Ok**	
h_a (in)	6.52		
ϕ Factor	0.7		
Type	CCC		
Width of the bearing	17		
Length of the bearing (l_b)	17		
Confinement Modification factor (m)	2		
Efficincy Factor (v)	A_B	R1	A_C
	0.65	0.85	0.85
Capacity of the face (ksi)	A_B	R1	A_C
	2.73	3.57	3.57
Force (kips)Applied On	A_B	R1	A_C
	231.7	175	151.9
Angle of the strut (Degrees)	49.0	90	0
Width of the strut/Bearing (l_b)(in)	8.13	5.10	6.52
Stress Applied by Strut/Load (ksi)	1.68	2.02	1.4
Utilization(%)	61.44	56.54	38.38

Figure 3-33: Nodal limits – example of successful node check.

Node	C		
h_a (in)	6.52	Nodal Failure	
ϕ Factor	0.7		
Type	CCT		
Width of the bearing	17		
Length of the bearing (l_b)	17		
Confinement Modification factor (m)	2		
Efficincy Factor (v)	C_D	R2	A_C
	0.65	0.7	0.7
Capacity of the face (ksi)	C_D	R2	A_C
	2.73	2.94	2.94
Force (kips)Applied On	C_D	R2	A_C
	540.70	408.3	354.4
Angle of the strut (Degrees)	49.0	90	0
Width of the strut/Bearing (l_b)(in)	13.26	11.90	6.52
Stress Applied by Strut/Load (ksi)	2.40	2.02	3.2
Utilization(%)	87.87	68.65	108.76

Figure 3-34: Nodal limits – example of nodal limit exceeded.

3.3.8 Step 8: Angle Check

AASHTO LRFD indicates that the angle between a strut and a tie should not be less than 25 degrees. The template checks the angles of the struts-and-ties given the geometry. At the bottom of the table, an indication is provided if the angles meet the requirement. If all angles are satisfactory, the word "*Ok*" will appear in green. If any angle is less than 25 degrees, the words "*Not Ok*" will appear in red. This is illustrated in Figure 3-35.

Angle Checks	
Angle	Degrees
ABD	53.13
BAC	126.87
CDE	36.87
ECD	53.13
EGD	53.13
GDE	36.87
GFH	36.87
FHG	53.13
IJH	53.13
HIJ	36.87
JLK	53.13
JKL	36.87
OMN	53.13
MNO	36.87
POQ	53.13
OQP	36.87
SPR	53.13
PRS	36.87
UST	53.13
STU	36.87
UVT	53.13
VTU	36.87
XWT	53.13
Angle Checks	Ok

Angle Checks	
Angle	Degrees
ABD	20.85
BAC	159.15
CDE	36.87
ECD	53.13
EGD	53.13
GDE	36.87
GFH	36.87
FHG	53.13
IJH	53.13
HIJ	36.87
JLK	53.13
JKL	36.87
OMN	53.13
MNO	36.87
POQ	53.13
OQP	36.87
SPR	53.13
PRS	36.87
UST	53.13
STU	36.87
UVT	53.13
VTU	36.87
XWT	53.13
Angle Checks	Not Ok

Figure 3-35: Example angle check table in template (Ok – left, Not ok – right).

3.3.9 Step 9: Template Summary

At the top of each template, there is a summary section that indicates whether the Nodal Strength Check, Angle Check, or Strut Check (Template Check) has passed or failed. An example summary can be seen in Figure 3-36.

Summary	
Nodal Strength Check	Ok
Angle Checks	Ok
Template Check	Ok

Summary	
Nodal Strength Check	Not Ok
Angle Checks	Ok
Template Check	Not Ok

Summary	
Nodal Strength Check	Not Ok
Angle Checks	Not Ok
Template Check	Not Ok

Figure 3-36: Example template summary table.

4 EXPERIMENTAL PROGRAM

A detailed survey of existing bent cap designs in the state of North Carolina was conducted in collaboration with the North Carolina Department of Transportation (NCDOT). The survey provided insights into the design parameters commonly used and typical practices. Based on the analysis of the available drawings, parameters such as shear span-to-depth (a/d) ratios, reinforcement ratios, and the heights of the bent caps were identified. The experimental program was designed to explore certain variables as representative portions of bent caps used. All members were designed to be limited by nodal strength rather than tie yielding. This is because members that are flexure critical (tie yielding) are more straightforward to predict using analytical models whereas members that are governed by nodal crushing (shear failures) are more challenging to reliably predict. The experiments in the series consisted of six beams labeled STC1 to STC6

The series of six shear critical deep beam tests were conducted at the Constructed Facilities Laboratory at North Carolina State University. The beams measured 20 ft. long, 4.5 ft. deep (STC1 through STC3) and 14 ft. long, 4 ft. deep (STC4 through STC6). Specimens STC1 through STC3 were 14 in. wide and STC4 through STC6 measured 12 in. wide. The specimens contained nine-headed No.10 bars for the bottom longitudinal reinforcement, resulting in a longitudinal reinforcement ratio of 1.75% for STC1 to STC3 and 1.57% for STC4 to STC6.

The transverse reinforcement consisted of No. 4 bars bent into two-legged stirrups. Both the longitudinal and transverse reinforcement were fabricated from the same grade of steel. Coupon tests conducted on three samples of each reinforcement type yielded average measured yield strengths of 65.0 ksi for the longitudinal bars ($f_{y,t}$) and 62.5 ksi for the transverse bars ($f_{y,w}$). The horizontal distribution reinforcement exhibited a yield strength of 62.5 ksi ($f_{y,d}$). The concrete compressive strength (f'_c), determined from 4 in. × 8 in. cylinders tested on the day of specimen testing, ranged from 4.82 ksi to 5.58 ksi.

Two shear-span-to-depth ratios are explored ranging between approximately 1 and 2. STC1 to STC3 have a shear-span-to-depth ratio of 1.810 and STC4 to STC6 have a shear-span-to-depth ratio of 1.180. These shear-span-to-depth ratios represent a common range observed in bent caps. It also provides experimental data for a range of compression strut angles. The height of the bent caps was kept as large as possible and to avoid significant influence from size effect when compared to large bent caps that may be used in practice.

The study explored three different reinforcement configurations to examine the influence of different transverse and longitudinal reinforcement quantities had on the ultimate and service performance of the members. Some of the bent caps in North Carolina were identified to have a transverse reinforcement ratio of approximately 0.13%, this corresponds approximately to the minimum, transverse reinforcement required using sectional methods. Specimens STC2 and STC5 contain 0.13% transverse and longitudinal reinforcement to explore the performance of the members in the context of the strut-and-tie method. STC1 and STC4 contained 0.30% transverse and longitudinal reinforcement to examine how utilizing the minimum reinforcement required to utilize the unpenalized nodal factors in the STM has on the performance at service and ultimate conditions.

Additionally, STC3 and STC6 investigates the effects of zero transverse reinforcement on the response of the bent caps. Members containing less than the 0.30% minimum reinforcement can be designed and

evaluated using the AASHTO LRFD STM but with reduced nodal factors. Specimens without any distributed reinforcement were tested to compare the crack widths and structural performance with those that included 0.30% and 0.13% reinforcement. These comparisons help evaluate the influence of reinforcement on service and ultimate behavior. This is particularly important since the AASHTO LRFD, and STM in general, lack guidance on how designs will perform under service loads. While deflections are typically not a concern for deep members, the members can crack at service. Ensuring the designs have controlled crack widths at service that are acceptable by the transportation authority for durability, rating, maintenance and aesthetic purposes is important. Additionally, very few experiments in the literature report multiple different crack widths throughout loading, thus, making this experimental series important for this study. Table 4-1 summarizes the dimensions, reinforcement ratios and the material properties of the experimental series.

Table 4-1: Summary of the dimensions, reinforcement ratios and material strengths of the experimental series.

Summary of Experiments											
Specimen	**Length (ft.)**	**Span (2a) (ft.)**	**Height (ft.)**	**Width (in.)**	**d**	**a/d**	**ρ_v and ρ_h (%)**	**ρ_l (%)**	**f'_c (ksi)**	**$f_{y,w}$ (ksi)**	**$f_{y,t}$ (ksi)**
STC 1	20.0	14.0	4.50	14.0	46.4	1.810	0.30	1.75	4.93	62.5	65.0
STC 2	20.0	14.0	4.50	14.0	46.4	1.810	0.13	1.75	5.14	62.5	65.0
STC 3	20.0	14.0	4.50	14.0	46.4	1.810	0.00	1.75	5.46	62.5	65.0
STC 4	14.0	8.00	4.00	12.0	46.4	1.180	0.30	1.57	4.82	62.5	65.0
STC 5	14.0	8.00	4.00	12.0	46.4	1.180	0.13	1.57	5.21	62.5	65.0
STC 6	14.0	8.00	4.00	12.0	46.4	1.180	0.00	1.57	5.58	62.5	65.0

The geometric and reinforcement details for the STC series of tests are presented in Figure 4-1 through Figure 4-6. Figure 4-1 through Figure 4-3 illustrate the dimensions and reinforcement ratios for beams STC1, STC2, and STC3, while Figure 4-4 through Figure 4-6 provide the corresponding details for beams STC4, STC5, and STC6. These figures provide an overview of the experimental setup, highlighting the variation in reinforcement ratios and beam dimensions across the test specimens.

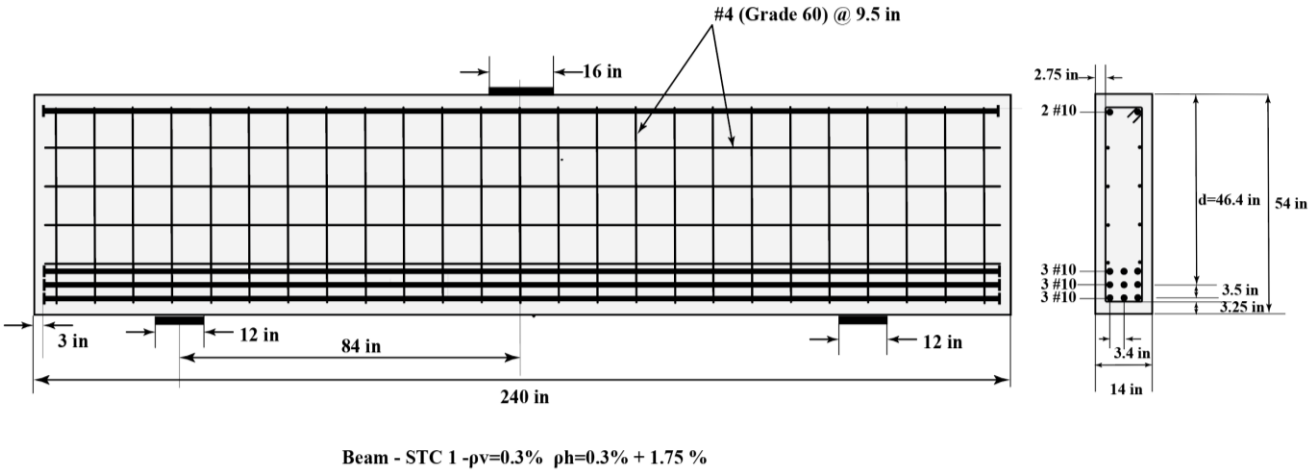

Figure 4-1: STC1 reinforcement details.

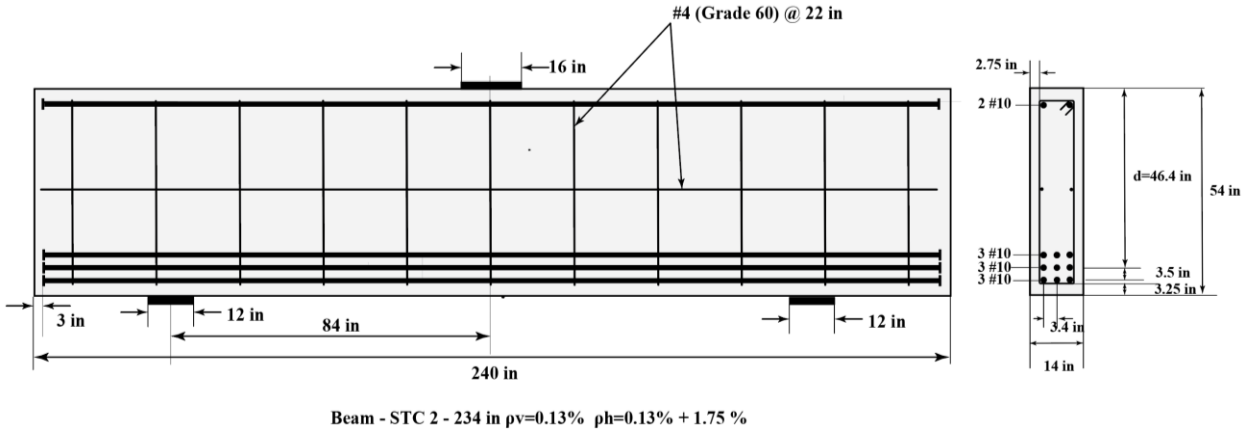

Figure 4-2: STC2 reinforcement details.

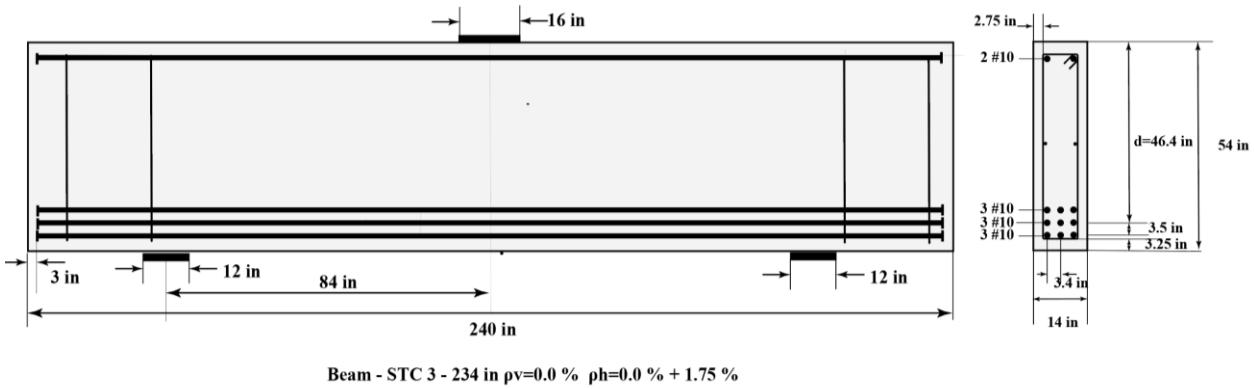

Figure 4-3: STC3 reinforcement details.

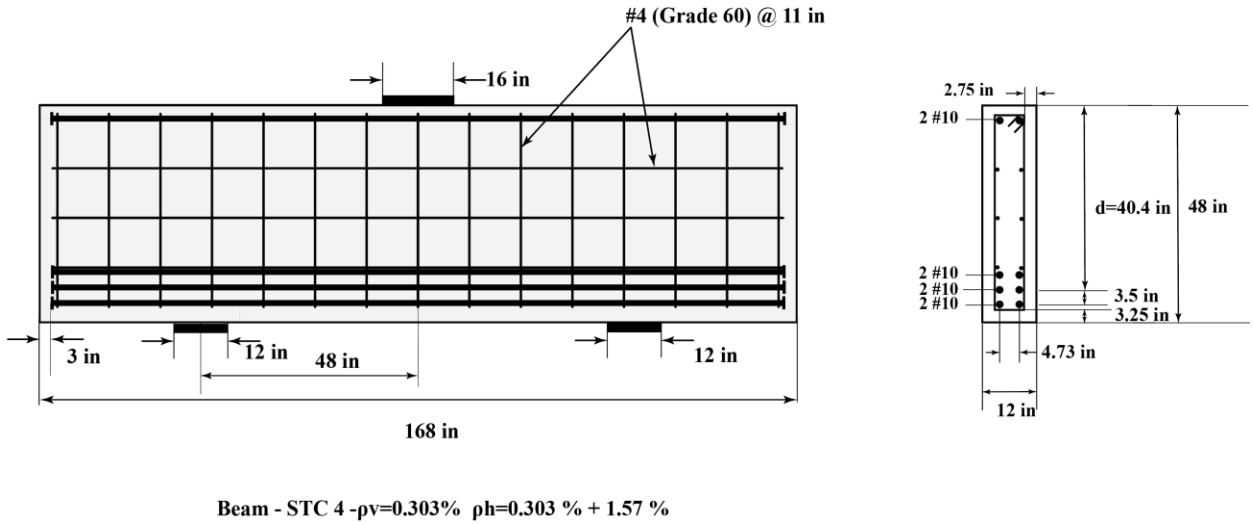

Figure 4-4: STC4 reinforcement details.

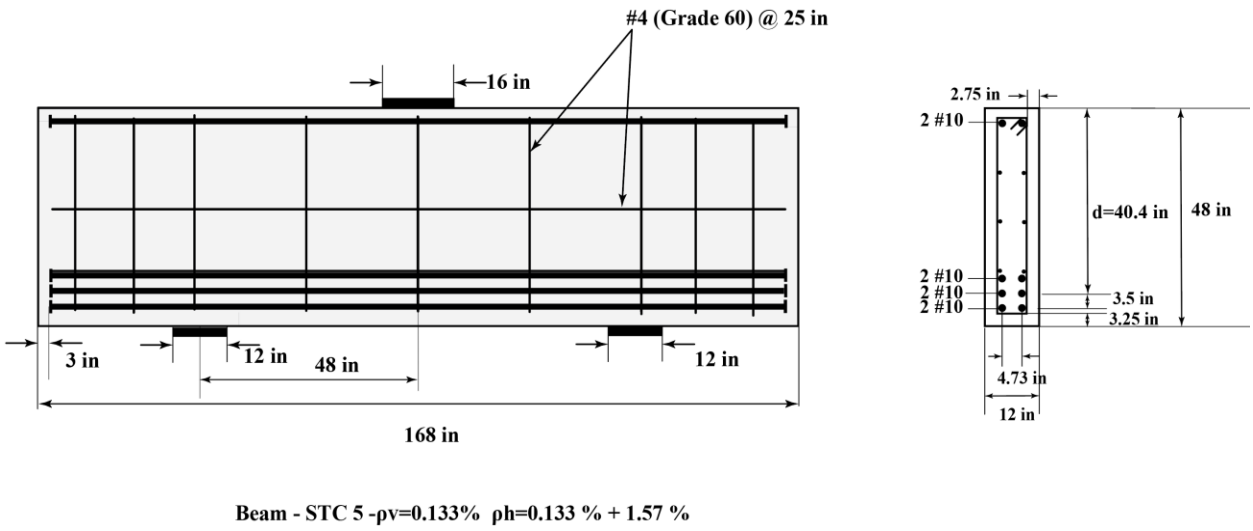

Figure 4-5: STC5 reinforcement details.

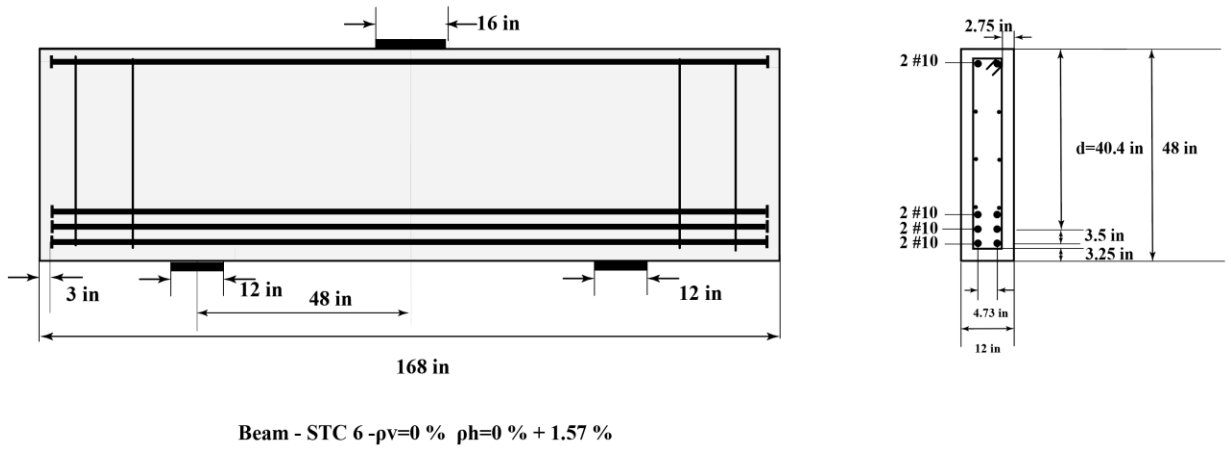

Figure 4-6: STC6 reinforcement details.

All six specimens were point loaded in the center of the span and simply supported. The support plates measured 12 in. x 14 in. x 2 in. (STC1 through STC3) and 12 in. x 12 in. x 2 in. (STC4 through STC6) and rested on roller supports. The loading plate measured 16 in. x 14 in. x 3 in. for STC1 through STC3, and 16 in. x 12 in. x 3 in. for STC4 through STC6. Hydro-Stone was used between the loading plate and the beam to ensure the load was evenly distributed on the top surface of the beam. A spherical bearing was used between the actuator head and the spreader beam to ensure that moments were not transmitted through the actuator. Figure 4-7 shows the experimental setup, where the beams were monotonically loaded until failure.

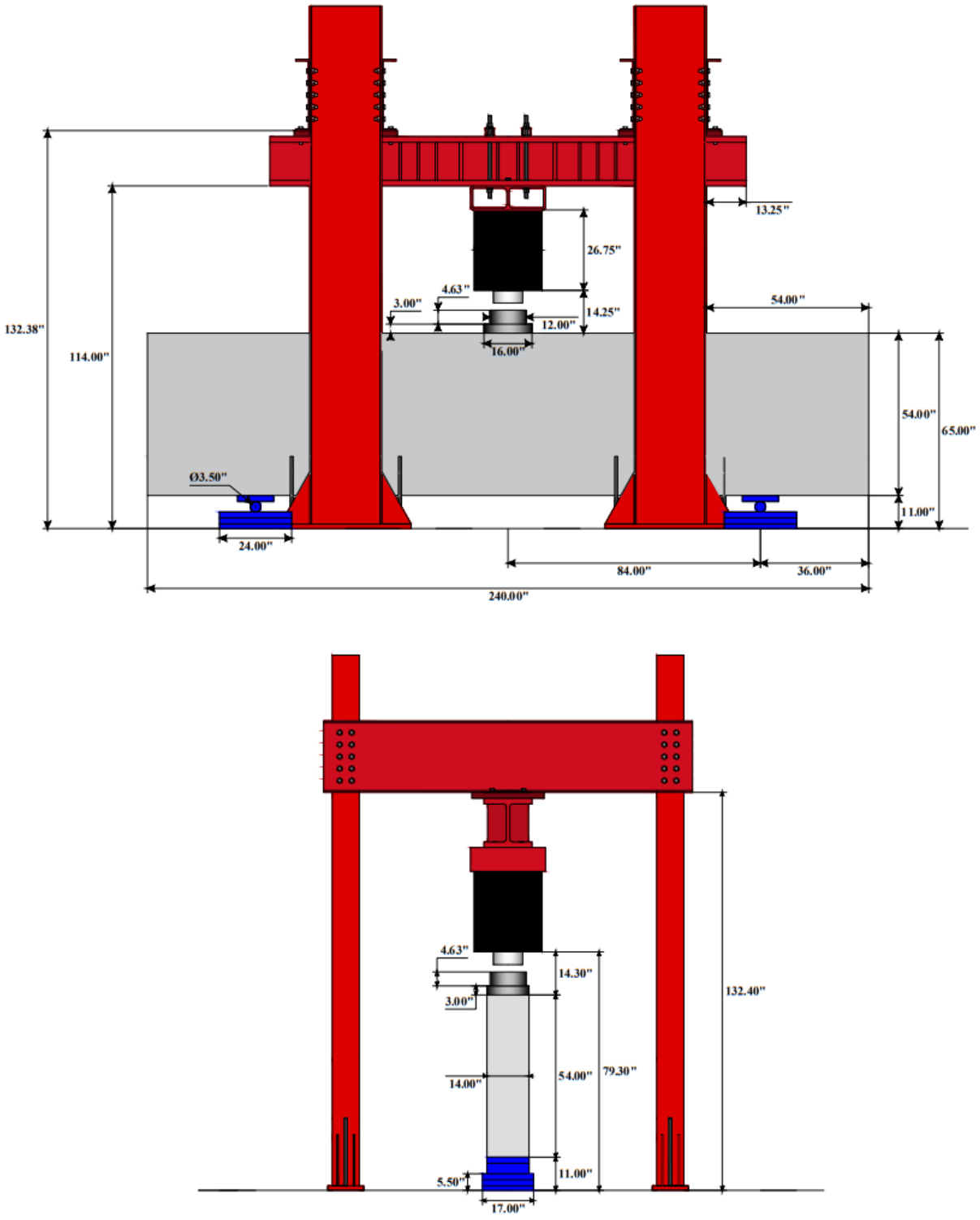

Figure 4-7: Experimental setup (specimen shape STC1-STC3 shown).

Strain gauges were included along some of the longitudinal and transverse reinforcement. See Appendix F for details. A displacement transducer was used to measure the vertical displacement of the midspan of the bottom of the beam with respect to the strong floor.

Understanding the internal force transfer mechanisms in deep beams, particularly the development of struts and nodal zones is challenging due to the complex, non-linear strain distributions and localized cracking that occur under loading. Traditional measurement techniques, such as strain gauges and linear transducers, provide data only at discrete points and often do not capture the full extent and evolution of these behaviors across the entire beam. Consequently, it becomes difficult to observe and quantify the member response. To address these limitations, this study employed Digital Image Correlation (DIC), which enables the full field of view deformation field response of the surface of the specimens throughout loading. These deformation fields can also be used to determine local strains on the surface of the test specimens. DIC is a non-contact optical technique that uses pairs of cameras to monitor how a speckle pattern surface changes throughout loading. The deformation fields can also be used to determine crack kinematics, crack widths and crack slips, at multiple locations along multiple cracks throughout loading.

To obtain high-resolution, full field-of-view deformation data, the entire surface of the west face of the beam was monitored with the three-dimensional DIC system. Maintaining an approximate resolution of 2 pixels/mm, three stereo-systems (north system, middle system, and south system) with two 12.3 MP cameras in each system, were used (shown in *Figure 4-8*). The data from the three systems were combined using a proprietary multi-view registration algorithm. A speckle pattern with speckles measuring approximately 2.5 mm in diameter was applied to the specimens. This arrangement resulted in 3-5 pixels per speckle. The speckle pattern was applied so the beam had approximately 50% black-white contrast.

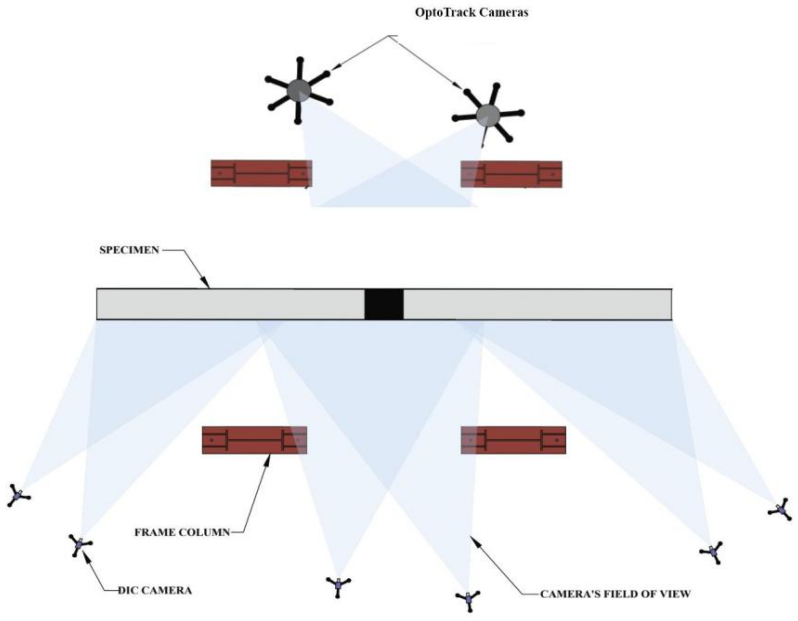

Figure 4-8: Plan view of the DIC cameras and LED arrangement.

The east face of the beam was instrumented with a 9 in. x 9 in. a grid of 138 infrared Light-Emitting Diode (LED) targets arranged in 6 rows and 23 columns. The three-dimensional position of the infrared targets was measured with OptoTrack cameras. This data was used to verify and validate the DIC deformation field data obtained.

4.1 Experimental Observations and Results

For all six members in the STC series, initial loading of the specimens resulted in flexural cracks at the bottom of the beam near mid-span. As the load increased, flexural cracks widened, and shear cracks formed between the support plate and near the edge of the loading plate. As loading continued, shear cracks extended and widened significantly, with all beams ultimately failing in shear. No splitting cracks were observed at the bottom of the specimens up to and at the last load stage.

A string potentiometer was attached to the center of the beam to measure the vertical displacement of the beam as the load was applied. The load–displacement responses of specimens STC1, STC2, and STC3 are presented in Figure 4-9 . This figure compares the response of the three members with different quantities of distributed orthogonal reinforcement for the members in the series with an *a/d* ratio of 1.810. The applied load (kips) is plotted against the mid-span displacement (in.).

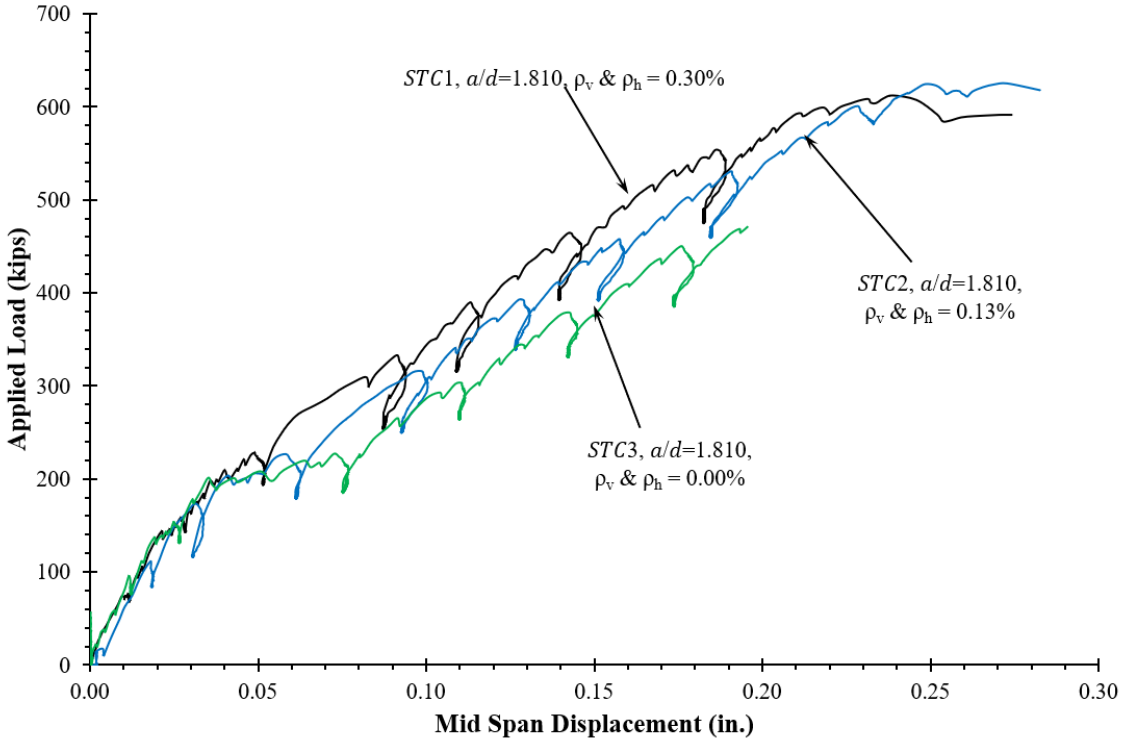

Figure 4-9: Load versus mid span displacement response for STC1-STC3.

Similarly, a string potentiometer was attached to the center of the beam to measure the vertical displacement of the beam as the load was applied. The load–displacement responses of specimens STC4-STC6 are presented in Figure 4-10. This figure compares the response of the three members with different quantities of distributed orthogonal reinforcement for the members in the series with an *a/d* ratio of 1.188. The applied load (kips) is plotted against the mid-span displacement (in.).

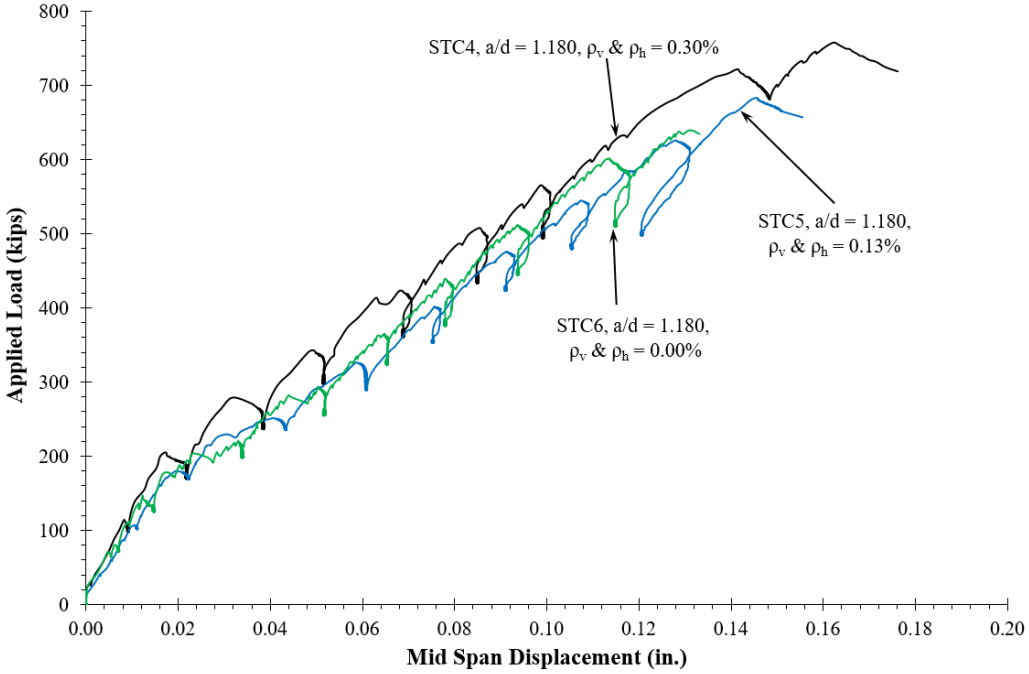

Figure 4-10: Load versus mid span displacement response for STC4-STC6.

Strain gauges were installed along the longitudinal reinforcement at two locations: at the mid-span and at the center of the shear span. Additionally, strain gauges were mounted at the mid-height of the beam within the shear span on transvers bars to monitor vertical strain development. Figure 4-11 presents the load versus mid-span strain response for specimens STC1-STC3, while Figure 4-12 shows the corresponding results for specimens STC4-STC6. Additional data and detailed results are provided in Appendix F. For a given strain at the mid-span, the corresponding load was observed to increase with the amount of transverse reinforcement provided in the beams. This trend highlights the role of transverse reinforcement in improving shear resistance and overall load-carrying capacity. It also indicates that the transverse reinforcement provided is engaged and providing crack control. As observed in Figure 4-11 and Figure 4-12, strain levels increase when the transverse and horizontal distribution reinforcement are reduced.

For a given strain at the mid-span, the corresponding load was observed to increase with the amount of orthogonal distributed reinforcement provided in the beams. This trend highlights the role of transverse reinforcement in improving shear resistance and overall load-carrying capacity. Additionally, beams with smaller span-to-depth (a/d) ratios exhibited lower strain levels under a given load compared to those with larger a/d ratios.

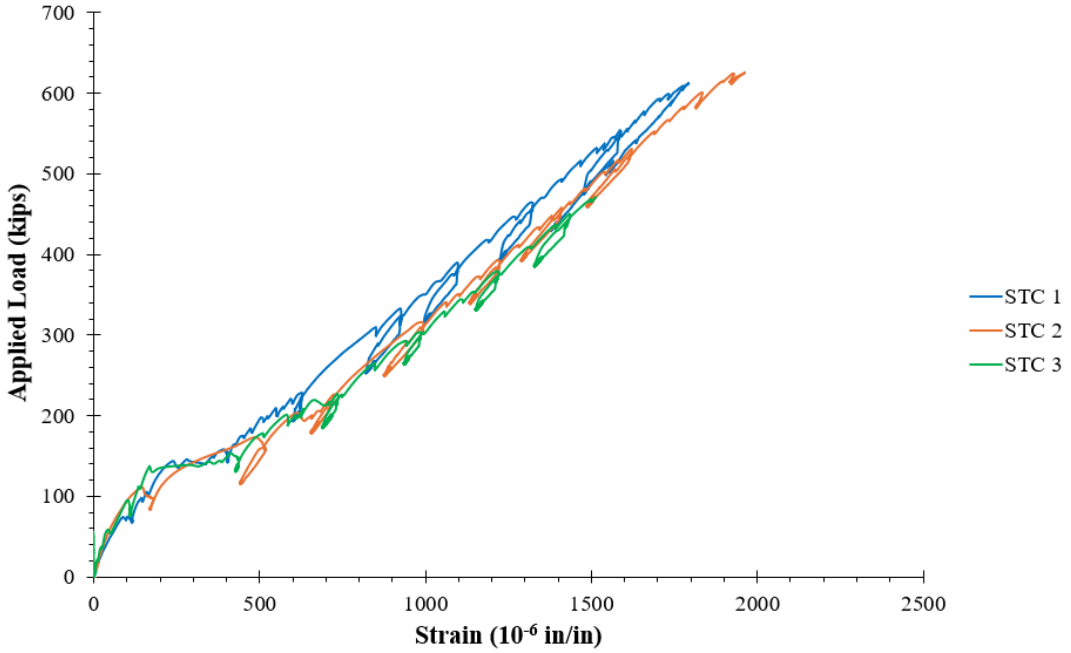

Figure 4-11: Load vs strain at mid span, STC1-STC3.

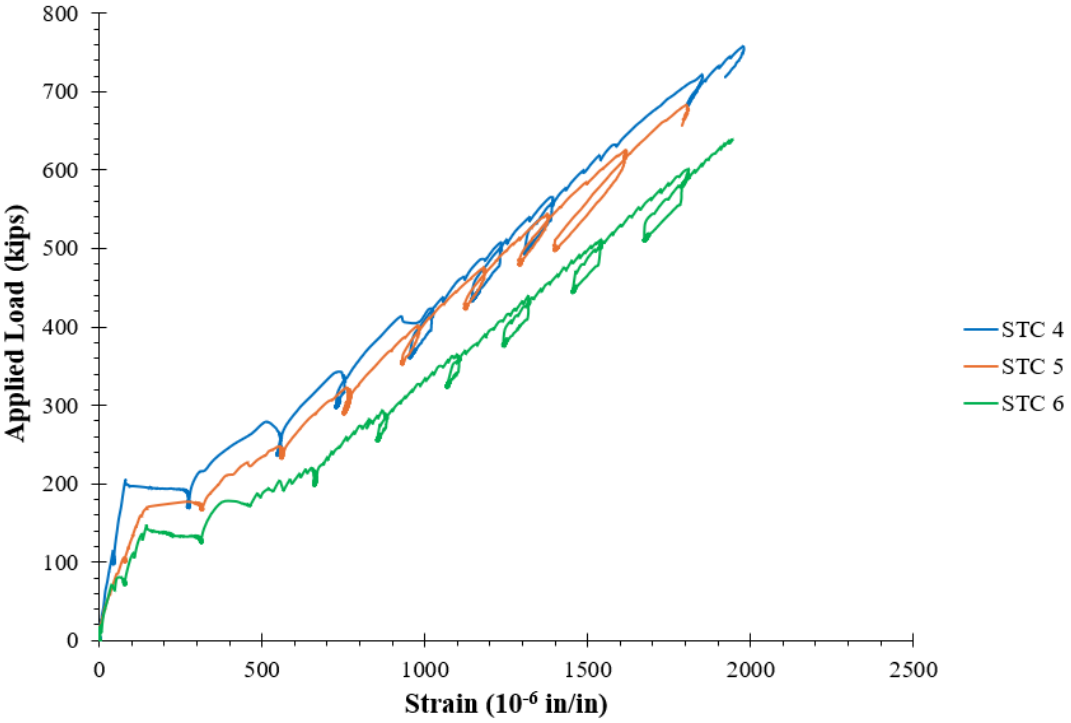

Figure 4-12: Load vs strain at mid span, STC4-STC6.

In this study, the failure loads of six deep beam specimens were predicted using two advanced modeling approaches in addition to strut-and-tie modeling approaches: the Two-Parameter Kinematic Theory (2PKT) and VecTor2, a nonlinear finite element program. The models were developed to examine their ability to predict the response of members so that the techniques can be used to verify and validate the template designs and to comment on aspects of the member response not investigated in the experimental program. See Appendix C. The predicted values were compared with experimental results.

The 2PKT model, developed by Mihaylov et al. (2013), is a kinematics-based analytical approach in which the shear behavior of reinforced concrete beams is described using two degrees of freedom: the average strain in the longitudinal reinforcement and the vertical displacement of the critical loading zone. The shear span is idealized as consisting of a rigid body above the critical crack and a crack fanning zone beneath it. The overall response is governed by equilibrium, kinematic conditions and constitutive relationships that define the contributions from shear carried in the uncracked zone near the loading plates, aggregate interlock, transverse reinforcement, and dowel action. This model has been verified and validated against experimental results and has been shown to effectively capture the key mechanisms that contribute to shear strength in disturbed regions.

The VecTor2 program is a nonlinear finite element analysis tool based on the Modified Compression Field Theory (MCFT) (Vecchio and Collins 1986) and the Disturbed Stress Field Model (Vecchio 2000). In this method, the behavior of cracked reinforced concrete is modeled by considering smeared, rotating cracks, compatibility and constitutive relationships. Effects such as tension stiffening, aggregate interlock, compression softening, and shear slip along cracks are incorporated through advanced constitutive models. The program allows for simulation of reinforced concrete behavior under load, including complex stress and strain distributions that arise in disturbed regions. VecTor2 has been successfully used in the analytical modeling of deep beams, as demonstrated in the study by Palipana and Proestos (2024), which evaluated shear-critical deep beams with high-strength headed shear reinforcement.

These predictions were also compared with those obtained using the AASHTO STM, both with and without applying the minimum reinforcement limitations. A summary of the predicted and actual failure loads, along with the associated predictions, is provided in Table 4-2. The nonlinear finite element program VecTor2 demonstrated the best predictive ability for the peak load, with a mean test-to-predicted shear capacity ratio of 1.03 and a coefficient of variation of 9%. Similarly, the 2PKT model predicted shear capacity with a mean test-to-predicted ratio of 1.33 and a coefficient of variation of 9%. In comparison, the strut-and-tie model gave a mean test-to-predicted ratio of 1.54 with a higher coefficient of variation of 16.9%. While all three methods were capable of capturing the overall response of the representative bent caps, VecTor2 provided the most accurate and consistent predictions among the approaches evaluated.

Table 4-2: Summary of STC1-STC6 peak shear strength and predictions from models.

Specimen	Predictions			Exp. Load (kips)	Test Load/ Prediction 2PKT	Test Load/ Prediction STM (AASHTO)	Test Load/ Prediction (VecTor2)
	2PKT (kips)	STM AASHTO (kips)	VecTor2 (kips)				
STC1	549	510	645	612	1.11	1.20	0.95
STC2	434	365	616	625	1.44	1.71	1.02
STC3	349	365	498	471	1.35	1.29	0.95
STC4	577	511	652	757	1.31	1.48	1.16
STC5	501	368	618	683	1.36	1.86	1.10
STC6	450	368	607	633	1.41	1.72	1.04
				Average	1.33	1.54	1.04
				CoV	0.09	0.169	0.09

4.2 Experimental Observations of Crack Widths

Periodically throughout the test the loading was paused and reduced by approximately 10-15%. The cracks on one side of each test specimen were marked, measured and photographed. Crack measurements were obtained using crack comparator gauges and were nominally measured on a grid aligned with the LED targets.

Figure 4-13 shows the development and evolution of crack patterns for all six specimens (STC1 - STC6) at different loading stages. For each specimen, the cracking behavior was captured at approximately 60–70% of the peak load and again after failure. This represents approximately the service load on the specimens, if the specimen's actual capacity and design capacity matched. As can be seen at this load level, shear cracks are observed in all specimens. Members with more transverse reinforcement have more distributed cracking whereas members without distributed reinforcement show fewer, larger cracks. It should be noted that the load applied to each member in Figure 4-13 differs. For example, the peak load for members without distributed reinforcement is lower than companion members with 0.30% reinforcement.

Figure 4-14 illustrates the crack patterns observed at the failure load for all six specimens (STC1 - STC6). These images capture the final stage of cracking behavior, reflecting the structural response at ultimate capacity. As shown, all specimens exhibit prominent shear cracking, with the severity and distribution of cracks varying based on the amount of distributed reinforcement. Specimens with higher transverse reinforcement ratios display a more distributed crack pattern, indicating enhanced crack control. In contrast, specimens without transverse reinforcement show fewer but more pronounced and wider cracks. It is important to note that the peak load applied to each specimen differs. For instance, specimens lacking transverse reinforcement reached lower ultimate loads compared to their counterparts reinforced with 0.30% distributed reinforcement.

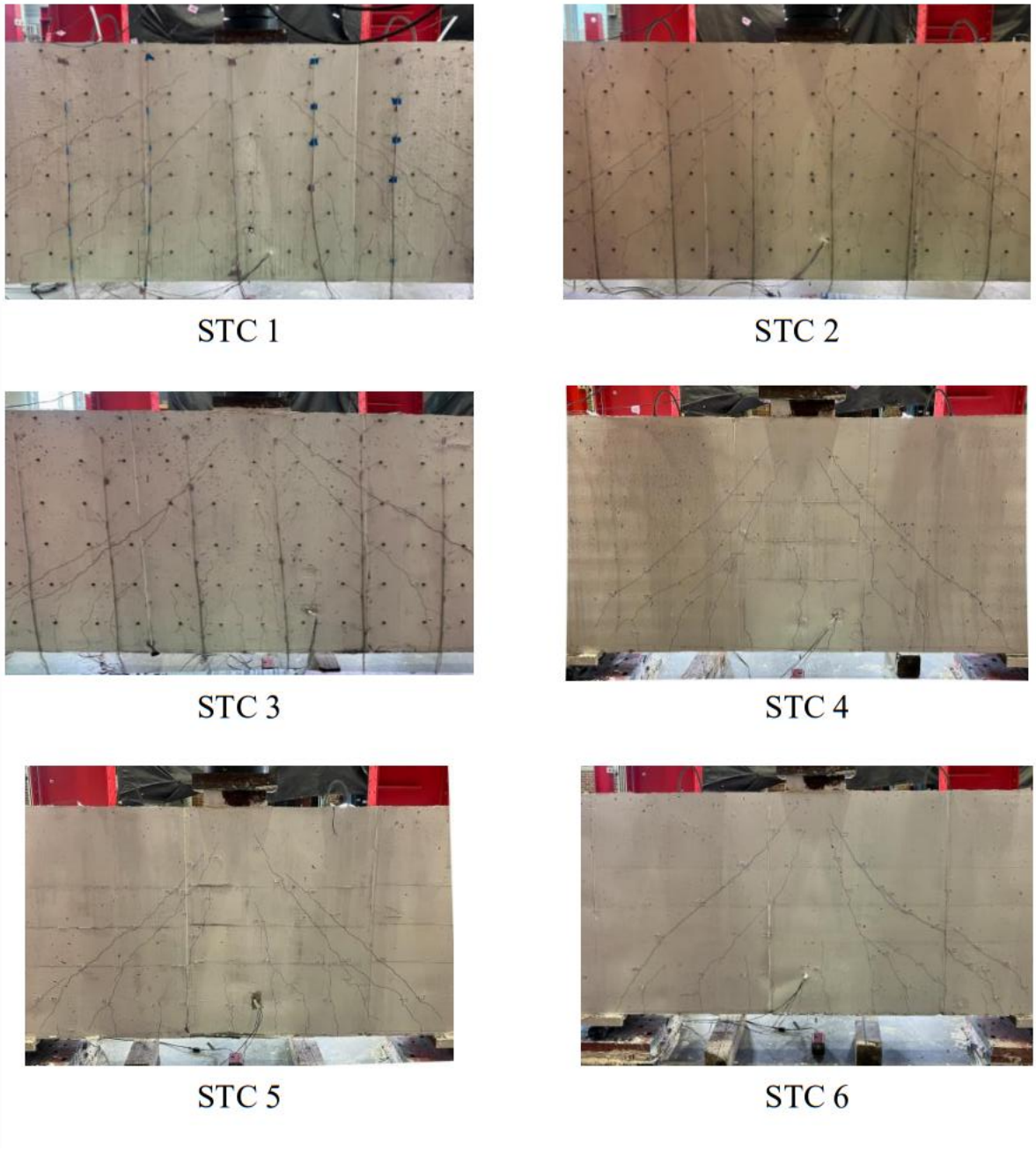

Figure 4-13: Crack patterns observed in beams STC1-STC6 at approximately 60% of peak load.

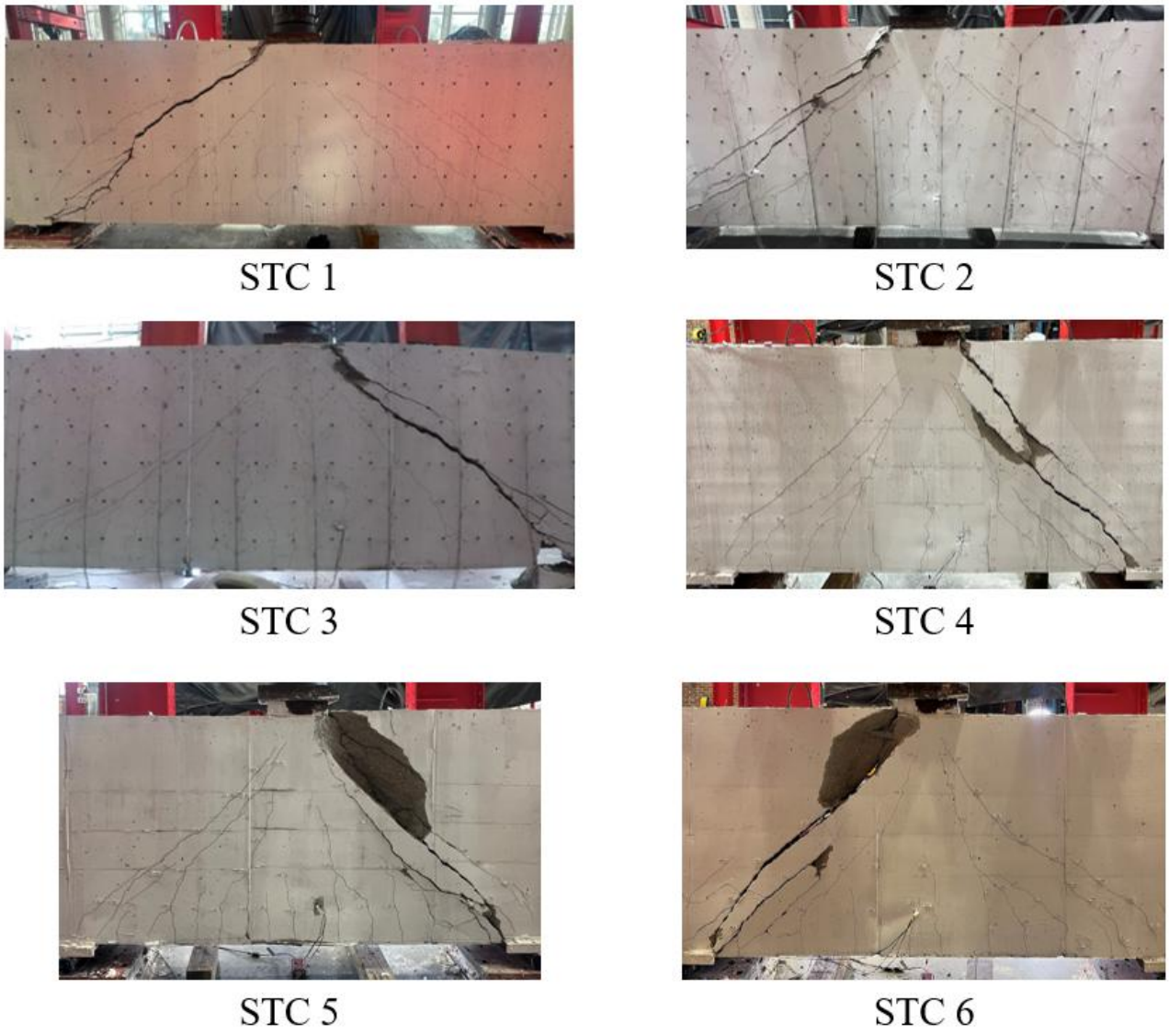

Figure 4-14: Crack patterns observed in beams STC1-STC6 after failure.

The crack patterns obtained for each specimen were digitized and are shown in Figure 4-15 through Figure 4-17. The critical cracks that lead to failure of the specimen are indicated in red. The critical crack is typically defined as the crack that extends from the inner edge of the support plate to near the edge of the loading plate and has the largest crack widths. In some cases, particularly those with at least minimum transverse reinforcement and members that have horizontal distributed reinforcement, multiple shear cracks with different widths can make it difficult to identify which crack is critical before failure.

Figure 4-15 shows the crack pattern determined for STC1. To compare the influence of shear reinforcement on crack patterns, Figure 4-16 shows the caparison of crack diagrams for STC1, STC2, and STC3. These three specimens contained the same longitudinal reinforcement (ρ_l) quantities. As can be seen, the crack

patterns, the crack shapes, and the crack locations were similar. However, the number of cracks decreases as the transverse reinforcement is increased. Crack patterns of all six beams can be found in Appendix F.

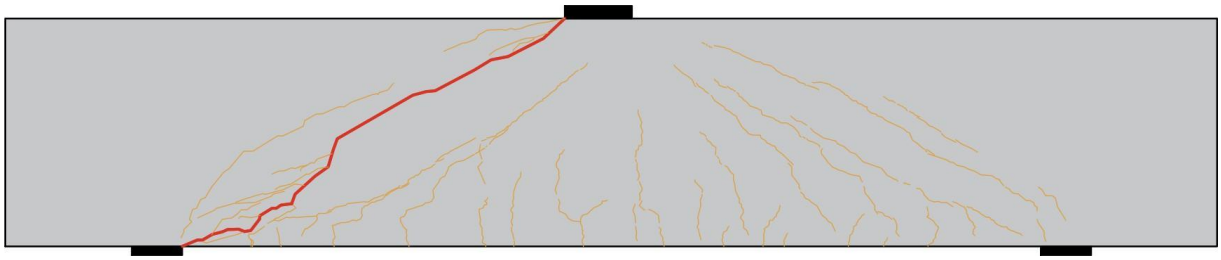

Figure 4-15: Crack pattern of STC1 at last load stage.

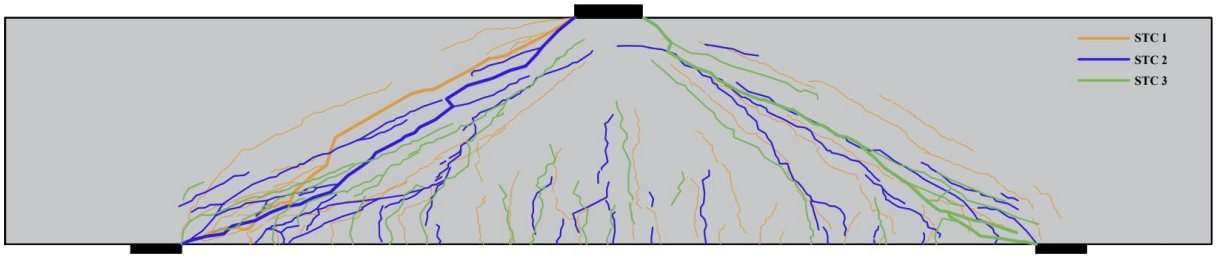

Figure 4-16: Overlapping crack patterns for beams STC1, STC2, and STC3.

Figure 4-17 presents the crack patterns observed in beams STC4, STC5, and STC6. These beams have a shear-span-to-depth (a/d) ratio of 1.18, which is significantly lower than that of beams STC1 to STC3.

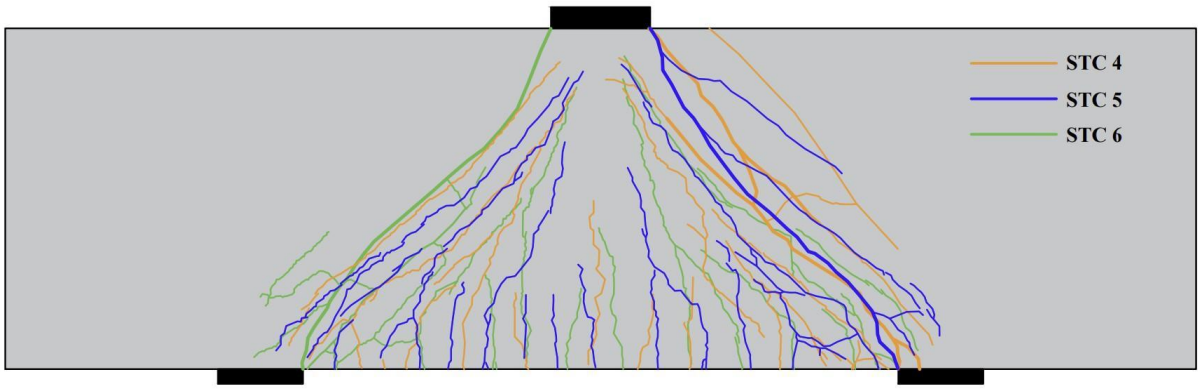

Figure 4-17: Overlapping crack patterns of beams STC4, STC5, and STC6.

In AASHTO LRFD Clause 5.6.7 of the Bridge Design Specifications, a crack width limit of 0.017 inches (0.43 mm) is referenced, particularly for Exposure category I (AASHTO 2020). Additionally, the American Concrete Institute (ACI) 224R-1 (2007) suggests a typical threshold limit for service-level cracking to be approximately 0.4 mm (0.016 in.).

Based on a crack width limit of 0.016 in. (0.41 mm), which is sometimes considered a serviceability threshold in structural design to ensure durability and prevent excessive cracking, the corresponding applied loads were determined from the experimental data. These values, which represent the load levels at which the crack width reached the serviceability limit, are presented in

Table *4-3*. The data was derived from the load-crack width relationships shown in Figure 4-18 and Figure 4-19, where the vertical line in each figure marks the designated crack width limit.

The observation that the loads corresponding to a 0.016 in. (0.41 mm) crack width in all tested beams were lower than those predicted by the AASHTO LRFD design specifications suggests that, at the load levels predicted by AASHTO, the crack widths would likely exceed 0.016 in. (0.41 mm).

According to the AASHTO Manual for Bridge Element Inspection (MBEI), (2019), the evaluation of cracks in reinforced concrete elements is based on observable characteristics, including width and extent, to assign appropriate condition states. Cracks narrower than 0.012 in. (0.3 mm) typically fall under Condition State 1, indicating no significant distress. Cracks between 0.012 in. (0.3 mm) and 0.05 in. (1.3 mm) are classified as Condition State 2, reflecting moderate deterioration that may require monitoring but not immediate action. In this context, a crack width threshold of 0.016 in. (0.41 mm) aligns with the transition into Condition State 2, serving as a reasonable value for serviceability assessments. This classification provides a framework for integrating experimental crack width data into a broader durability evaluation, ensuring consistency with national bridge inspection practices.

To better understand the behavior of cracks in the specimens, crack width data were obtained using both manual measurements and Digital Image Correlation (DIC). Unlike manual measurements, DIC provides continuous, high-resolution tracking of crack development throughout the loading process. This results in smoother and more detailed curves that capture subtle changes in crack width, including abrupt increases associated with crack propagation. Figure 4-20 shows the graph of STC1 to STC3 based on DIC data, while Figure 4-21 shows the graph of STC4 to STC6 based on DIC data.

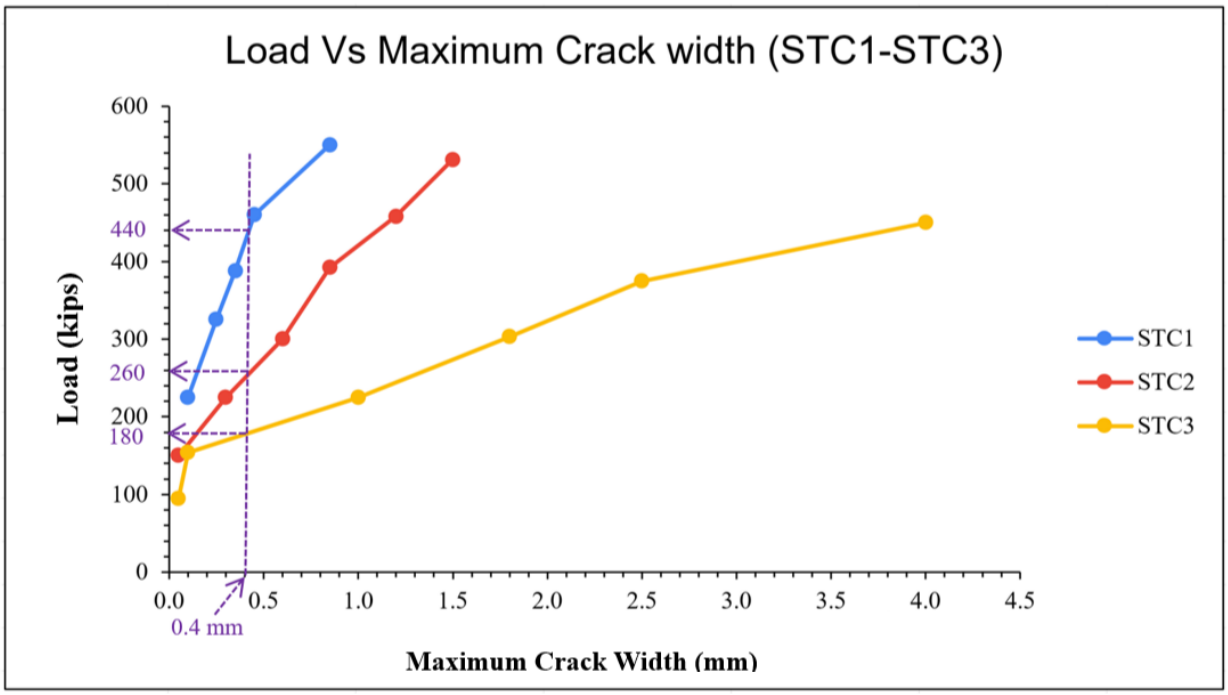

Figure 4-18: Load vs crack width - STC1 -STC3.

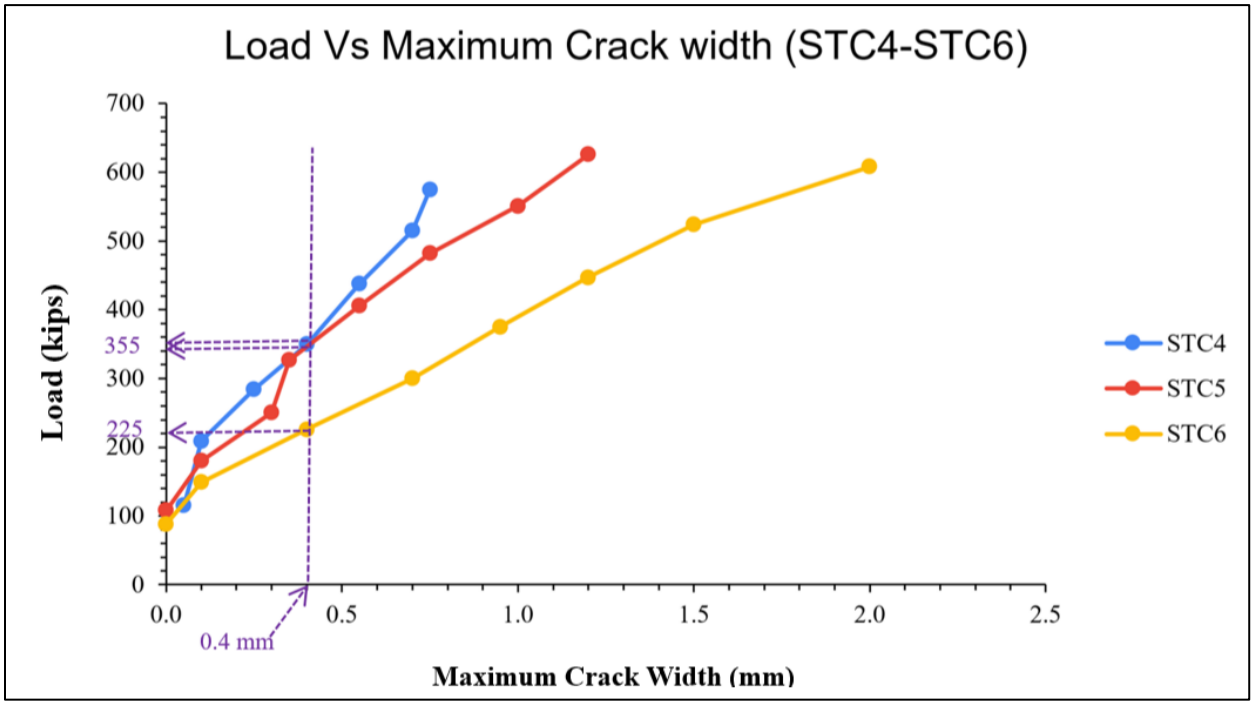

Figure 4-19: Load vs crack width - STC4-STC6.

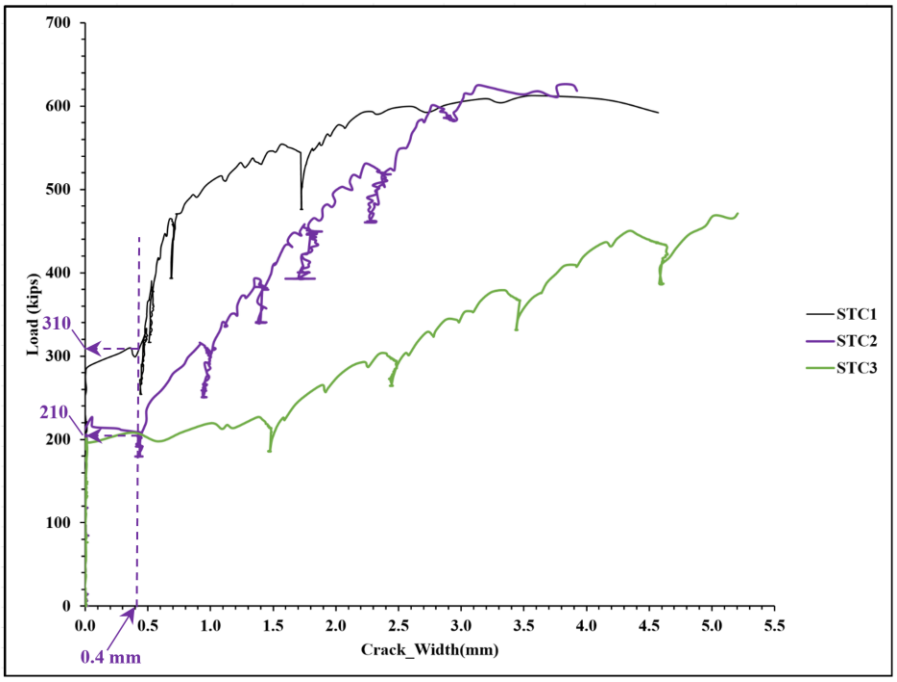

Figure 4-20: Load vs. Maximum Crack Width for specimens STC1-STC3 obtained using Digital Image Correlation (DIC).

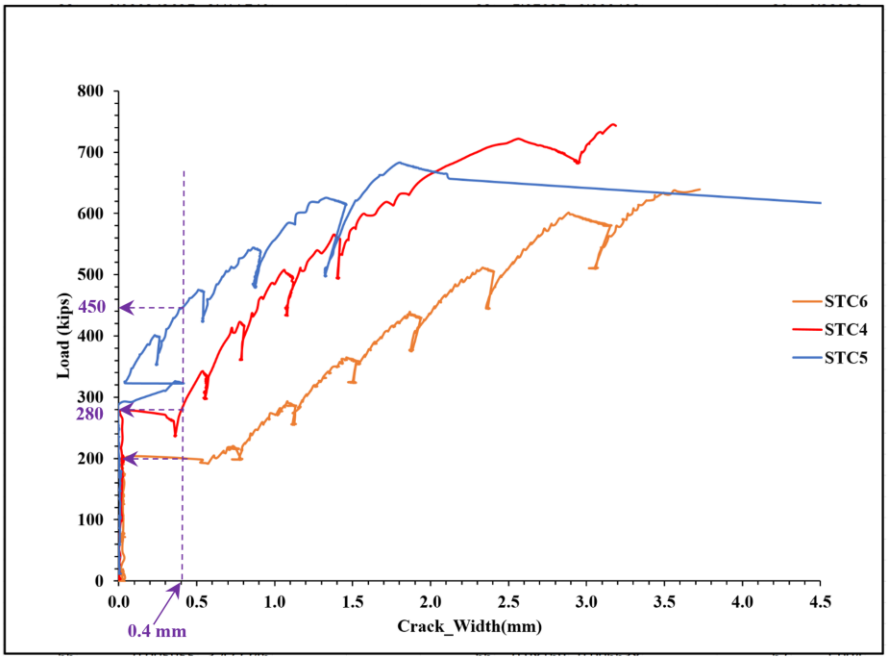

Figure 4-21:Load vs. Maximum Crack Width for specimens STC4-STC6 obtained using Digital Image Correlation (DIC).

Table 4-3: Comparison of STM predictions and loads corresponding to the crack width of 0.016 in. (0.41 mm)

Specimen	Reinforcement Ratios		Predictions			Load corresponding to manually measured experimental crack width 0.016 in. (kips)
	$\rho_v$and ρ_h (%)	ρ_l (%)	2PKT (kips)	STM AASHTO (kips)	VecTor2 (kips)	
STC1	0.30	1.75	549	510	645	440
STC2	0.13	1.75	434	365	616	260
STC3	0.00	1.75	349	365	498	180
STC4	0.30	1.57	577	511	652	360
STC5	0.13	1.57	501	368	618	350
STC6	0.00	1.57	450	368	607	225

As shown in

Table 4-3, the applied loads corresponding to a crack width of 0.016 in (0.41 mm) obtained through manual measurements. The manual measurements represent average crack widths over a small localized region, making them more representative of the actual cracking behavior. Nevertheless, the average percentage difference between the two methods across all specimens is approximately 18.2%**,** with DIC loads consistently lower. The maximum difference observed is about 29.6% for STC1, while the remaining specimens show considerably smaller deviations. This close agreement highlights that both methods provide consistent and comparable estimates for identifying the serviceability limit state, despite their inherent differences in measurement technique.

4.3 DIC Analysis

Figure 4-22-Figure 4-27 shows principal tensile strains and principal compressive strains at the peak load and at an estimate of the service load (approximately 60% of the peak load) for STC4 - STC6. The principal tensile strain plots are useful to determine the crack patterns, where the high-strain regions indicate the cracked regions. For the compressive strains, the maps show high compressive strains beneath and near the edges of the loading plates. The strains below the plate are not uniform and increase near the edges of the plate.

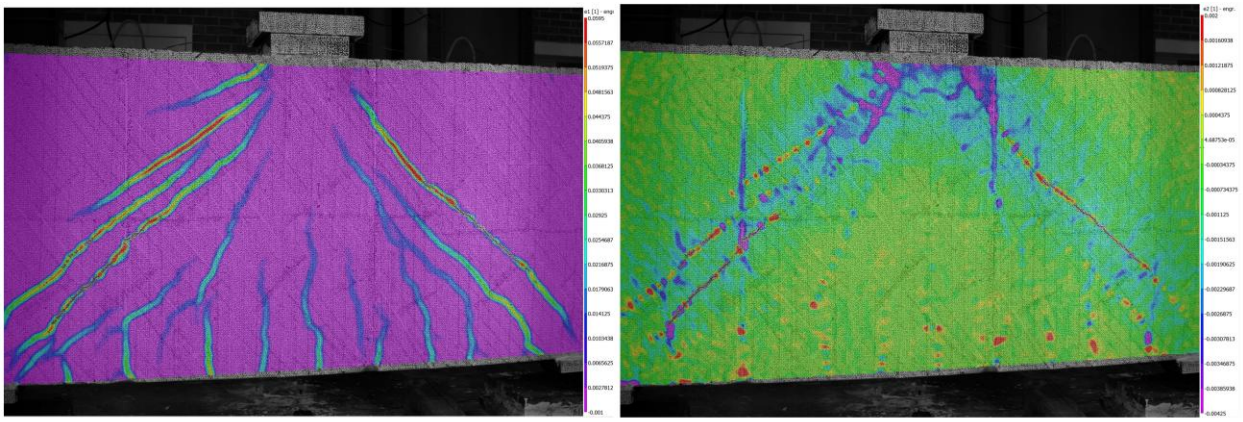

Figure 4-22: Principal tensile strains (ϵ_1) and principal compressive strains (ϵ_2) of STC4 at peak load.

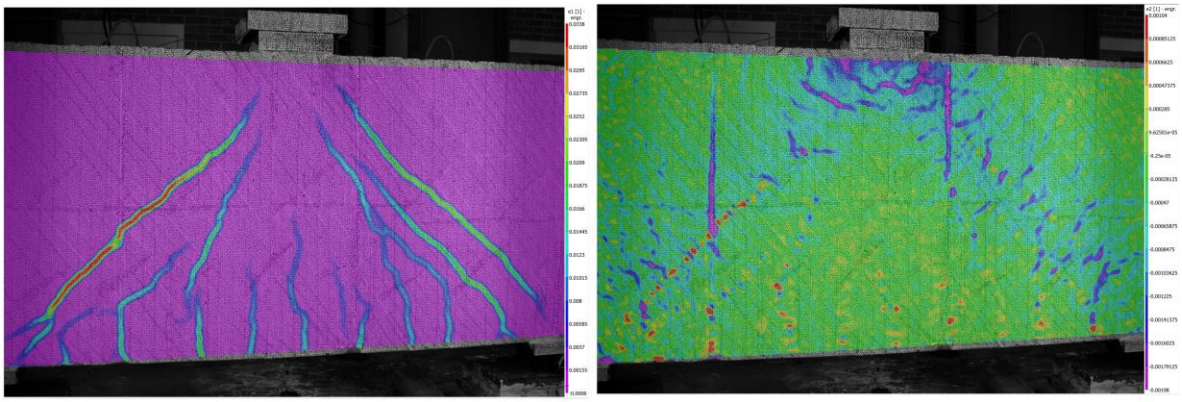

Figure 4-23: Principal tensile strains (ϵ_1) and principal compressive strains (ϵ_2) of STC4 at service load (60% of peak load).

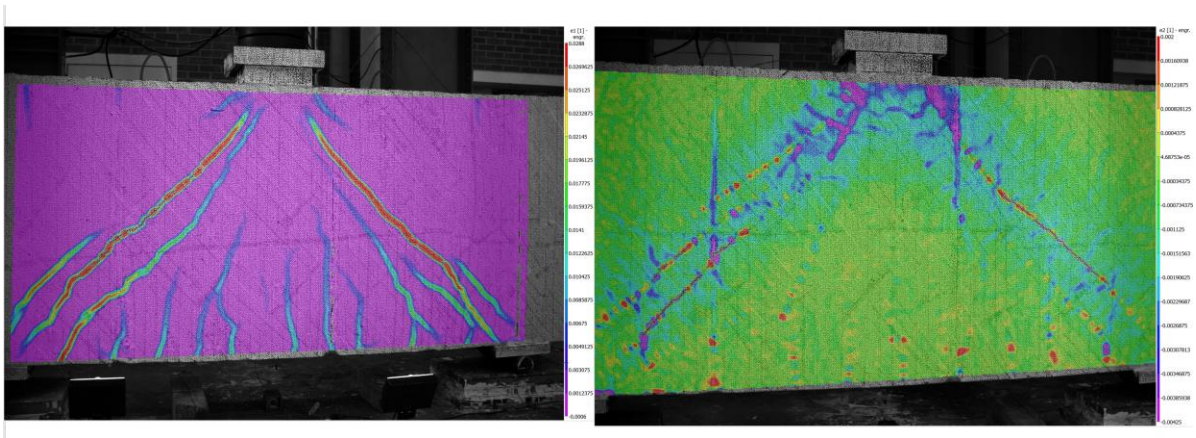

Figure 4-24: Principal tensile strains (ϵ_1) and principal compressive strains (ϵ_2) of STC5 at the peak load.

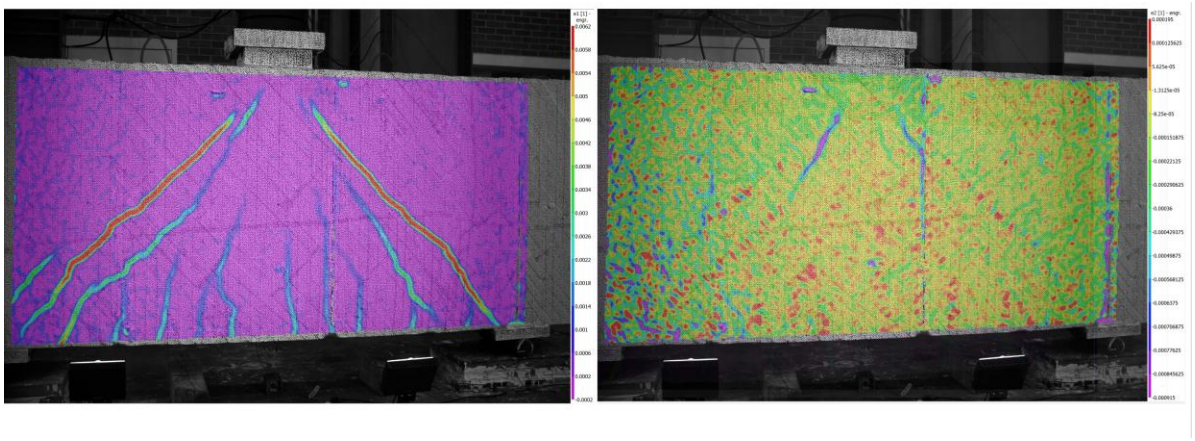

Figure 4-25: Principal tensile strains (ϵ_1) and principal compressive strains (ϵ_2) of STC5 at service load (60% of peak load).

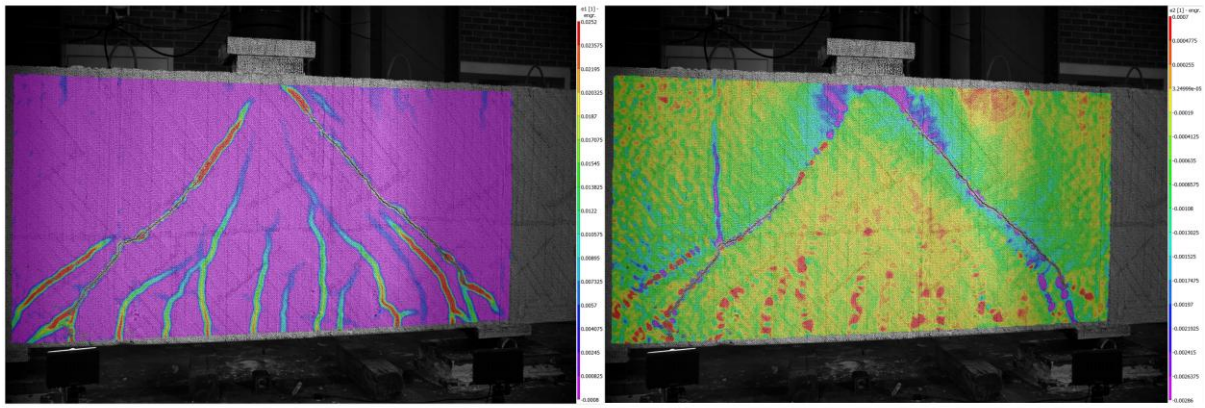

Figure 4-26: Principal tensile strains (ϵ_1) and principal compressive strains (ϵ_2) of STC6 at the peak load.

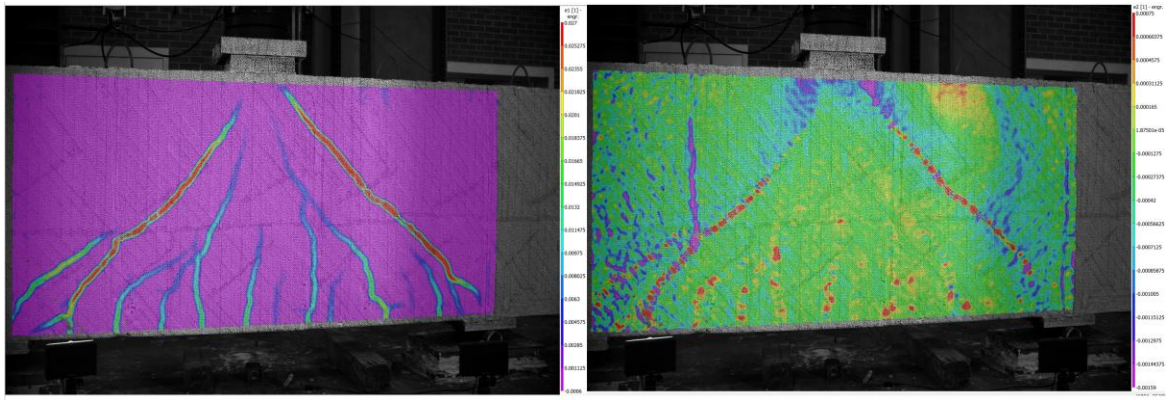

Figure 4-27: Principal tensile strains (ϵ_1) and principal compressive strains (ϵ_2) of STC6 at service load (60% of peak load).

4.4 Summary of Experimental Observations

The following provides a summary of key experimental observations from the STC test series. It highlights differences in performance at service and ultimate load levels based on varying reinforcement quantities and shear span-to-depth ratios. The summary also evaluates the performance of the members in the context of the AASHTO Strut-and-Tie Method (STM).

1. Based on the series of STC experiments, the use of minimum distributed reinforcement in shear-critical deep beams improves the shear performance of the members and their performance is reasonable compared to the AASHTO STM predictions.
    a. STC3 and STC6, which contained no orthogonal distributed reinforcement, achieved peak shear capacities of 471 kips and 633 kips, respectively—values that are 1.29 and 1.72 times greater than the shear capacities predicted by the AASHTO STM.
    b. STC2 and STC5, which contained 0.13% distributed reinforcement, achieved peak shear capacities of 625 kips and 683 kips, respectively—values that are 1.71 and 1.86 times greater than the shear capacities predicted by the AASHTO STM.
2. STC1, with a shear span-to-depth ratio of 1.81 and 0.30% orthogonal distributed reinforcement performed well compared to similar members that contain no distributed reinforcement.
    a. STC1, which had 0.30% of distributed reinforcement, achieved a peak shear force of 1.30 times STC3, which contained no distributed reinforcement.
    b. STC1 achieved a peak shear force nearly identical to that of STC2, which contained 0.13% distributed reinforcement. It is important to note that the concrete cylinder strength at the time of testing was 0.20 ksi (4.3%) higher for STC2 than for STC1.
3. STC4 with a shear span-to-depth ratio of 1.18 and with 0.30% distributed reinforcement performed well compared to similar members that contain no distributed reinforcement.
    a. STC4, which had 0.30% orthogonal distributed reinforcement, reached a crack width of 0.3 mm (0.012 in.) at 60% of the peak load and 0.7 mm (0.028 in.) at the peak load.
    b. STC4 achieved a peak shear force of 1.1 times the capacity of STC5, which contained 0.13% distributed reinforcement. It is important to note that the concrete cylinder strength at the time of testing was 0.6 ksi (10.75 %) higher for STC3 than for STC1.
4. For the STC series experiments, it was observed the transverse reinforcement yielded across the critical shear crack for the deep beams tested (see Appendix F).
5. The inclusion of orthogonal distributed reinforcement improved crack control. All the members with 0.13% or 0.30% shear reinforcement exhibited controlled distributed crack patterns.
6. For both shear span-to-depth ratios, higher transverse reinforcement led to smaller crack widths, indicating the effectiveness of distributed reinforcement in controlling cracking.
7. Beams with lower a/d ratios (1.18) exhibited smaller crack widths overall for members with the same reinforcement ratios compared to those with a higher a/d ratios (1.81). For example, STC4 (a/d = 1.18, ρ_v = 0.30%) exhibited a maximum crack width of 0.7 mm (0.028 in.) at the peak load versus STC1 (a/d = 1.81, ρ_v = 0.30%) which exhibited 0.8 mm (0.031 in.). Similarly, STC6 (no distributed reinforcement) had a crack width of 1.6 mm (0.063 in.) at the peak versus STC3 which exhibited a crack width of 4.0 mm (0.157 in.). This shows that shorter shear spans (lower a/d) results in smaller

crack widths even when no distributed reinforcement is present. It also highlights the importance of variables, other than reinforcement quantity, on crack widths.

8. A clear trend was observed in the behavior of beams STC1 through STC3, where the crack width progressively decreased with the increase in orthogonal distributed reinforcement ratio for a given load. This indicates that the presence of higher amounts of transverse reinforcement effectively controls cracks.
9. STC1 with a shear span-to-depth ratio of 1.81 and 0.30% distributed reinforcement, exhibited smaller crack widths compared to similar members without distributed reinforcement.
    a. STC1, which had 0.30% distributed reinforcement, reached a crack width of 0.35 mm (0.014 in.) at 60% of the peak load and 0.8 mm (0.031 in.) at the peak load.
    b. STC1 achieved a peak shear force nearly identical to that of STC2, which contained 0.13% distributed reinforcement. The maximum crack width of STC2 at 60% of the peak load was 0.6 mm (0.024 in.) and 1.5 mm (0.059 in.) at the peak load. At 60% of the peak load, the maximum crack width of STC2 was 66.7% larger than that of STC1. At the peak load, the crack width of STC2 was 87.5% larger than that of STC1.
    c. The maximum crack width of STC3 at 60% of the peak load was 1.5 mm (0.059 in.) and 4 mm (0.157 in.) at the peak load. The crack width of STC2 at 60% of the peak load was 0.6 mm (0.024 in.) and 1.5 mm (0.059 in.) at the peak load. At 60% of the peak load, the crack width of STC2 was 66.7% larger than that of STC1, and STC3 showed a 100% larger crack width compared to STC1. At the peak load, the maximum crack width for STC2 was 87.5% larger than that of STC1, while the maximum crack width of STC3 was 400% larger than that of STC1.
10. STC4, with a shear span-to-depth ratio of 1.18 and 0.30% distributed reinforcement, exhibited smaller crack widths compared to similar members without distributed reinforcement.
    a. STC4, which had 0.30% distributed reinforcement, reached a crack width of 0.3 mm (0.012 in.) at 60% of the peak load and 0.7 mm (0.028 in.) at the peak load.
    b. STC4 achieved a peak shear force 10.83% higher than that of STC5, which contained 0.13% transverse reinforcement. The maximum crack width of STC5 at 60% of the peak load was 0.45 mm (0.018 in.), and 1.5 mm (0.059 in.) at the peak load. At 60% of the peak load, the crack width of STC5 was 50% larger than that of STC4. At the peak load, the crack width of STC5 was approximately 114% larger than that of STC4.
    c. The maximum crack width of STC6 at 60% of the peak load was 0.95 mm (0.037 in.) and 1.6 mm (0.063 in.) at the peak load. The maximum crack width of STC5 at 60% of the peak load was 0.45 mm (0.018 in.) and 1.5 mm (0.059 in.) at the peak load. At 60% of the peak load, the crack width of STC5 was 50% larger than that of STC4, and STC6 showed a 217% larger crack width compared to STC4. At the peak load, the crack width in STC5 was approximately 114% larger than that of STC4, while the crack width in STC6 was about 129% larger than that of STC4.

5 CONCLUSION AND RECOMMENDATIONS

Reinforced concrete bridge bent caps are structural components that carry large loads over relatively short spans between columns or other supporting elements. In many cases the resulting shear span-to-depth ratios are less than 2-2.5. These short shear spans indicate that many bent caps behave as deep beams or disturbed regions, resulting in nonlinear strain distributions through the depths of the members. The strut-and-tie method (STM) is an approach that has been codified in most standards around the world and provides a basis to design disturbed regions. The STM has the advantage that it gives great flexibility to the designer as to how the internal flow of forces in a member can be designed. Multiple acceptable STM can be developed. While an advantage, this poses challenges in practice, as questions can arise as to what strut-and-tie typologies are most appropriate to begin with, which set of assumptions are a reasonable place to start and how checks be conducted for strut-and-tie models presented by others. This study aimed to summarize the literature on the design of bridge bent cap structures using the STM, identify typical reinforced concrete bridge bent caps in North Carolina that are conducive to design by the STM, develop STM templates for typical bent cap typologies, conduct experiments to explore the response of members under several variables and supplement the results with nonlinear finite element modelling.

This study summarized the relevant literature as it relates to strut-and-tie design and evaluation of bridge bent cap structures. The literature contains relevant information regarding assumptions related to items such as equivalent bearing sizes, consideration of complex nodal regions and overall strut-and-tie layout. The literature reviewed includes codes and standards, technical reports, journal papers, peer department of transportation studies and federal guidance documents.

The study identified typical bridge bent cap typologies in North Carolina conducive to design using the STM. Twelve typologies and sub typologies were identified. These represent a breadth of typologies the NCDOT often utilizes. Examining these typologies provides the basis upon which the strut-and-tie models for other typologies and sub typologies can be developed. These twelve typologies consist of symmetric and asymmetric loading conditions for two, three and four column bent caps. The symmetrical and asymmetrical conditions arise when the loading from the superstructure induces symmetric or asymmetric loading conditions on the bent cap. These different loading conditions result in different typologies for the strut-and-tie models. Namely, the arrangement of struts and ties change.

These templates were developed to input the loads, properties, and geometric conditions and output checks for compliance consistent with the AASHTO LRFD strut-and-tie provisions and tie reinforcement required. The process is initiated by selecting an appropriate strut-and-tie typology from a predefined set, based on the given loading and support conditions. Structural dimensions, material strengths, support and bearing dimensions, and applied loads are entered into the template. The templates were also developed to conduct the internal analysis of forces in the strut-and-tie model truss elements. To allow the NCDOT to reproduce the calculations presented and extend the methods suggested, the process was made as transparent as possible. This was accomplished by solving the truss using the method of joints, set up in a matrix of equations. In situations where the bent cap is statically indeterminate, the reactions should be input from a structural analysis conducted by the designer using an elastic model of the bent cap with the given applied loads. Additionally, in many structural analyses of the bent caps, there is often an assumption that the

supporting elements can transmit moments. To ensure a consistent load path between the analysis conducted by the designer and the strut-and-tie model, those moments should be accounted for in the strut-and-tie model. This has been incorporated into the templates. That is, each supporting element can carry two reactions separated by a distance; thus, an axial load and moment can be transmitted into the supporting elements. Once the model is analyzed, its validity is verified through nodal checks in accordance with AASHTO LRFD provisions, and the necessary longitudinal and transverse reinforcement is determined.

Six large-scale experiments were conducted to investigate different geometric conditions and reinforcement ratios on the performance of representative portions of bent caps at service and ultimate conditions. A series of experiments showed that using minimum distributed reinforcement improves the shear performance of shear-critical deep beams. Members without orthogonal distributed reinforcement, STC3 and STC6, achieved peak shear capacities of 471 kips and 633 kips, 1.29 and 1.72 times greater than AASHTO STM predictions. With 0.13% transverse reinforcement, STC2 and STC5 reached 625 kips and 683 kips, 1.71 and 1.86 times the AASHTO STM predictions. STC1, with a shear span-to-depth ratio of 1.81 and 0.30% reinforcement, reached 1.30 times the strength of STC3 and was similar in strength of STC2. Similarly, STC4, with a shear span-to-depth ratio of 1.18 and 0.30% reinforcement, achieved 1.20 times the capacity of STC6 and 1.10 times that of STC5. These results in this experimental series indicate the effectiveness of transverse and horizontal reinforcement in enhancing shear performance but also indicate that in terms of ultimate strength there is not a significant increase in strength for members compared to when approximately 0.13% of orthogonal distributed reinforcement is used.

The performance at service loads, however, is influenced by the amount of orthogonal distributed reinforcement. Specifically, at approximately 60% of the peak load, the crack widths in members without transverse reinforcement, STC3 and STC6 had significantly larger shear crack widths than STC2 and STC5, which contained 0.13% distributed reinforcement or STC1 and STC4 which contained 0.30% reinforcement. For scenarios where 0.13% or 0.30% reinforcement were used, the cracks were well controlled. More distributed reinforcement resulted in multiple smaller cracks rather than fewer wider cracks. It was also observed that members with smaller shear span-to-depth ratios, exhibited smaller crack widths at service than similarly reinforced members with larger shear-span-to-depth ratios.

The six experiments were compared to strut-and-tie models developed based on the AASHTO LRFD STM. The results indicate that the AASHTO method conservatively predicted the strength for the members in this series. Specimens STC3, STC6, STC2 and STC5 contain less than 0.30% distributed reinforcement. As a result AASHTO LRFD suggests a nodal efficacy factor of 0.45 should be used for these members. When this reduced value is applied, AASHTO LRFD provides very conservative results for the prediction of ultimate strength of the members. When this reduced value is ignored and the nodal efficiency factors are applied as if minimum reinforcement was included, the AASHTO LRFD still provides conservative predictions for the ultimate strength of the specimens tested.

The six large-scale experiments conducted were also compared to models developed in VecTor2. The nonlinear finite element program VecTor2 was able to predict the capacity of the experiments with a mean test-to-predicted ratio of 1.03 and a coefficient of variation of 9%. The results indicate the program is

reliably able to predict the response of these disturbed regions which represent typical bent caps in North Carolina.

VecTor2 was also used to evaluate the performance of designs generated from the templates. Appendix C provides several examples of typical bent caps designed using the appropriate template typology. The resulting design was then modelled in VecTor2 to determine if the design adequately performed. In all the cases described in Appendix C the results indicate that the templates provided for the typical typologies identified provide conservative designs.

5.1 Recommendations

The recommendations associated with this study can be categorized into three areas: general recommendations, recommendations regarding strut-and-tie modelling and associated assumptions and recommendations related to minimum reinforcement requirements. The following are the recommendations based on the results of the study, experimental investigation and modelling conducted.

5.1.1 General Recommendations

1. Bent caps in North Carolina often have shear span-to-depth ratios less than 2 or 2.5 and are conducive to design using the AASHTO LRFD STM.
    a. In scenarios where shear span-to-depth ratios exceed 2 or 2.5 it may be more appropriate to apply sectional methods and treat the member as slender (e.g., not a disturbed region).
2. The templates outlined for the twelve typologies and sub-typologies identified provide a basis upon which strut-and-tie designs and evaluations can be conducted.
    a. The templates and typologies identified represent a broad range of scenarios that can be extended or modified to accommodate other bent cap arrangements.
3. The AASHTO LRFD STM appears to give conservative designs for the ultimate capacity of members. However, consideration of the desired service performance is needed as the STM method does not guarantee any particular service level performance. It is recommendations, to consider the reinforcement provided to ensure adequate performance at service loads is achieved (see recommendations below).
4. The use of the strut-and-tie method for the design of the bent caps should be conducted in a manner that is consistent with the assumed load path in the structure.
    a. Consistent assumptions regarding the superstructure loads, and how the loads are transmitted into the columns or other supporting elements is needed.
    b. If the structural analysis assumes the columns or other supporting elements transmit moments at the bent cap interface, this should be considered in the strut-and-tie model.
5. Templates were developed as a part of this study to conduct the analysis of the forces in the strut-and-tie model as well as conducting nodal checks and proportioning of the longitudinal and transverse reinforcement. A significant amount of effort was placed on conducting the analysis of

the forces for the strut-and-tie model so that the calculations are transparent. The NCDOT may however, wish to conduct this step manually or using computer software. In this case the development of strut-and-tie models for different typologies and scenarios becomes an application of the nodal checks and related checks discussed in this study. These checks are direct extensions of those provided and it is expected that these can be conducted without significant effort or re-development of templates. That is, once designers are comfortable laying out the arrangement of the struts and ties, the corresponding checks can be readily conducted. It is expected that the process will be straightforward for the NCDOT to develop their own models moving forward.

5.1.2 Strut-and-Tie Modelling and Recommended Assumptions

1. The flowchart reproduced and shown in Figure 5.1 serves as a recommended guide for integrating STM into the existing design process followed by NCDOT. See Appendix D for additional details.
2. Strut-and-tie models can be developed using the template models, or other strut-and-tie models can be developed.
3. Factored loads should be applied onto the strut-and-tie model.
4. All resistance factors should be applied for ties and struts.
5. Every strut-and-tie model must satisfy equilibrium.
    a. Envelope forces and loading generally, cannot be used with strut-and-tie models.
6. In scenarios where strut-and-tie models are statically indeterminate:
    a. An elastic analysis of the bent cap is recommended to assign the reaction forces. That is, the bent cap can be assumed to be a linear elastic beam with multiple supports and reasonable stiffness assumptions. Once the reactions are determined the forces in the struts and ties can be calculated without any assumption of their stiffness.
    b. Assumptions for how the flow of forces occurs, other than the elastic analysis of the bent cap can be assumed. However, it should be emphasized that any assumptions made for the distribution of the reactions, including the moments transmitted to the supporting elements should be consistent with the load path assumptions in the structural analysis of the entire structure.
    c. It is not recommended to assume strut or tie stiffnesses to solve indeterminate trusses in strut-and-tie models using stiffness methods.
7. In scenarios where moments and vertical loads are transmitted at the bent cap and supporting element interface, it is recommended this be modelled by representing the vertical load and moment by two forces separated by a flexural lever arm. The two forces separated by the lever arm should be statically equivalent to the single vertical load and moment. The flexural lever arm can be any reasonable assumption for the flexural lever arm in the column or supporting element (for example 7/8d may be an appropriate approximation).
8. In scenarios where multiple bearing pads are used through the thickness of the bent cap (e.g., from multiple girders supported on either side of the bent cap), the multiple bearings can be idealized as a single bearing.
    a. In scenarios where there can be significant differences in bearing loads through the width of the bent cap, significant torsions could arise in the bent cap. In these scenarios it is

recommended that the bent cap be divided (along its width) and two strut-and-tie models be developed one for each side of the bent cap. In scenarios where torsions are not significant, a single model is recommended.

9. In scenarios where non-rectangular bearing pads or supporting elements, such as circular columns are used, it is recommended an equivalent area rectangle or square be utilized.
10. In many scenarios, particularly in members with overhangs or multiple spans, the top or bottom chord of the strut-and-tie model of the bent cap can switch from compression to tension. So that more complex strut-and-tie models are not needed at these transition points, it is recommended a constant top chord and bottom chord position is used for the entire length of the bent cap.
11. Consistent with AASHTO LRFD, it is recommended that ties and/or struts are no less than 25 degrees apart.
12. It is recommended to apply all the AASHTO LRFD nodal checks and tie checks as outlined in in AASHTO LRFD and described in this study.
13. It is recommended to ensure that all reinforcement provided is adequately detailed and developed as required by AASHTO LRFD.
14. It is recommended, that while the proposed templates can be used, it may be more efficient for the templates provided to be converted into scripts that are consistent with the internal NCDOT processes. This may be particularly useful if design checks are needed for many load cases that arise from structural analysis software.

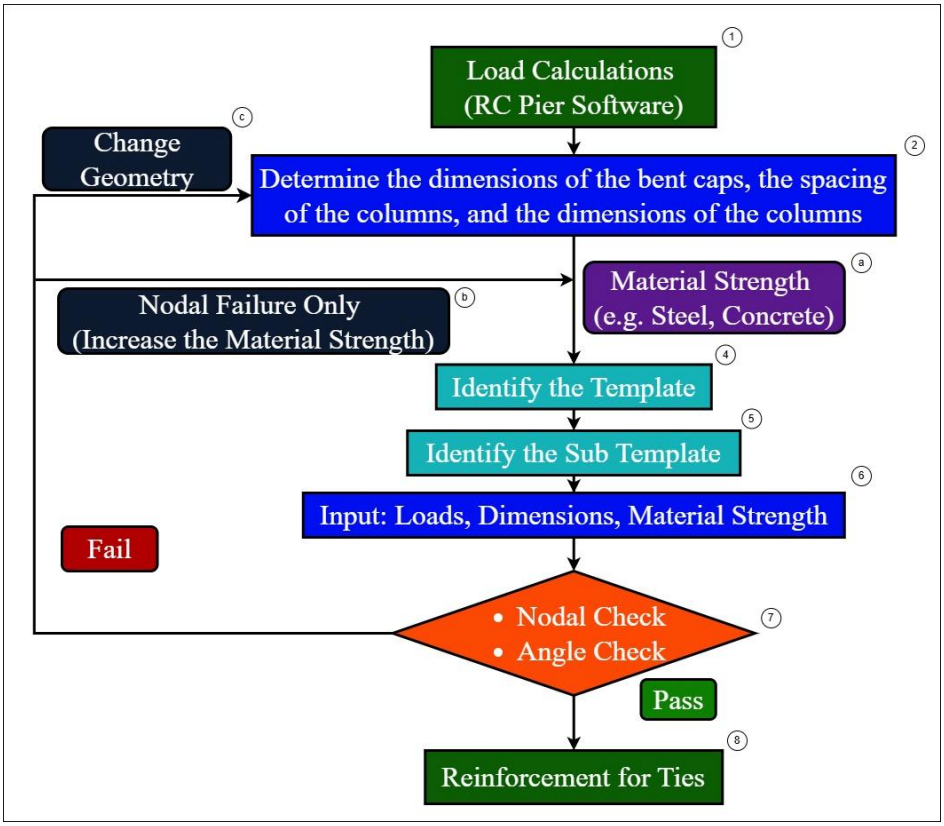

Figure 5-1: Design flow chart.

5.1.3 Minimum Reinforcement Requirement Recommendations

As a part of this study, the recommend minimum reinforcement requirements relating to the strut-and-tie provisions were investigated. The experimental series explored the use of no distributed reinforcement, 0.13% orthogonal reinforcement and 0.30% orthogonal reinforcement in both the vertical and horizonal directions. Based on the review of the literature, experimental results, and analytical modeling the following are recommendations related to minimum distributed reinforcement in both orthogonal directions.

1. In the design of bent caps using AASHTO LRFD STM, it is generally recommended to use the 0.30% minimum required reinforcement so that the larger nodal efficiency factors in AASHTO LRFD Table 5.8.2.5.3a-1 can be employed. It is expected that this will give conservative designs under ultimate limit state conditions. This quantity of reinforcement will assist in crack control under service conditions.
    a. In members that are not heavily loaded in shear, the designer can reduce this quantity of distributed reinforcement, and use the lower nodal efficiency factor (a value of 0.45) as described in the AASHTO LRFD STM provisions.
2. The Manual for Bridge Element Inspection (Federal Highway Administration, 2019) for reinforced concrete bent caps suggests crack widths as large as 0.0625 in. – 0.125 in. (1.6 mm to 3.2 mm) corresponds to "narrow to moderate" crack widths, resulting in a Condition State less than 3. Shear cracks in disturbed regions can be come concerning at lower values. Additionally, ACI 224R-1 (ACI 2007) guidance documents suggest that crack widths near service loads should be limited to approximately 0.016 in. (0.40 mm). Based on the results of this study, a minimum quantity of distributed reinforcement in both orthogonal directions of approximately 0.13% to 0.30% is recommended to achieve this level of service for members designed using the AASHTO STM.
    a. It should be noted that as the shear span-to-depth ratio, concrete strength, quantity of flexural reinforcement, concrete clear cover, reinforcement bar sizes and other member specific factors change, the minimum amount of distributed reinforcement to achieve the desired performance at service loads may also change.
3. In evaluating existing members that may contain less than 0.30% distributed reinforcement, but more than zero distributed reinforcement, the results of this study indicate that it may be appropriate to use the nodal factors in AASHTO LRFD Table 5.8.2.5.3a-1, rather than using a value of 0.45. This could be considered in evaluating existing bent caps or bent caps that, for example, may have been designed using sectional methods and contain lower quantities of transverse reinforcement (approximately 0.13%).

6 IMPLEMENTATION AND TECHNOLOGY TRANSFER PLAN

The deliverables for this project included a final report, technical presentation, lecture, workshop training, software tools, data, and user manuals. The manuals, provided in the appendices, demonstrate how to use the developed templates. The software is delivered as a series of Excel spreadsheets, enabling users to input design parameters and receive outputs and verification checks in accordance with the AASHTO LRFD strut-and-tie design methodology. The workshops, training materials, and manuals are intended to help users understand, apply, and potentially expand the use of these templates within their own design workflows.

The findings of this research provide a foundation for NCDOT to implement and apply the AASHTO LRFD strut-and-tie method for the design and assessment of bridge bent caps in North Carolina. The study also offers valuable insights into the behavior of bent caps under service and ultimate loads, particularly in relation to different levels of transverse reinforcement. These insights inform decisions on minimum reinforcement requirements and serviceability performance. The tools and guidance developed through this project are intended for use in both new designs and the evaluation of existing structures, and they are expected to influence NCDOT policy on bent cap design and assessment. The templates offer an efficient alternative design method that can be applied in scenarios where they offer structural or economic benefits.

Implementation of this research is expected in four key areas. First, it will support the training of engineers in the application of the strut-and-tie method, using the provided report and templates for hands-on learning. Second, the methodology can guide the development of additional templates for other structural configurations, using Excel or similar tools. Third, the current templates can be used for the design and evaluation of bent caps that match the typologies identified in this study. Fourth, the approach may be incorporated into automated workflows, allowing for integration into NCDOT's standard design processes.

The success of this project will be measured by the extent to which the strut-and-tie method is used to more accurately represent internal force flow in bent caps. This ultimately impacts safety, as the method ensures proper performance under service and ultimate loads. For heavily loaded bent caps, the method may also reduce the amount of required reinforcement, alleviating congestion and lowering material and construction costs. In some cases, it may influence the geometry of the bent caps, such as their depth, further improving efficiency, constructability, and overall economy.

7 CITED REFERENCES

1. AASHTO. (2020). *LRFD Bridge Design Specifications and Commentary*, Ninth Edition, Washington, DC: American Association of State Highway Transportation Officials, 1912 pp.
2. American Concrete Institute. (2007). *ACI 224R-01: Control of Cracking in Concrete Structures* (Reapproved 2007). Farmington Hills, MI: American Concrete Institute.
3. ACI Committee 318. (2019). *Building code requirements for structural concrete (ACI 318-19) and commentary (ACI 318R-19)*. Farmington Hills, MI: American Concrete Institute.
4. American Concrete Institute. (2002). *Examples for the design of structural concrete with strut-and-tie models (ACI SP-208)*. Farmington Hills, MI: American Concrete Institute.
5. American Concrete Institute, Committee 445. (2021). Strut-and-Tie Method Guidelines for ACI 318-19—Guide (ACI PRC-445.2-21). Farmington Hills, MI: American Concrete Institute. ISBN 978-1-64195-146-3.
6. American Society of Civil Engineers. (2025). Report Card for America's Infrastructure. ASCE, 25 Mar. 2025, https://infrastructurereportcard.org/.
7. Brown, M. D., Sankovich, C. L., Bayrak, O., Jirsa, J. O., Breen, J. E., & Wood, C. L. (2006). *Design for shear in reinforced concrete using strut-and-tie models*. Austin, TX: Center for Transportation Research, Bureau of Engineering Research, University of Texas at Austin. (Texas Department of Transportation, Research and Technology Implementation Office).
8. Collins, M. P., & Mitchell, D. (1997). *Prestressed concrete structures*. Toronto, Canada: Response Publications.
9. CSA (Canadian Standards Association). (2004). *Design of concrete structures* (CSA-A23.3-04). Mississauga, Ontario: Canadian Standards Association.
10. CSA (Canadian Standards Association). (2019). *Design of concrete structures* (CSA-A23.3:19). Mississauga, Ontario: Canadian Standards Association.
11. Federal Highway Administration. (2019). *Manual for bridge element inspection* (2nd ed., Publication No. FHWA-HIF-20-002). U.S. Department of Transportation. https://www.fhwa.dot.gov/bridge/pubs/hif20002.pdf.
12. Frosch, R. J., Kreger, M. E., Fanous, F. S., & Abu-Hawash, A. (2012). Strut-and-Tie Model Design Examples for Bridge Structures (NCHRP Report 681). Washington, D.C.: Transportation Research Board of the National Academies. ISBN 978-0-309-15538-9.
13. Hooke, R. (1678). *Lectures de potentia restitutiva, or of spring: Explaining the power of springing bodies; to which are added some collections*. London: J. Martyn.
14. Kani, M. W., Huggins, M. W., & Wittkopp, R. R. (1979). In *Kani on shear in reinforced concrete* (p. 225). Toronto, Canada: University of Toronto, Department of Civil Engineering.
15. Kelly, D. W., & Elsley, M. (1995). A procedure for determining load paths in elastic continua. *Engineering Computations*, 12(5), 415–424. https://doi.org/10.1108/02644409510799721.

16. Leonhardt, F., & Walther, R. (2005). *The Stuttgart shear tests* (Report No. 318). Stuttgart, Germany: University of Stuttgart.

17. Liang, Q. Q., Xie, Y. M., & Steven, G. P. (2001). Generating optimal strut-and-tie models in prestressed concrete beams by performance-based optimization. *ACI Structural Journal*, 98(2), 226–232. https://doi.org/10.14359/10191.

18. Mihaylov, B. I., Bentz, E. C., & Collins, M. P. (2013). Two-parameter kinematic theory for shear behavior of deep beams. *ACI Structural Journal*, 110(3). https://doi.org/10.14359/51685602.

19. Nawy, E. G. (2006). *Reinforced concrete: A fundamental approach* (5th ed.). Upper Saddle River, NJ: Prentice Hall.

20. North Carolina Department of Transportation. (2021, April 8). *North Carolina bridge information*. NCDOT. https://www.ncdot.gov/initiatives-icies/Transportation/bridges.

21. Palipana, D. K. and Proestos, G. T. (2024), "Experimental Investigation of Deep Beams with High-Strength Headed Shear Reinforcement, Part I," ACI Structural Journal, V. 121, No. 3, May 2024. doi: 10.14359/51740486.

22. Perkins, S. M. (2011). *Shear behaviour of deep reinforced concrete members subjected to uniform load* (Master's thesis). University of Toronto.

23. Proestos, G. T., Palipana, D. K., & Mihaylov, B. I. (2021). Evaluating the shear resistance of deep beams loaded or supported by wide elements. *Engineering Structures*, 226, 113668. https://doi.org/10.1016/j.engstruct.2020.111368.

24. Qambar, M. (2020). *Effect of wide loading elements and shear span-to-depth ratio on the behavior of shear critical reinforced concrete deep beams* (Master's thesis). North Carolina State University.

25. Trandafir, A. N., Palipana, D. K., Proestos, G. T., & Mihaylov, B. I. (2022). Framework for crack-based assessment of existing lightly reinforced concrete deep members. *ACI Structural Journal*, 119(1), 255–266. https://doi.org/10.14359/51733143.

26. Vecchio, F. J. (2000). Disturbed stress field model for reinforced concrete: Formulation. Journal of Structural Engineering, 126(9), 1070–1077. https://doi.org/10.1061/(asce)0733-9445(2000)126:9(1070).

27. Vecchio, F. J., & Collins, M. P. (1986). The modified compression-field theory for reinforced concrete elements subjected to shear. *ACI Structural Journal*, 83(2), 219–231. https://doi.org/10.14359/10416.

APPENDIX

A LITERATURE REVIEW

A.1 B and D Regions in Concrete Beams

Reinforced concrete deep beams are common structural elements used in bridge substructure components such as bent caps. As a result of concentrated loads and geometric properties, the strain distribution in deep members does not remain linear and shear strains govern the response. Since plane sections do not remain plane, sectional design and analysis methods may not result in an accurate characterization of the member response. Members with shear-span-to-depth ratios less than approximately 2 or 2.5 often exhibit this type of behavior. The shear span is the distance between points of application of concentrated load to its adjacent reaction force/support, and clear span is the distance between supports/columns.

Typically, reinforced concrete members are designed to resist shear and flexural forces based on the assumption that the strains vary linearly through the depth of the section. This assumption is based on Hooke's hypothesis (Hooke 1678), also known as the beam theory, where the mechanical behavior of a beam is commonly determined by assuming that plane sections remain plane. The regions where the strain distribution is linear are known as B regions (i.e., the region where the beam theory remains valid). In B regions, the internal state of stresses can be determined from equilibrium and compatibility conditions at a discrete cross-section. Therefore, the design of these regions is often referred to as sectional design, and it employs sectional design methods. Methods used for sectional designs are discussed in subsequent sections.

In contrast, D regions are regions where the nonlinear strains through the depth of the member and shear strains dominate the behavior. In these D regions, plane sections do not remain plane, and more advanced approaches are needed to conduct design or analysis. Nonlinear strain distributions are caused by abrupt changes in geometry or loading conditions. Localized effects of a concentrated load or geometric discontinuity have been observed to have an effect on the strain distribution for about one member depth, d, away from a discontinuity (St. Venant's principle). For this reason, D regions extend approximately one member depth from the point of change in the load or abrupt change in the geometry. Deep beams are often comprised of both a load and support discontinuity. Therefore, in cases where the load is a point load, nonlinear behavior can be expected when disturbed regions merge with each other; in other words, when the load point is located less than about twice the member depth, $2d$, away from the support. Figure A.1.a depicts some common examples of geometric discontinuities, and Figure A.1.b provides some examples of static discontinuities.

A.2 Deep Beams – D Regions

Deep beams are widely used in load-distributing elements and are commonly encountered in bridges and high-rise buildings. They are often used for transfer girders, bent caps, cross beams, corbels, etc. Figure A-1.a and Figure A-1.b show a deep beam transferring loads from above to the supporting columns. Due to changes in the column layout on upper floors, deep beams are becoming increasingly popular in

condominium apartments and commercial buildings. Figure A-2.a and Figure A-2.b show a hammer head pier where deep beams are used.

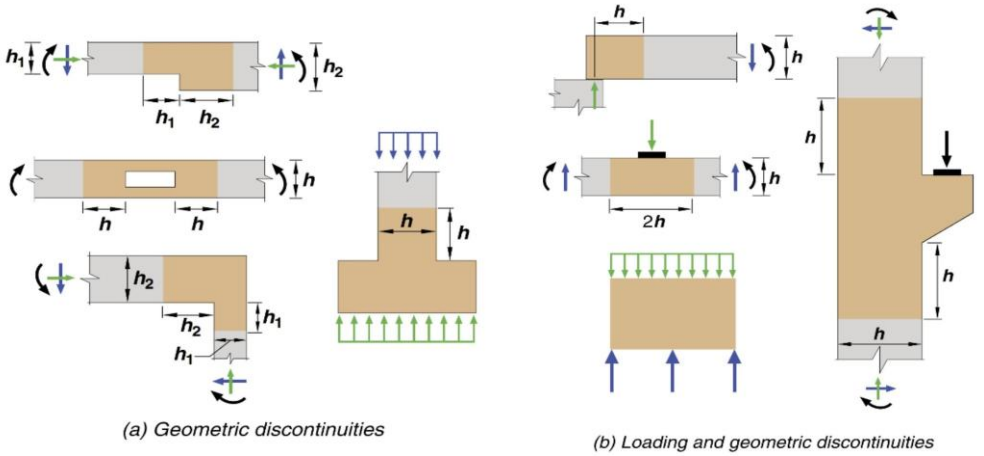

Figure A-1: a: Geometric discontinuity and b: Static/geometric discontinuities (ACI 318-19 Fig R23.1).

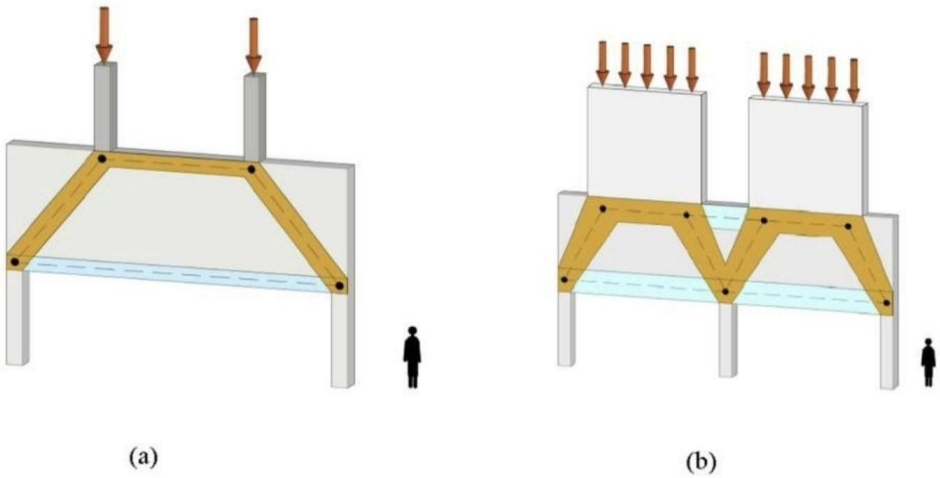

Figure A-2: a: Application of deep beams: Transfer beam supporting columns and b: Application of deep beams: Transfer girder supporting Walls (Proestos, Palipana, Mihaylov 2021)

Bent caps (also known as pier caps) are widely used in bridges, and various types of bent caps exist. Bent caps can be categorized based on materials, load transfer mechanisms, and shapes. Common bent caps include cantilever bent caps, column bent caps, solid bent caps, and hammerhead bent caps. Figure A-3 shows a hammerhead bent cap transferring the loads from the girders above to the supporting pier. Figure A-4 shows a two-column bent cap from the Marc Basnight Bridge, NC, with the loads from the supported girders and reactions (idealized as point loads).

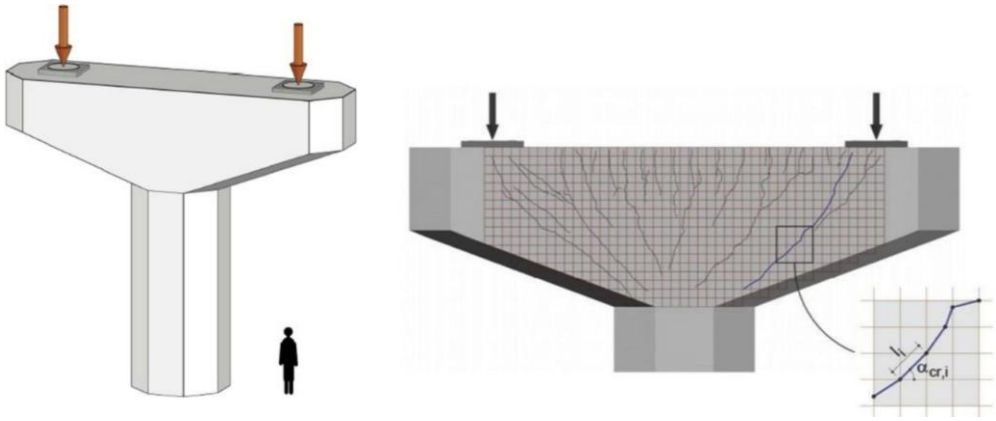

Figure A-3: a: Hammerhead pier cap and b: Measured crack shape in the pier cap (Trandafir, Palipana, Proestos, Mihaylov, 2022).

Figure A-4: Bent cap of Marc Basnight Bridge, NC, and idealization of loads.

In deep beams, the strain distribution across the section does not remain linear, and shear deformations that are neglected in traditional beam theory, govern the response of deep beams. Figure A-5.a shows the linear distribution of strain in a slender beam, and Figure A-5.b depicts the nonlinear distribution of strain across the cross-section of a deep beam. The nonlinear behavior of such elements necessitates a detailed-local design rather than a sectional design. Figure A-6 shows the variation of stress trajectories of a continuous beam under a uniformly distributed load.

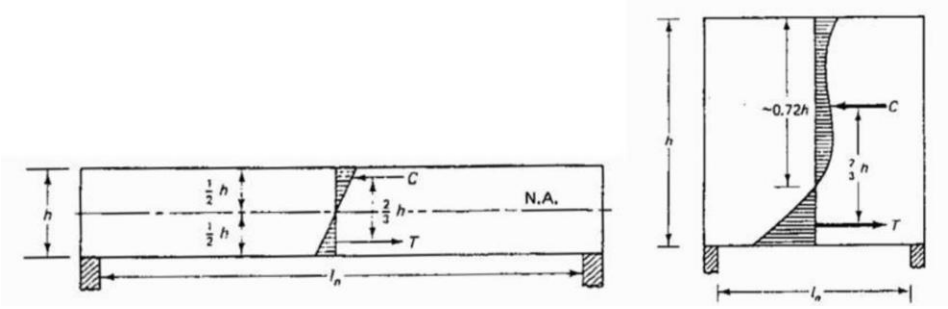

Figure A-5: a: Linear distribution of strains in a Bernoulli's beam (Nawy 2006 Fig 6.13) and b: Nonlinear distribution of strains in a deep beam (Nawy 2006 Fig. 6.13).

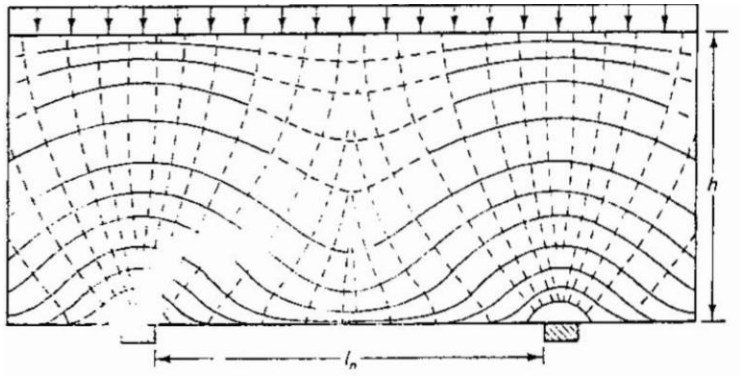

Figure A-6: Stress trajectories of a continuous beam under uniformly distributed load (Nawy 2006 Fig. 6.15).

The Canadian Standard CSA A23.3-19 states that flexural members with a clear span to an overall depth ratio of less than 2 shall be designed as deep beams, and the nonlinear distribution of strains should be considered (CSA 2019). *Figure 1-2* illustrates the effect of the shear span-to-depth ratio on the shear strength of the beams. As discussed earlier, a sharp increase occurs when the shear span-to-depth ratio is reduced below 2.5-3. When the shear span-to-depth ratio exceeds this range, shear resistance increases due to arch action. When the shear-span-to-depth ratio is high (as in slender beams), sectional methods are used for the design, whereas tools such as the strut-and-tie method are used and are more efficient when the shear-span-to-depth ratio is small.

A.3 The Strut-and-Tie Method

The Strut-and-Tie Method (STM), which is based on a lower bound approach, is more efficient at capturing the flow of forces in deep concrete members than sectional methods. The STM has been adopted into several design codes, including AASHTO LFRD, ACI 318, and CSA A23.3. Figure A-7 compares the shear strength predictions of various codes using sectional methods and the STM. AASHTO LRFD allows the use of strut-and-tie procedures for the design of these members (AASHTO, 2020). The STM takes advantage of the

direct strut action that occurs in deep beams, which is not accounted for in sectional methods. This means that designs can be more efficient and require smaller depths, less longitudinal reinforcement, or less transverse reinforcement. There are many advantages to using strut-and-tie procedures as they are general in nature and give designers significant flexibility. Oftentimes, multiple design alternatives can be developed and are considered acceptable. This is particularly true in situations with multiple supporting elements, where the support reactions are statically indeterminate. However, this can make verifying unique engineering calculations or design alternatives more difficult.

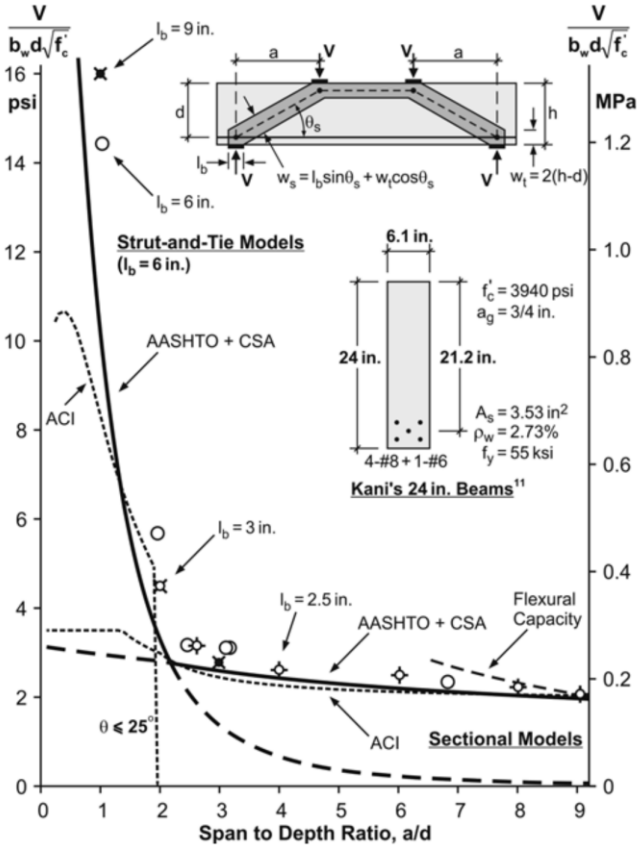

Figure A-7: Effect of shear-span-to-depth ratio on the shear strength of the beam based upon Kani's experiments (1979). The picture is adopted from (Mitchel and Collins 1997).

A.3.1 Description and theory of strut-and-tie methods

A strut-and-tie model idealizes the complex flow of stresses in a concrete member as axial elements. Concrete struts resist the compressive stress fields, and reinforcing steel ties resist the tensile stress fields. Struts and ties intersect at regions called nodes. Nodes are named based on the nature of the elements that frame them. Nodes also define the zone where the forces in the struts and ties are anchored. Loads are idealized as point loads or as a series of point loads (as in the case of uniformly distributed loads) and are transferred to the struts through nodes. The angle of struts, the types of struts, and the ties are completely dependent on the load path assumed. As mentioned earlier, the STM allows engineers to select any feasible

typology of struts and ties that satisfy equilibrium. This leaves designers and engineers a significant amount of flexibility in design. Although there may be multiple acceptable designs, not all designs are equal. Since the STM provides many load path solutions, selecting an efficient strut-and-tie model is crucial. The load path needs to be selected keeping in mind the efficiency of the strut-and-tie model. As an example, one can use direct struts, as shown in Figure A-8.a or all of the transverse steel can be grouped into a single stirrup and represented as a single tie at the middle of the clear span (see Figure A-8.b). This second option will split the direct compression strut into two separate struts, increasing the angle of the bottom diagonal strut and its capacity. These are just two of the ways strut-and-tie models can be constructed for deep beams with transverse reinforcement. In general, as long as the stresses, limit states, and static equilibrium of the members are satisfied, and the direction of the internal truss follows the stress fields, the solution is viable.

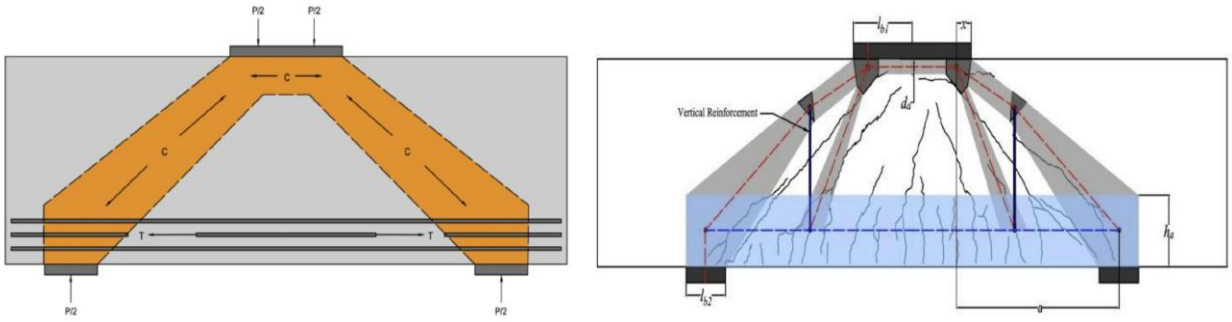

Figure A-8: a: Strut-and-tie model of a deep beam without transverse reinforcement and b: Strut-and-tie model of a deep beam with transverse reinforcement (Qambar 2020).

Selecting a feasible and efficient strut-and-tie model requires engineering judgment and experience. An efficient strut-and-tie model is one that carries the highest load among many other possible typologies. This means that even though a selected truss arrangement satisfies the equilibrium condition, the selected truss might not be the most efficient solution. Proportioning is the process of defining the cross-sectional areas and strength that is required to resist the assumed load through the assumed load path. Proportioning of ties, or finding the tension force carried by the reinforcement, is relatively straightforward and calculated by multiplying the area of steel by the yield stress (with appropriate reduction factors). However, proportioning the size of the nodes and the compression strut is not as straightforward and is discussed in detail in section A.3.4.

A.3.2 Selecting the geometry and shape of the strut-and-tie model

The selection of the shape and geometry is important to ensure an efficient flow of forces. Developing of STM using conventional methods involves an iterative process and judgment of the designer (He, Liu, Wang, & Ma 2020, Kelly & Elsley 1995). Recently, various techniques have been developed to select the most suitable strut-and-tie arrangement for a particular structure under a particular load configuration (see Figure A-9).

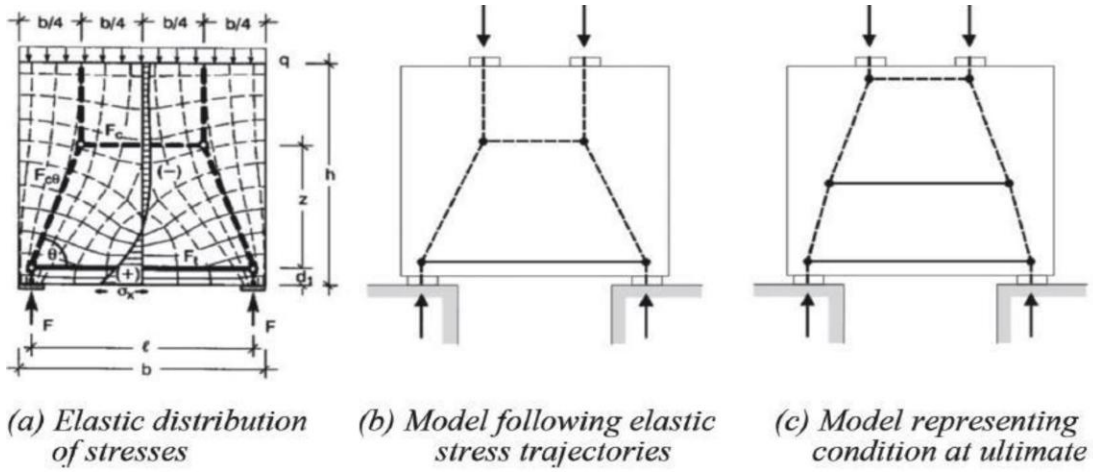

Figure A-9: Possible models of strut-and-tie designs (image adapted from Leonhardt & Walther 2005).

Recent advancements in computational power have significantly reduced the time and resources required for nonlinear analysis, improving its efficiency. Finite element software, such as VecTor2, can now handle nonlinear analyses of concrete structures with complex geometries. While these nonlinear models can provide valuable insight into the behavior of structures, including crack patterns and load paths, they are often not practical for routine design due to their computational complexity and the time required for analysis. Nonlinear analysis requires significant computational resources, making it less accessible for everyday design practice. In contrast, strut-and-tie models (STM) offer a simplified yet effective approach for capturing the essential load transfer mechanisms in deep beams and other complex structural elements. By observing the crack patterns from nonlinear models, STMs can be developed that provide a more practical, efficient method for engineers to design and analyze structures while still reflecting the essential behavior of the system.

A.4 Nodal Zones in Strut-and-Tie Models

The stress levels in the node are limited in various codes using different approaches. A comparison made among AASHTO LFRD, CSA A23.3, and ACI 318-19 STM is presented following sub-chapters.

A.4.1 ACI 318 - Building Code Requirements for Structural Concrete and Commentary

A nodal zone is a volume of concrete surrounding the node, assumed to transfer strut and tie forces through the node (ACI Committee 318, 2019). These nodes are classified based on the types of loads (tension or compression) that intersect at the node. There are three main types of nodes: CCC, CCT, and CTT According to ACI, a CCT node is bounded by two compression struts (C) and one tension tie (T). It is important to note that nodes are limited to a maximum of three intersecting forces. If the number of intersecting forces is more than three, the forces have to be reduced by using projections and summation of forces in the same sense.

- CCT: nodes consisting of tension tie(s) intersecting in one direction with a diagonal compressive strut.
- CCC: nodes consisting of only compressive struts.
- CTT: nodes consisting of tension tie(s) intersecting in two directions.

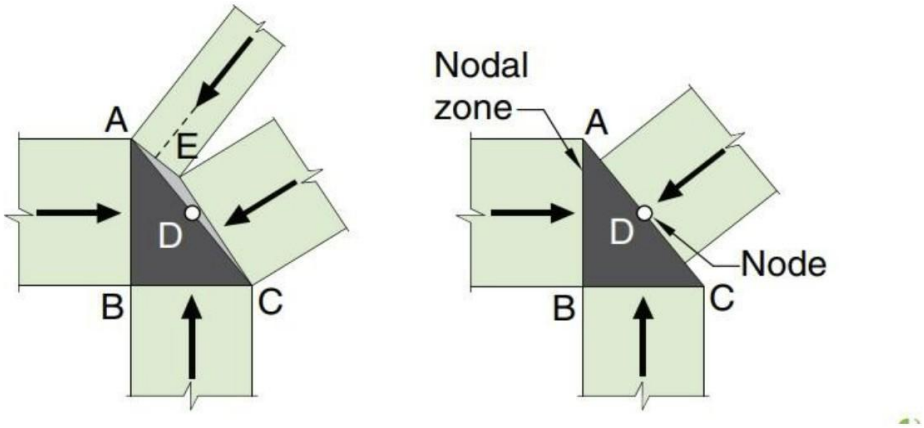

Figure A-10: Two forces on the face AC can be resolved into one force as shown in the figure (ACI Committee 318 2019).

According to ACI 318, the design of nodal zones within the Strut-and-Tie Method is governed by specified strength limits expressed as fractions of the concrete compressive strength. These limits vary depending on the type of nodal zone, reflecting differences in the stress conditions and anchorage of reinforcement. A summary of the nodal stress limits is presented below. In addition, ACI SP-208 and ACI CI PRC-445.2-21 provides further explanations and illustrative examples that demonstrate the application of these limits in practical design situations.

Stress limits in nodes according to ACI 318:

- CCC node (compression–compression–compression) = 0.85 f'_c
- CCT node (compression–compression–tension) = 0.75 f'_c
- CTT node (compression–tension–tension) = 0.60 f'_c

A.4.2 CSA A23.3 - Design of Concrete Structures

The Canadian standard addresses nodal strength as a whole. The nodes are categorized based on the type of forces that they withstand. The more tensile forces on the node, the less stress is permitted on the node.

Stress limits in nodes according to A23.3:

- Nodes bounded by struts and bearing areas = $0.85 \cdot \emptyset_c \cdot m \cdot f'_c$

- Nodes with anchoring tie in only one direction = $0.75 \cdot \emptyset_c \cdot m \cdot f'_c$
- Nodes with anchoring tie in more than one direction = $0.65 \cdot \emptyset_c \cdot m \cdot f'_c$

Where:
ϕ_c = Resistance factor for concrete, where ϕ_c = 0.65 unless the elements are produced in accordance with CSA A23.4.
m = Confinement modification factor, taken as $q_{A2} \leq 2$, provided that sufficient reinforcement is included for crack control.
f'_c = Specified compressive strength of concrete.

A.4.3 AASHTO LFRD Bridge Design Specifications

ASHTO LFRD Bridge Design Specifications (2020) approaches the nodal strength face-wise rather than approaching it as a whole. The following equation gives the factored resistance of the node face:

$$f_{cu} = m \cdot v \cdot f'_c \qquad (A.1)$$

Where:
v = Efficiency factor
m = Confinement modification factor, taken as $q_{A2} \leq 2$, provided that sufficient reinforcement is included for crack control.
A_2 = The notional area defined in Clause 5.6.5 AASHTO LFRD.
A_1 = Area under the bearing device (in^2)
f'_c = Specified compressive strength of concrete.
Nodal strength checks must be completed for all the nodes and load cases. The strength of a face of the node is given by Equation (A.2).

$$P_n = f_{cu} \cdot A_{cn} \qquad (A\text{-}2)$$

Where:
A_{cn} : Area of the face of the node.

The factored resistance (P_r) can be calculated is given by Equation (A-3).

$$P_r = \phi \cdot P_n \qquad (A\text{-}3)$$

Where ϕ is the resistance factor for compression specified in AASHTO LRFD code (AASHTO 2020), Article 5.5.4.2, and is equal to 0.7.

As shown in Figure A-11, at bearing the load is assumed to spread at a slope of 2 horizontal to 1 vertical (2H:1V) through the depth of the member. Based on this assumption, the effective loaded area A_1 is defined, and the corresponding notional area A_2 is determined on the section under consideration. This dispersion model provides the basis for calculating the bearing strength of concrete. The parameter *m* in the design equations relates to the slope of this assumed load dispersion (2H:1V).

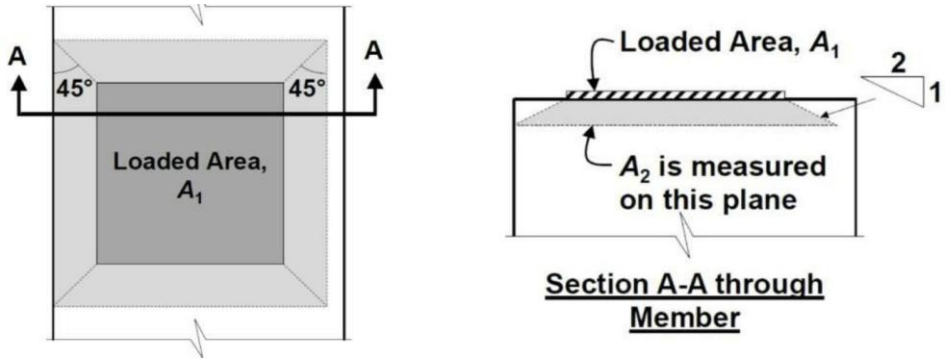

Figure A-11: Determining the A1 and A2. Adapted from AASHTO (AASHTO 2020).

v = concrete efficiency factor. A value of 0.45 is used for structures that do not contain sufficient crack control reinforcement. Values of *v* for structures with crack control reinforcement are given below in Table A.1. Efficiency factors are shown graphically in Figure A-12.

Table A.1: Efficiency factors for nodes with crack control reinforcement- Table 5.8.2.5.3a-1 AASHTO LFRD (2020).

	Node Type		
Face	**CCC**	**CCT**	**CTT**
Bearing Face	0.85	0.70	$0.85-\frac{f'_c}{20\ \text{ksi}}$ $0.45 \le v \le 0.65$
Back Face			
Strut-to-Node Interface	$0.85-\frac{f'_c}{20\ \text{ksi}}$ $0.45 \le v \le 0.65$	$0.85-\frac{f'_c}{20\ \text{ksi}}$ $0.45 \le v \le 0.65$	

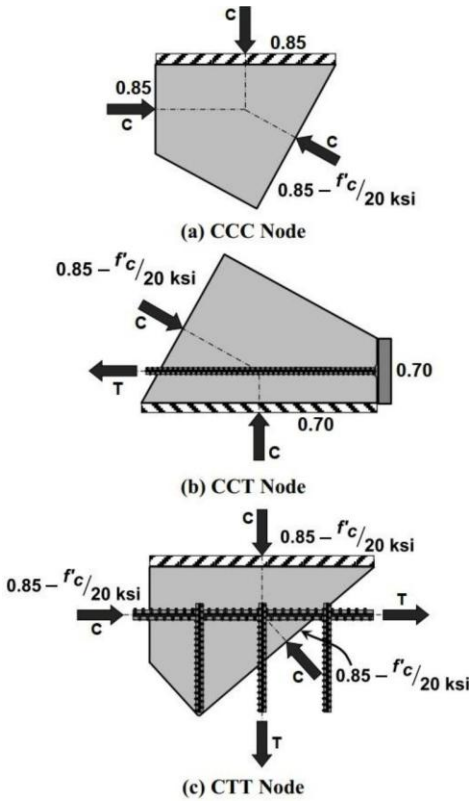

Figure A-12: Efficiency factors (AASHTO 2020).

A.5 Strut Capacities

As discussed in Section A.3.4, struts carry compression in the strut-and-tie model. Struts can be comprised of either concrete or concrete with reinforcement. Three shapes of struts that are primarily used in the STM are the prismatic strut, the bottle-shaped strut (see Figure A-13), and compression fanning strut (see Figure A-14). Strut capacity is a function of the compressive strength of concrete and the tensile strain in the transverse direction. When bottle-shaped struts are applied to the design, longitudinal cracks may occur due to tensile forces acting perpendicular to the struts, so confining reinforcement should be placed in the direction perpendicular to the strut axis.

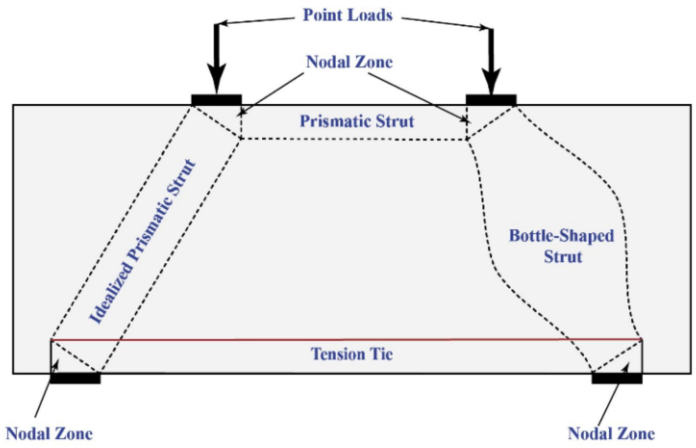

Figure A-13: Prismatic and bottle shaped struts.

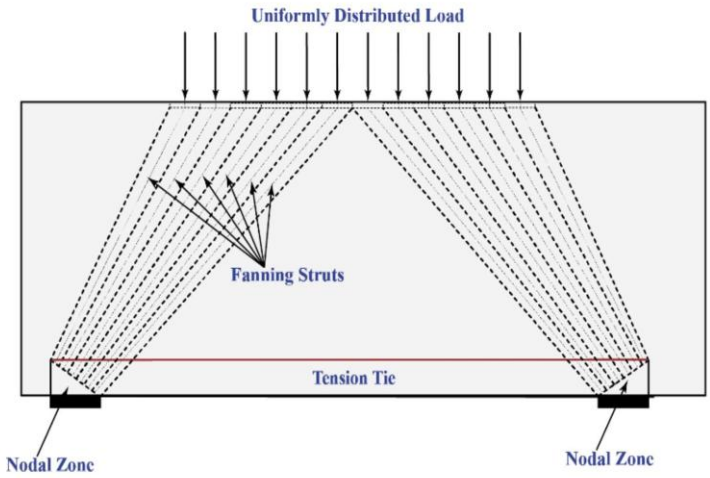

Figure A-14: Compression fanning struts.

ACI 318-19 classifies the struts based on the location (see Figure A-15) within the structural element as following

- Boundary Struts – Struts that occur within the uniform compressive stress field or regions where the compression field is not intersected by the tension field.
- Interior strut – Compressive field is spread in the lateral direction in these types of struts and is crossed by tension field.

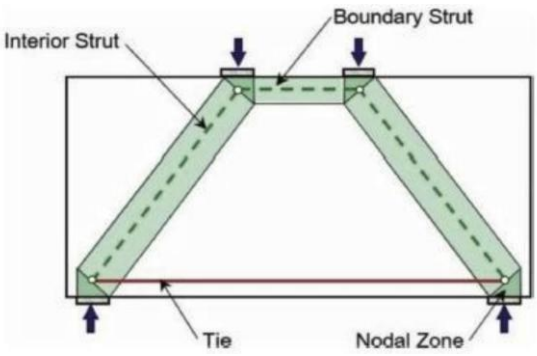

Figure A-15: Defining interior struts, boundary struts, and nodal zones (ACI Committee 318 2019).

CSA A23.3 gives a detailed description of how to proportion fanning compression struts. The following is guidance provided by the code. The beam with UDL can be idealized in two ways, as described below.

- The UDL can be idealized as twelve-point loads over the entire span. Each of the point loads is assigned to a fanning strut, and the tie is located in the narrow area of the fanning strut (see Figure A-16).
- The UDL can be idealized as just two point loads acting at the quarter of the span, and the compression field is simulated by just one strut rather than six fanning compression struts (see Figure A-17).

The width of the strut is dependent on the nodal dimensions, dimensions of the support, and the dimensions of the loading plate The dimensions of the prismatic strut were discussed in section A.3.7. The proportioning of fanning struts is summarized in Figure A.17 (CSA, 2019). CSA discusses proportioning the struts near supports and proportioning the struts at the loading point. The ACI and AASHTO codes give similar definitions.

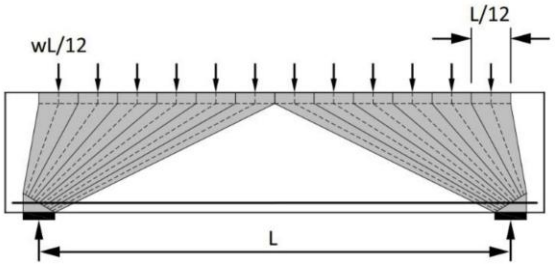

Figure A-16: Compression fanning struts idealization (CSA 2019).

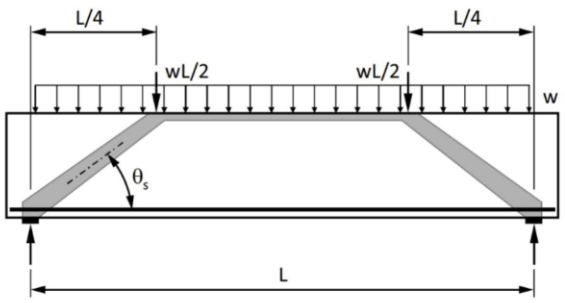

Figure A-17: UDL idealized as two-point loads acting at the quarter span (CSA 2019).

Martin and Sanders (2007) conducted a comprehensive study as part of NCHRP Project 20-07/Task 217 to improve and implement Strut-and-Tie Modeling (STM) procedures within the AASHTO LRFD Bridge Design Specifications. A key focus of their work was the idealization of uniformly distributed loads (UDLs) in STM applications, which is relevant in the design of deep beams, bent caps, and D-regions in reinforced concrete structures.

Martin and Sanders (2007) emphasizes that distributed loads, such as UDLs from superstructures or bearing areas, cannot be directly applied in STM. Instead, these loads must be represented as an equivalent system of concentrated point loads. This transformation ensures that the forces entering the D-region can be correctly transferred through the nodes of the STM framework.

Figure A-18, adapted from the report, illustrates this transformation process. It shows how a typical pier cap subjected to uniformly distributed loads (UDLs) is idealized using an array of discrete point loads along the span. These concentrated loads serve as input forces for the STM, enabling the development of a truss-like internal force path that aligns with the actual stress flow in the D-region. This step is essential to satisfy equilibrium conditions and ensure accurate modeling of load transfer through strut, ties and node in STM based design.

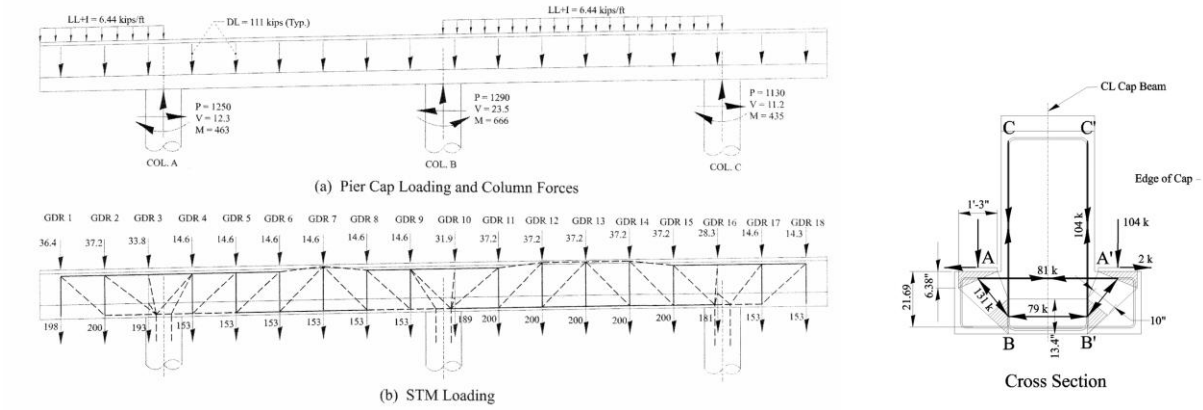

Figure A-18: Idealization of Uniformly Distributed Loads (UDLs) into Discrete Point Loads for Strut-and-Tie Modeling (STM) in an Inverted-T Bent Cap (Martin and Sanders (2007).

A.5.1 ACI 318 - Building Code Requirements for Structural Concrete and Commentary

The strength of a concrete strut is given by ACI 318-19 using the following equation in terms of compressive strength (f'_c) of the concrete:

$$f_{ce} = 0.85.\beta_c.\beta_s.f'_c \qquad (A.2)$$

Where:

- β_c = Strut/Node confinement modification factor:
  - For the end of a strut node that has a bearing surface as a side: $q_{A2} \leq 2$.
  - For all other cases: $\beta_c = 1$.
- β_s = Strut coefficient (given in Table A.2).

Table A.2: Strut coefficient β_s.

Strut location	Strut type	Criteria	β_s	
Tension members or tension zones of members	Any	All cases	0.4	(a)
All other cases	Boundary struts	All cases	1	(b)
	Interior struts	Reinforcement satisfying (a) or (b) of Table 23.5.1	0.75	(c)
		Located in regions satisfying 23.4.4	0.75	(d)
		Beam-column joints	0.75	(e)
		All other cases	0.4	(f)

A.5.2 CSA A23.3 - Design of Concrete Structures

The compression force in the strut is limited to $\emptyset_c \times f_{cu} \times A_{cs}$, where ϕ_c is the reduction factor, f_{cu} is the compressive strength, and A_{cs} is the effective cross-sectional area. A_{cs} is calculated based on the concrete area available and the anchorage conditions at the end (see Figure A-19).

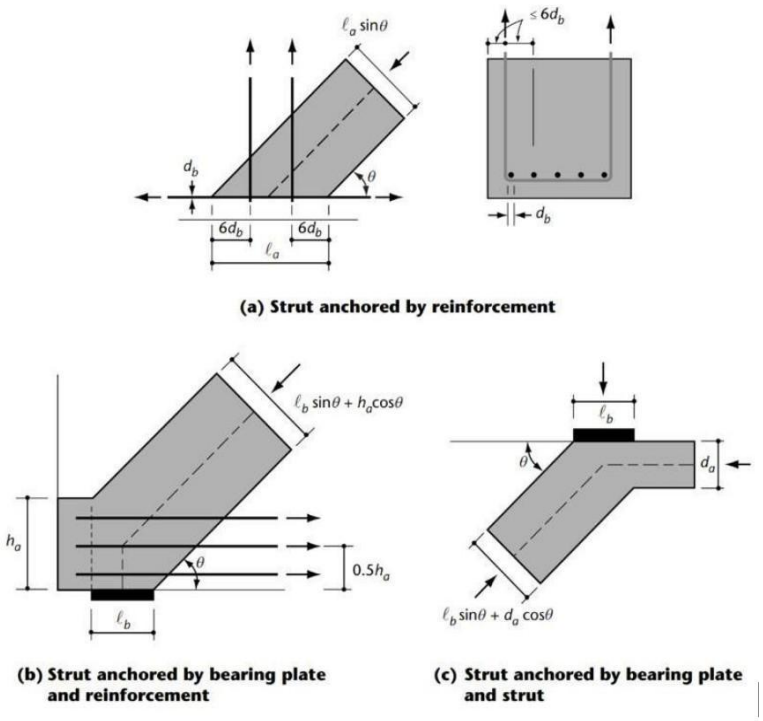

Figure A-19: Influence of bar diameter, bearing, and anchorage conditions on selecting the cross-section of the strut (CSA 2019).

The compressive strength (f_{cu}) is limited based on Equation A.3. According to the equation, the compressive strength decreases with the tensile strain (ϵ_1) in the orthogonal direction of the strut. The relationship is known as the compression softening relationship, and was first developed as a part of the Modified Compression Field Theory (Vecchio & Collins 1986).

$$f_{cu} = \frac{f'_c}{0.8 + 170\ \epsilon_1} \qquad (A.3)$$

Where ϵ_1 = Strain perpendicular to the strut and it is governed by $\epsilon_1 = \epsilon_s + (\epsilon_s + 0.002) \times cot^2(\theta)$ f'_c = Compressive strength of concrete. Figure A-20 shows the relationship between f_{2max} (f_{cu} in this case) and α (θ in this case).

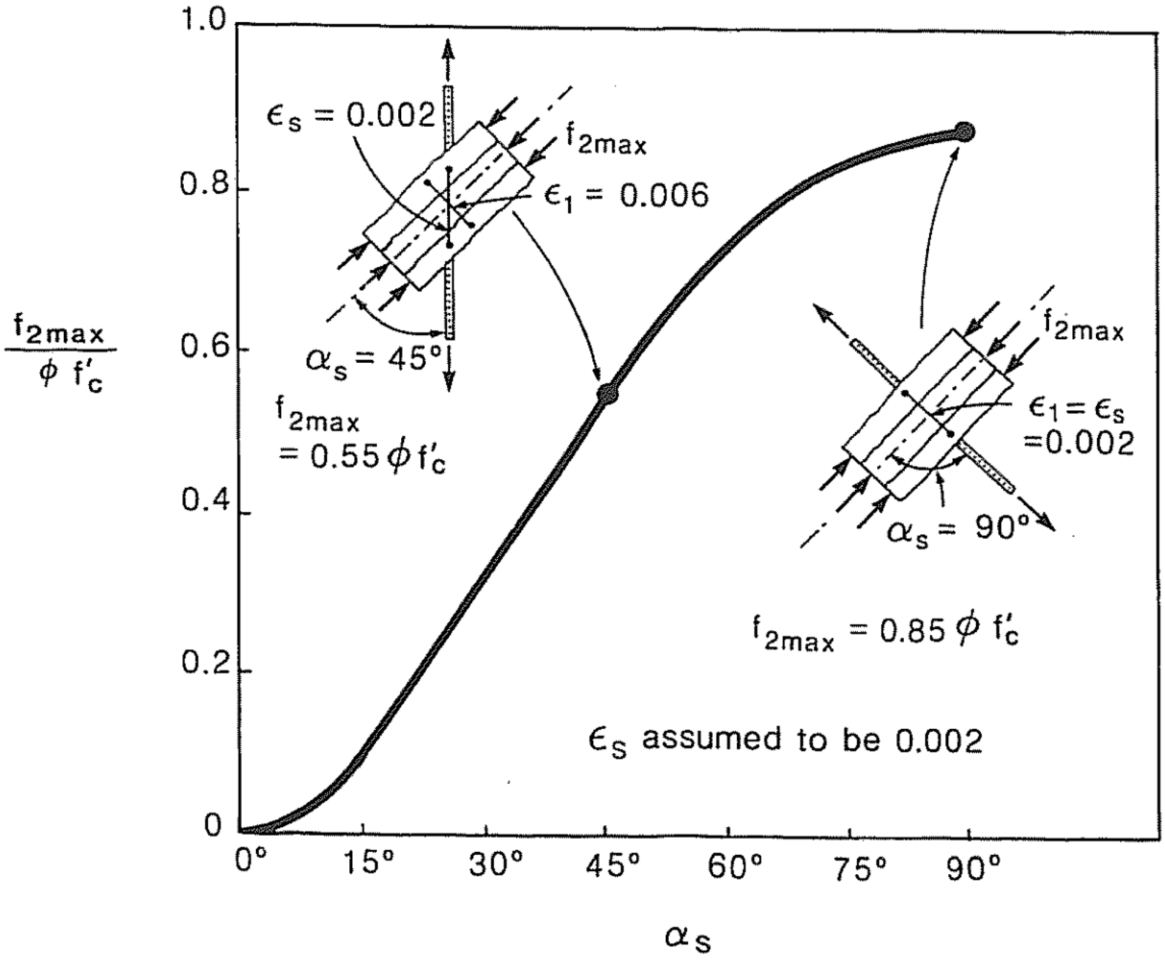

Figure A-20: Crushing strength versus orientation of tensile reinforcement passing through the strut (Collins and Mitchell 1997).

Both CSA and AASHTO set a minimum angle between compressive struts and tension ties of 25 degrees. This minimum is established to mitigate cracking and assist in minimizing excess strains. It is also limited since it is unlikely ties and struts are occurring adjacent to each other in the same directions. The angle of 25 degrees is established as the minimum threshold.

The AASHTO 9th Edition has updated its guidelines regarding strut and tie modeling. It no longer requires the strut checks that were part of previous editions. The focus is on the nodal checks as described earlier.

A.6 Texas Department of Transportation – Experiments on Bent Caps

Brown, Sankovich, Bayrak, Jirsa, Breen, and Wood (2006) conducted a study for the Texas Department of Transportation (TxDOT) on shear design of reinforced concrete beams using strut-and-tie models and sectional methods. The first series (Series I) of beams were tested with uniformly distributed loads and point loads with varying horizontal and vertical reinforcement. The second test series (Series II) of beams was tested to identify the effect of the width of the beam on the shear strength and to check the effect of the span-to-depth ratio on shear strength. The third test series (Series III) was tested to see the effect of load distribution on the shear strength. In test Series I, 10 beams were tested with the dimensions of 6 in. width and 30 in depth (the effective depth (d) was 27 in.). The beams were loaded with various load configurations, such as UDL and concentrated loads with asymmetry (not symmetric around the mid-point of the beam). In all the tests, the load was placed asymmetrically within the middle 10 ft. (120 in.) of the beam (see Figure A-21). In addition to the variables discussed above, the bearing plate sizes on both sides were selected so that they differed. The bearing plate on the north side/right side (marked with a triangle) was smaller than the plate on the left support (marked with a circle) (see Figure A-22). The smaller bearing plate was 6 in x 6 in., whereas the larger plate was 6 in x 8 in.

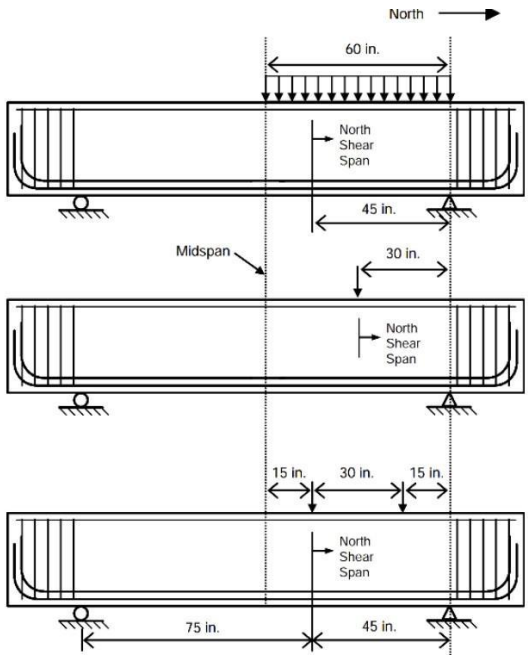

Figure A-21: The UDL was applied with 30 jacks, each with a capacity of 10 kips (See Figure 2.21).

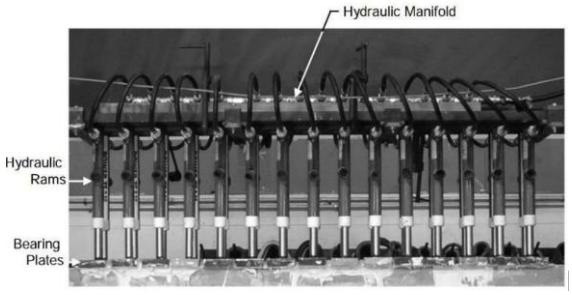

Figure A-22: UDL arrangement using series of jacks adapted from (Brown, Sankovich, Bayrak, Jirsa, Breen, and Wood 2006).

Details of the 10 beams tested are shown below in Table A.3, and the results are tabulated in Table A.4.

Table A.3: Details of beams tested in Series I. adapted from (Brown, Sankovich, Bayrak, Jirsa, Breen, and Wood 2006).

Specimen	Concrete Strength [psi]	Stirrup Spacing, s_v [in.]	Spacing of Horizontal Shear Reinforcement, s_h [in.]
I-UL-8.5-0a	2440	8.5	N/A
I-UL-8.5-0b	2640	8.5	N/A
I-UL-0-0	3230	N/A	N/A
I-UL-0-8.5	2640	N/A	8.5
I-UL-17-17	2660	17	17
I-UL-17-0	2660	17	N/A
I-2C-8.5-0	3210	8.5	N/A
I-2C-0-0	3210	N/A	N/A
I-CL-8.5-0	2580	8.5	N/A
I-CL-0-0	2370	N/A	N/A

Table A.4: Summary of shear failure loads of beams tested in Series I).

Specimen	North Reaction [kip]	South Reaction [kip]	Failure Load [kip]	Diagonal Cracking Load [kip]	$\sum \frac{A_{si}}{bs_i} sin\alpha_i$
I-UL-8.5-0a	161.7	59.7	221.4	64.3	0.003
I-UL-8.5-0b	142.5	56.6	199.1	69.9	0.003
I-UL-0-0	135.8	49.6	185.5	83.6	0
I-UL-0-8.5	123.9	48.7	172.6	103.5	0.003
I-UL-17-17	138.5	52.6	191.0	84.1	0.003
I-UL-17-0	143.4	57.5	200.9	82.7	0.0015
I-2C-8.5-0	120.8	45.4	109.1	54.6	0.003
I-2C-0-0	91.1	33.6	125.7	82.6	0
I-CL-8.5-0	79.1	30.0	166.2	41.1	0.003
I-CL-0-0	92.2	33.5	124.6	68.3	0

The Series I tests concluded that beams with uniformly distributed loads fail at higher loads than point loads in terms of total shear resistance. In addition, it was concluded that there is no significant increase in the shear strength when horizontal shear reinforcement is included. Interestingly, it was found that beams containing both vertical and horizontal shear reinforcement carried slightly less loads than beams with only vertical shear reinforcement. From the observation of I-UL-0-0, It could be observed that beyond a certain limit (I- UL-17-0), decreasing the spacing of vertical reinforcement did not increase the shear capacity. From the observation of test Series I, it could be noticed that all the tests involved the crushing of diagonal struts. Two parallel cracks were observed between 70%-80% of the failure load before the final failure occurred. Similarly, Series II and Series III experiments were designed and tested.

It is important to note that the test results from Series I and Series III beams suggest that a uniformly distributed load can be modeled by two-point loads spaced equally. The failure mechanism observed in the Series III-2 specimen, induced by two-point loads spaced similarly, closely resembles the mechanism created by a uniformly distributed load. This observation is also supported by previous research, including that of Kani, Huggins, and Wittkopp (1979) and Perkins (2011). The relevance of this conclusion lies in its application to the design of bent caps subjected to uniformly distributed loads, particularly when using the STM.

A.7 Minimum Reinforcement Requirements when using the Strut-And-Tie Method

Traditionally, minimum distributed reinforcement in both orthogonal directions has been recommended when applying strut-and-tie methods. This is theoretically based on the idea that, since any internal load paths are permitted, the structure may require to undergo some internal redistribution and thus some reinforcement should be provided to achieve this. In the CSA A23.3-19 (Canadian Standards Association), the minimum reinforcement for strut-and-tie models, is addressed in Section 14.1.8.5. The CSA 2019 standard specifies the minimum area of 0.20% in both orthogonal directions. Similarly, AASHTO and ACI 318 suggests, a value of 0.30% and 0.25%, respectively.

Experimental results related to concrete beam tests were collected from the literature and compiled into a comprehensive database by Brown, Sankovich, Bayrak, Jirsa, Breen, and Wood (2006). Based on the analysis of this data, an experimental program was developed to address gaps in the existing technical literature. Using the data compiled, the code provisions in ACI 318 and AASHTO LRFD were examined. The analysis revealed that both codes often produce unconservative estimates of strength. In response to this, a new design procedure was developed to improve safety levels and simplify the implementation of the STM. As part of this procedure, a new method for determining the minimum reinforcement required within a strut was introduced.

As part of the research conducted by Brown, Sankovich, Bayrak, Jirsa, Breen, and Wood (2006), an observation was made that when the minimum reinforcement requirements were applied to the specimens

listed in the database, only 49 specimens met the AASHTO LRFD requirements. Of these 49 specimens, 92% had measured strengths greater than the nominal capacities determined using the STM provisions.

Brown, Sankovich, Bayrak, Jirsa, Breen, and Wood (2006) developed a new model, for the minimum reinforcement required to carry the transverse tension in a bottle-shaped strut was developed based solely on strength. The minimum reinforcement ratio required across the crack can be calculated by the equation given below.

$$\rho_{min} = \frac{k_s \cdot v \cdot f'_c \cdot A_c \cdot sin\,(\theta)}{f_y \cdot b \cdot d \cdot m} \qquad (A.4)$$

Where:
v = Efficiency factor.
f'_c = Specified compressive strength of concrete.
A_c = Minimum cross-sectional area of the strut.
θ = Angle of the strut
m = Slope of the dispersion of compression.
k_s = Conversion factor for the efficiency of the face of a node abutting a strut

For a majority of the specimens in the database, minimum reinforcement of 0.15% was adequate for strength purposes. Any increase in reinforcement beyond that amount did not result in substantial additional strength in the specimens. In order to reduce crack widths under service loads, the newly developed procedure set the minimum perpendicular reinforcement ratio at 0.003 Brown et al. (2006). Therefore, the equation was modified as shown below.

$$\rho_{min} = \frac{k_s \cdot v \cdot f'_c \cdot A_c \cdot sin\,(\theta)}{f_y \cdot b \cdot d \cdot m} \geq 0.003 \qquad (A.5)$$

Even though this approach provides an estimate for the minimum reinforcement required, it does not offer any information about the distribution of crack widths.

However, AASHTO has adopted more stringent reinforcement requirements values (0.30% in both orthogonal directions).

B DETAILED ANALYSIS OF A TWO-COLUMN BENT CAP: EXAMPLE AND SUMMARY OF NODAL STRENGTHS

B.1 Summary of Forces on A Two Column Bent Cap for 9 Load Cases and a Dead Load Only Case

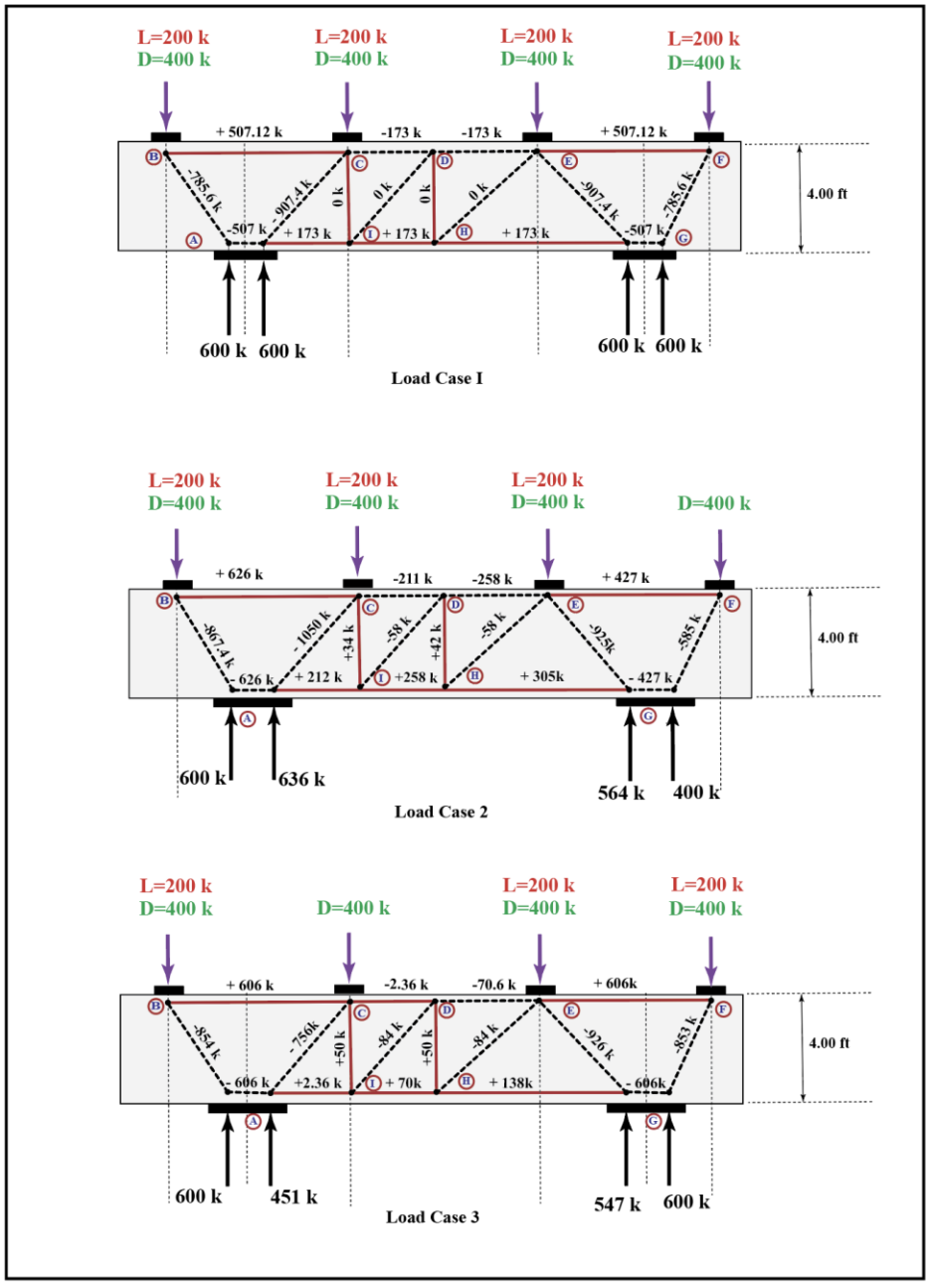

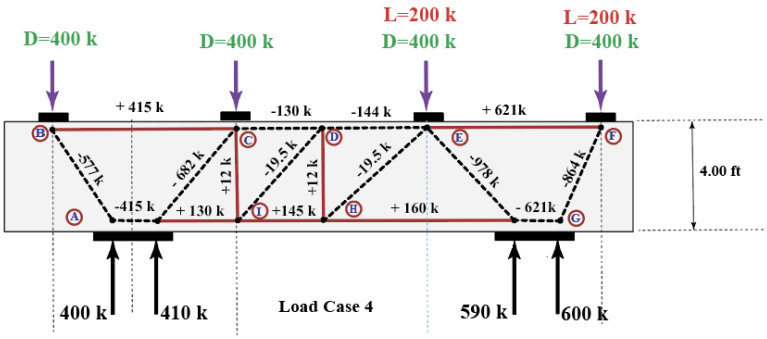
D=400 k
D=400 k
L=200 k
D=400 k
L=200 k
D=400 k
+ 415 k
-130 k
-144 k
+ 621k
-577 k
- 682 k
+12 k
-19.5 k
+12 k
-19.5 k
-978 k
-864 k
4.00 ft
-415 k
+ 130 k
+145 k
+ 160 k
- 621k
400 k
410 k
Load Case 4
590 k
600 k

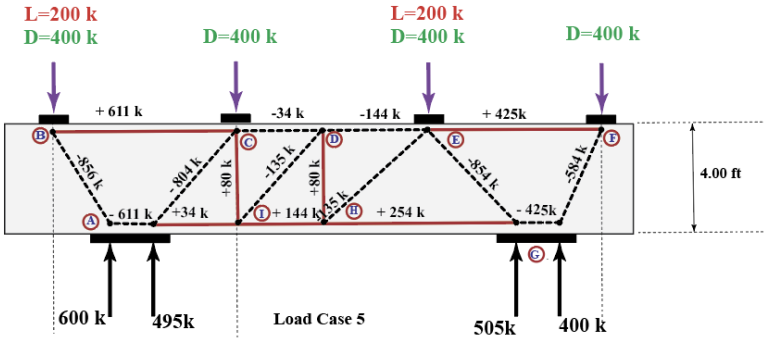
L=200 k
D=400 k
D=400 k
L=200 k
D=400 k
D=400 k
+ 611 k
-34 k
-144 k
+ 425k
-856 k
- 804 k
+80 k
-135 k
+80 k
-854 k
-584 k
4.00 ft
- 611 k
+34 k
+ 144 k
+ 254 k
- 425k
600 k
495k
Load Case 5
505k
400 k

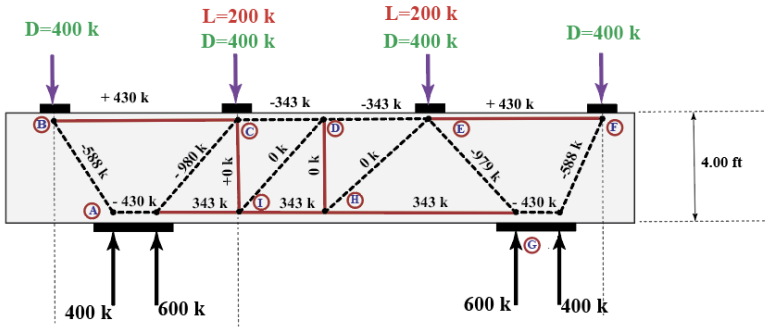
D=400 k
L=200 k
D=400 k
L=200 k
D=400 k
D=400 k
+ 430 k
-343 k
-343 k
+ 430 k
-588 k
- 980 k
+0 k
0 k
0 k
0 k
-979 k
-588 k
4.00 ft
- 430 k
343 k
343 k
343 k
- 430 k
400 k
600 k
Load Case 6
600 k
400 k

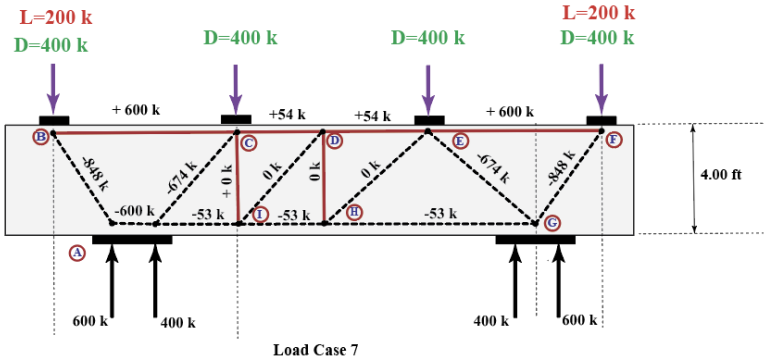
L=200 k
D=400 k
D=400 k
D=400 k
L=200 k
D=400 k
+ 600 k
+54 k
+54 k
+ 600 k
-848 k
-674 k
+ 0 k
0 k
0 k
0 k
-674 k
-848 k
4.00 ft
-600 k
-53 k
-53 k
-53 k
600 k
400 k
Load Case 7
400 k
600 k

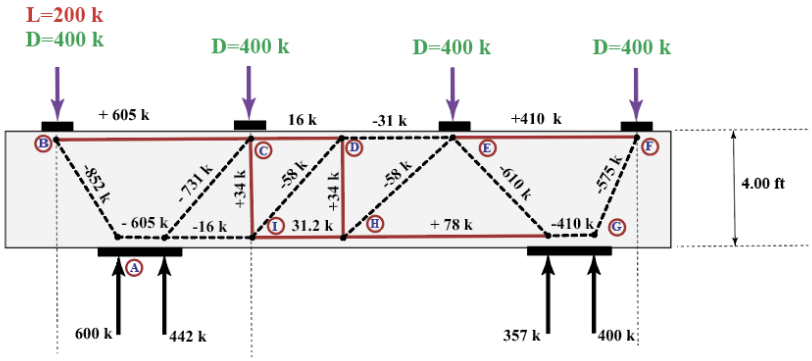

Load Case 8

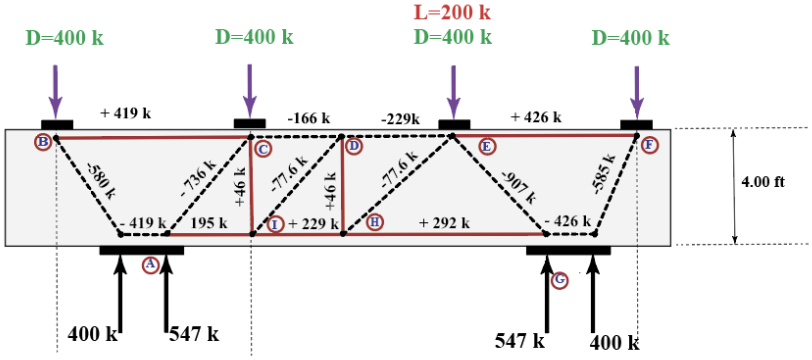

Load Case 9

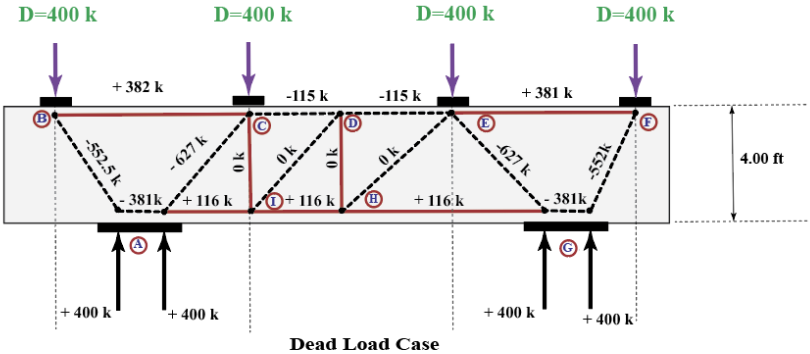

Dead Load Case

B.2 Summary of Nodal Efficiency Factors and Nodal Strengths

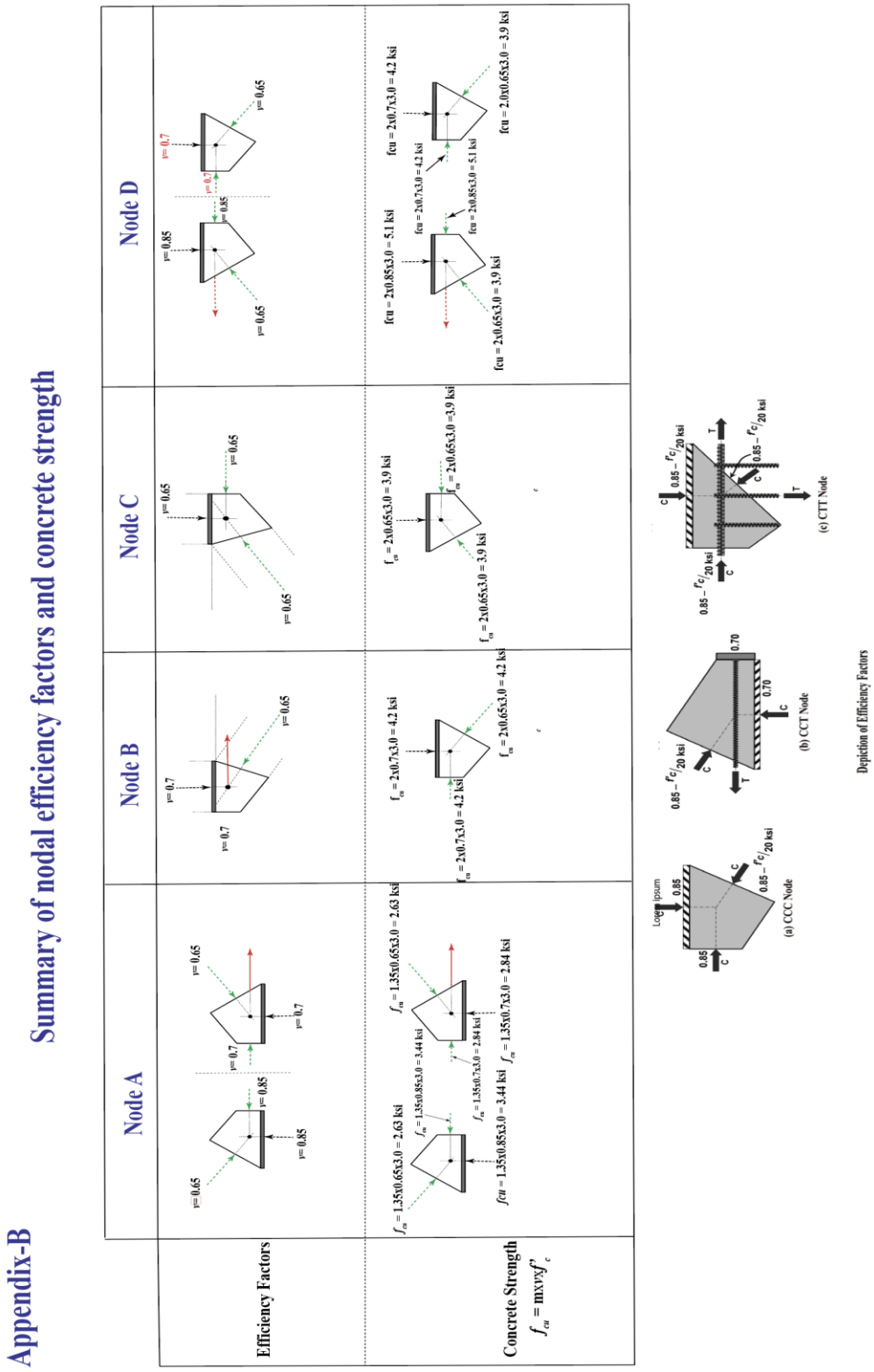

C NONLINEAR FINITE ELEMENT ANALYSIS RESULTS FOR TYPICAL BENT CAP TYPOLOGIES

VecTor2 is a nonlinear finite element analysis tool based on the Modified Compression Field Theory (MCFT) (Vecchio & Collins 1986) and the Disturbed Stress Field Model (DSFM) (Vecchio 2000). In VecTor2, the behavior of cracked reinforced concrete is modeled by considering smeared, rotating cracks. Effects such as tension stiffening, compression softening, and shear slip along cracks are incorporated through detailed constitutive models. The program allows for realistic simulation of reinforced concrete behavior under load, including complex stress and strain distributions. Through the use of compatibility, equilibrium, and constitutive relationships, accurate predictions of load-carrying capacity and deformation patterns can be obtained.

Dimensions and loading configurations of typical NCDOT bent cap typologies were extracted from drawings provided by the NCDOT. These dimensions were input into a relevant STM template and the details of the members were entered into the STM Excel design templates developed as a part of this study. Material strengths were also input into the templates. Assumptions were made for concrete strength (f'_c = 4.5 ksi) as well as longitudinal and transverse reinforcement strengths (f_{yl} = 60 ksi, and f_{yv} = 60 ksi). These values were kept consistent between VecTor2 and the STM design templates.

Nonlinear finite element models were developed in VecTor2 for each beam configuration to validate the STM based design templates. These models were carefully constructed to replicate the geometry, loading conditions, and material properties used in the templates, ensuring a direct comparison. After determining the maximum load capacities and required reinforcement areas using the Excel based templates, corresponding VecTor2 models were created to match those configurations. VecTor2, with its ability to simulate the complex behavior of reinforced concrete—including cracking, tension stiffening, and strut softening—provided a robust benchmark for evaluating the design templates. The maximum loads obtained from the VecTor2 simulations were then compared to those predicted by the templates to assess their accuracy and conservativeness.

This comparison allowed for an evaluation of the templates and whether they provided conservative estimates. Table C.1 presents a comparison of the results for each beam.

Table C.1: Design template and VecTor2 maximum load comparison.

Beam	Design Template Maximum Loads (kips)	VecTor2 Maximum Load (kips)
2 CBC 4 Loads	372	540
3 CBC 4 Loads	464	755
3 CBC 10 Loads	200	420
4 CBC 5 Loads	851	1852

The first beam is a two column bent cap four loads from Davidson County as shown below in Figure C-1. Figure C-2 shows the dimensions, typology, and VecTor2 analysis at maximum load.

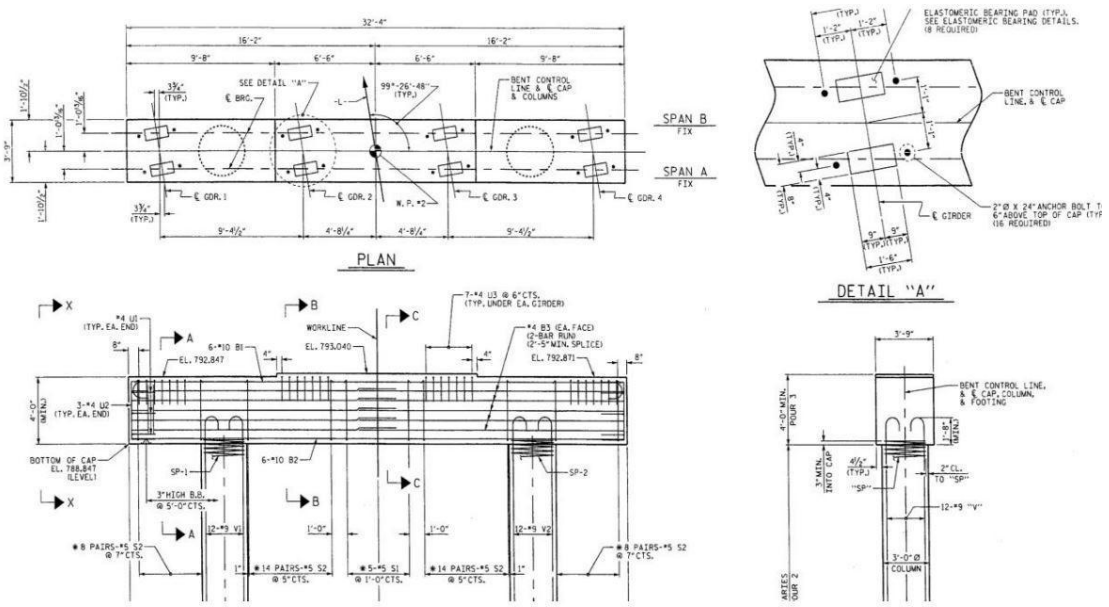

Figure C-1: Plan and elevation of two-column skew bent cap and section (Ref: Project No. B-4499, Davidson County, Sheet No. S-22).

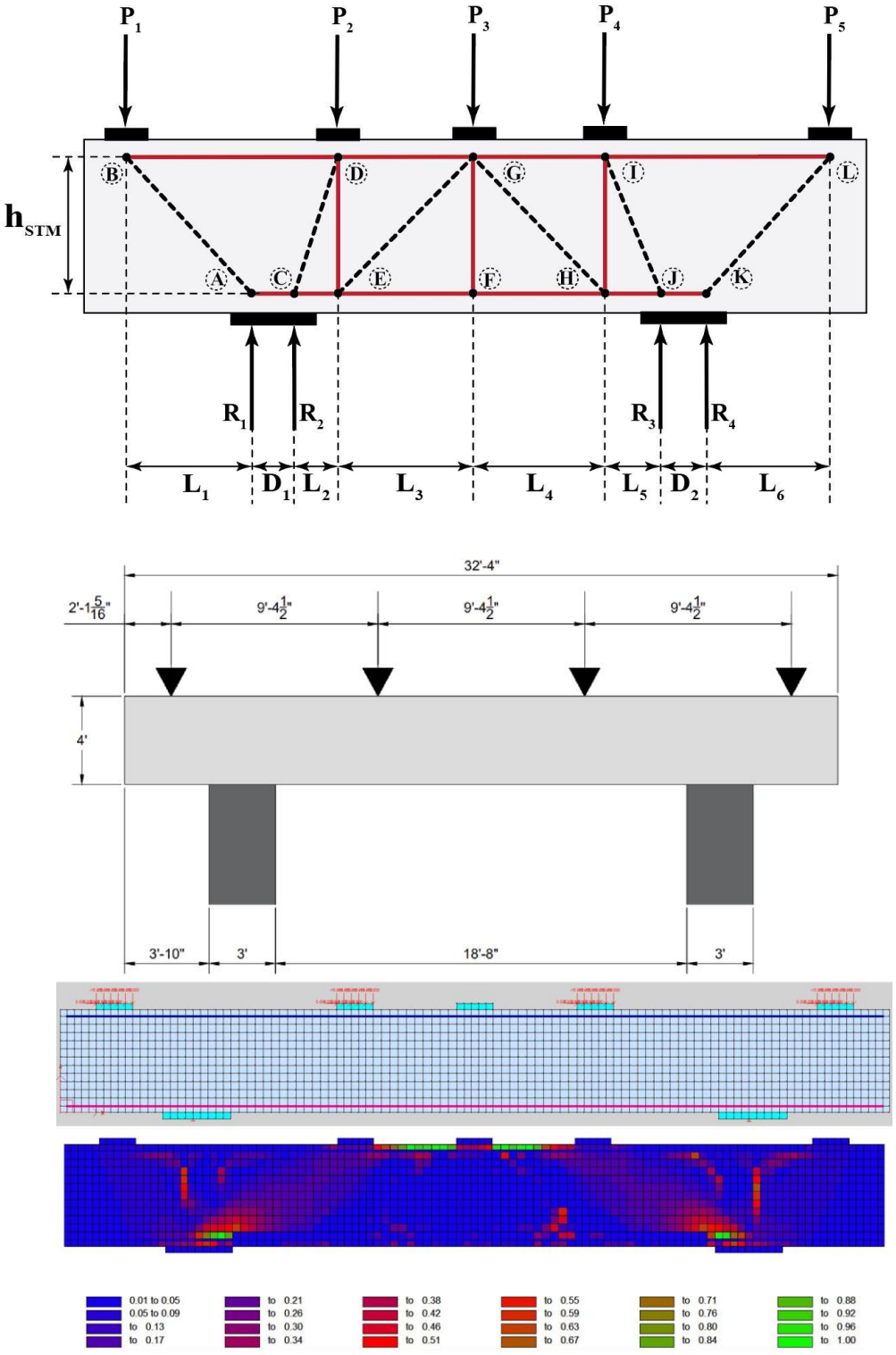

Figure C-2: Two column bent caps four loads: design template, topology and VecTor2 analysis.

The second beam is a three column bent cap with four loads as shown below in Figure C-3. The general dimensions were determined from NCDOT structures but the structure does not relate to a specific bent cap.

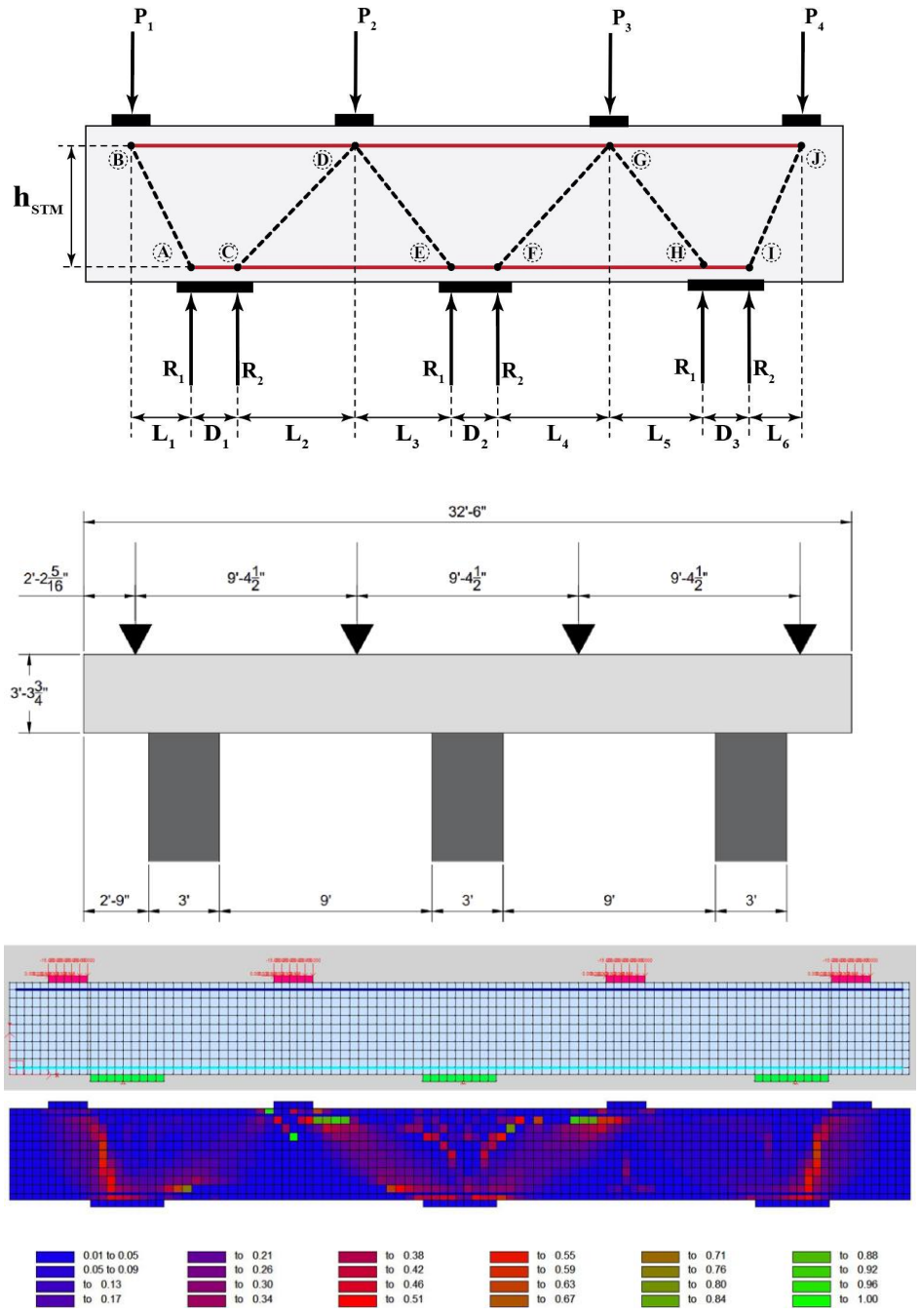

Figure C-3: Three column bent caps four loads: design template, topology and VecTor2 analysis.

The third beam is a three column bent cap with ten loads from Anson County as shown below in Figure C-4. Figure C-5 shows the dimensions, typology, and VecTor2 analysis at maximum load.

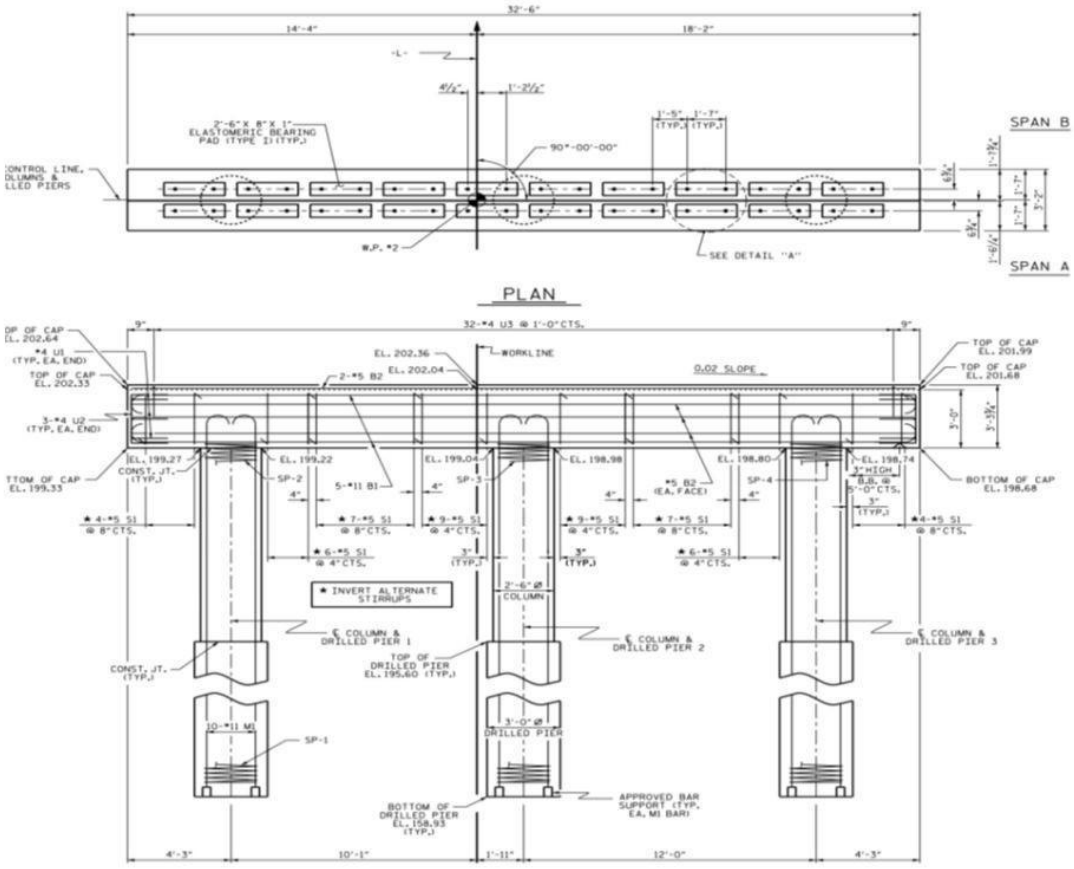

Figure C-4: Plan and elevation views of three-column bent cap (Ref: Project No. B-2506, Anson County, Sheet No. S-17).

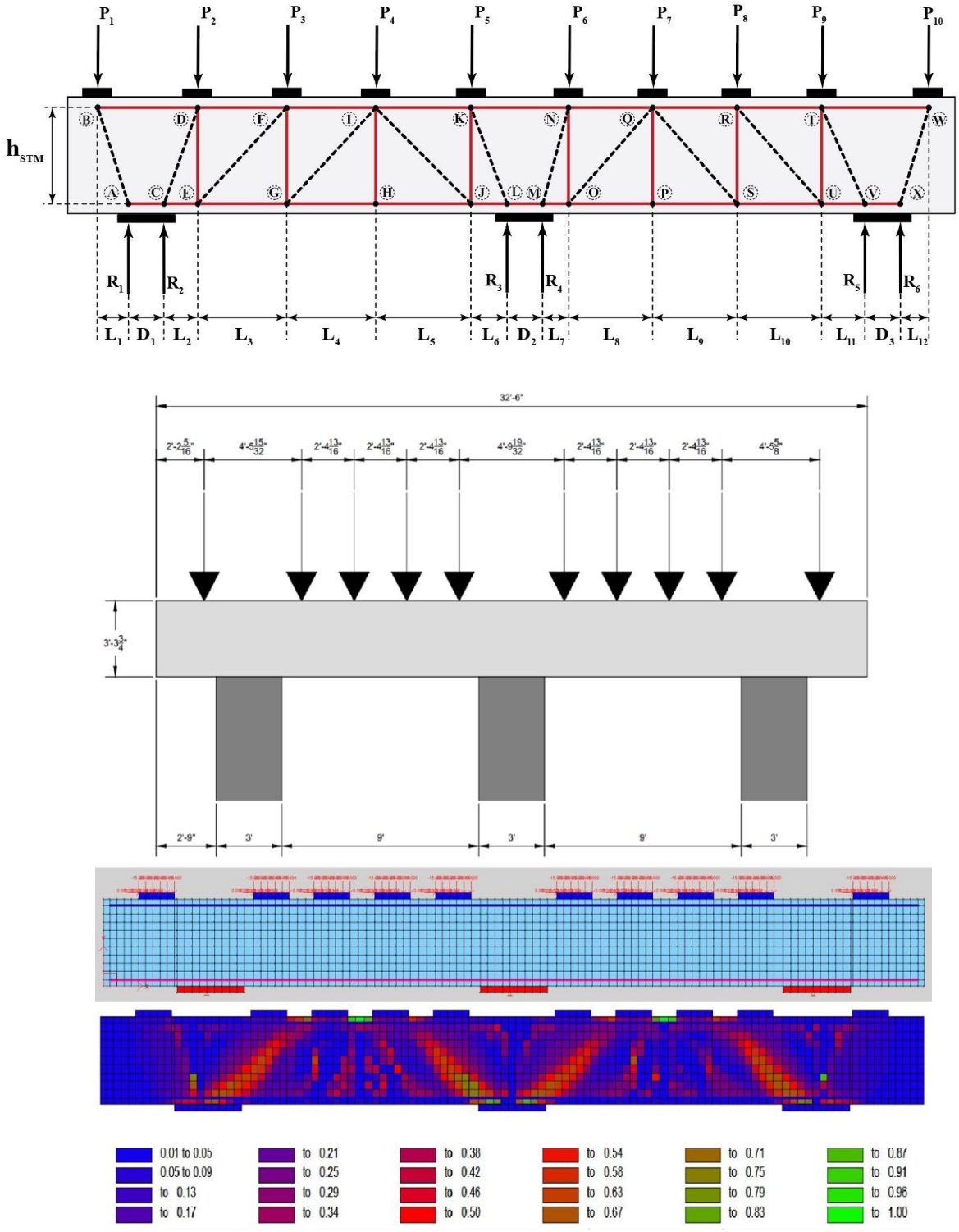

Figure C-5: Three column bent Caps ten Loads: design template, topology and VecTor2 analysis.

The fourth beam is a four column bent cap five loads from Wake County as shown below in Figure C-4. Figure C-5 shows the dimensions, typology, and VecTor2 analysis at maximum load.

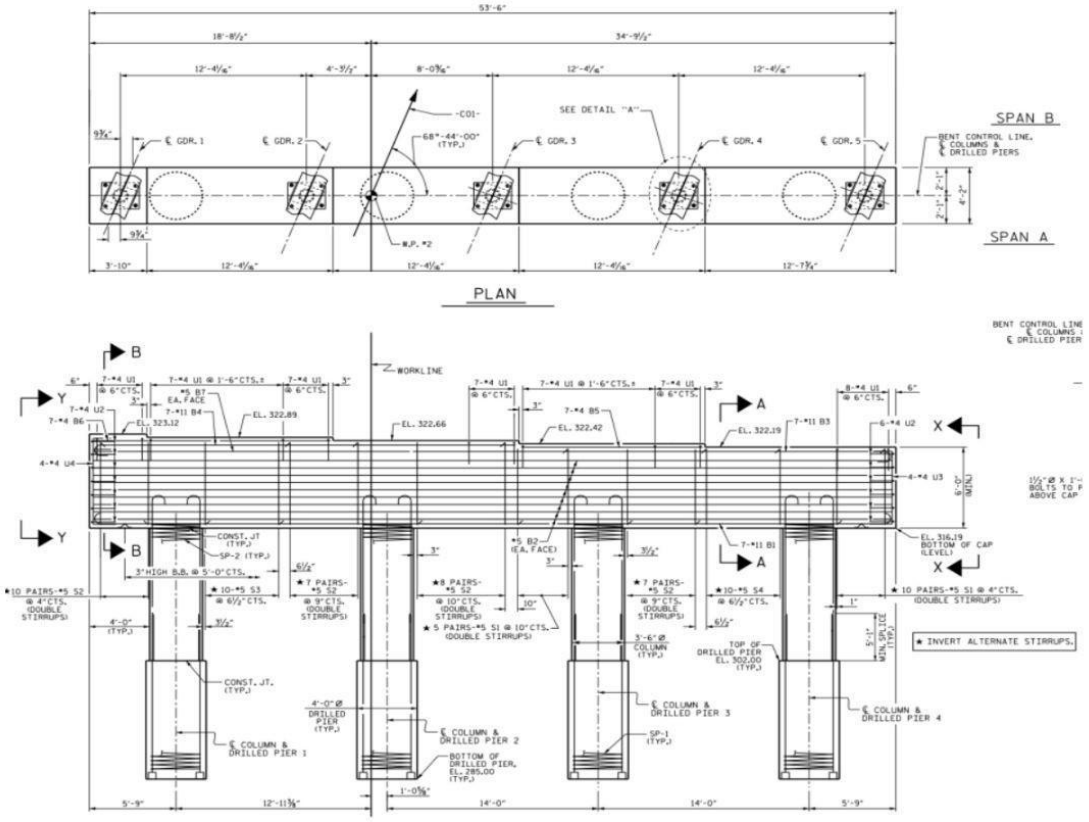

Figure C-6: Plan and elevation of four column stepped bent cap (Ref: Project No. I-5700, Wake County, Sheet No. S1-23).

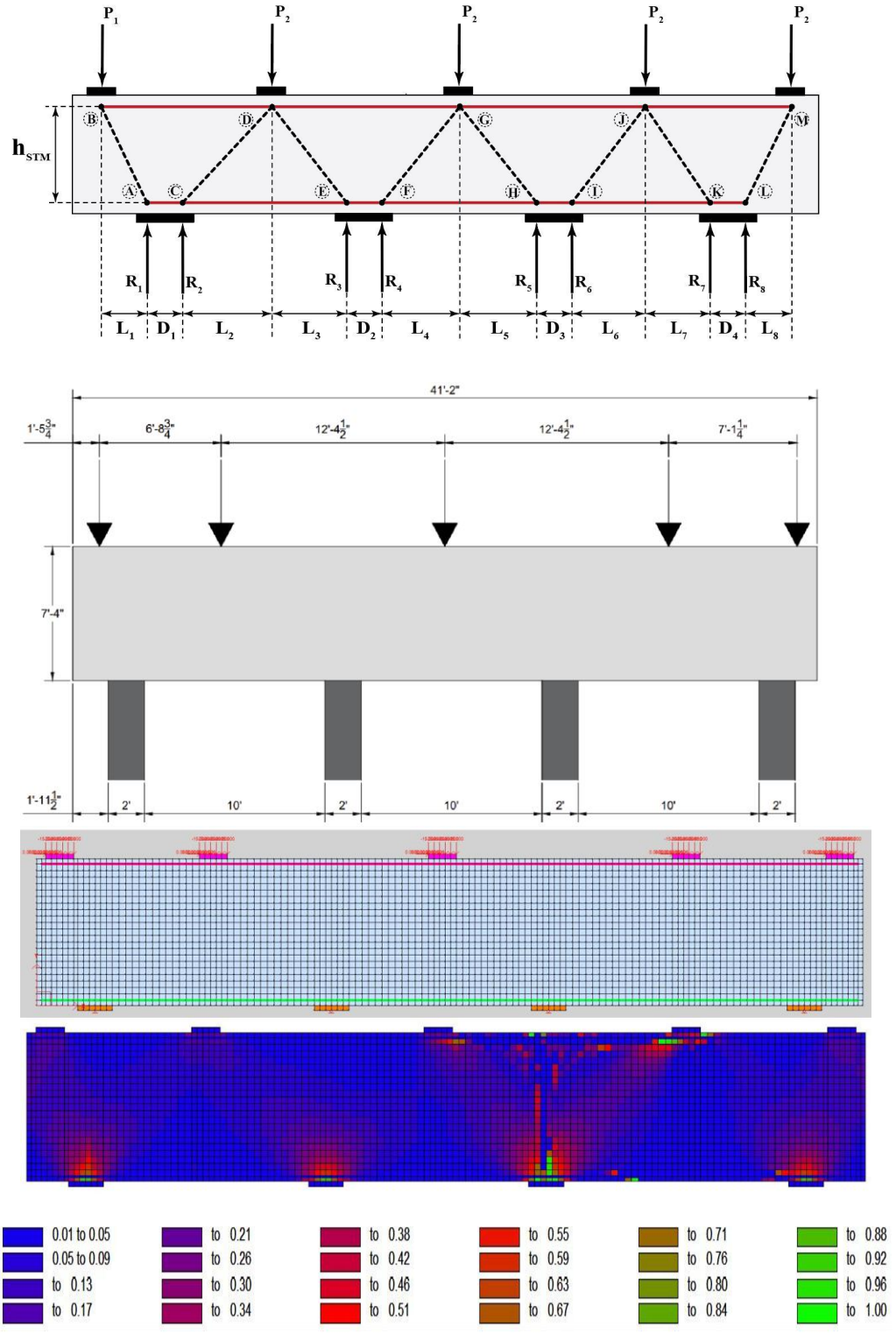

Figure C-7: Four column bent caps five loads: design template, topology and VecTor2 analysis.

C.1 Comparison of Design Templates Against Nonlinear Finite Element Analysis

The comparison between the STM-based design templates and the nonlinear VecTor2 models demonstrates that the templates generally provide conservative estimates of load-carrying capacity. In most cases, the VecTor2 models predicted significantly higher maximum loads than those obtained from the design templates. This outcome is desirable in practice, as it reflects a built-in safety margin in the design process. It should be noted that the comparisons do not apply load factors or resistance factors.

For the 2 CBC 4 Loads configuration, the design template predicted a maximum load of 372 kips, while the VecTor2 model reached 540 kips. This is 31% higher, indicating that the template provided a conservative estimate of strength. A similar trend was observed in the 3 CBC 10 Loads configuration, where the design template estimated a capacity of 200 kips, and the VecTor2 model predicted 420 kips. This corresponds to an estimated 52 % higher capacity. The most pronounced difference occurred in the 4 CBC 5 Loads configuration. The design template predicted a capacity of 851 kips, while VecTor2 calculated a maximum capacity of 1852 kips. This reflects about 54% higher capacity compared to the STM template prediction.

The 3 CBC 4 Loads configuration also followed this observation. The design template predicted a maximum load of 464 kips, while the VecTor2 model reached 750 kips. This represents a 38% higher predicted load capacity. All four beam configurations showed that the design templates produced lower load capacities than the VecTor2 models. These results assist in verifying and validating the STM based design templates for typical NCDOT bent cap typologies.

D Integrating Strut-and-Tie Templates into NCDOT Bridge Design Workflows

This appendix outlines how the strut-and-tie model templates can be integrated into existing NCDOT bridge substructure workflows using the existing workflow, including RC-Pier and LEAP Bridge Concrete. This section summarizes the flow of information from structural analysis to the determination of reinforcement quantities using the strut-and-tie method.

In current NCDOT processes, engineers rely on software such as LEAP Bridge Concrete (including the CONSPAN module) and RC-Pier to generate design loads and perform substructure design. LEAP Bridge Concrete is used primarily for superstructure modeling, including prestressed I-girders and box girders. It outputs reaction loads due to dead loads (DC), wearing surfaces (DW), live loads (LL), and impact (IM), but these reactions are not yet factored according to AASHTO LRFD.

RC-Pier is used in this workflow. It serves as the platform where all unfactored loads from LEAP Bridge are combined using AASHTO LRFD load combinations, such as Strength I, Strength II, and Service Limit States. RC-Pier automates the application of load factors (e.g., 1.25DC + 1.5LL + 0.5 IM for Strength I) and calculates the resulting bearing reactions at each girder location. These factored reactions are then used for structural design of pier caps, columns, and foundations.

Figure D-1 shows bearing layout on the bent cap. It shows that there are two bearing lines (double), each from the centerline. The grid below lists each bearing point's distance from the cap end (either left or right), establishing the exact spatial arrangement of applied loads. This configuration is used for determining strut and tie positions in STM templates and models.

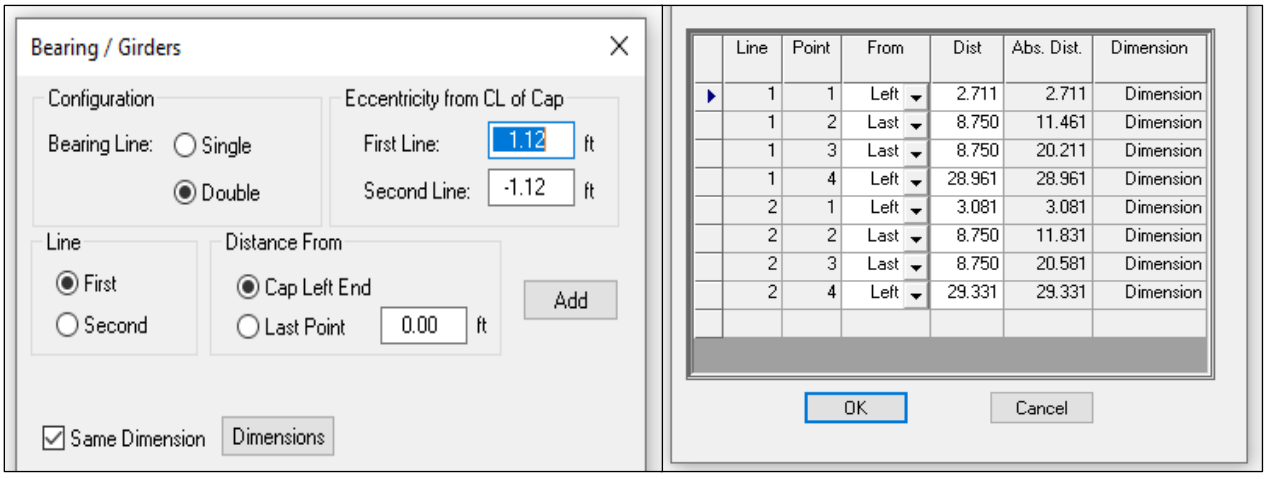

Figure D-1: Bearing and girders geometry configuration (RC-Pier).

Figure D-2 shows the inputs, representing structural dead loads, live loads, impact loads, etc. In addition to bearing loads, this case includes uniformly distributed loads (UDLs) applied across the cap. The UDLs are

defined by their magnitude (in klf) and location across the span (as fractions of the cap length from x_1/L to x_2/L). These loads also remain unfactored at this stage.

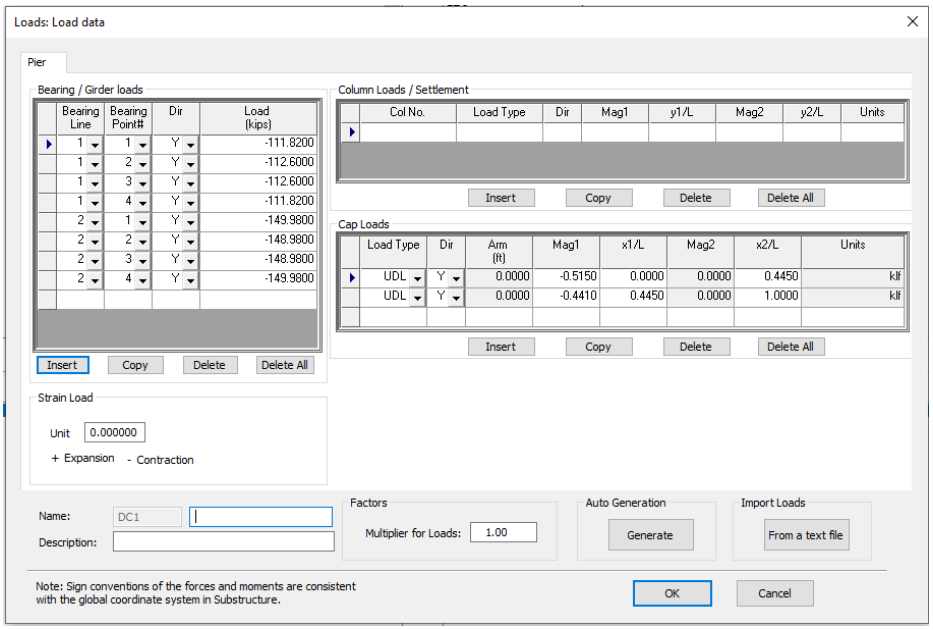

Figure D-2: Loads– Bearing and Cap Loads

Figure D-3 shows some of the combinations considered by RC Piers based on AASHTO LFRD provisions.

```
LOAD COMBINATIONS - AASHTO LRFD 9

Comb #     1  (STR GP 1        ) = 1.00 (  1.25 DC1 + 1.50 DW1 + 1.75 LL1 + 1.75 CE1
                                       + 1.75 BR1 + 0.50 SH1 )
Comb #     2  (STR GP 1        ) = 1.00 (  1.25 DC1 + 1.50 DW1 + 1.75 LL2 + 1.75 CE2
                                       + 1.75 BR2 + 0.50 SH1 )
Comb #     3  (STR GP 1        ) = 1.00 (  1.25 DC1 + 1.50 DW1 + 1.75 LL3 + 1.75 CE3
                                       + 1.75 BR3 + 0.50 SH1 )
Comb #     4  (STR GP 1        ) = 1.00 (  1.25 DC1 + 1.50 DW1 + 1.75 LL4 + 1.75 CE4
                                       + 1.75 BR4 + 0.50 SH1 )
Comb #     5  (STR GP 1        ) = 1.00 (  1.25 DC1 + 1.50 DW1 + 1.75 LL5 + 1.75 CE5
                                       + 1.75 BR5 + 0.50 SH1 )
Comb #     6  (STR GP 1        ) = 1.00 (  1.25 DC1 + 1.50 DW1 + 1.75 LL6 + 1.75 CE6
                                       + 1.75 BR6 + 0.50 SH1 )
Comb #     7  (STR GP 1        ) = 1.00 (  1.25 DC1 + 1.50 DW1 + 1.75 LL7 + 1.75 CE7
                                       + 1.75 BR7 + 0.50 SH1 )
```

Figure D-3: RC –Pier output- load combinations.

Figure D-4 shows a sample output from RC-Pier report, presenting the internal forces at each node of the bent cap under factored load combinations based on AASHTO LRFD provisions. This table includes the factored reactions at all girder support locations for a specific load combination.

To extract the bearing loads for STM design, the engineer identifies the nodes corresponding to bearing locations along the bent cap. The vertical applied loads at these nodes represent the factored bearing reactions that are directly used as input in the STM templates. These values incorporate all relevant dead

and live load effects, including impact, and have been combined and factored per AASHTO specifications within RC-Pier.

The RC Pier analysis provides both the vertical reactions and the corresponding moments at the bearings (nodes). In order to input these results into the strut-and-tie templates, the reactions and moments should be represented as two separate vertical forces spaced apart horizontally. The summation of these two forces is equal to the total vertical reaction obtained from RC Pier, while the couple generated by the two forces corresponds to the moment at the support. They should be statically equivalent. This ensures that both the equilibrium of forces and the moment effects from RC Pier are correctly represented in the template.

This output eliminates the need for manual load combination or factoring, providing a set of bearing loads that can be used in STM templates for reinforcement design and nodal checks.

Combination No. 2661
Group Id: STR GP 5 Name: STRENGTH GROUP V

Memb	Node	Fx kip	Fy kip	Fz kip	Mx kft	My kft	Mz kft
1	1	10.76	624.69	-2.24	-182.53	0.42	-137.83
1	2	-8.60	-589.86	3.49	94.55	-0.42	-150.64
2	3	13.31	751.26	-1.25	-172.96	0.32	-188.72
2	4	-11.15	-716.44	2.50	114.80	-0.32	-176.52
3	5	15.19	617.32	-2.34	-184.15	0.23	-232.92
3	6	-13.03	-582.49	3.59	93.14	-0.23	-189.04
4	7	0.00	0.00	0.00	0.00	0.00	0.00
4	8	0.00	8.32	0.11	0.00	0.13	-10.18
5	8	0.00	-8.32	-0.11	0.00	-0.13	10.18
5	9	0.00	10.43	0.14	0.00	0.21	-16.02

Figure D-4: Sample RC-Pier output showing factored support reactions for Strength Group V, used to extract bearing loads for STM-based bent cap design.

The STM templates developed in this research are designed to function independently of upstream load combination logic and are applied after factored bearing reactions are determined. Specifically, the templates require the following inputs: factored vertical bearing reactions (obtained from RC-Pier), bearing locations and spacing, bent cap geometry (including length, depth, and column spacing), and material properties such as concrete compressive strength (f'_c) and steel yield strength (f_y). Based on these inputs, the STM template calculates the required tie reinforcement and checks the nodal capacity for the particular STM selected.

The output from the STM template includes the required area of steel (A_s) for each tie, a check of the nodal capacities and a check of the minimum angle requirements. Since the template uses factored bearing loads, it fits into the existing design workflow and can replace or complement sectional design methods without requiring changes to upstream load modeling processes or software tools such as RC-Pier or LEAP Bridge.

Table D.1 shows a summary of the steps involved in incorporating the STM templates into the NCDOT bridge substructure workflow.

Table D.1: Step-by-step integration of the STM template into the standard bridge substructure design workflow.

Step 1: Load Generation (LEAP Bridge)	• Model the superstructure using LEAP Bridge (e.g., span layout, girder type, geometry) • Obtain girder reaction loads: DC, DW, LL, IM (unfactored)
Step 2: Load Combination and Factoring (RC-Pier)	• Input all loads into RC-Pier • RC-Pier applies AASHTO LRFD load combinations (e.g., Strength I) • Output: factored bearing reactions at each girder support
Step 3: STM Template Selection and Input	• Choose the appropriate STM template based on cap geometry and support configuration • Enter the factored loads and bearing reactions, spacing, and material properties into the template
Step 4: Reinforcement Detailing and Nodal Checks	• Review output reinforcement requirements from the STM template • Detail all reinforcement as required by AASHTO LRFD • Ensure each node satisfies the capacity limits and stress checks on each face • Ensure the minimum angle requirements are adhered to for the geometry and typology

The implementation of STM templates using factored load inputs from RC-Pier provides a viable path for bent cap design in NCDOT structures. It builds on existing workflows and maintains compatibility with software used by NCDOT such as LEAP Bridge and RC-Pier.

E ADDITIONAL DETAILS OF THE EXPERIMENTAL PROGRAM

To obtain high-resolution, full field-of-view deformation data, the entire surface of the west face of the beam was monitored with a full field-of-view DIC system. Maintaining an approximate resolution of 2 pixels/mm, three stereo-systems (north system, middle system, and south system) with two 12.3 MP cameras in each system, were used (shown in Figure E-1). The data from the three systems were combined using a proprietary multi-view registration algorithm. A speckle pattern with speckles measuring approximately 2.5 mm in diameter was applied to the specimens. This arrangement resulted in 3-5 pixels per speckle. The speckle pattern was applied so the beam had approximately 50% black-white contrast.

Throughout loading, the entire specimen surface 3D deformation field was captured. The east face of the beam was instrumented with a 9 in x 9 in a grid of 138 Infrared Light-Emitting Diode (LED) targets arranged in 6 rows and 23 columns. The entire specimen surface 3D deformation field was captured throughout loading. This data was used to help verify and validate the DIC deformation field data obtained (see Figure E-1).

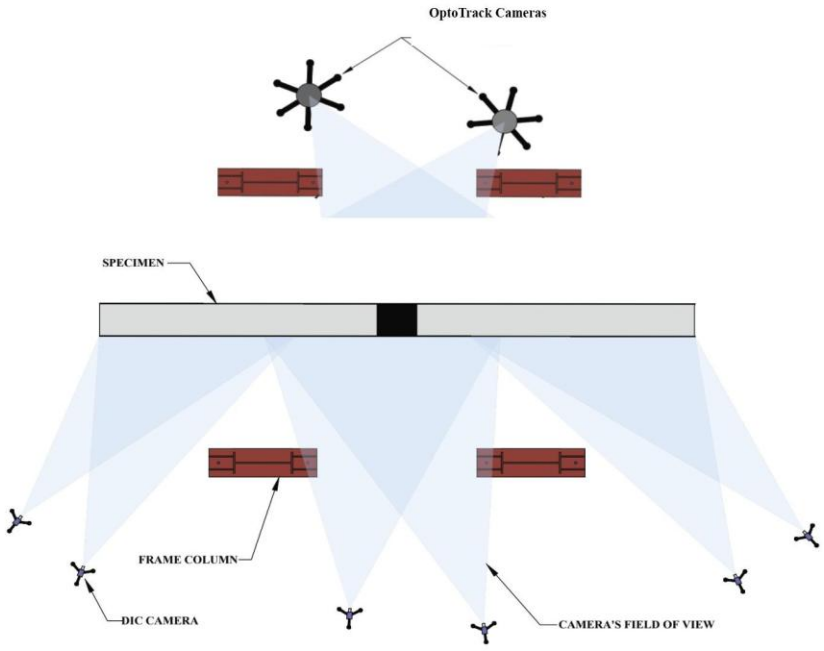

Figure E-1: Plan view of the DIC cameras and LED arrangement.

The specimens were loaded monotonically to failure. Throughout the tests, load stages were conducted, where at a load stage, the loading was halted and reduced by approximately 10-15% (for safety). The cracks were marked and measured on the east face of the member using crack comparator gauges. In addition to

the DIC photos, high resolution photos were taken locally on the specimen at each load stage and after failure. Throughout loading, high-resolution videos were recorded on the east face of the specimen.

The reaction frame was used to test the STC series. The load was applied with a 2000-kip hydraulic cylinder. The cylinder was used to apply a monotonically increasing load to the center of the reinforced concrete deep beam specimen. The applied load was measured by monitoring the pressure applied from the advance valve of the cylinder. The hydraulic cylinder was attached to the middle of the spreader beam to apply the load and evenly distribute the reaction between the two frames. All of the specimens rested on roller-roller supports. Figure E-2 shows the experimental setup for STC1-STC3. Figure E-3 shows the experimental setup for STC4-STC6.

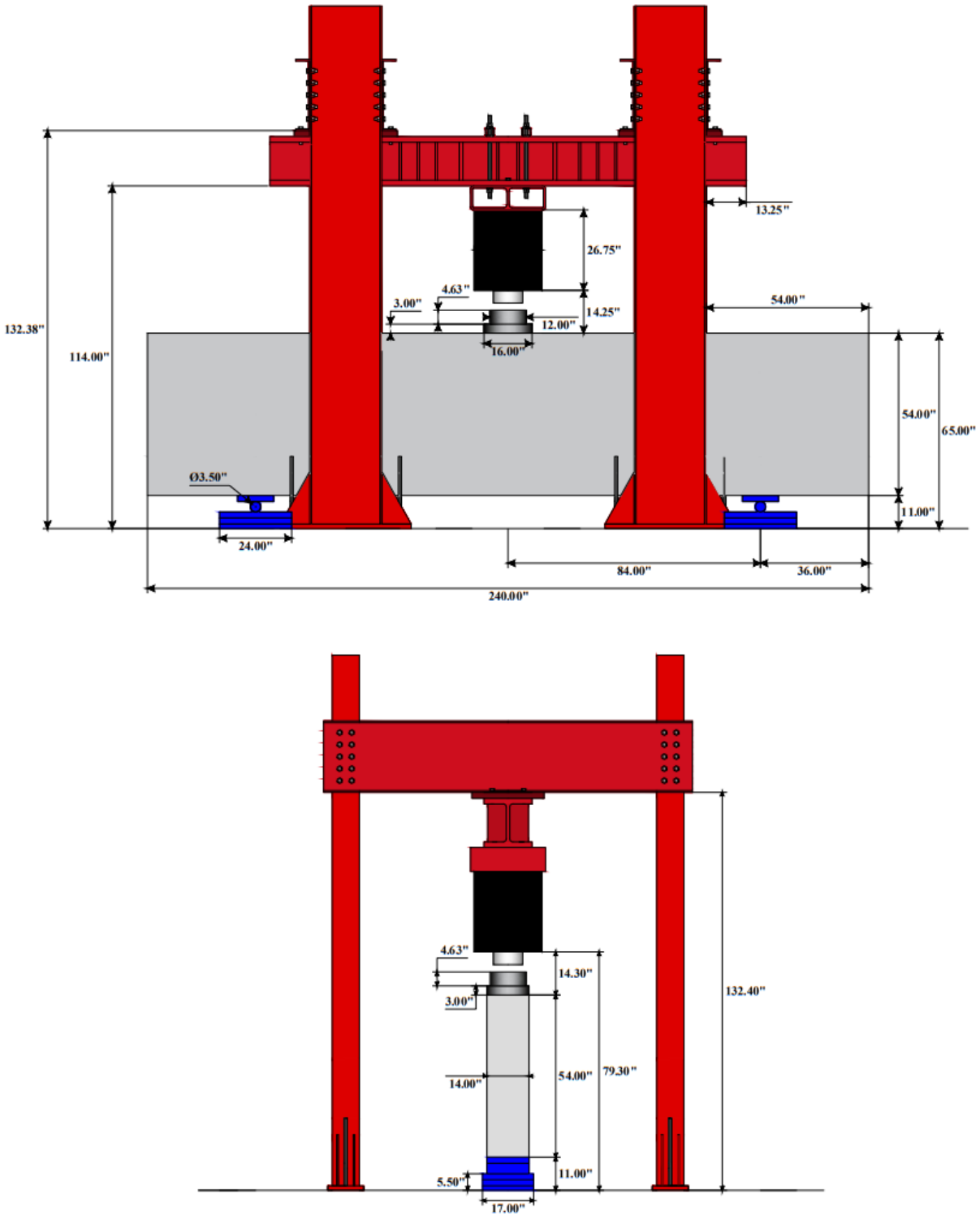

Figure E-2: Experimental setup STC1-STC3.

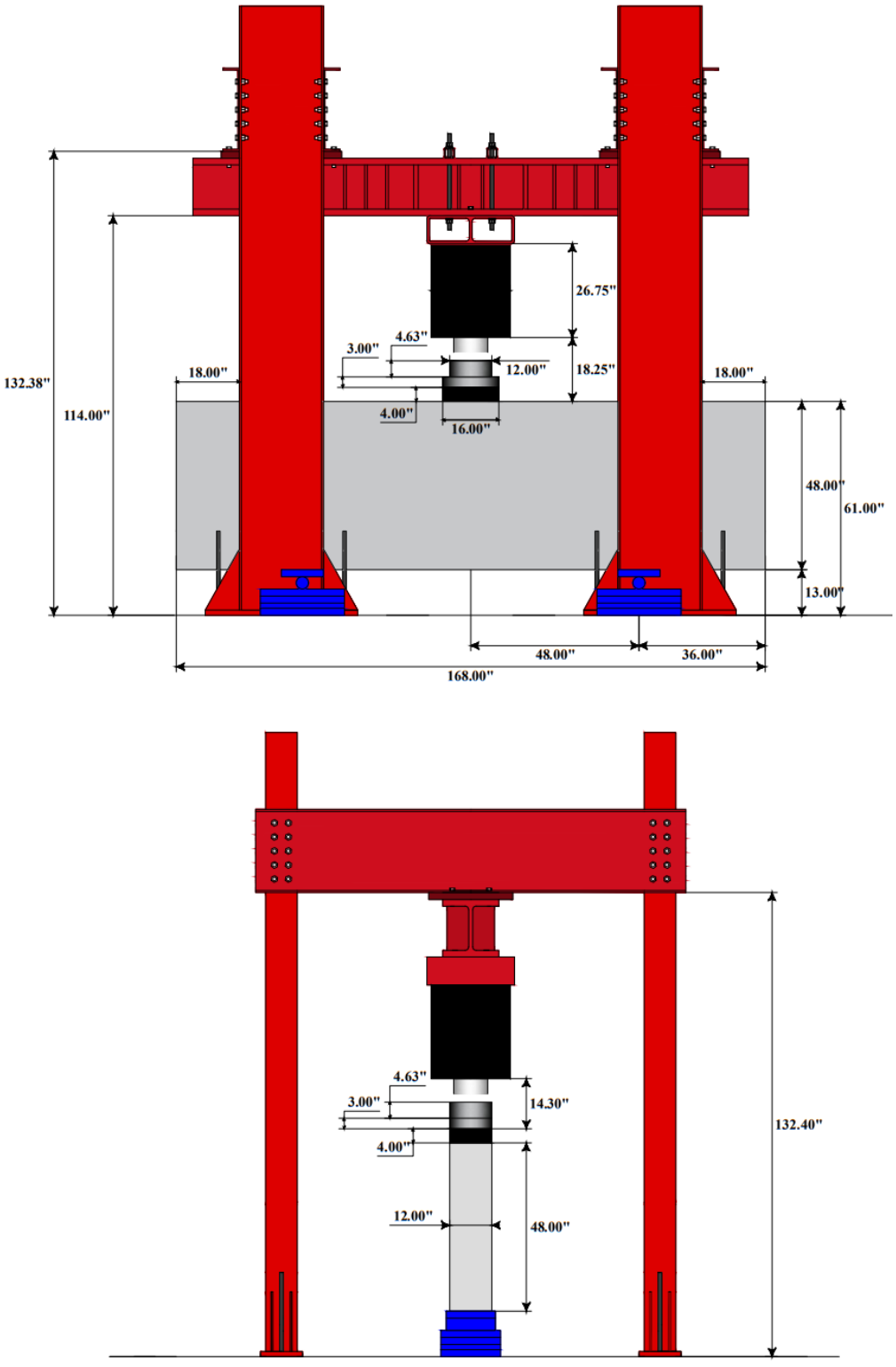

Figure E-3: Experimental setup STC4-STC6.

The STC experimental program consisted of six deep beam specimens designed to investigate shear behavior under varying reinforcement configurations and geometries. STC1 - STC3 measured 240 in. (6096 mm) in length, 54 in. (1372 mm) in height, and 14 in. (356 mm) in width, while STC4 – STC6 measured 168 in. (4267 mm) in length, 48 in. (1219 mm) in height, and 14 in. (356 mm) in width. All specimens were supported on two 12 in. × 14 in. × 2 in. (305 mm × 356 mm × 51 mm) steel plates resting on roller supports. A 16 in. × 14 in. × 3 in. (407 mm × 356 mm × 76 mm) steel loading plate was used for all tests, with Hydro-Stone applied between the plate and the beam to ensure uniform contact. A spherical bearing between the actuator head and the loading plate allowed load application without moment transfer. The primary variable was the amount of distributed reinforcement in each orthogonal direction (ρ_v and ρ_h): STC1 and STC4 had 0.30%, STC2 and STC5 had 0.13%, and STC3 and STC6 had no distributed reinforcement. Longitudinal reinforcement ratios (ρ_l) ranged from 1.57% to 1.75%, and compressive strength ($f'c$) varied from 4.8 to 5.6 ksi. All beams used Grade 60 steel reinforcement ($f_{y,w}$ = 62.5 ksi, $f_{y,t}$ = 65 ksi). The shear span-to-depth ratio (a/d) was approximately 1.81 for STC1 - STC3 and 1.18 for STC4 - STC6.

E.1 Material Properties

E.1.1 Concrete Properties

The specified concrete cylinder strength was approximately 3.0 ksi. The aggregate size used was 0.375 in. The concrete strength at the day of testing were higher than 3.0 ksi. The summary of concrete strengths, f'_c, measured on test day are provided in Table E.1.

Table E.1: Concrete cylinder strengths for STC1-STC6 measured on test day.

Cylinder Test Data	
Beam	f'_c **(ksi)**
STC 1	4.93
STC 2	5.14
STC 3	5.46
STC 4	4.82
STC 5	5.21
STC 6	5.58

E.1.2 Steel Reinforcement Properties

As previously described, two sets of steel reinforcement bars were used in the experimental series: No. 4 Grade 60 deformed reinforcing bars and No. 10. Grade 60 deformed reinforcing bars. The material properties of all the reinforcement in the experimental series was obtained from steel coupon tests. The yield stress (f_y) against yield strain (ε_y) is shown in Figure E-4 and Figure E-5.

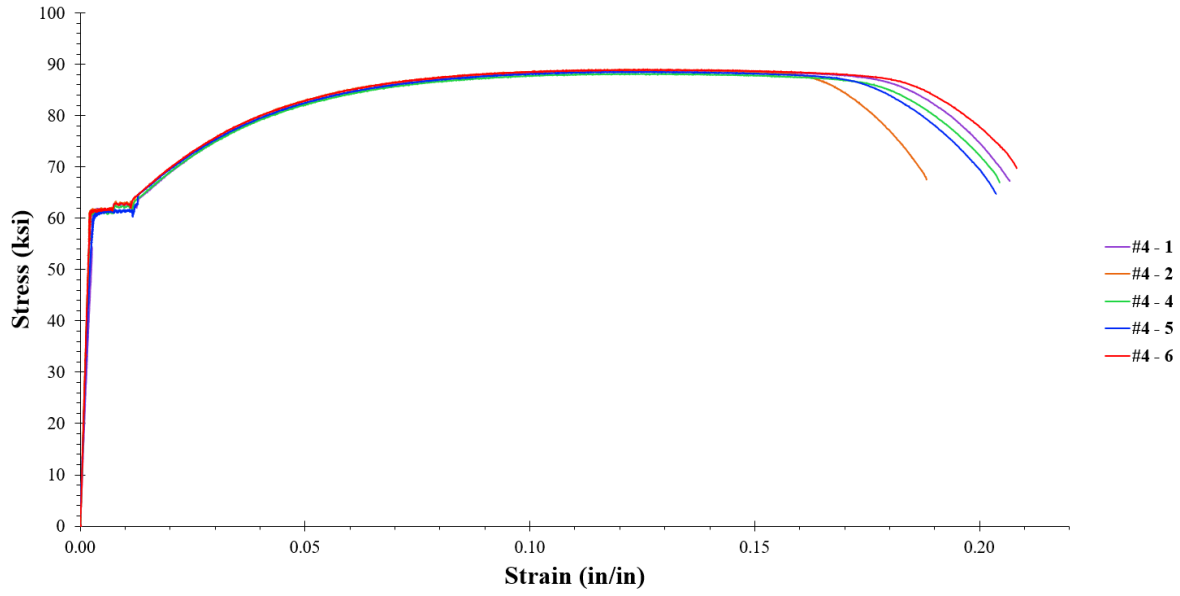

Figure E-4: Stress versus strain response of steel No. 4 steel coupons.

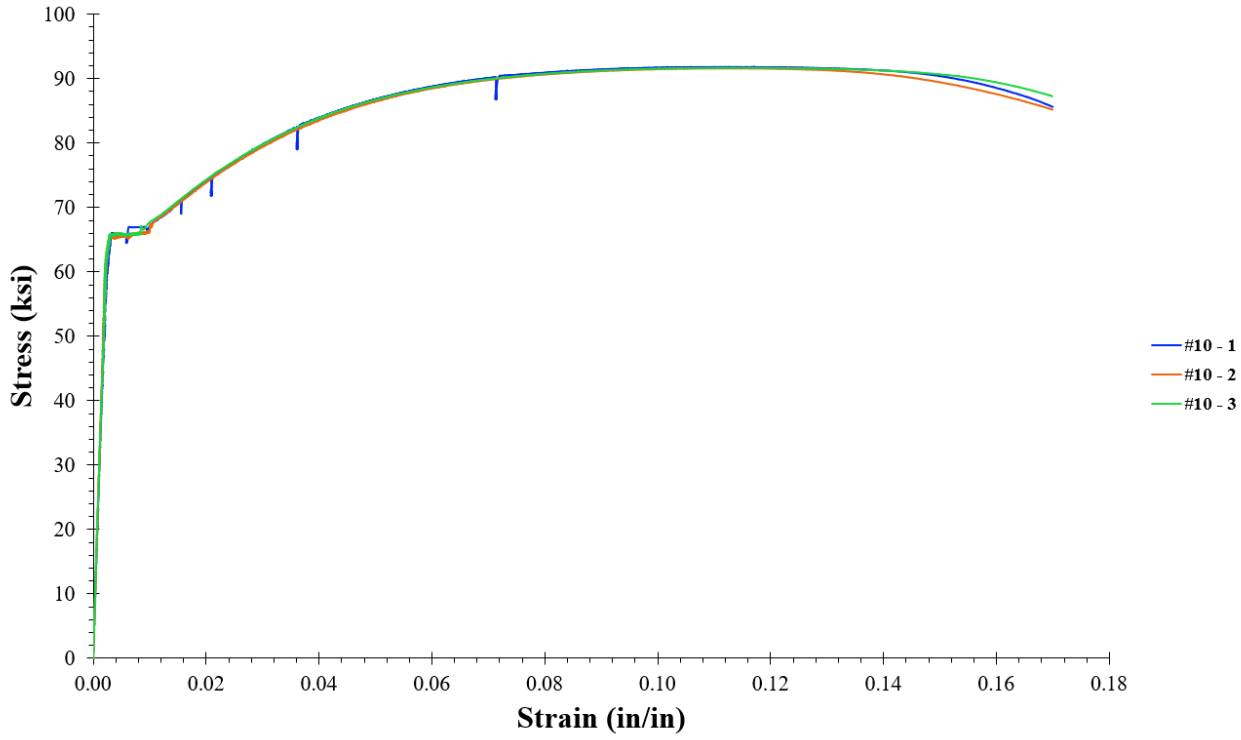

Figure E-5: Stress versus strain response of steel No. 10 steel coupons.

F STRAIN ANALYSIS AND CRACK PATTERNS AT FAILURE LOADS

F.1 Strain Analysis

Figure F-1 shows the placement of strain gauges in each beam. Beams without transverse reinforcement contain a total of three strain gauges placed on the longitudinal reinforcement: one at midspan and two located halfway between the loading plate and the support plate on each side. The other beams, which include transverse reinforcement, have two additional strain gauges installed on the transverse reinforcement near the center of the shear span.

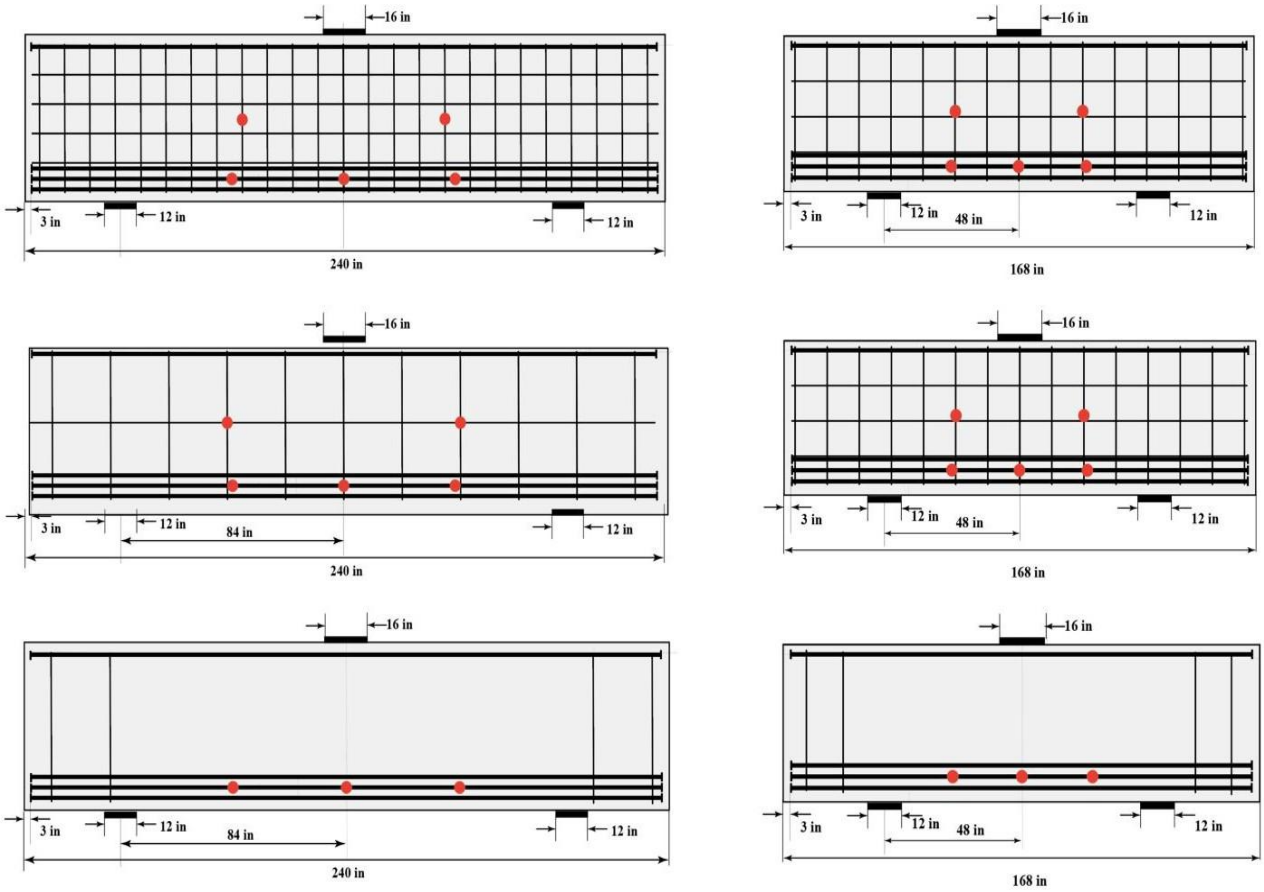

Figure F-1: Arrangement of strain gauges.

Figure F-2 presents the load versus strain response for strain gauges 1 through 3, located on the longitudinal reinforcement of STC1. Figure F-3 shows the load versus strain response for strain gauges 4 and 5, positioned on the transverse reinforcement of STC1.

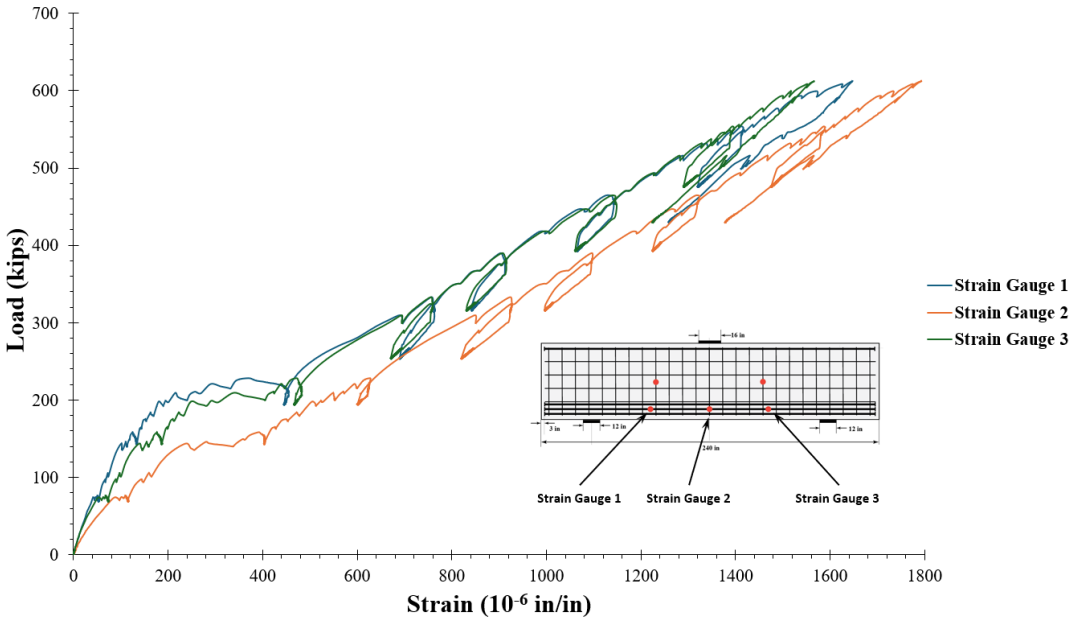

Figure F-2: STC1: Load versus strain of strain gauges 1, 2, and 3.

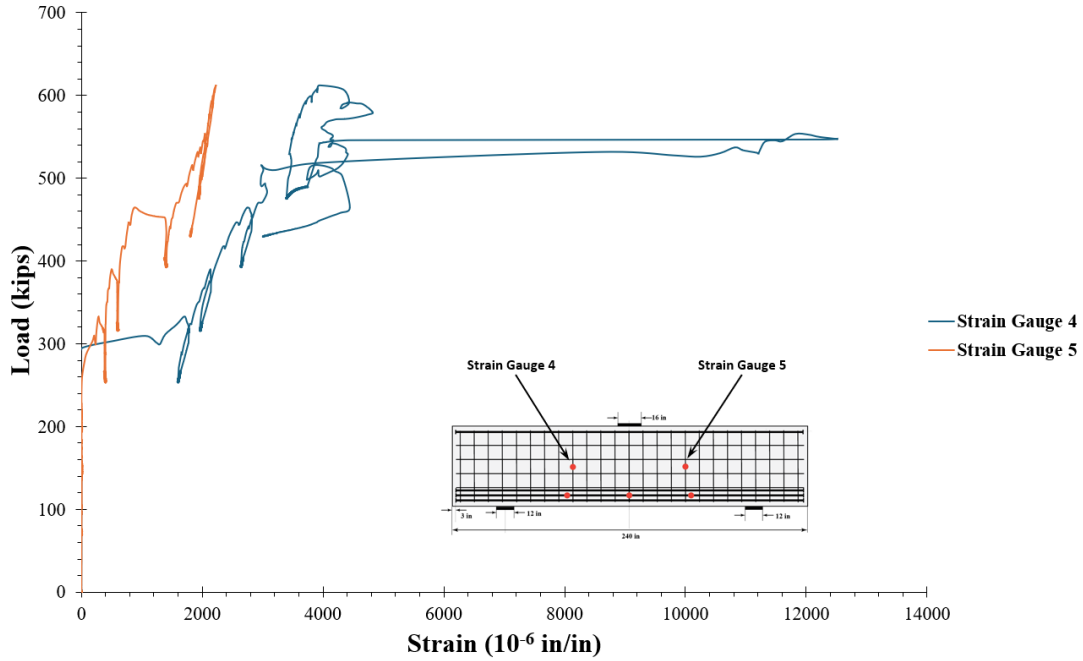

Figure F-3: STC1: Load versus strain of strain gauges 4 and 5.

Figure F-4 presents the load versus strain response for strain gauges 1 through 3, located on the longitudinal reinforcement of STC2. Figure F-5 shows the load versus strain response for strain gauges 4 and 5, positioned on the transverse reinforcement of STC2.

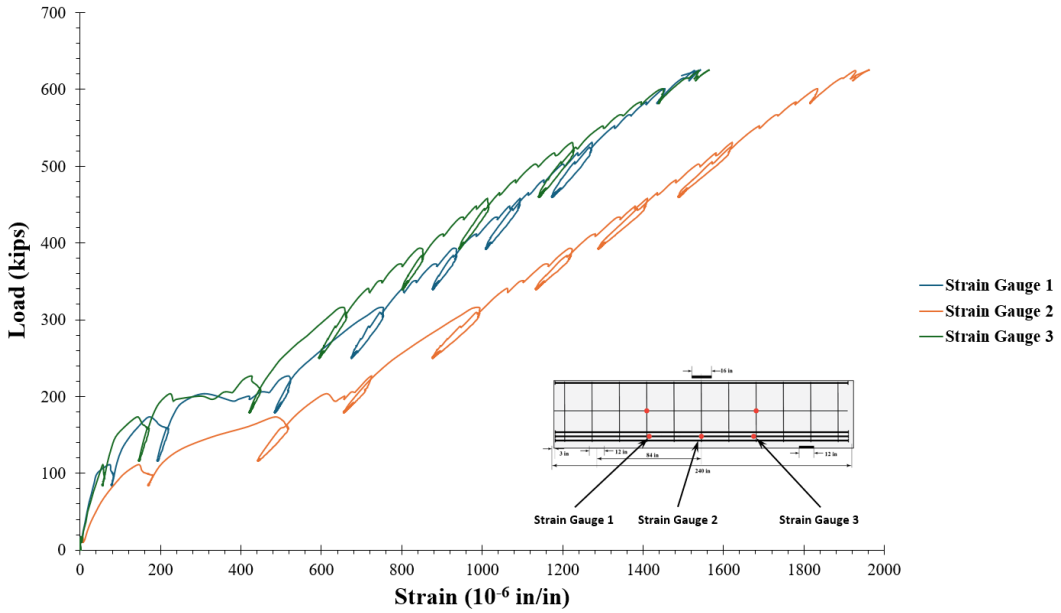

Figure F-4: STC2: Load versus strain of strain gauges 1, 2, and 3.

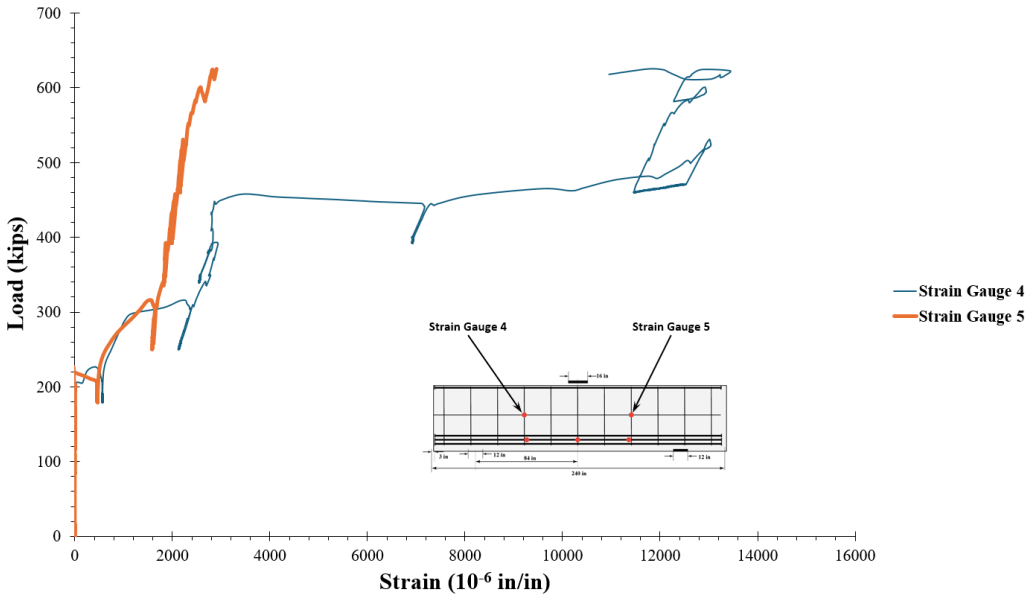

Figure F-5: STC2: Load versus strain of strain gauges 4 and 5.

Figure F-6 presents the load versus strain response for strain gauges 1 through 3, located on the longitudinal reinforcement of STC3.

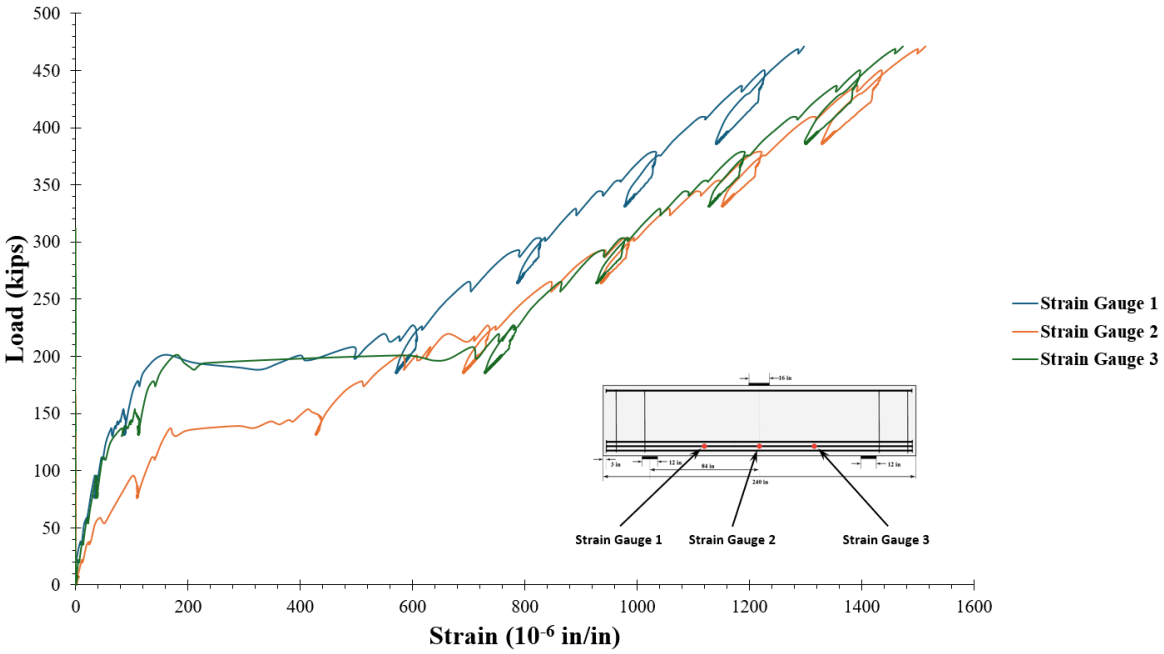

Figure F-6: STC3: Load versus strain of strain gauges 1, 2, and 3.

Figure F-7 presents the load versus strain response for strain gauges 1 through 3, located on the longitudinal reinforcement of STC4. Figure F-8 shows the load versus strain response for strain gauges 4 and 5, positioned on the transverse reinforcement of STC4.

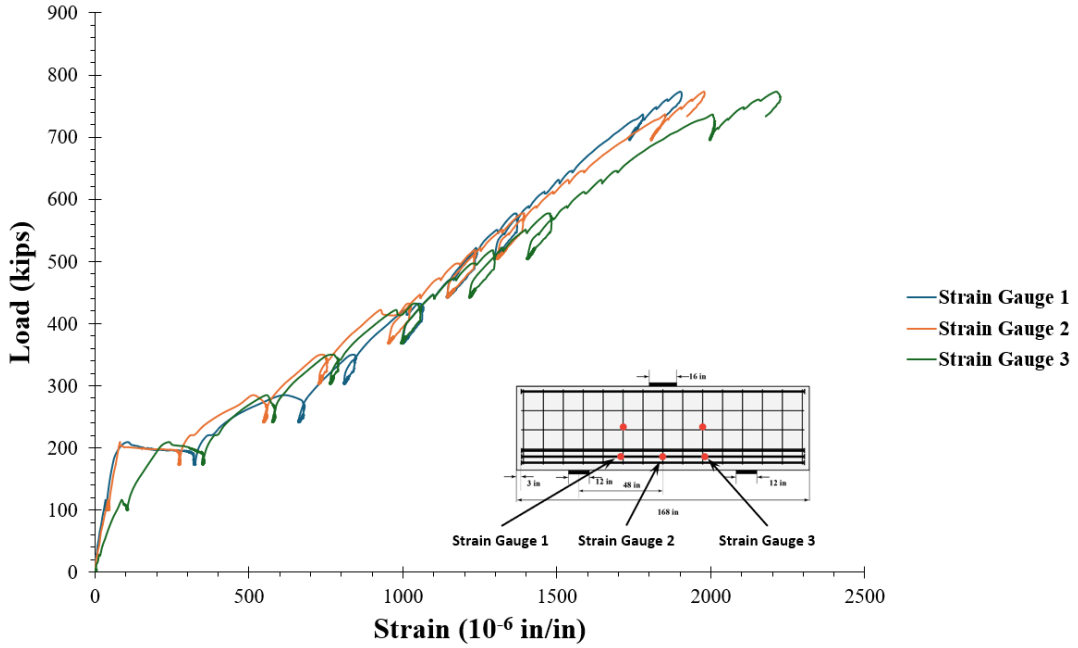

Figure F-7: STC4: Load versus strain of strain gauges 1, 2, and 3.

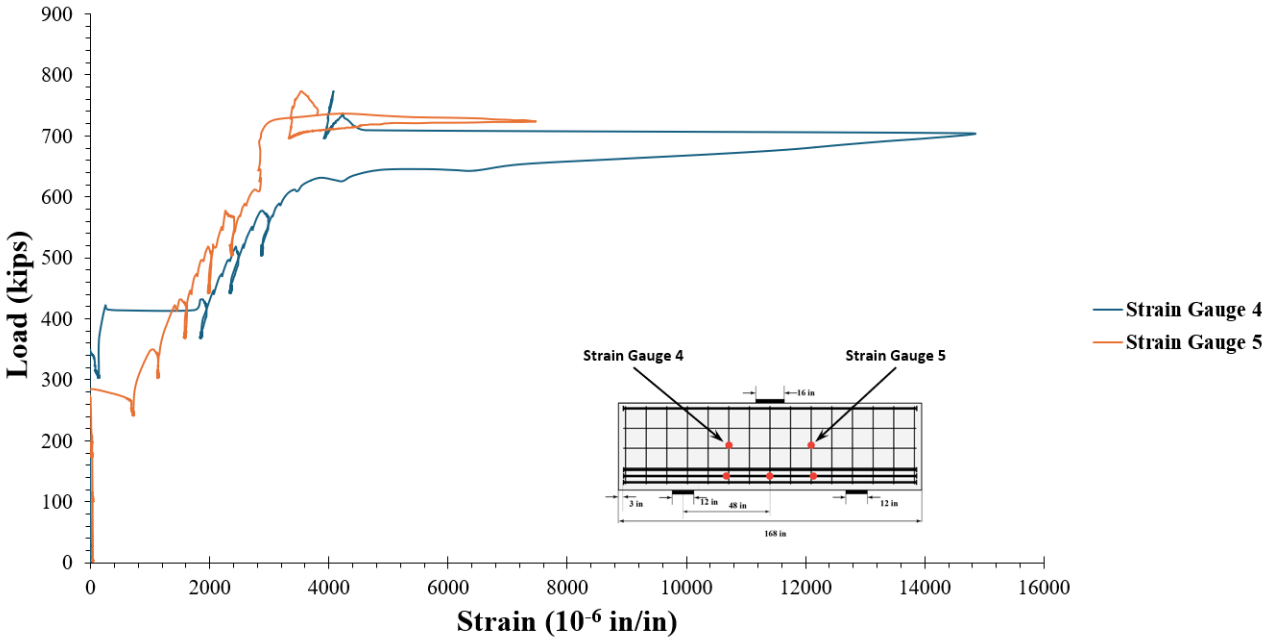

Figure F-8: STC4: Load versus strain of strain gauges 4 and 5.

Figure F-9 presents the load versus strain response for strain gauges 1 through 3, located on the longitudinal reinforcement of STC5. Figure F-10 shows the load versus strain response for strain gauge 4, positioned in the transverse reinforcement of STC5.

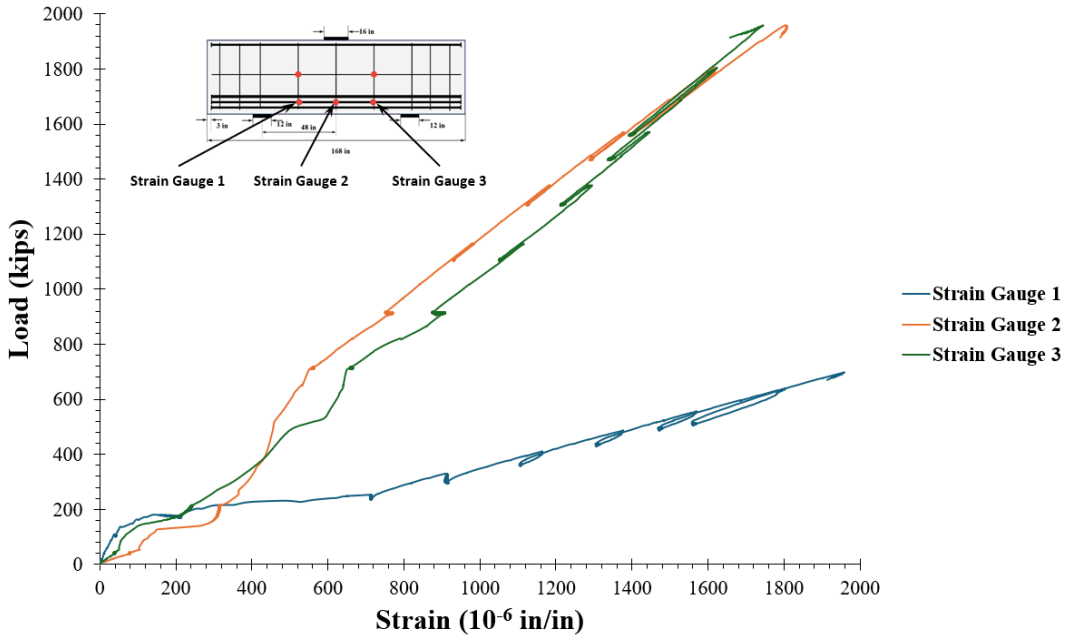

Figure F-9: STC5: Load versus strain of strain gauges 1, 2, and 3.

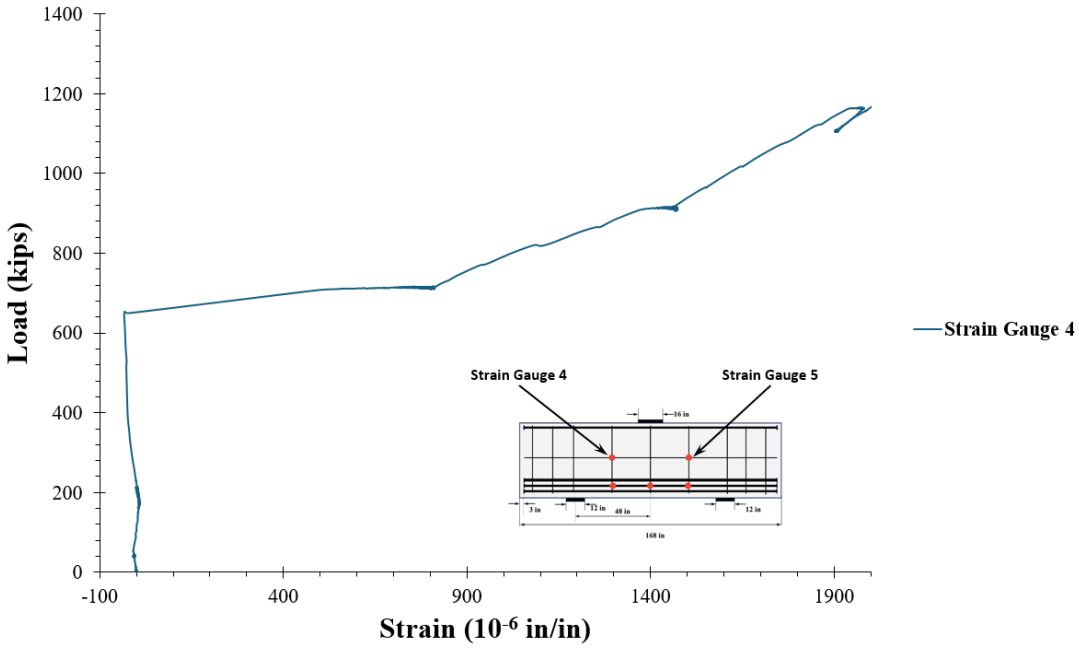

Figure F-10: STC5: Load versus strain of strain gauge 4.

Figure F-11 presents the load versus strain response for strain gauges 1 through 3, located on the longitudinal reinforcement of STC6.

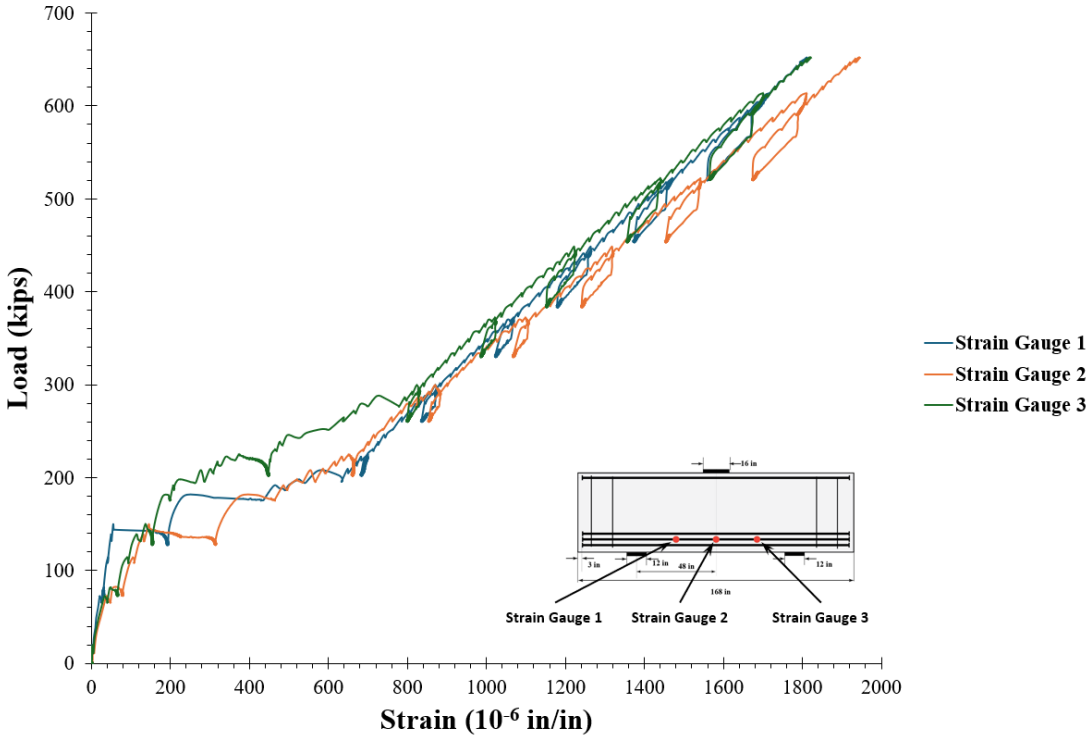

Figure F-11: STC6: Load versus strain of strain gauges 1, 2, and 3.

F.2 Crack Patterns

The crack patterns obtained for STC1-STC3 and STC4-STC6 are shown in Figure F-12 through Figure F-14 and Figure F-16 through Figure F-18, respectively. The critical cracks for each specimen are indicated with a thicker line. The critical crack is typically defined as the crack that extends from the inner edge of the support plate to near the edge of the loading plate and has the largest crack widths. Figure F-15 shows the combined crack widths of STC1, STC2 and STC3. Figure F-19 shows the combined crack widths of STC4, STC5 and STC6. As it can be seen in the figures, the number of cracks is reduced as the transverse reinforcement ration is increased.

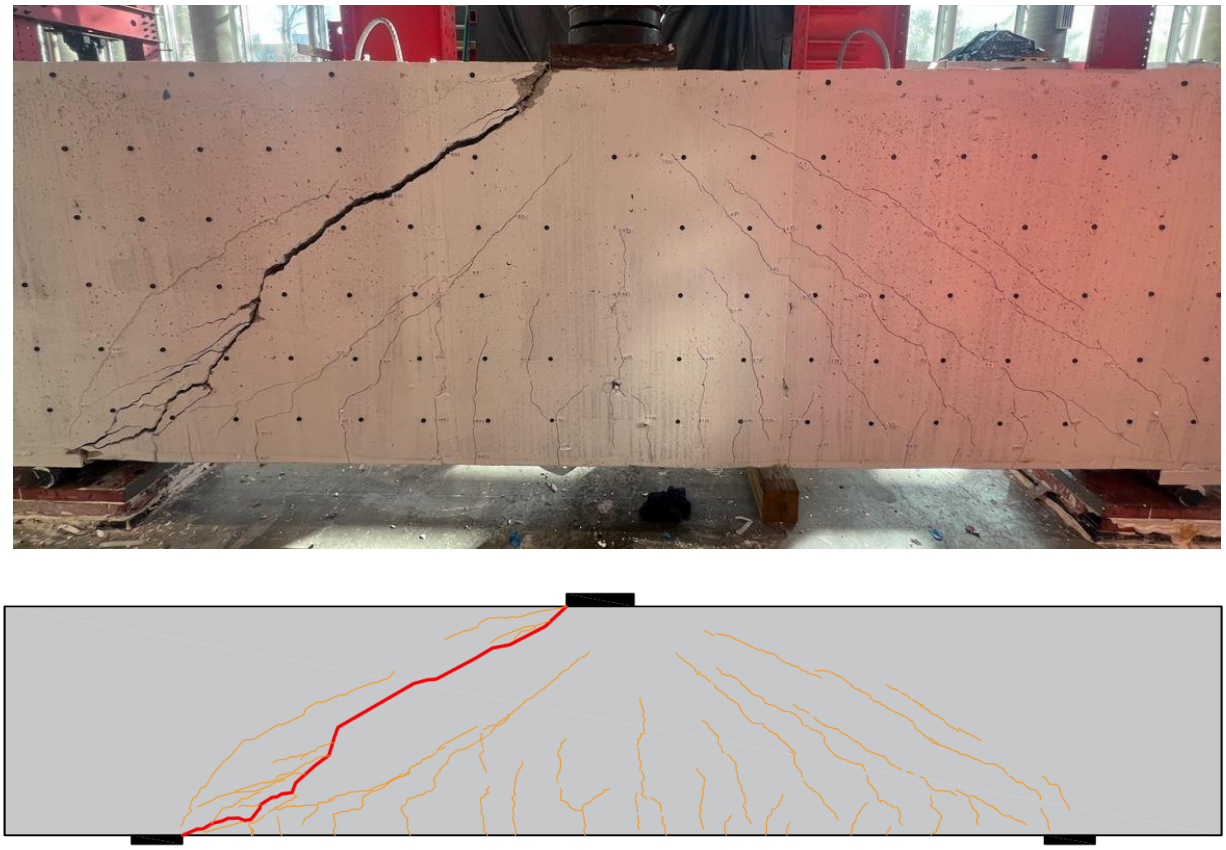

Figure F-12: Crack pattern of beam STC1 at failure load.

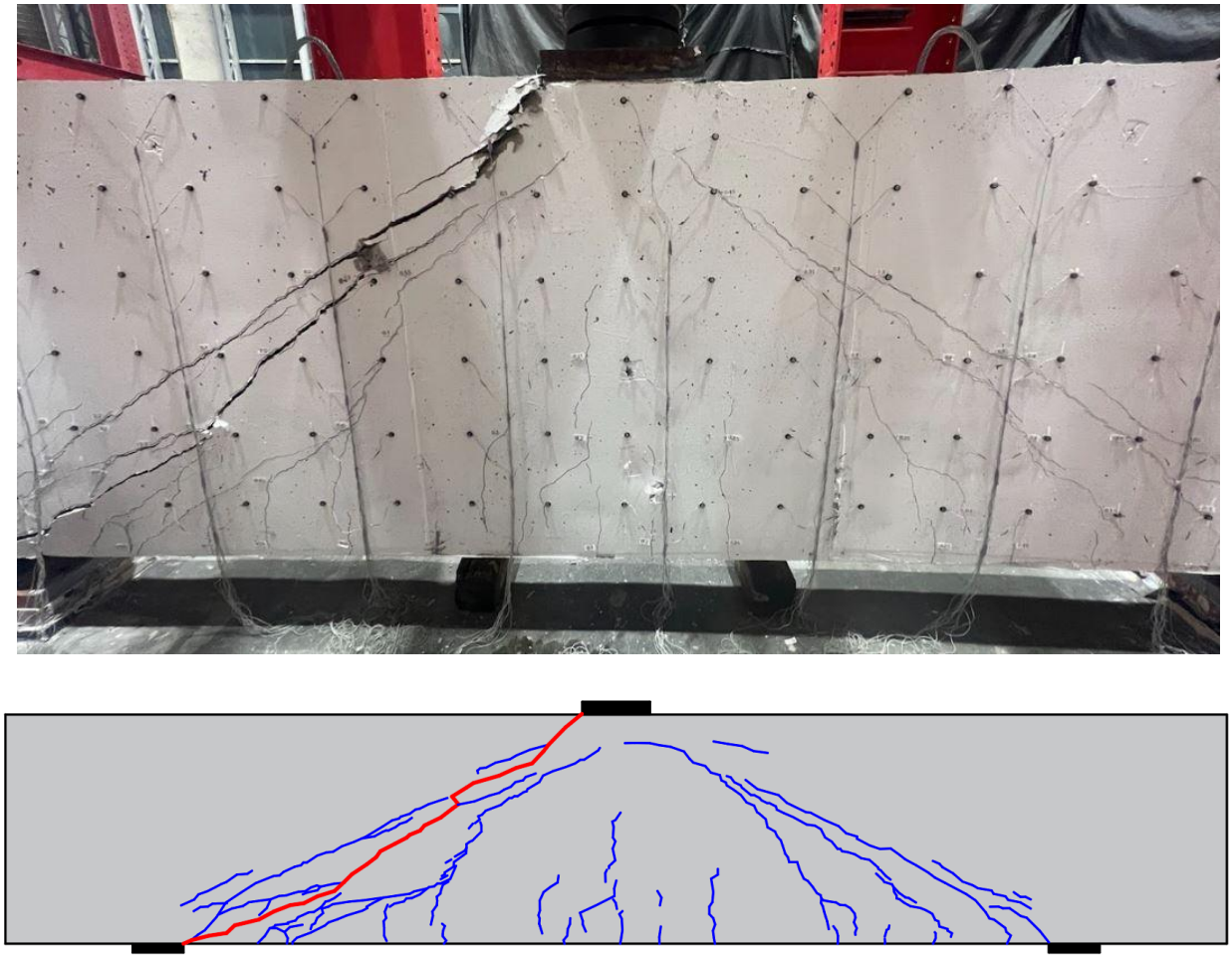

Figure F-13: Crack pattern of beam STC2 at failure load.

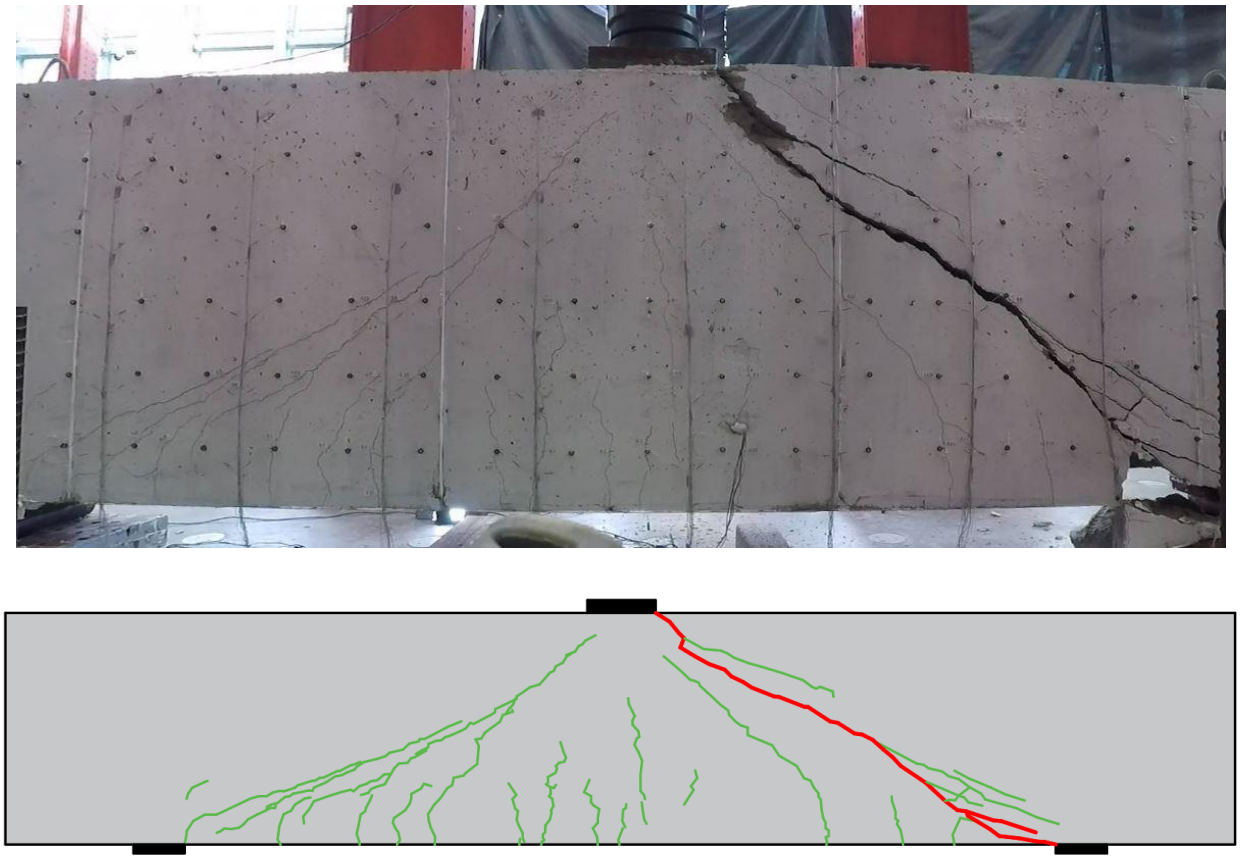

Figure F-14: Crack pattern of beam STC3 at failure load.

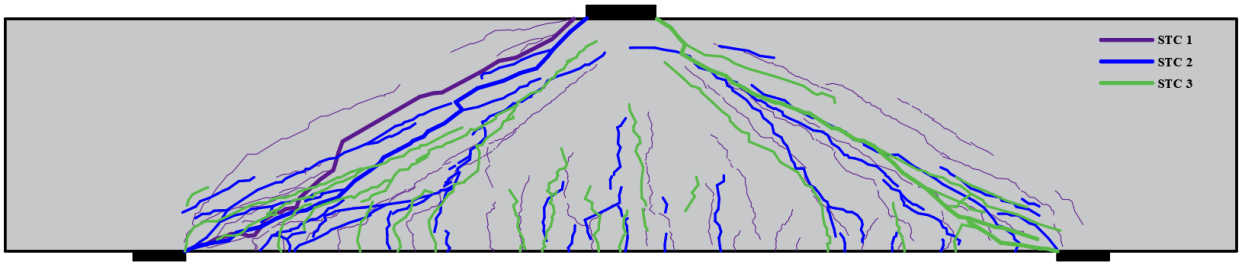

Figure F-15: Overlapping crack patterns of beams STC1, STC2, and STC3.

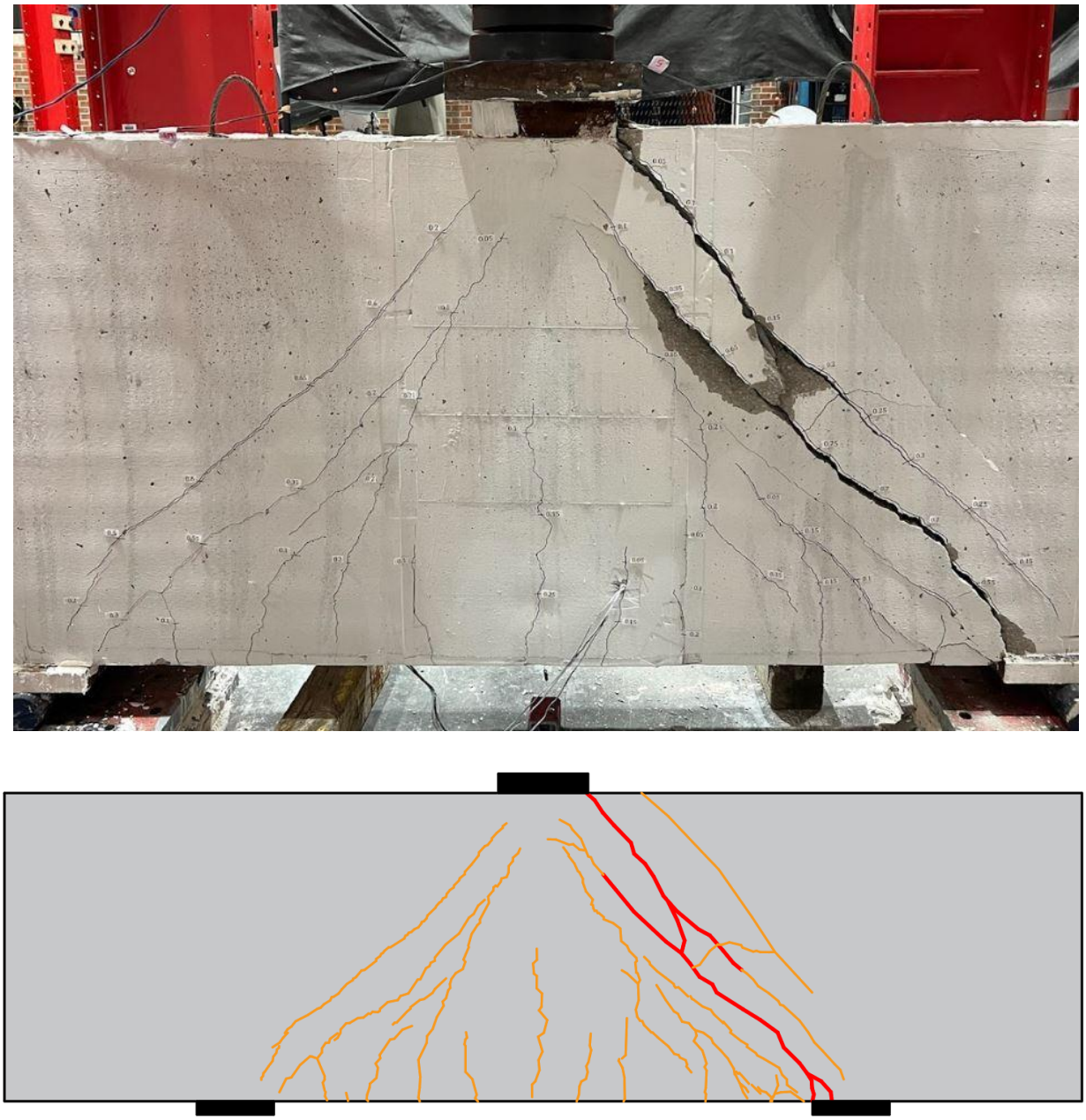

Figure F-16: Crack Pattern of beam STC4 at failure load.

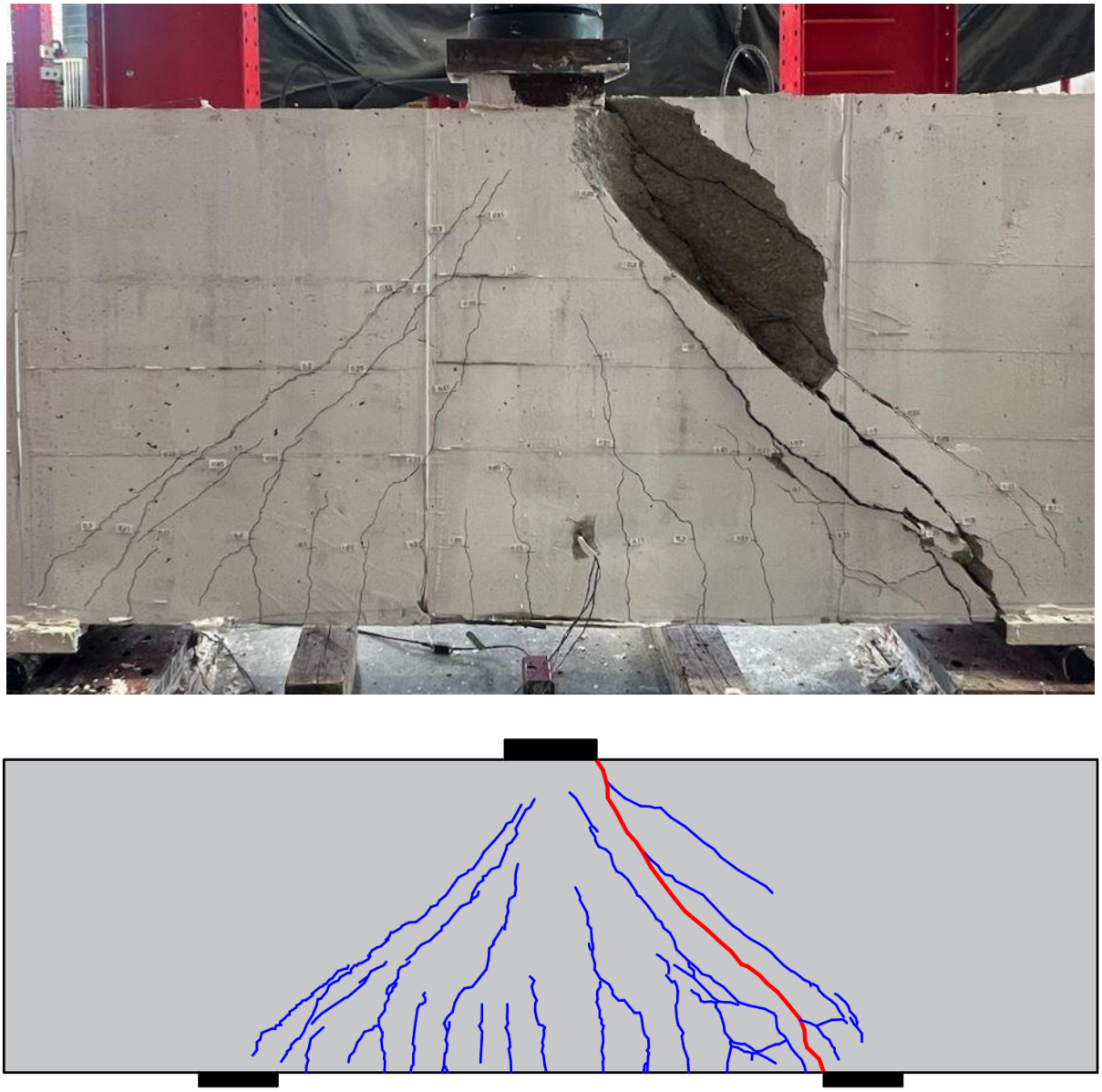

Figure F-17: Crack Pattern of beam STC5 at failure load.

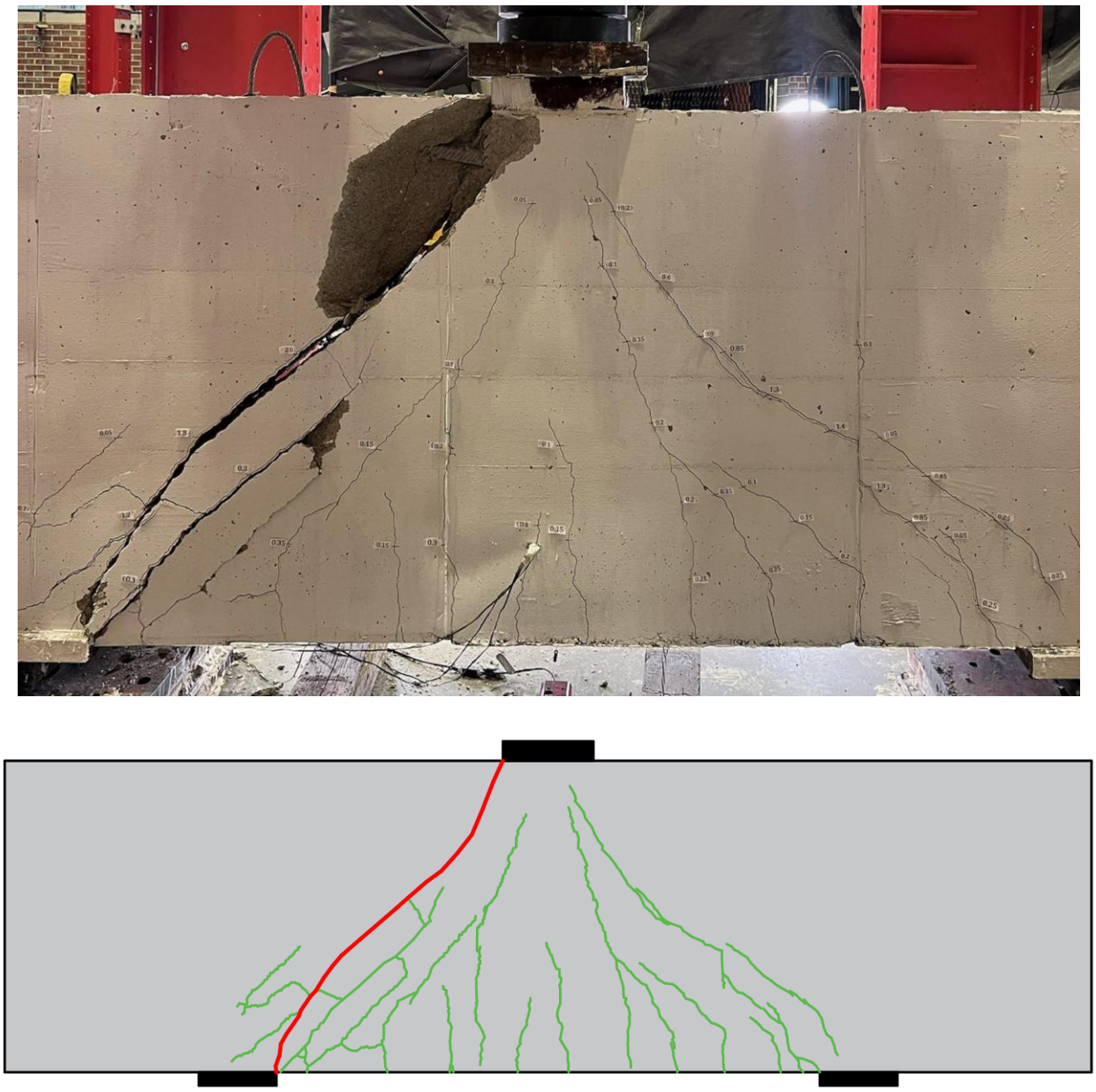

Figure F-18: Crack pattern of beam STC6 at failure load.

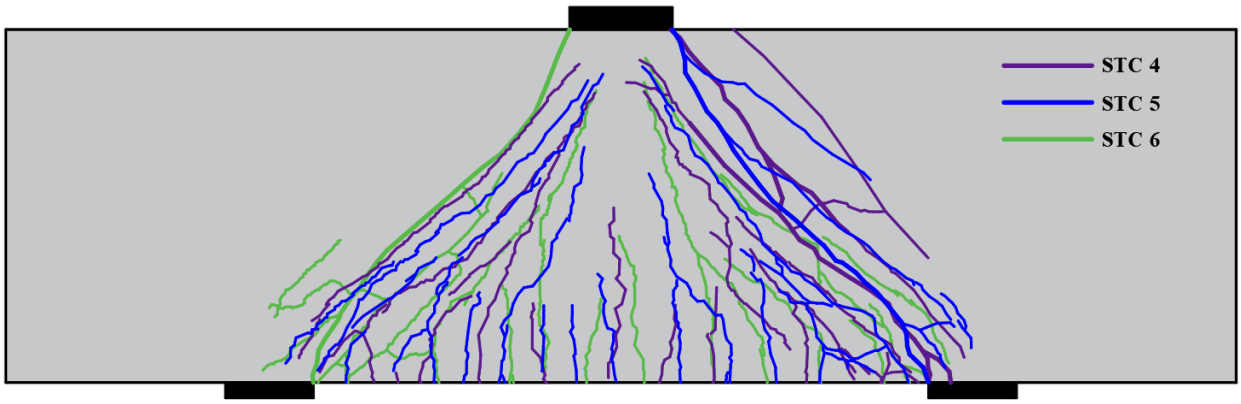

Figure F-19: Overlapping crack patterns of beams STC4, STC5, and STC6.

G SUMMARY OF LITERATURE REVIEWED FOR THIS PROJECT

This chapter presents a comprehensive compilation of the reference materials consulted throughout the course of this research project. While the previous literature review chapter focused on summarizing selected studies and codes that directly influenced the conceptual framework and methodology, this section lists a broader range of technical documents, design specifications, and code provisions that supported various aspects of the study. These references provided essential background knowledge, theoretical foundations, and guidance on best practices relevant to the project, and were instrumental in shaping the experimental design, analysis procedures, and interpretation of results.

Barbary, A., Beshara, F., Mahmoud, A. (2015). STATE OF ART—High strength Steel Fiber Reinforced Concrete Deep Beams. Performance of Steel Fibers Reinforced Concrete Deep Beam; Repository of Benha University: Benha, Egypt, 9-96.

Bentz, E. C., Vecchio, F. J., Collins, M. P. (2006). Simplified Modified Compression Field Theory for Calculating Shear Strength of Reinforced Concrete Elements. ACI Structural Journal, 103(4), 614-624. doi:10.14359/16438.

Brown, M. D., Sankovich, C. L., Bayrak, O., Jirsa, J. O., Breen, J. E., Wood, C. L. (2006). Design for shear in reinforced concrete using strut-and-tie models (Texas Department of Transportation, Research and Technology Implementation Office). Austin, TX: Center for Transportation Research, Bureau of Engineering Research, University of Texas at Austin.

Collins, M. P., Mitchell, D. (1980). Shear and Torsion Design of Prestressed and Non-Prestressed Concrete Beams. PCI Journal, 25(5), 32-100. doi:10.15554/pcij.09011980.32.100.

Collins, M. P., Mitchell, D. (1981). Discussion and Closure. PCI Journal, Vol. 26, No. 6, Nov-Dec, 1981. Pp.96-118.

Collins, M. P., Mitchell, D. (1997). Prestressed concrete structures. Toronto: Response Publications.

Collins, M.P., Mitchell, D. (1974). Diagonal compression field theory-A rational model for structural concrete in pure torsion. ACI Journal Proceedings, 71(28), 396-408. https:doi.org/10.14359/7103.

Colorito, A., Wilson, K., Bayrak, O., Russo, F. (2017). Strut-and-Tie Modeling (STM) for Concrete Structures, Design Examples [Review of Strut-and-Tie Modeling (STM) for Concrete Structures, Design Examples]. Federal Highway Administration.

EN 1992-1-1 (2004) (English): Eurocode 2: Design of concrete structures – Part 1-1: General rules and rules for buildings [Authority: The European Union Per Regulation 305/2011, Directive 98/34/EC, Directive 2004/18/EC].

He, Z.-Q., Liu, Z., Wang, J., Ma, Z. J. (2020). Development of strut-and-tie models using load path in structural concrete. Journal of Structural Engineering,146(5). https.doi.org/(asce)st.1943-541x.0002631.

Hooke, Robert. (1678). Lectures de potential restitutive, or, Of spring explaining the power of springing bodies : to which are added some collections. London : Printed for J. Martyn.

Joint ACI-ASCE Committee 326. (2008). Shear and diagonal tension. ACI Journal Proceedings, 11(3), 352–396. https://doi.org/10.14359/7921.

Kani, M.W., Huggins, M.W., Wittkopp, R.R. (1979). In Kani on shear in reinforced concrete (p. 225). University of Toronto, Dept. of Civil Engineering, Canada.

Kelly, D.W., Elsley M. (1995). A procedure for determining load paths in Elastic continua. Engineering Computations, 12(5), 415-424. https://doi.org/10.1108/02644409510799721.

Klein, G. J. (2008). Curved-Bar Nodes: A detailing tool for strut-and-tie models. Concrete International, 42-A.11. Leonhardt, F., Walther, R. (2005). The Stuttgart Shear Tests. 318Reference, 11(28).

Liang, Q. Q., Xie, Y. M., Steven, G. P. (2001). Generating optimal strut-and-tie models in prestressed concrete beams by performance-based optimization. ACI Structural Journal, 98(2), 226–232. https://doi.org/10.14359/10191.

Martin, B. T. & Sanders, D. H. (2007)**.** *Verification and Implementation of Strut-and-Tie Model in LRFD Bridge Design Specifications*, NCHRP 20-07, Task 217, a report under the National Cooperative Highway Research Program.

Mihaylov, B. I., Bentz, E. C., Collins, M. P. (2013). Two-Parameter Kinematic Theory for Shear Behavior of Deep Beams. ACI Structural Journal, 110(3), 447-456. doi:10.14359/51685602.

Mihaylov, B. I., Hunt, B., Bentz, E. C., Collins, M. P. (2015). Three-Parameter Kinematic Theory for Shear Behavior of Continuous Deep Beams. ACI Structural Journal, 112(1), 47-58. doi:10.14359/51687180.

Mörsch, E. (1922). Der Eisenbetonbau (Reinforced Concrete Construction, Verlag con Konrad Wittwer. Struttgart, West Germany. 460 pp.

N.C. Department of Transportation. (2021, April 8). North Carolina Bridge Information. NCDOT. https://www.ncdot.gov/initiatives-policies/Transportation/bridges/Pages/default.aspx

Nawy, E. G. (2006). Reinforced concrete: A fundamental approach (5th ed.). Upper Saddle River, NJ.: Prentice Hall.

Orcutt, C., Cook, W. D., Mitchell, D. (2020). Response of Variable-Depth Reinforced Concrete Pier Cap Beams.

Perkins, S. M. (2011). Shear Behaviour of Deep Reinforced Concrete Members Subjected to Uniform Load (Unpublished master's thesis). University of Toronto.

Proestos, G. T., Bentz, E. C., Collins, M. P. (2018). Maximum shear capacity of reinforced concrete members. ACI Structural Journal, 115(5), 1463–73.

Proestos, G. T., Palipana, D. K., Mihaylov, B. I. (2021). Evaluating the shear resistance of deep beams loaded or supported by wide elements. Engineering Structures, 226(11368).

Qambar, M. (2020). Effect of wide loading elements and shear span-to-depth ratio on the behavior of shear critical reinforced concrete deep beams (Master's thesis). North Carolina State University, Raleigh, NC.

Qambar, M. (2020). Effect of Wide Loading Elements and Shear Span-to-Depth Ratio on the Behavior of Shear Critical Reinforced Concrete Deep Beams (Unpublished master's thesis). North Carolina State University.

Ritter, W. (1899), Die Bauweise Heurchique (Construction Techniques of Hennebique), Schweizerische Bauzeitung, Zurich.

Schlaich, J., Schafer, K., Jennewein, M. (1987). Toward a Consistent Design of Structural Concrete. PCI Journal, 32(3), 74-150. doi:10.15554/pcij.05011987.74.150.

Trandafir, A. N., Palipana, D. K., Proestos, G. T., Mihaylov, B. I. (2022). Framework for crack-based assessment of existing lightly reinforced concrete deep members. ACI Structural Journal, 119(1), 255–266.

Vecchio, F. J. (2000). Disturbed stress field model for reinforced concrete: Formulation. Journal of Structural Engineering, 126(9), 1070–1077. https://doi.org/10.1061/(asce)0733-9445(2000)126:9(1070).

Vecchio, F. J., Collins, M. P. (1986). The Modified Compression-Field Theory for Reinforced Concrete Elements Subjected to Shear. ACI Journal Proceedings, 83(2), 219-231. doi:10.14359/10416.

Williams, C. S., Deschenes, D. J., Bayrak, O. (2012). Strut-and-tie model design examples for bridges: Final report (Texas Department of Transportation, Research and Technology Implementation Office). Austin, TX: Center for Transportation Research, University of Texas at Austin.

Zeller, W. (1983). Bruchversuche an stahlbetonkonsolen bei vera¨nderung des bewehrungsgrades abschlußbericht zum forschungsvorhaben. Univ.

Zeller, W. (1991). Conclusions from Tests on Corbels. IABSE Colloquium, Structural Concrete, International Association for Bridge and Structural Engineering, Stuttgart, 577-582.